https://doi.org/10.35662/unine-thesis-3140

University of Neuchâtel

Faculty of Sciences

Laboratory of Plant Molecular and Cellular Biology

Lateral root formation in *Arabidopsis thaliana* and *Brachypodium distachyon*: comparison of spatial accommodating responses

A dissertation submitted to the
University of Neuchâtel
For the degree of
Doctor ès Sciences

Presented by

Cristóvão de Jesus Vieira Teixeira

Thesis Director:

Prof. Dr. Josephus Vermeer

Committee Members:

Prof. Dr. Christian S. Hardtke (University of Lausanne)

Prof. Dr. Felix Kessler (University of Neuchâtel)

Prof. Dr. Michael T. Raissig (University of Bern)

Defended on 03/09/2024

Neuchâtel, 2024

unine
Université de Neuchâtel
Faculté des sciences

Rue Emile-Argand 11
CH-2000 Neuchâtel
doctorat.sciences@unine.ch

IMPRIMATUR POUR THESE DE DOCTORAT

La Faculté des sciences de l'Université de Neuchâtel autorise l'impression de la présente thèse soutenue par

Monsieur Cristóvão DE JESUS VIEIRA TEIXEIRA

Titre :

"Lateral root formation in *Arabidopsis thaliana* and *Brachypodium distachyon*: comparison of spatial accommodating responses"

sur le rapport des membres du jury composé comme suit :

- **Prof. Josephus Vermeer,** directeur de thèse, UniNE
- **Prof. Felix Kessler,** UniNE
- **Prof. Christian S. Hardtke,** uniL, Suisse
- **Prof. Michael T. Raissig,** UniBE, Suisse

Neuchâtel, le 24 septembre 2024

Le Doyen, Prof. P. Brunner

ACKNOWLEDGEMENTS

We are never truly alone. Anyone who claims to have achieved success without any help discredits the countless individuals who have contributed to their journey. The completion of this doctoral thesis is no exception. Coming from a background where even the most optimistic predictions did not foresee me reaching this point, I am deeply grateful for the faith and support of those who believed in my potential. Expressing my gratitude is the least I can do.

First and foremost, I owe a deep debt of thanks to my parents for always prioritizing my education and supporting my decisions, even when those decisions seemed unattainable at first glance. They had faith in me, made numerous sacrifices, and did the best they could within the circumstances they faced. Now, as a father myself, I more fully understand the challenges they confronted. So, from the bottom of my heart, thank you, Mr. Sinval Domingos and Mrs. Zilda Teixeira. I also thank my grandparents, Mrs. Maria Domingues and Mr. Vani Delfino, who looked after me and my sister during a hard time in our lives.

Beyond my parents, many individuals have profoundly impacted my journey, from the time I left home to the beginning of my PhD. However, none have had as transformative an influence as my beloved wife, Julia Dias. She supported me throughout the entire PhD, from start to finish. There was not a single day when I felt I couldn't count on her. She has been the foundation that strengthened me and made me more confident. She embodies nobility and insight, and I am the luckiest man to call her my wife and the mother of our son, Gabriel. From the bottom of my heart, a big thank you to my wife.

My early years were enriched by the presence of many family members and friends: my sister Jessica Vieira, and my friends Markênio Peixoto, Fernando Bretner, Michael Christiano, Julio Cesar, Juliana Oliveira, Viniycius Americo, Tavvs Alves, Guilherme Costa, Thais and Thalita Marra, Camilla Gomes, Paulo Bahia, Fabio Cesarino, Denner Araujo, Julio Andrade, Pedro Cumino, Yona Marscarenhas, Erica Lidia, Diogo Careca, Léo Iporá, Claudio Americo, Donalvan Maia, Renan Botan, Murilo Carrera, Henrique Castro, and so many others. I deeply appreciate the support you all provided, and my sincerest apologies to those I may not have mentioned — you are no less important to me.

PhD life introduced me to new experiences and responsibilities. Living in Switzerland was an exceptional experience, made even better by the people who supported me throughout. I am particularly grateful to Prof. Dr. Joop Vermeer for accepting me as his PhD student and providing invaluable guidance during my time in his lab. He was always available for advice and offered support as I balanced the challenges of writing this thesis while being a new father. Thank you, Joop!

Of course, my journey would not have been as fulfilling without the incredible colleagues (now friends) I worked alongside. I owe a special thanks to my long-term-best office and running mate, Milica Nenadic, who generously provided advice and valuable tips during the writing phase. To Kevin and Thomas Badet, who always welcomed my questions and fully embraced the "Brachy Project" as their own — thank you. I also extend my thanks to Thai Buy and Zsofia Winter for their teamwork during the teaching semesters. I believe we made a great team! A heartfelt thank you to Vinay Shekhar, Doro Stöckler, and Martha Thellmann for their attention during my early PhD years, and to Mrs. Sophie Marc-Martin and Mrs. Pauline Udriet for their support in the lab and the great morning conversations. Also, thank you to Diego Beltrame and Zoe Cano, who were great colleagues in the lab day-to-day.

Lastly, I would like to acknowledge the many others who, in various ways, offered their time, attention, and belief in my ability to succeed on this PhD journey. Thank you.

ABSTRACT

Roots are essential for anchoring plants to the soil and for the uptake of water and nutrients. Root branching significantly enhances the morphological adaptability of the root system in response to various biotic and abiotic factorsDespite significant findings in recent decades within the LR context, there remain major questions about the role of the endodermis during the emergence of the LRP. Our research has identified two important groups of auxin-mediated enzymatic components (GDSL-type esterase/lipase proteins - GELPs) that regulate suberin polymerization and likely its degradation. Additionally, we have demonstrated that developmental plasticity of the endodermis is necessary for normal LR emergence. Higher order mutants, almost completely lacking suberization in the endodermis, were highly sensitive to stress conditions. The wild grass *Brachypodium distachyon*, with its small genome, short life cycle, and small stature, is suitable for genetic transformation and has been developed as a model organism for both laboratory and field studies. However, it presents considerable challenges for studying LRs in their early developmental stages. We adapted a clearing method that significantly reduces clearing time, is compatible with various fluorescence dyes, and allows deep imaging of early cell divisions in the LRP. Using this toolkit, we were able to systematically categorize each LRP stage similar to what is used in Arabidopsis. We also demonstrated that, unlike in Arabidopsis, in Brachypodium the endodermis reactivates the cell cycle during LR formation. Moreover, we could show that the LRP appears to modify its Casparian strips to allow the emergence of the new organ. Surprisingly, the auxin reporter DR5 was not detected in early stages of LR formation, which does not necessarily imply that auxin is not involved in the initiation steps since we observed expression of auxin transporters during LR initiation events. We employed a root tip excision (RTE) method to synchronize LR development in Brachypodium, revealing distinct responses between accessions Bd21 and Bd21-3. In the latter accession, LRs appeared to be delayed in their emergence towards the nutrient medium along the root axis compared to Bd21. Additionally, osmotic stresses and hormonal treatments significantly reduced LR number and size in Bd21-3. Histological analyses suggested that the observed challenges in LRP emergence could be caused by early lignification of the exodermis in Bd21-3, unlike Bd21, where a delayed lignification was associated with facilitated LRP emergence. Integrating RTE with RNA-seq analysis of selected time points revealed a rapid induction of genes with a predicted function in cell-wall modification following the synchronized LR formation. Further studies, such as single-cell sequencing, will be essential to investigate the genetic programs underlying cell wall remodelling during LRP emergence in Brachypodium. In conclusion, we believe that this thesis contributed to advance our understanding of LR development in a wild grass, particularly emphasizing the pivotal role of the endodermis and its interactions with hormonal pathways and suberin dynamics.

Keywords: Lateral root (LR), endodermis, suberization, auxin, Brachypodium distachyon, root branching, Casparian strips, lignification, root tip excision (RTE), cell-wall modification.

RÉSUMÉ

Les racines sont essentielles pour ancrer les plantes au sol et pour l'absorption de l'eau et des nutriments. La ramification des racines améliore considérablement l'adaptabilité morphologique du système racinaire en réponse à divers facteurs biotiques et abiotiques. Notre compréhension de la formation des racines latérales (RL) provient principalement d'études sur Arabidopsis. L'endoderme joue un rôle crucial lors de l'émergence des primordiums des racines latérales (PRL). Malgré des découvertes importantes au cours des dernières décennies dans le contexte des RL, des questions majeures subsistent quant au rôle de l'endoderme lors de l'émergence des PRL. Nos recherches ont identifié deux groupes importants de composants enzymatiques médiés par l'auxine (protéines estérase/lipase de type GDSL - GELPs) qui régulent la polymérisation de la subérine et probablement sa dégradation. De plus, nous avons démontré que la plasticité développementale de l'endoderme est nécessaire pour une émergence normale des RL. Les mutants de haut rang, presque totalement dépourvus de subérisation dans l'endoderme, étaient très sensibles aux conditions de stress. L'herbe sauvage *Brachypodium distachyon*, avec son petit génome, son cycle de vie court et sa petite taille, est adaptée à la transformation génétique et a été développée comme organisme modèle pour les études en laboratoire et sur le terrain. Cependant, elle présente des défis considérables pour l'étude des RL à leurs premiers stades de développement. Nous avons adapté une méthode de clarification qui réduit considérablement le temps de clarification, est compatible avec divers colorants fluorescents, et permet l'imagerie en profondeur des premières divisions cellulaires dans les PRL. En utilisant cet outil, nous avons pu systématiquement catégoriser chaque étape des PRL, comme cela est utilisé chez Arabidopsis. Nous avons également démontré que, contrairement à Arabidopsis, chez Brachypodium, l'endoderme réactive le cycle cellulaire lors de la formation des RL. De plus, nous avons montré que les PRL semblent modifier leurs bandes de Caspary pour permettre l'émergence du nouvel organe. Fait surprenant, le rapporteur d'auxine DR5 n'a pas été détecté aux premiers stades de la formation des RL, ce qui n'implique pas nécessairement que l'auxine ne soit pas impliquée dans les étapes initiales, car nous avons observé l'expression de transporteurs d'auxine lors des événements d'initiation des RL. Nous avons utilisé une méthode d'excision de la pointe racinaire (RTE) pour synchroniser le développement des RL chez Brachypodium, révélant des réponses distinctes entre les accessions Bd21 et Bd21-3. Chez cette dernière accession, les RL semblaient être retardées dans leur émergence vers le milieu nutritif le long de l'axe racinaire par rapport à Bd21. De plus, les stress osmotiques et les traitements hormonaux ont considérablement réduit le nombre et la taille des RL chez Bd21-3. Des analyses histologiques ont suggéré que les difficultés observées dans l'émergence des PRL pourraient être causées par une lignification précoce de l'exoderme chez Bd21-3, contrairement à Bd21, où une lignification retardée était associée à une émergence facilitée des PRL. L'intégration de la RTE avec l'analyse RNA-seq de points temporels sélectionnés a révélé une induction rapide de gènes avec une fonction prédite dans la modification de la paroi cellulaire après la formation synchronisée des RL. Des études supplémentaires, telles que le séquençage à cellule unique, seront essentielles pour étudier les programmes génétiques sous-jacents au remodelage de la paroi cellulaire pendant l'émergence des PRL chez Brachypodium. En conclusion, nous pensons que cette thèse a contribué à faire progresser notre compréhension du développement des RL chez une herbe sauvage, en mettant particulièrement l'accent sur le rôle crucial de l'endoderme et ses interactions avec les voies hormonales et la dynamique de la subérine.

Mots-clés : Racine latérale (RL), endoderme, subérisation, auxine, *Brachypodium distachyon*, ramification des racines, bandes de Caspary, lignification, excision de la pointe racinaire (RTE), modification de la paroi cellulaire.

TABLE OF CONTENTS

	CHAPTER 1 - INTRODUCTION	***15***
1.1	Importance of root system architecture (RSA)	16
1.2	Lateral root development is essential for RSA formation	16
1.3	The Role of Indole-3-Acetic Acid (IAA) in Lateral Root Organogenesis	18
1.4	Lateral root development in Arabidopsis thaliana	20
1.5	Lateral root development in monocots and other plant species.	22
1.6	Utilizing Brachypodium as a model for studying lateral root development	22
1.7	Tools for Observing Lateral Root Development in large species	24
1.7.1	Tissue clearing	24
1.7.2	Approaches for synchronizing LR development	26
1.8	Reference list	27
2.	**CHAPTER 2 - GDSL-domain proteins have key roles in suberin polymerization and degradation**	***33***
2.1	Brief introduction	34
2.2	Publication and follow-up assays	56
3.	**CHAPTER 3 - An updated toolset for observing lateral root development in Brachypodium**	***59***
3.1	Abstract	60
3.2	Introduction	61
3.3	Results	62
3.3.1	Brachypodium from seed to seed	62
3.3.2	CleaSee is unsuitable for clearing of Brachypodium root tissue	64
3.3.3	Deep-Clear is compatible with fluorescent proteins and -dyes	67
3.3.4	DEEP-Clear facilitates Brachypodium root tissue clearing	69
3.3.5	LR synchronization in Brachypodium	70
3.4	Discussion and applications	73
3.5	APPENDIX: Step by step protocols and chemical references.	74
3.6	Reference list	80
4.	**CHAPTER 4 - An atlas of Brachypodium distachyon lateral root development.**	***83***
4.1	Abstract	84
4.2	Introduction	86
4.3	Results	96
4.3.1	Lateral roots initiate from phloem pole pericycle cells in Brachypodium	87
4.3.2	DR5pro::ER-mRFP does not detect transcriptional auxin responses during early stages of LR development	89
4.3.3	Endodermal-derived cells form the root cap of new LRs.	92
4.3.4	Suberin deposition in the exodermis of Brachypodium roots is delayed compared to the endodermis	92
4.3.5	Dividing endodermal cells overlying the LRP appear not to establish a Casparian strip.	93
4.4	Discussion	95
4.5	Concluding remarks	98

4.6	Material and methods	98
4.7	Reference list	101
4.8	Supplementary figures	106
5.	**CHAPTER 5 - Root Tip excision uncovers differences in lateral root emergence in Brachypodium accessions**	***115***
5.1	Abstract	116
5.2	Introduction	117
5.3	Results	119
5.3.1	Bd21 and Bd21-3 show distinct LR developmental responses after RTE	119
5.3.2	Brachypodium Bd21-3 shows delayed LR emergence under abiotic stresses and hormonal treatments	121
5.3.3	Exodermal lignification correlates with delayed LR emergence	123
5.3.4	Cell-wall-related genes are rapidly induced after RTE	125
5.4	Discussion	127
5.5	Material and methods	131
5.6	Supplementary figures	134
5.7	Reference list	138
6	**CHAPTER 6 - General Discussion**	***141***
6.1	Introduction	142
6.2	Conclusion and future prospects	152
6.3	Final remarks	154
6.4	Reference list	156

THESIS OUTLINE

Chapter 1 is an introduction to key concepts related to root system architecture (RSA) with a focus on comparing and contrasting LR development between dicots and monocots. Here, we also discuss the use of *Brachypodium distachyon* as a plant model for studying LR development and the major tools for circumventing the challenges of observing the initial LRP cell divisions in this plant model.

Chapter 2 is team effort in which we show that specialized Arabidopsis endodermal cells respond to auxin by activating genes that remodel cell walls. We identified two groups of auxin-controlled GDSL lipases: one group is essential for the synthesis suberin, and the other breaks it down. These enzymes play crucial roles in modifying root suberin and also influencing LR formation.

Chapter 4 demonstrates the successful application of the tools developed in Chapter 3. It describes the major stages of LRP development in *Brachypodium* and provides insights into auxin signaling and cell wall modifications during the emergence of the LRP.

Chapter 5 employs the methodologies established in earlier chapters to explore a distinct RSA developmental pattern following the RTE-LR synchronization in two *Brachypodium* accessions. Through RNA-seq analysis, we demonstrate in this chapter the unique early and late responses in both accessions post-LR synchronization.

Chapter 6 summarizes the main findings and presents perspectives for future research.

CHAPTER 1

1. INTRODUCTION

Cristovão De Jesus Vieira Teixeira[1] *; Joop E.M. Vermeer*[1]

[1]*Laboratory of Molecular and Cellular Biology, Institute of Biology, University of Neuchâtel, Rue Emile Argand 11, CH-2000, Neuchâtel, Switzerland.*

Author contributions: Chapter 1 was fully written by *Cristovão De Jesus Vieira Teixeira* with suggestions and corrections by *Prof Dr. Joop E.M. Vermeer*.

1.1 Importance of root system architecture (RSA)

Currently, one of the most important challenges to achieve food security is the intensification of global food production. Crop plants, particularly cereals, are a vital, important food supply both directly and through use in animal feed: an estimated 75% of the human energy demand is fulfilled by cereal starch. According to FAO (2022), cereal crops production worldwide reached more the 2,6 million tons and wheat (monocot) contributes to one third of this total. However, hunger and malnutrition remain as major issues in many parts of the world even with the pronounced increase in cereal yield since the introduction of the Green Revolution technologies (Morris *et al.*, 2017).

Additionally, climate change can dramatically impact crop yields with long-term trends in average rainfall and extended drought periods (Kumar et al., 2019). Regardless of the numerous efforts to fully describe the response of crops to climate change, little is known about the complex mechanisms underlying plant adaptation to abiotic stresses (Jiang et al., 2020). This is in part due to the fact that most research in plant biology has been focused on aboveground responses such as flowering and grain development although root system architecture (RSA) is also strongly affected by climate change (Jiang et al., 2020). A strong and well-developed RSA is also associated with plants that are better adapted to extreme conditions. Therefore, understanding how root systems of major crops grow and develop is crucial as it allows for a fundamental understanding of plant development that can address challenges in cereal breeding.

1.2 Lateral root development is essential for RSA formation

RSA is referred to as the 3D spatial arrangement of roots in the soil (Pandey et al., 2021; Schäfer et al., 2022). The major components of RSA are root length, spread, number, and length of LRs. Allorhizic and homorhizic root types are the predominant root forms observed in plants (Orman-Ligeza et al., 2013; Amtmann, Bennett and Henry, 2022). In allorhizic, also known as dicotyledonous, the primary root is formed from the embryo and then LRs arise from the primary root (**Figure 1A**). RSA is also referred to as tap root systems since the primary root is the major originator of LRs. In less common cases, tap root systems also produce adventitious roots (hypocotyl or shoot-borne roots). In the case of homorhizic root systems also known as fibrous roots (in monocotyledonous), the primary root is also present, but embryonically formed seminal roots and adventitious roots are often present (**Figure 1B**) (Hochholdinger and Zimmermann, 2008; Sebastian et al., 2016). In later developmental stages, fibrous roots tend to lack the dominant axis and present a shallower growth pattern but with higher complexity compared to tap root systems (Fitter, 1987; Hochholdinger et al., 2004; Sebastian et al., 2016).

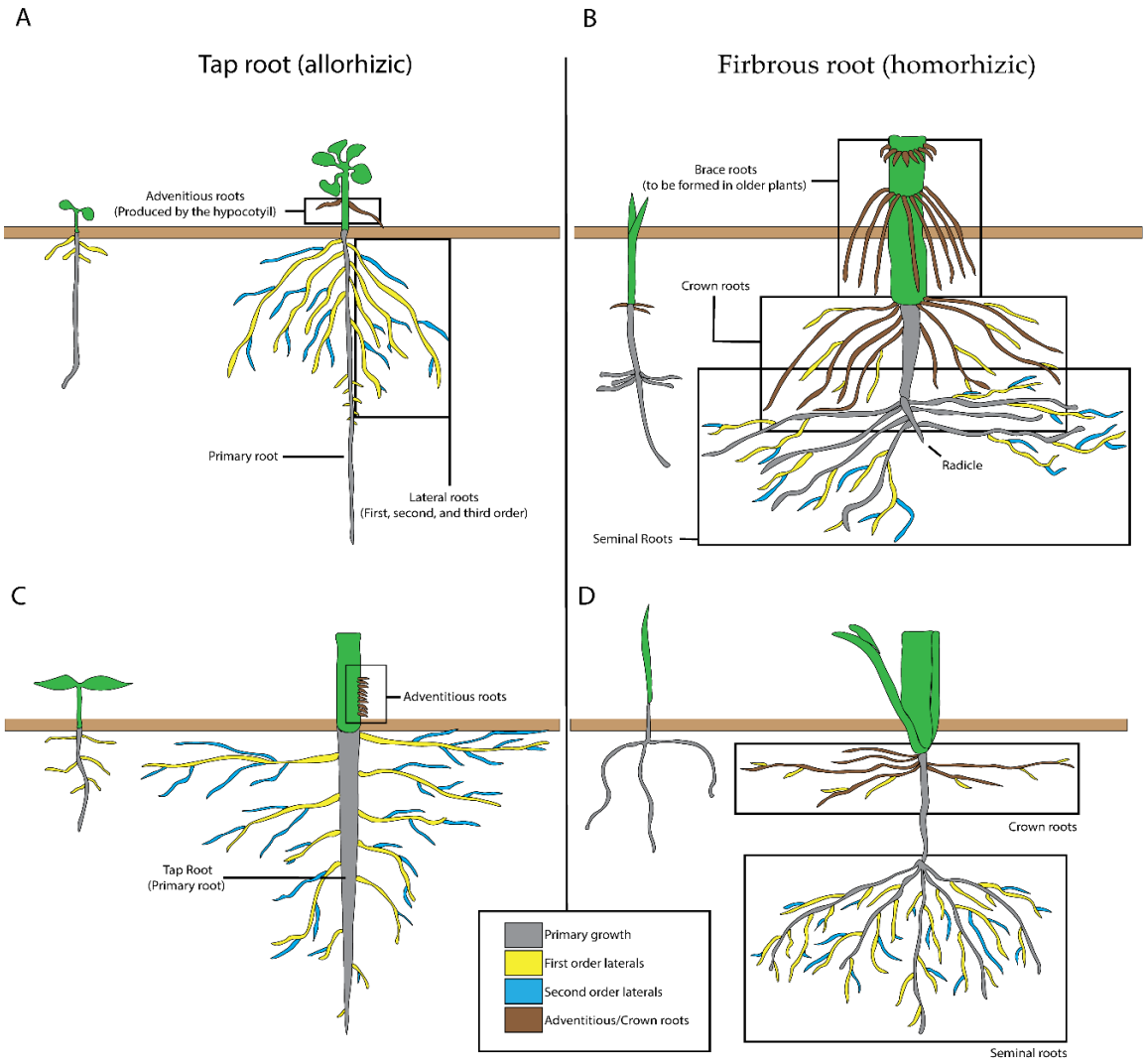

Figure 1. **A** to **D**, Schematics showing diversity in root system architecture at both seedling (left) and mature (right) stages in eudicots (**A** and **C**) and monocots (**B** and **D**). **A**, *Arabidopsis thaliana* (Arabidopsis) root system. **B**, Maize root system. **C**, Tomato root system (for clarity, stem-derived adventitious roots are only shown in the labeled region). **D**, Wheat root system. Modified from Atkinson et al. (2014).

For instance, in cereals, these include two classes of nodal roots: the crown and brace roots, which develop from belowground and aboveground nodes, respectively (**Figure 1B** and **D**). Crown roots in wheat (**Figure 1D**) form at the lower three to seven nodes, and in maize, they are organized on average into six underground whorls (**Figure 1B**). (Curtis, Rajaram and Macpherson, 2002). Maize also has two to three whorls of aboveground brace roots (also termed stilt or prop roots), which are functional for water and nutrient uptake and also important for support (Hostetler et al., 2022). In both monocots and dicots, the growth angle and number of LRs are central components of the overall architecture of the plant (Banda et al., 2019). LR formation is essential for RSA development as it increases the plant's capability to explore the soil for water and nutrients. Additionally, it enhances plant stress response and adaptation, improves anchorage and stability and facilitates interaction with microbes in the rhizosphere (Laskowski et al., 2006; Ambastha, Friedmann and

Leshem, 2020). Therefore, the importance of investigating the developmental mechanisms governing LR formation.

1.3 The Role of Indole-3-Acetic Acid (IAA) in Lateral Root Organogenesis

The plant hormone indole-3-acetic acid (IAA) or auxin is one of the major regulators of LR organogenesis. Intensive research efforts on understanding the mechanisms of RSA formation have validated the role of IAA (and other derived metabolites) as a major player in both embryonic (Mo and Weijers, 2009; Hao et al., 2021) and postembryonic developmental processes (Zazimalová, Petrasek and Benková, 2014). This knowledge also assisted the understanding of the molecular basis of the auxin-driven pathways, IAA production and transport thorough plant tissues (Blakely et al., 1988; Laskowski, 2013; Smetana et al., 2019; Israeli, Reed and Ori, 2020). IAA is a derivative from the tryptophan (Trp) pathway (Ursache et al., 2014; Israeli, Reed and Ori, 2020; Kou et al., 2022). Trp is firstly converted to indole-3-pyruvate (IPA) by the TRYPTOPHAN AMINOTRANSFERASE OF ARABIDOPSIS (TAA) family of amino transferases and subsequently IAA is produced from IPA by the YUCCA family of flavin monooxygenases (YUC gene family, named YUCCA after the yucca plant). The two-step conversion of Trp to IAA is the main auxin biosynthesis pathway that plays an essential role in many developmental processes. Additionally, the TAA/YUC pathway is highly conserved in the plant kingdom as the main IAA biosynthesis pathway since its disturbance leads to various developmental and responsive events in several species (Péret et al., 2012; Zhao, 2012; Cheung et al., 2020). IAA is produced mostly in the above ground parts of the plant, in the root meristem and in small amounts at sites of LR formation (Cavallari, Artner and Benkova, 2021). Subsequently, the IAA efflux proteins PIN-FORMED (PIN), the IAA influx proteins AUXIN RESISTANT 1 (AUX1) and LIKE AUX1 (LAX) facilitate the transport of IAA through plant tissues (Blilou et al., 2005). In opposite direction, a subset of ATP-binding cassette transporters/multidrug (ABCB) also function as auxin efflux carriers. However, recent data suggest that at least one of these ABCB transporters rather transports brassinosteroids, instead of IAA (Geisler and Murphy, 2006; Bailly et al., 2012; Cho et al., 2014; Ying et al., 2024). Once arriving at the sites of action, IAA is promptly sensed by a complex set of receptors, including the nuclear TRANSPORT INHIBITOR RESISTANT 1/AUXIN RESPONSE F-BOX (TIR1/AFB) F-box proteins, members of the SCFTIR1/AFB complex, which convey an auxin-induced transcriptional signal (Hayashi et al., 2008; Dindas et al., 2018). The auxin receptors form a co-receptor complex with the AUXIN/INDOLE-3-ACETIC ACID (Aux/IAA) transcriptional co-regulators that are ubiquitinated degraded by the proteasome after binding auxin (Ramos et al., 2001; Irina et al., 2012). This degradation relieves the repression of the AUXIN RESPONSE FACTOR (ARF) transcription factors by the Aux/IAA proteins (Zhou et al., 2018). ARFs have

a DNA-binding domain that interacts with the auxin response element (AuxRE) in promoters of auxin-responsive genes. When free from Aux/IAA interaction, ARF proteins act as either transcriptional activators or repressors of their target genes. This in turn guides the auxin response to the appropriate developmental output (Weijers and Wagner, 2016; Israeli, Reed and Ori, 2020).

The synthetic DR5 promoter 'Direct Repeat 5' is widely used as a reporter of auxin response (Liao et al., 2015). It consists of 7-9 AuxRE repeats and marks sites of transcriptional auxin response by activating fused reporter genes such as β-glucuronidase (Ulmasov *et al.*, 1997), fluorescent proteins (Vieten *et al.*, 2003), or luciferase (Moreno-risueno *et al.*, 2010). Highly coordinated activity of auxin signalling reporter DR5 in the basal meristem and gradients of DR5 activities have been linked to LRFC specification and LR initiation, respectively (Dubrovsky *et al.*, 2008; Swarup *et al.*, 2008). Further work on the analysis of crystal structures of 2 functionally divergent ARFs revealed that the AuxRE in DR5 is not a high-affinity binding site. Therefore, it likely that the limited sensitivity of DR5 reporters is due to its element being medium ARF affinity. A more updated version of a DR5 reporter named DR5v2 that relies on the replacement of the 9 original AuxREs in the original DR5-rev promoter was engineered to address this question (Ulmasov, Hagen and Guilfoyle, 2003; Liao *et al.*, 2015). These additional DR5v2 expression domains matched the predicted auxin accumulation sites based on the convergence of polar auxin transporter localization (Scarpella *et al.*, 2006). Although the addition of a novel binding site for ARF transcription factors shows promising results in increasing the sensitivity and precision of auxin response visualization, further work will be necessary to adapt this auxin reporter to other plant species, especially monocots. Another sensor to map auxin response is provided by DII-VENUS (Liao *et al.*, 2015). Conceptually different from the DR5 auxin sensor, it consists of a fusion of the auxin-dependent degradation domain II of an Aux/IAA protein to the Venus fluorescent protein. In this case, the absence of fluorescence reports auxin accumulation. Interfering with IAA biosynthesis, transport or response often leads to alterations in LR formation. Increased concentrations of IAA leads to higher numbers of LRs, while mutants impaired in auxin transport or one of the components of the signaling cascade form fewer LRs (Péret, Larrieu and Bennett, 2009). A large part of the knowledge about LR formation and its control by auxin comes from the model dicot Arabidopsis. Although some studies have been performed in rice (Smith and de Smet, 2012), it is still not clear whether these mechanisms are conserved in other Poaceae species.

Auxin efflux transporters, for instance, PIN1, PIN3, PIN4, PIN6, and PIN7 (Benková *et al.*, 2003; Marhavý *et al.*, 2013), AUX1, and AUX3 (LAX3) (Marchant *et al.*, 2002; Péret *et al.*, 2012) also play a major role during LR formation. In *pin1* mutants, LRP development

is delayed, and LR number is decreased (Benková *et al.*, 2003). Loss of LAX3 function causes a delay in LRP emergence (Swarup *et al.*, 2008). Additionally, the LATERAL ORGAN BOUNDARY REGION (LBD) genes are reported to disrupt LRP development in single and higher order mutants (Porco *et al.*, 2016). The findings that LBD proteins directly or indirectly can promote the expression of auxin importers (AUX1 and LAX3) explains some of these phenotypes (Porco *et al.*, 2016; Lee *et al.*, 2017). In Arabidopsis, PROHIBITIN 3 (PHB3) was demonstrated to cause endogenous nitric oxide (NO) accumulation by regulating the expression of SHI-RELATED SEQUENCE5 (SRS5). The expression of SRS5 also leads to the degradation of IAA14 and IAA28, thereby increasing the expression of *GATA23* and *LBD16*, ultimately regulating the development of LR formation (Luo et al., 2022). In monocots plants, the family of auxin transporters is expanded and frequently consists of duplicated genes that share a significant degree of sequence similarity. Certain proteins within these groups have undergone changes in function and structure, as well as in their expression patterns, particularly in organs like adventitious roots, panicles, tassels, and ears. Most of the current knowledge of the role and mechanisms of these auxin transporters in monocots come from rice, maize, sorghum, and Brachypodium. However, very little is known on their localization and function during LR formation.

1.4 Lateral root development in Arabidopsis thaliana

Arabidopsis thaliana (Arabidopsis) is the major plant model used for RSA studies (Atkinson *et al.*, 2014; Bellini, Pacurar and Perrone, 2014). It presents a tap root system; therefore, a single primary root elongates and LR are formed later (**Figure 2A**). LR development in Arabidopsis initiates from the pericycle adjacent to the xylem, the so-called xylem pole pericycle (XPP) in the parent root (**Figure 2C**). Remarkably, before the first visible cell divisions in the differentiation zone, a range of pre-initiation events are reported in the basal meristem of Arabidopsis roots (Vanneste et al., 2005; De Smet et al., 2007; De Rybel et al., 2010; Pacheco-Villalobos et al., 2016). In this transition zone or oscillation zone (OZ), a sharp decrease in cell divisions and cell elongation is observed. Additionally, a process named “priming” is associated to the specification of XPP into pre-branch sites (Laskowski and ten Tusscher, 2017). LRs initiate from a pair of Lateral Root Founder Cells (LRFCs), and a series of highly coordinated cell divisions lead to the development of a new LR primordium (LRP) (Casero, Casimiro and Lloret, 1995; Ditengou et al., 2008; Stoeckle, Thellmann and Vermeer, 2018).

The first morphological event of LRP initiation takes place in the differentiation zone where LRFCs divide asymmetrically and anticlinal. Cell division and expansion of pericycle cells are tightly controlled by auxin and other plant hormones. The endodermis also plays

an important role during LRP formation due to the presence of lignified Caparian Strips (CS) and many other cell wall modifications (Lehman, Smertenko and Sanguinet, 2017; Vilches Barro et al., 2019; Ursache et al., 2021; Stöckle et al., 2022). For instance, the elimination of endodermal cells activates pericycle cells to re-enter the cell cycle and promotes periclinal cell divisions. Only when exogenous auxin is supplied, the endodermis elimination result sin LR initiation (Marhavý et al., 2016). Likewise, auxin (discussed later) is associated with the activation of transcription Gly-Asp-Ser-Leu (GDSL) lipases for suberin synthesis and degradation in the endodermis to facilitate the emergence of LRP (Ursache et al., 2021). Additionally, SHORT HYPOCOTYL 2 (SHY2)/IAA3 (member of the auxin-induced Aux/IAA gene family) is also known to be induced in endodermal cells overlying the LRP. Expression of its gain-of-function mutant only in the elongating endodermis (*CASP1pro::shy2-2*), to locally block Aux/IAA-mediated auxin signalling was shown to completely disrupt LR development (Vermeer et al., 2014; Vermeer and Geldner, 2015). Furthermore, a coordinated reorganization of the cytoskeleton in response to the phytohormone auxin in both the XPP and endodermis is required for normal LR morphogenesis (Vilches Barro et al., 2019; Stöckle et al., 2022). After several rounds of cell divisions, the LRP forms an ellipsoid-shape eventually reacting the outer layers and emerging from the root surface (Van Norman et al., 2013).

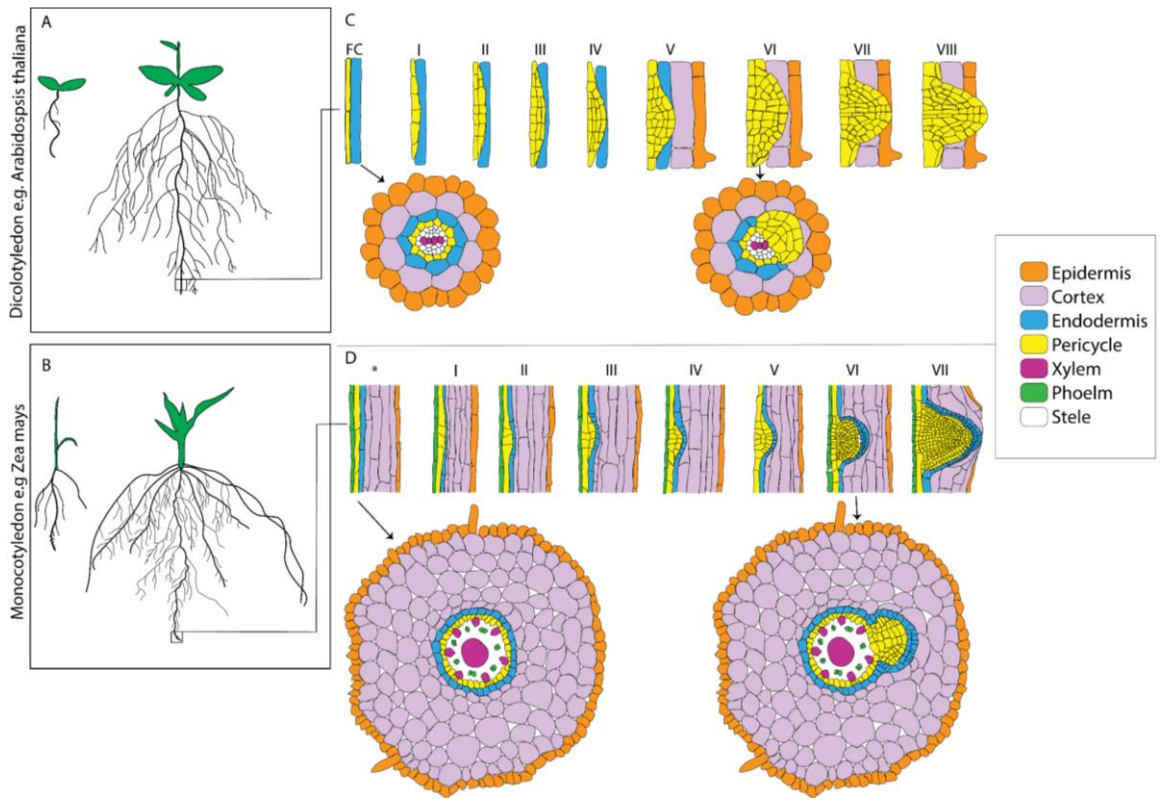

Figure 2. **Schematic representation of lateral root development in monocots and dicots.** (**A**) Arabidopsis thaliana and (**B**) Barley (*Hordeum vulgare*). The stages of lateral root development are depicted for Arabidopsis (**C**) and Barley. **Note**: the image is not drawn to scale. Adapted from (Péret, Larrieu and Bennett, 2009; Orman-Ligeza et al., 2013; Yue and Beeckman, 2014; Stoeckle, Thellmann and Vermeer, 2018)

Interestingly, Arabidopsis shows LR development on the side of the main root in contact with water in the soil or agar (Bao et al., 2014).This environmental stimulus known as hydropatterning was shown a conserved process in maize and rice and reveal the importance of auxin biosynthesis and transport in regulating this process (Bao et al., 2014).

Additionally, it also involves a posttranslational modification of transcription factor ARF7 in Arabidopsis evidencing how environmental inputs modulate the auxin response machinery (Orosa-Puente et al., 2018). However, it remains unclear whether these and other developmental processes are fully or partially conserved in a wider range of plant species.

1.5 Lateral root development in monocots and other plant species.

In monocots, LRP initiate from pericycle cells associated with the phloem poles (**Figure 2D**) (Orman-Ligeza et al., 2013; Yu et al., 2016). This contrasts with dicot species like Arabidopsis where LRP arise exclusively from the XPP (Malamy and Benfey, 1997). The polyarchy stellar organization of cereal roots leads to LRP formation in several longitudinal files. Similar to Arabidopsis, LRP formation in monocots follows an acropetal sequence with younger LRs closer to the root tip; however, with higher variability due to formation of different LR types. Notably, in cereals and many other plant species, the endodermis cells adjacent to the diving pericycle dedifferentiate, undergo anticlinal divisions thereby contributing to the development of the LRP (Xiao et al., 2019). Later, cells derived from the endodermis further divide to generate the inner and outer layers of the root cap (**Figure 2D**). For instance, in barley, cortical cells also undergo cell division but their direct contribution to the LRP is still unclear (Kirschner et al., 2017). The endodermal and cortical cell divisions are thought to assist LR emergence, potentially facilitated by the loss of CS during the endodermal cell division. However, it is unclear which mechanisms regulate the dedifferentiation and cell cycle activation of the endodermis and the role of hormones, especially auxin, in this process.

1.6 Utilizing Brachypodium as a model for studying lateral root development

Arabidopsis LR development has been a model system to study root morphogenesis for the last two decades (Scheres and Wolkenfelt, 1998; Dubrovsky and Forde, 2012; Banda et al., 2019). Many of the genes involved in LR organogenesis have been identified over the last decade using forward and reverse genetic approaches (De Rybel et al., 2010; Lavenus et al., 2015; Banda et al., 2019). Although impressive progress has recently been made in crops such as rice, maize and barley (Ni et al., 2014; Sebastian et al., 2016; Kirschner et al., 2017), Arabidopsis remains the main experimental system for studying LR development and the underlying hormone signalling pathways (Benková and Bielach, 2010; Orosa-Puente et al., 2018; Leftley et al., 2021). In monocots, LR studies have mostly been conducted on rice,

which is considered as a model plant for cereal crops (Wang et al., 2002; Uga et al., 2013; Lu et al., 2018; Meng et al., 2019). However, handling rice as a large, outbreeding plant with a long life-cycle and demanding growth requirements is quite problematic as model for high-throughput LR studies. Instead, the non-domesticated, temperate grass *Brachypodium distachyon* (Brachypodium) has all the attributes to make it an excellent model to study root systems architecture in cereal crops (Vogel, 2008; Chochois, Vogel and Watt, 2012; Hardtke and Pacheco-Villalobos, 2015a). Important features such as relatively small genome size, simple growth conditions, fast regeneration time and self-pollination make this plant model a strong candidate for LR research in major monocots.

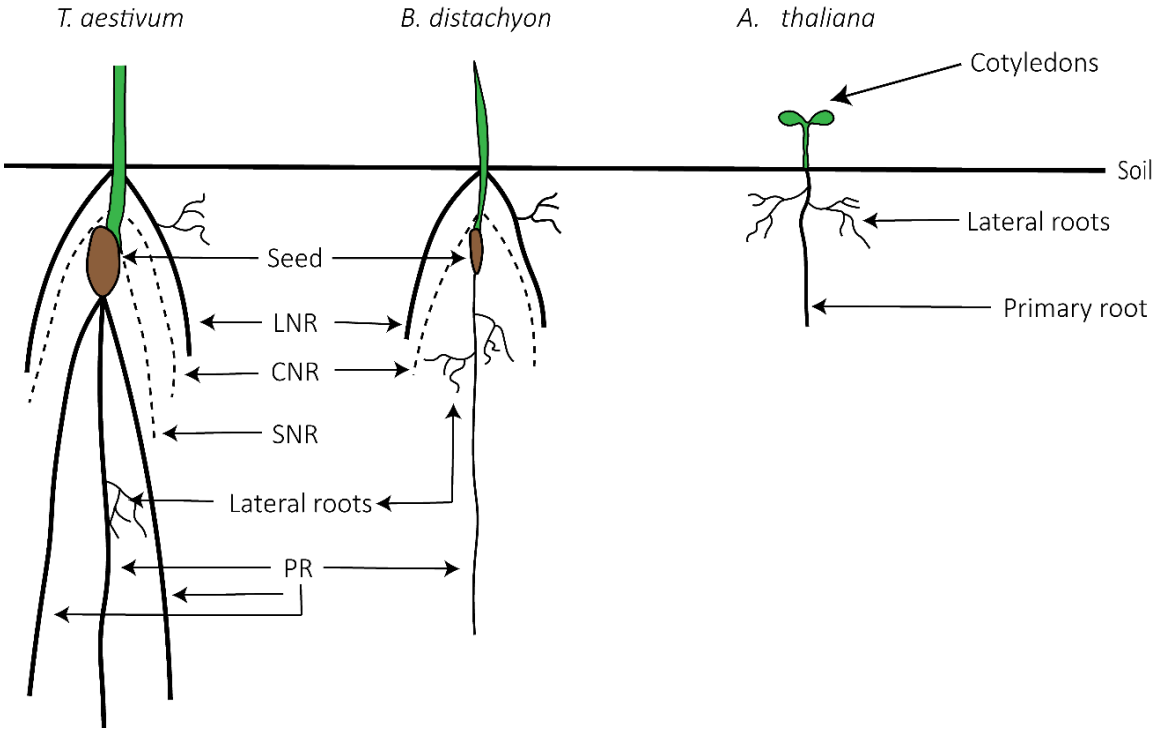

Figure 3. **Comparison of wheat (*T. aestivum*), *Brachypodium distachyon*, and *A. thaliana* root systems**. Horizontal line, soil level. Abbreviations: CNR, coleoptile node axile root; LNR, leaf node axile root; PR, primary axile root; SNR, scutellar node axile root. Modified from (Catalan et al., 2014).

This makes it very suitable to conduct studies and transfer the knowledge to, for instance, wheat, barley and maize (Vogel et al., 2006; van der Schuren et al., 2018).

The Brachypodium root system presents a high degree of developmental and anatomical similarity to cereal crops, for instance wheat and maize, especially at the adult plant stages (Garvin, 2007), presented in a much less complex structure (Catalan et al., 2014; Hardtke and Pacheco-Villalobos, 2015b; Scholthof et al., 2018) (**Figure 3**). The root system of Brachypodium (Bd21) has one primary axile root, two coleoptile node axile roots that emerge above the seed, and successive leaf node axile roots (Pacheco-Villalobos and Hardtke, 2012; Catalan et al., 2014; Scholthof et al., 2018). The Brachypodium vasculature system shows on average six to eight meta-xylem elements with two or three xylem poles

each and one central meta-xylem (eventually two). Phloem poles can be found in a similar number alternating with xylem tissues in the vascular cylinder (**Figure 2D**). Analogous to Arabidopsis, the inner vascular system is surrounded by a single layer of pericycle cells from which LRs are known to initiate. However, in contrast to Arabidopsis, in Brachypodium, the endodermis appears to become a part of the new LR primordium, similar as reported for maize (Bell and McCully, 1970; Jansen et al., 2012). However, still additional investigation is required to confirm the precise tissue coordination and developmental sequences during LR development in Brachypodium relative to the main vascular tissues.

1.7 Tools for Observing Lateral Root Development in large species

1.7.1 Tissue clearing

Arabidopsis is a valuable model for studying plant roots because the simplicity of the tissue organization and almost transparent cell layers (Péret et al., 2009). In contrast, Brachypodium has thicker root layers with increased autofluorescence challenging visualization of deep tissues (van der Schuren et al., 2018). To study early LRP development in Brachypodium effectively, histological methods such sectioning and clearing will need to be employed. Sectioning tissues into thin slices has been the standard practice in histology (Yadav 2021). However, biological structures are inherently three-dimensional (3-D), therefore, the spatial information of the sample is lost after the sections are made. In contrast, clearing methods provide subcellular level optical access to intact tissues, organs, or entire specimens. When such approaches are combined, for instance with confocal microscopy and automated approaches for image processing, it can speed up research by increasing output and considerably lowering the costs in resources (Ursache et al., 2018; Piccinini, Nirina Ramamonjy and Ursache, 2024). Most of clearing methods were developed for mammalian tissues and subsequently adapted for other specimens, including plants (Pende et al., 2020; Ueda et al., 2020). Clearing tissues consists of reducing absorption by eliminating or changing the refraction index (RI) of pigments to make the tissue transparent without losing its integrity. Plants exhibit a wide diversity of cell types (e.g., parenchymal and epidermal cells), organelles (e.g., chloroplasts and amyloplasts), and components (e.g., waxes and pigments) with specific optical properties (Richardson et al., 2021). Consequently, these factors influence how light penetrates the tissue layers, thereby affecting light absorption and scattering. Clearing protocols for plant tissues are divided into two main categories (**Figure 4**). Solvent-based (SBC) clearing and Aqueous-based clearing (ABC).

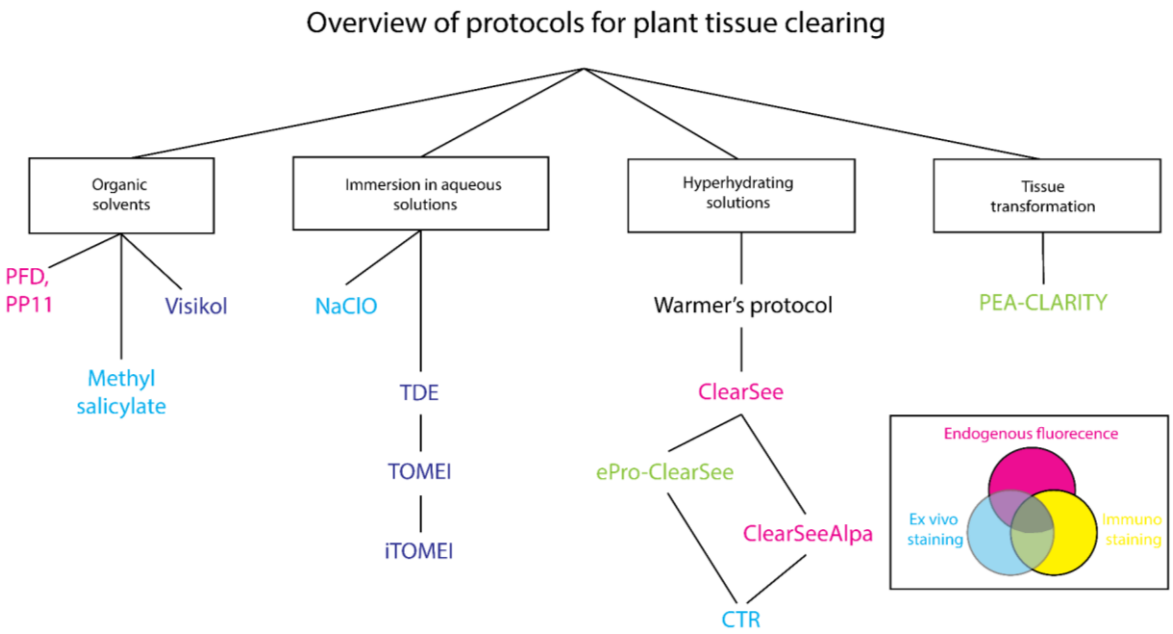

Figure 4. **Overview of clearing protocols (CPs) for plant tissues.** Abbreviations: BABB, benzyl benzoate/benzyl alcohol; CTR: clearing tannic roots; ePro-ClearSee, enzymes 2 propanol ClearSee; iTOMEI: improved TOMEI; PEA CLARITY, plant-enzyme-assisted CLARITY; PFD, perfluorodecalin; PP11, perfluoroperhydrophenanthrene; SeeDB, See Deep Brain; TDE: 2,2′-thiodiethanol; TOMEI, transparent plant organ method for imaging – Modified from (Hériché et al., 2022).

SBC approaches were the pioneering protocols for tissue clearing based on dehydration, lipid solvation, and incubation in a high-RI solution (Richardson and Lichtman, 2015). However, the dehydration step is often associated with damaging of the tissue integrity. Additionally, most of SBC approaches are not compatible with fluorescent proteins (FP) or fluorescent dyes (FD). ABC methods offer alternatives that generally keep the stability of FP, increased compatibility with a diversity of FD, but slower clearing than the SBC methods (Yadav et al., 2021). ABC methods rely on the passive immersion, protein hyperhydration and hydrogel embedding of the sample (Ueda et al., 2020). For instance, CLARITY involves the infusion of a hydrogel matrix into the specimen, which supports the structural integrity of the tissue while allowing for the removal of lipids that contribute to light scattering and absorption (Palmer et al., 2015). PEA-CLARITY, a derivative of the CLARITY technique (**Figure 4**), further optimizes this process for plant tissues, which often require different conditions due to their unique composition and density (Palmer et al., 2015).

The most recent and efficient method for clearing plant tissue is ClearSee (Kurihara et al., 2015). ClearSee is a water-based solution that offers effective clearing and is suitable for a wide range of endogenous FPs. It is compatible with many FDs and has been tested across various organs and plant species (Ursache et al., 2018). Specific variants of the ClearSee protocol have been created to meet particular needs. For instance, ePro-ClearSee was developed for immunostaining, and another variant was designed to enhance

compatibility with additional FDs (Nagaki, Yamaji and Murata, 2017). In the latest update of this protocol, named ClearSeeAlpha, a reductant, sodium sulphite, is added to prevent brown pigmentation caused by polyphenol oxidation (Kurihara et al., 2021). However, the addition of SS limits the compatibility of the clearing agent with some FDs, such as Basic Fuchsin, which is used for observing lignin (Kurihara et al., 2021). The original ClearSee protocol also induces browning issues in Brachypodium root tissue as reported in (Kurihara et al., 2021). Therefore, a combination and adaptation of other clearing protocols might be necessary for clearing Brachypodium roots and observed lignification within the same sample set while preserving the endogenous FP.

1.7.2 Approaches for synchronizing LR development

Understanding the formation of LR development can become a major challenge due to the small number of cells involved in the initiation events (Dubrovsky *et al.*, 2006). This issue is aggravated by the lack of synchrony within the different initiation sites. A range of Lateral Root Inducible Systems (LRIS) has been developed to attempt to solve this problem. In Arabidopsis, LR initiation can be, for instance, induced mechanically either by gravitropic curvature or by the transient bending of a root by hand (Ditengou et al., 2008). In this case, the plant hormone auxin accumulates at the site of LR induction prior to initiation. Therefore, LRP tissue in different developmental stages can be harvested from zero to approximately 42 hours after the bending. Although its simplicity, this approach generates a small amount of tissue sample and it has not been demonstrated to work in monocots. Another LR inducing system relies on seed germination in the presence of the auxin transport inhibitor N-1-naphthylphthalamic acid (NPA) followed by transfer to growth medium containing the auxin 1-naphthalene acetic acid (NAA) (Crombez et al., 2016). The latter method has also been demonstrated to be functional for maize (Jansen et al., 2012). Although this approach increases the number of LRPs at a specific stage, it remains unclear to what extent these early hormone treatments affect other plant hormones. (Jansen et al., 2013) also reports that seed germination is inefficient in the presence of NPA. Therefore, seeds would initially need to be grown in the absence of NPA and then transferred to NPA-treated plates potentially inducing LRP initiation before LR induction with NAA treatment increasing variability in the developmental stages of LRPs. An alternative method relies in the excision of the root tip and in the ability of compensatory root growth via LR formation (Kawai et al., 2022). In rice, main root tip cutting induced LR development in the remaining proximal portions and promoted elongation of first-order LRs and higher-order branching (Sasaki et al., 1984; Kawai et al., 2017). Although this method presents the most straightforward approach for inducing LRP development, to this point, it has not been extensively tested in other plant species.

REFERENCE LIST

Ambastha, V., Friedmann, Y. and Leshem, Y. (2020) 'Laterals take it better – Emerging and young lateral roots survive lethal salinity longer than the primary root in Arabidopsis', *Scientific Reports*, 10(2391), pp. 1–11. Available at: https://doi.org/10.1038/s41598-020-60163-7.

Amtmann, A., Bennett, M.J. and Henry, A. (2022) 'Root Phenotypes for the Future', *Plant, Cell & Environment* [Preprint]. Available at: https://doi.org/10.1111/PCE.14269.

Atkinson, J.A. *et al.* (2014) 'Branching Out in Roots: Uncovering Form, Function, and Regulation', *Plant Physiology*, 166(2), pp. 538–550. Available at: https://doi.org/10.1104/pp.114.245423.

Bailly, A. *et al.* (2012) 'Plant Lessons: Exploring ABCB Functionality Through Structural Modeling', *Frontiers in plant science*, 2, p. 108. Available at: https://doi.org/10.3389/fpls.2011.00108.

Banda, J. *et al.* (2019) 'Lateral Root Formation in Arabidopsis: A Well-Ordered LRexit', *Trends in Plant Science*, 24(9), pp. 826–839. Available at: https://doi.org/10.1016/j.tplants.2019.06.015.

Bao, Y. *et al.* (2014) 'Plant roots use a patterning mechanism to position lateral root branches toward available water', *Proceedings of the National Academy of Sciences*, 111(25), pp. 9319–9324. Available at: https://doi.org/10.1073/pnas.1400966111.

Bellini, C., Pacurar, D.I. and Perrone, I. (2014) 'Adventitious roots and lateral roots: Similarities and differences', *Annual Review of Plant Biology*. Annual Reviews Inc., pp. 639–666. Available at: https://doi.org/10.1146/annurev-arplant-050213-035645.

Bell, J. and McCully, M. (1970) 'A histological study of lateral root initiation and development inZea mays', *Protoplasma*, 205, pp. 179–205. Available at: http://www.springerlink.com/index/H534X7JN67X81711.pdf.

Benková, E. *et al.* (2003) 'Local, Efflux-Dependent Auxin Gradients as a Common Module for Plant Organ Formation', *Cell*, 115(5), pp. 591–602. Available at: https://doi.org/10.1016/S0092-8674(03)00924-3.

Benková, E. and Bielach, A. (2010) 'Lateral root organogenesis - from cell to organ', *Current Opinion in Plant Biology*, 13(6), pp. 677–683. Available at: https://doi.org/10.1016/j.pbi.2010.09.006.

Blakely, L.M. *et al.* (1988) 'Experimental Studies on Lateral Root Formation in Radish Seedling Roots: II. Analysis of the Dose-Response to Exogenous Auxin', *Plant Physiology*, 87(2), pp. 414–419. Available at: https://doi.org/10.1104/pp.87.2.414.

Blilou, I. *et al.* (2005) 'The PIN auxin efflux facilitator network controls growth and patterning in Arabidopsis roots', *Nature*, 433(7021), pp. 39–44. Available at: https://doi.org/10.1038/nature03184.

Casero, P.J., Casimiro, I. and Lloret, P.G. (1995) 'Lateral root initiation by asymmetrical transverse divisions of pericycle cells in four plant species:Raphanus sativus, Helianthus annuus, Zea mays, andDaucus carota', *Protoplasma*, 188(1), pp. 49–58. Available at: https://doi.org/10.1007/BF01276795.

Catalan, P. *et al.* (2014) 'Update on the genomics and basic biology of Brachypodium. International Brachypodium Initiative (IBI)', *Trends in Plant Science*, 19(7), pp. 414–418. Available at: https://doi.org/10.1016/j.tplants.2014.05.002.

Cavallari, N., Artner, C. and Benkova, E. (2021) 'Auxin-regulated lateral root organogenesis', *Cold Spring Harbor Perspectives in Biology*, 13(7). Available at: https://doi.org/10.1101/cshperspect.a039941.

Cheung, A.Y. *et al.* (2020) 'Update on Receptors and Signaling', *Plant Physiology*, 182(4), pp. 1527–1530. Available at: https://doi.org/10.1104/pp.20.00275.

Chochois, V., Vogel, J.P. and Watt, M. (2012) 'Application of Brachypodium to the genetic improvement of wheat roots', *Journal of Experimental Botany*, 63(9), pp. 3467–3474. Available at: https://doi.org/10.1093/jxb/ers044.

Cho, H. *et al.* (2014) 'A secreted peptide acts on BIN2-mediated phosphorylation of ARFs to potentiate auxin response during lateral root development', *Nature Cell Biology*, 16(1), pp. 66–76. Available at: https://doi.org/10.1038/ncb2893.

Crombez, H. *et al.* (2016) 'Lateral Root Inducible System in Arabidopsis and Maize', *J. Vis. Exp*, 107, p. 53481. Available at: https://doi.org/10.3791/53481.

Curtis, B., Rajaram, S. and Macpherson, H. (2002) *Bread wheat: improvement and production.*, …. Food and Agriculture Organization of the United Nations. Available at: https://doi.org/ISBN 92-5-104809-6.

Dindas, J. *et al.* (2018) 'AUX1-mediated root hair auxin influx governs SCFTIR1/AFB-type Ca2+ signaling', *Nature Communications*, 9(1). Available at: https://doi.org/10.1038/s41467-018-03582-5.

Ditengou, F.A. *et al.* (2008) 'Mechanical induction of lateral root initiation in Arabidopsis thaliana', *Proceedings of the National Academy of Sciences of the United States of America*, 105(48), pp. 18818–18823. Available at: https://doi.org/10.1073/pnas.0807814105.

Dubrovsky, J.G. *et al.* (2006) 'Lateral Root Initiation in Arabidopsis: Developmental Window, Spatial Patterning, Density and Predictability', *Annals of Botany*, 97(5), pp. 903–915. Available at: https://doi.org/10.1093/aob/mcj604.

Dubrovsky, J.G. *et al.* (2008) 'Auxin acts as a local morphogenetic trigger to specify lateral root founder cells', *Proceedings of the National Academy of Sciences*, 105(25), pp. 8790–8794. Available at: https://doi.org/10.1073/pnas.0712307105.

Dubrovsky, J.G. and Forde, B.G. (2012) 'Quantitative Analysis of Lateral Root Development: Pitfalls and How to Avoid Them', *The Plant Cell*, 24(1), pp. 4 LP – 14. Available at: https://doi.org/10.1105/tpc.111.089698.

Garvin, D.F. (2007) 'Brachypodium: a new monocot model plant system emerges', *Journal of the Science of Food and Agriculture*, 87(7), pp. 1177–1179. Available at: https://doi.org/10.1002/jsfa.2868.

Geisler, M. and Murphy, A.S. (2006) 'The ABC of auxin transport: The role of p-glycoproteins in plant development', *FEBS Letters*, 580(4), pp. 1094–1102. Available at: https://doi.org/10.1016/j.febslet.2005.11.054.

Hao, Z. *et al.* (2021) 'Conserved, divergent and heterochronic gene expression during Brachypodium and Arabidopsis embryo development', *Plant Reproduction*, 34(3), pp. 207–224. Available at: https://doi.org/10.1007/S00497-021-00413-4/FIGURES/7.

Hardtke, C.S. and Pacheco-Villalobos, D. (2015a) 'The Brachypodium distachyon Root System: A Tractable Model to Investigate Grass Roots', pp. 245–258. Available at: https://doi.org/10.1007/7397_2015_6.

Hardtke, C.S. and Pacheco-Villalobos, D. (2015b) 'The Brachypodium distachyon Root System: A Tractable Model to Investigate Grass Roots', in, pp. 245–258. Available at: https://doi.org/10.1007/7397_2015_6.

Hayashi, K. *et al.* (2008) 'Small-molecule agonists and antagonists of F-box protein–substrate interactions in auxin perception and signaling', *Proceedings of the National Academy of Sciences*, 105(14), pp. 5632 LP – 5637. Available at: https://doi.org/10.1073/pnas.0711146105.

Hériché, M. *et al.* (2022) 'Imaging plant tissues: advances and promising clearing practices', *Trends in Plant Science*, 27(6), pp. 601–615. Available at: https://doi.org/10.1016/j.tplants.2021.12.006.

Hochholdinger, F. and Zimmermann, R. (2008) 'Conserved and diverse mechanisms in root development', *Current Opinion in Plant Biology*, pp. 70–74. Available at: https://doi.org/10.1016/j.pbi.2007.10.002.

Irina, L. *et al.* (2012) 'system for differential sensing of auxin', 8(april). Available at: https://doi.org/10.1038/nchembio.926.

Israeli, A., Reed, J.W. and Ori, N. (2020) 'Genetic dissection of the auxin response network', *Nature Plants*, 6(9), pp. 1082–1090. Available at: https://doi.org/10.1038/s41477-020-0739-7.

Jansen, L. *et al.* (2012) 'Phloem-associated auxin response maxima determine radial positioning of lateral roots in maize'. Available at: https://doi.org/10.1098/rstb.2011.0239.

Jansen, L. *et al.* (2013) 'Comparative transcriptomics as a tool for the identification of root branching genes in maize', *Plant Biotechnology Journal*, 11(9), pp. 1092–1102. Available at: https://doi.org/10.1111/pbi.12104.

Jiang, Q. *et al.* (2020) 'Assessing climate change impacts on greenhouse gas emissions, N losses in drainage and crop production in a subsurface drained field', *Science of The Total Environment*, 705, p. 135969. Available at: https://doi.org/10.1016/j.scitotenv.2019.135969.

Kawai, T. *et al.* (2022) 'WUSCHEL-related homeobox family genes in rice control lateral root primordium size', *Proceedings of the National Academy of Sciences of the United States of America*, 119(1). Available at: https://doi.org/10.1073/PNAS.2101846119/-/DCSUPPLEMENTAL.

Kirschner, G.K. *et al.* (2017) 'Unique and Conserved Features of the Barley Root Meristem', *Frontiers in Plant Science*, 8, p. 1240. Available at: https://doi.org/10.3389/fpls.2017.01240.

Kou, X. *et al.* (2022) 'Auxin Response Factors Are Ubiquitous in Plant Growth and Development, and Involved in Crosstalk between Plant Hormones: A Review', *Applied Sciences 2022, Vol. 12, Page 1360*, 12(3), p. 1360. Available at: https://doi.org/10.3390/APP12031360.

Kumar, J. *et al.* (2019) 'Towards Exploitation of Adaptive Traits for Climate-Resilient Smart Pulses', *International journal of molecular sciences*, 20(12), p. 2971. Available at: https://doi.org/10.3390/ijms20122971.

Kurihara, D. *et al.* (2015) 'ClearSee: a rapid optical clearing reagent for whole-plant fluorescence imaging.', *Development (Cambridge, England)*, 142(23), pp. 4168–79. Available at: https://doi.org/10.1242/dev.127613.

Kurihara, D. *et al.* (2021) 'ClearSeeAlpha: Advanced Optical Clearing for Whole-Plant Imaging', *Plant and Cell Physiology* [Preprint]. Available at: https://doi.org/10.1093/pcp/pcab033.

Laskowski, M. *et al.* (2006) 'Expression profiling of auxin-treated Arabidopsis roots: Toward a molecular analysis of lateral root emergence', *Plant and Cell Physiology*, 47(6), pp. 788–792. Available at: https://doi.org/10.1093/pcp/pcj043.

Laskowski, M. (2013) 'Lateral root initiation is a probabilistic event whose frequency is set by fluctuating levels of auxin response', *Journal of Experimental Botany*, 64(9), pp. 2609–2617. Available at: https://doi.org/10.1093/jxb/ert155.

Laskowski, M. and ten Tusscher, K.H. (2017) 'Periodic Lateral Root Priming: What Makes It Tick?', *The Plant Cell*, 29(3), pp. 432–444. Available at: https://doi.org/10.1105/tpc.16.00638.

Lavenus, J. *et al.* (2015) 'Inference of the Arabidopsis Lateral Root Gene Regulatory Network Suggests a Bifurcation Mechanism That Defines Primordia Flanking and Central Zones', *The Plant Cell*, 27(5), pp. 1368 LP – 1388. Available at: https://doi.org/10.1105/tpc.114.132993.

Lee, D.O. *et al.* (2017) 'Cross-species functional diversity within the PIN auxin efflux protein family'. Available at: https://doi.org/10.7554/eLife.31804.001.

Leftley, N. *et al.* (2021) 'Uncovering How Auxin Optimizes Root Systems Stresses', pp. 1–16. Available at: https://doi.org/10.1101/cshperspect.a040014.

Lehman, T.A., Smertenko, A. and Sanguinet, K.A. (2017) 'Auxin, microtubules, and vesicle trafficking: conspirators behind the cell wall', *Journal of Experimental Botany*, 68(13), pp. 3321–3329. Available at: https://doi.org/10.1093/jxb/erx205.

Liao, C.Y. *et al.* (2015) 'Reporters for sensitive and quantitative measurement of auxin response', *Nature Methods*, 12(3), pp. 207–210. Available at: https://doi.org/10.1038/nmeth.3279.

Lu, Y. *et al.* (2018) 'MiR393 and miR390 synergistically regulate lateral root growth in rice under different conditions', *BMC Plant Biology*, 18(1), p. 261. Available at: https://doi.org/10.1186/s12870-018-1488-x.

Malamy, J.E. and Benfey, P.N. (1997) 'Organization and cell differentiation in lateral roots of Arabidopsis thaliana', *Development*, 124(1), pp. 33 LP – 44. Available at: http://dev.biologists.org/content/124/1/33.abstract.

Marchant, A. *et al.* (2002) 'AUX1 Promotes Lateral Root Formation by Facilitating Indole-3-Acetic Acid Distribution between Sink and Source Tissues in the Arabidopsis Seedling', *The Plant Cell*, 14(3), pp. 589–597. Available at: https://doi.org/10.1105/tpc.010354.

Marhavý, P. *et al.* (2013) 'Auxin reflux between the endodermis and pericycle promotes lateral root initiation', *EMBO Journal*, 32(1), pp. 149–158. Available at: https://doi.org/10.1038/emboj.2012.303.

Marhavý, P. *et al.* (2016) 'Targeted cell elimination reveals an auxin-guided biphasic mode of lateral root initiation', *Genes & Development*, 30(4), pp. 471–483. Available at: https://doi.org/10.1101/gad.276964.115.

Meng, F. *et al.* (2019) 'Molecular Mechanisms of Root Development in Rice', *Rice (New York, N.Y.)*, 12(1), p. 1. Available at: https://doi.org/10.1186/s12284-018-0262-x.

Mo, B. and Weijers, D. (2009) 'Auxin Control of Embryo Patterning', pp. 1–13.

Moreno-risueno, M.A. *et al.* (2010) 'Oscillating Gene Expression Arabidopsis Root Branching', 329(September), pp. 1306–1312.

Morris, E.C. *et al.* (2017) 'Shaping 3D Root System Architecture', *Current Biology*, 27(17), pp. R919–R930. Available at: https://doi.org/10.1016/j.cub.2017.06.043.

Nagaki, K., Yamaji, N. and Murata, M. (2017) 'ePro-ClearSee: a simple immunohistochemical method that does not require sectioning of plant samples', *Scientific Reports*, 7(1), p. 42203. Available at: https://doi.org/10.1038/srep42203.

Ni, J. *et al.* (2014) 'Histological characterization of the lateral root primordium development in rice', *Botanical Studies*, 55(1), pp. 1–6. Available at: https://doi.org/10.1186/s40529-014-0042-x.

Orman-Ligeza, B. *et al.* (2013) 'Post-embryonic root organogenesis in cereals: branching out from model plants', *Trends in Plant Science*, 18(8), pp. 459–467. Available at: https://doi.org/10.1016/J.TPLANTS.2013.04.010.

Orosa-Puente, B. *et al.* (2018) 'Root branching toward water involves posttranslational modification of transcription factor ARF7', *Science*, 362(6421), pp. 1407–1410. Available at: https://doi.org/10.1126/science.aau3956.

Pacheco-Villalobos, D. *et al.* (2016) 'The Effects of High Steady State Auxin Levels on Root Cell Elongation in Brachypodium[OPEN]'. Available at: https://doi.org/10.1105/tpc.15.01057.

Palmer, W.M. *et al.* (2015) 'PEA-CLARITY: 3D molecular imaging of whole plant organs', *Scientific Reports*, 5(1), p. 13492. Available at: https://doi.org/10.1038/srep13492.

Pandey, B. *et al.* (2021) 'Plant roots sense soil compaction through restricted ethylene diffusion', *Science*, In press(January), pp. 276–280.

Pende, M. *et al.* (2020) 'A versatile depigmentation, clearing, and labeling method for exploring nervous system diversity', *Science Advances*, 6(22). Available at: https://doi.org/10.1126/sciadv.aba0365

Péret, B. *et al.* (2009) 'Arabidopsis lateral root development: an emerging story', *Trends in Plant Science*, 14(7), pp. 399–408. Available at: https://doi.org/10.1016/j.tplants.2009.05.002.

Péret, B. *et al.* (2012) 'Auxin regulates aquaporin function to facilitate lateral root emergence', *Nature Cell Biology*, 14(10), pp. 991–998. Available at: https://doi.org/10.1038/ncb2573.

Péret, B., Larrieu, A. and Bennett, M.J. (2009) 'Lateral root emergence: A difficult birth', *Journal of Experimental Botany*, 60(13), pp. 3637–3643. Available at: https://doi.org/10.1093/jxb/erp232.

Piccinini, L., Nirina Ramamonjy, F. and Ursache, R. (2024) 'Imaging plant cell walls using fluorescent stains: The beauty is in the details', *Journal of Microscopy* [Preprint]. John Wiley and Sons Inc. Available at: https://doi.org/10.1111/jmi.13289.

Porco, S. *et al.* (2016) 'Lateral root emergence in Arabidopsis is dependent on transcription factor LBD29 regulation of auxin influx carrier LAX3', *Development (Cambridge)*, 143(18), pp. 3340–3349. Available at: https://doi.org/10.1242/DEV.136283/264091/AM/LATERAL-ROOT-EMERGENCE-IN-ARABIDOPSIS-IS-DEPENDENT.

Ramos, J.A. *et al.* (2001) 'Rapid Degradation of Auxin / Indoleacetic Acid Proteins Requires Conserved Amino Acids of Domain II and Is Proteasome Dependent', 13(October), pp. 2349–2360.

Richardson, D.S. *et al.* (2021) 'Tissue clearing', *Nature Reviews Methods Primers*, 1(1), p. 84. Available at: https://doi.org/10.1038/s43586-021-00080-9.

Richardson, D.S. and Lichtman, J.W. (2015) 'Clarifying Tissue Clearing', *Cell*, 162(2), pp. 246–257. Available at: https://doi.org/10.1016/j.cell.2015.06.067.

De Rybel, B. *et al.* (2010) 'A novel Aux/IAA28 signaling cascade activates GATA23-dependent specification of lateral root founder cell identity', *Current Biology*, 20(19), pp. 1697–1706. Available at: https://doi.org/10.1016/j.cub.2010.09.007.

Scarpella, E. *et al.* (2006) 'Control of leaf vascular patterning by polar auxin transport', *Genes & Development*, 20(8), pp. 1015–1027. Available at: https://doi.org/10.1101/gad.1402406.

Schäfer, E.D. *et al.* (2022) 'Modeling root loss reveals impacts on nutrient uptake and crop development', *Plant Physiology*, 190(4), pp. 2260–2278. Available at: https://doi.org/10.1093/plphys/kiac405.

Scheres, B. and Wolkenfelt, H. (1998) 'The Arabidopsis root as a model to study plant development', *Plant Physiology and Biochemistry*, 36(1), pp. 21–32. Available at: https://doi.org/https://doi.org/10.1016/S0981-9428(98)80088-0.

Scholthof, K.-B.G. *et al.* (2018) 'Brachypodium: A monocot grass model system for plant biology', *The Plant Cell*, 30(August), p. tpc.00083.2018. Available at: https://doi.org/10.1105/tpc.18.00083.

van der Schuren, A. *et al.* (2018) 'Broad spectrum developmental role of Brachypodium AUX1', *New Phytologist*, 219(4), pp. 1216–1223. Available at: https://doi.org/10.1111/nph.15332.

Sebastian, J. *et al.* (2016) 'Grasses suppress shoot-borne roots to conserve water during drought.', *Proceedings of the National Academy of Sciences of the United States of America*, 113(31), pp. 8861–6. Available at: https://doi.org/10.1073/pnas.1604021113.

Smetana, O. *et al.* (2019) 'High levels of auxin signalling define the stem-cell organizer of the vascular cambium', *Nature*, p. 1. Available at: https://doi.org/10.1038/s41586-018-0837-0.

De Smet, I. *et al.* (2007) 'Auxin-dependent regulation of lateral root positioning in the basal meristem of Arabidopsis', *Development*, 134(4), pp. 681–690. Available at: https://doi.org/10.1242/dev.02753.

Stöckle, D. *et al.* (2022) 'Microtubule-based perception of mechanical conflicts controls plant organ morphogenesis', *Sci. Adv*, 8, p. 4974. Available at: https://doi.org/10.1126/SCIADV.ABM4974.

Stoeckle, D., Thellmann, M. and Vermeer, J.E. (2018) 'Breakout — lateral root emergence in Arabidopsis thaliana', *Current Opinion in Plant Biology*. Elsevier Ltd, pp. 67–72. Available at: https://doi.org/10.1016/j.pbi.2017.09.005.

Swarup, K. *et al.* (2008) 'The auxin influx carrier LAX3 promotes lateral root emergence', *Nature Cell Biology*, 10(8), pp. 946–954. Available at: https://doi.org/10.1038/ncb1754.

Ueda, H.R. *et al.* (2020) 'Tissue clearing and its applications in neuroscience', *Nature Reviews Neuroscience*. Nature Research, pp. 61–79. Available at: https://doi.org/10.1038/s41583-019-0250-1.

Uga, Y. *et al.* (2013) 'Control of root system architecture by DEEPER ROOTING 1 increases rice yield under drought conditions', *Nature Genetics*, 45(9), pp. 1097–1102. Available at: https://doi.org/10.1038/ng.2725.

Ulmasov, T. *et al.* (1997) 'Aux/IAA proteins repress expression of reporter genes containing natural and highly active synthetic auxin response elements.', *The Plant Cell*, 9(11), pp. 1963–1971. Available at: https://doi.org/10.1105/tpc.9.11.1963.

Ulmasov, T., Hagen, G. and Guilfoyle, T.J. (2003) *ARF1, a Transcription Factor That Binds to Auxin Response Elements*. Available at: http://science.sciencemag.org/ (Accessed: 14 June 2020).

Ursache, R. *et al.* (2014) 'Tryptophan-dependent auxin biosynthesis is required for HD-ZIP III-mediated xylem patterning', *Development (Cambridge)*, 141(6), pp. 1250–1259. Available at: https://doi.org/10.1242/dev.103473.

Ursache, R. *et al.* (2018) 'A protocol for combining fluorescent proteins with histological stains for diverse cell wall components', *The Plant Journal*, 93(2), pp. 399–412. Available at: https://doi.org/10.1111/tpj.13784.

Ursache, R. *et al.* (2021) 'GDSL-domain proteins have key roles in suberin polymerization and degradation', *Nature Plants*, 7(3), pp. 353–364. Available at: https://doi.org/10.1038/s41477-021-00862-9.

Vanneste, S. *et al.* (2005) 'Cell cycle progression in the pericycle is not sufficient for SOLITARY ROOT/IAA14-mediated lateral root initiation in Arabidopsis thaliana', *Plant Cell*, 17(11), pp. 3035–3050. Available at: https://doi.org/10.1105/tpc.105.035493.

Vermeer, J.E.M. *et al.* (2014) 'A spatial accommodation by neighboring cells is required for organ initiation in arabidopsis', *Science*, 343(6167), pp. 178–183. Available at: https://doi.org/10.1126/SCIENCE.1245871.

Vermeer, J.E.M. and Geldner, N. (2015) 'Lateral root initiation in Arabidopsis thaliana: a force awakens', *F1000Prime Reports*, 7. Available at: https://doi.org/10.12703/P7-32.

Vieten, A. *et al.* (2003) 'Efflux-dependent auxin gradients establish the apical – basal axis of Arabidopsis', pp. 147–153.

Vilches Barro, A. *et al.* (2019) 'Cytoskeleton Dynamics Are Necessary for Early Events of Lateral Root Initiation in Arabidopsis', *Current Biology*, 29(15), pp. 2443-2454.e5. Available at: https://doi.org/10.1016/j.cub.2019.06.039.

Vogel, J. (2008) ‘Unique aspects of the grass cell wall’, *Current Opinion in Plant Biology*, 11(3), pp. 301–307. Available at: https://doi.org/10.1016/j.pbi.2008.03.002.

Vogel, J.P. *et al.* (2006) ‘EST sequencing and phylogenetic analysis of the model grass Brachypodium distachyon’, *Theoretical and Applied Genetics*, 113(2), pp. 186–195. Available at: https://doi.org/10.1007/s00122-006-0285-3.

Wang, S. *et al.* (2002) *Lateral root formation in rice (Oryza sativa): promotion effect of jasmonic acid*, *J. Plant Physiol*. Available at: http://www.urbanfischer.de/journals/jpp.

Weijers, D. and Wagner, D. (2016) ‘Transcriptional Responses to the Auxin Hormone’, *Annual Review of Plant Biology*, 67(1), pp. 539–574. Available at: https://doi.org/10.1146/annurev-arplant-043015-112122.

Xiao, T.T. *et al.* (2019) ‘Lateral root formation involving cell division in both pericycle, cortex and endodermis is a common and ancestral trait in seed plants’, *Development (Cambridge)*, 146(20). Available at: https://doi.org/10.1242/dev.182592.

Yadav, V. *et al.* (2021) ‘Histochemical Techniques in Plant Science: More Than Meets the Eye’, *Plant and Cell Physiology*, 62(10), pp. 1509–1527. Available at: https://doi.org/10.1093/pcp/pcab022.

Ying, W. *et al.* (2024) ‘Structure and function of the *Arabidopsis* ABC transporter ABCB19 in brassinosteroid export’, *Science*, 383(6689). Available at: https://doi.org/10.1126/science.adj4591.

Yue, K. and Beeckman, T. (2014) ‘Cell-to-cell communication during lateral root development’, *Molecular Plant*, 7(5), pp. 758–760. Available at: https://doi.org/10.1093/mp/ssu012.

Yu, P. *et al.* (2016) ‘Genetic Control of Lateral Root Formation in Cereals’, *Trends in Plant Science*. Elsevier Ltd, pp. 951–961. Available at: https://doi.org/10.1016/j.tplants.2016.07.011.

Zazimalová, E., Petrasek, J. and Benková, E. (2014) *Auxin and Its Role in Plant Development*, *Auxin and Its Role in Plant Development*. Available at: https://doi.org/10.1007/978-3-7091-1526-8.

Zhao, Y. (2012) ‘Auxin biosynthesis: A simple two-step pathway converts tryptophan to indole-3-Acetic acid in plants’, *Molecular Plant*, 5(2), pp. 334–338. Available at: https://doi.org/10.1093/mp/ssr104.

Zhou, X. *et al.* (2018) ‘Identification, characterization, and expression analysis of auxin response factor (ARF) gene family in Brachypodium distachyon’, *Functional & Integrative Genomics*, 18(6), pp. 709–724. Available at: https://doi.org/10.1007/s10142-018-0622-z.

CHAPTER 2

1. GDSL-domain proteins have key roles in suberin polymerization and degradation

Robertas Ursache[1], Cristovao De Jesus Vieira-Teixeira[2], Valérie Dénervaud Tendon[1], Kay Gully[1], Damien De Bellis[1,4], Emanuel Schmid-Siegert[5§,] Tonni Grube Andersen1[$], Vinay Shekhar[2,3,] Sandra Calderon5,6, Sylvain Pradervand5,6, Christiane Nawrath1, Niko Geldner[1*] and Joop E.M. Vermeer[2,3*1]*

[1]Department of Plant Molecular Biology, University of Lausanne, 1015 Lausanne, Switzerland

[2]Laboratory of Cell and Molecular Biology, Institute of Biology, University of Neuchâtel, 2000, Neuchâtel, Switzerland

[3]Department of Plant and Microbial Biology & Zurich-Basel Plant Science Centre, University of Zurich, 8008 Zurich, Switzerland

[4]Electron Microscopy Facility, University of Lausanne, 1015 Lausanne, Switzerland

[5]Vital-IT Competence Center, Swiss Institute of Bioinformatics, 1015 Lausanne, Switzerland

[6]Genomic Technologies Facility, University of Lausanne, 1015 Lausanne, Switzerland

[$] Current address: Max Planck Institute for Plant Breeding Research, Carl-Von-Linne-Weg 10, 50829 Cologne, Germany

[§] Current address: NGSAI, Route de Corniche 3, CH-1066 Epalinges, Switzerland

[*]Corresponding authors: Robertas.Ursache@unil.ch, Niko.Geldner@unil.ch, Joop.Vermeer@unine.ch

Author contributions: *Cristovão De Jesus Vieira Teixeira* participated in the writing of the manuscript, performed the genotyping and phenotyping of the mutants, generated (Extended Data Figure 8), conducted experiments involving osmotic stress and tetrazolium tests (Extended Data Fig. 9 & 10), and created figures to meet reviewers' requirements.

2.1 Brief introduction

In parallel to the adventure of improving the methodology to better understand LR development in *Brachypodium*, a considerable part of my work also focused on helping to uncover the role of the GDSL-domain proteins (GELPS) in suberin deposition and degradation during root development. The findings of this research were published as Robertas Ursache, Cristovão De Jesus Vieira Teixeira, Valérie Dénervaud Tendon, Kay Gully, Damien De Bellis1, Emanuel Schmid-Siegert, Tonni Grube Andersen, Vinay Shekhar, Sandra Calderon, Sylvain Pradervand, Christiane Nawrath, Niko Geldner, and Joop E. M. Vermeer to *Nature Plants* volume 7, pages 353–364 (2021).

In this article, we show that differentiated endodermal cells have a distinct auxin-mediated transcriptome. We analysed this dataset and identified a set of ten GDSL-motif-containing enzymes that are differentially regulated after auxin treatment. We confirmed that all ten of these GDSL-motif containing enzymes were expressed in the endodermis, and were either repressed or induced during auxin treatment or LR formation. We showed that five of the auxin-repressed GDSL-motif-containing enzymes are redundantly required for suberin biosynthesis; the quintuple knockout of these enzymes essentially abrogated suberin accumulation in the endodermis. Among the five auxin-induced GDSL-motif-containing genes, we identified enzymes that we demonstrated to be sufficient for suberin degradation and required for correct LR emergence. The quintuple mutants of the suberin-biosynthetic, GDSL-motif-containing enzymes were highly sensitive to mild salt stress. Single-knockout mutants of members of the suberin-degrading class displayed delays in LR emergence. The enzymes identified in this work are strong candidates to be suberin polymerases and degradases in plants. This work advances our understanding of in vivo suberin formation, as well as the mechanisms underlying its developmental plasticity.

nature plants

ARTICLES

https://doi.org/10.1038/s41477-021-00862-9

GDSL-domain proteins have key roles in suberin polymerization and degradation

Robertas Ursache[1]✉, Cristovão De Jesus Vieira Teixeira[2], Valérie Dénervaud Tendon[1], Kay Gully[1], Damien De Bellis[1,3], Emanuel Schmid-Siegert[4,7], Tonni Grube Andersen[1,8], Vinay Shekhar[2,5], Sandra Calderon[4,6], Sylvain Pradervand[4,6], Christiane Nawrath[1], Niko Geldner[1]✉ and Joop E. M. Vermeer[2,5]✉

Plant roots acquire nutrients and water while managing interactions with the soil microbiota. The root endodermis provides an extracellular diffusion barrier through a network of lignified cell walls called Casparian strips, supported by subsequent formation of suberin lamellae. Whereas lignification is thought to be irreversible, suberin lamellae display plasticity, which is crucial for root adaptative responses. Although suberin is a major plant polymer, fundamental aspects of its biosynthesis and turnover have remained obscure. Plants shape their root system via lateral root formation, an auxin-induced process requiring local breaking and re-sealing of endodermal lignin and suberin barriers. Here, we show that differentiated endodermal cells have a specific, auxin-mediated transcriptional response dominated by cell wall remodelling genes. We identified two sets of auxin-regulated GDSL lipases. One is required for suberin synthesis, while the other can drive suberin degradation. These enzymes have key roles in suberization, driving root suberin plasticity.

Plants require a dynamic and adaptive root system, which enables optimal anchorage and foraging of the soil environment for water and nutrients, while managing interactions with the soil microbiome[1–3]. Lateral root formation is a key factor modulating root system architecture. In most angiosperms, including *Arabidopsis thaliana*, these organs initiate in xylem-pole associated pericycle cells (XPPs). Auxin is required for both initiation and development of lateral roots[4,5]. Lateral roots need to traverse the overlying endodermis to develop and emerge, and this cell layer therefore has an essential role during lateral root formation, as it has to actively accommodate the expansion growth of the XPPs through remodelling of cell shape and volume.

Moreover, to minimize both the leakage of nutrients from the stele into the rhizosphere and the entry of soil-borne pathogens, opening and sealing of the lignified and suberized endodermal barriers needs to be tightly controlled. Therefore, a dynamic desuberization and resuberization is bound to have an important role in this process. However, we still lack an understanding of the basic molecular machineries that regulate the dynamics of suberin deposition and degradation during root development[6–9]. The lignified Casparian strip appears to be locally modified to allow the growth of the lateral root through this cell layer[10] and it suberin has been shown to be deposited in the cell walls of endodermal cells in contact with the later lateral root primordium after emergence[8]. However, endodermal cells are often already suberized when lateral roots form and it is unknown how suberin is first degraded and later resynthesized.

All these responses are regulated via auxin-mediated signalling in the endodermis, and expression of *short hypocotyl 2-2* (*shy2-2*)—a dominant repressor of auxin signalling—in this cell layer blocks lateral root formation, demonstrating the crucial role of SHY2-mediated endodermal auxin signalling in this process[10].

In this Article, we show that differentiated endodermal cells have a distinct auxin-mediated transcriptome. We analysed this dataset and identified a set of ten GDSL-motif-containing enzymes that are differentially regulated after auxin treatment. We confirmed that all ten of these GDSL-motif-containing enzymes were expressed in the endodermis, and were either repressed or induced during auxin treatment or lateral root formation. We showed that five of the auxin-repressed GDSL-motif-containing enzymes are redundantly required for suberin biosynthesis; the quintuple knockout of these enzymes essentially abrogated suberin accumulation in the endodermis. Among the five auxin-induced GDSL-motif-containing genes, we identified enzymes that we demonstrated to be sufficient for suberin degradation and required for correct lateral root emergence. The quintuple mutants of the suberin-biosynthetic, GDSL-motif-containing enzymes were highly sensitive to mild salt stress. Single-knockout mutants of members of the suberin-degrading class displayed delays in lateral root emergence. The enzymes identified in this work are strong candidates to be suberin polymerases and degradases in plants. This work advances our understanding of in vivo suberin formation, as well as the mechanisms underlying its developmental plasticity.

Results

A genotype for obtaining specific endodermal auxin responses. Drastic changes in endodermal cell volume and Casparian strip modification during lateral root emergence[10] are mediated by

[1]Department of Plant Molecular Biology, University of Lausanne, Lausanne, Switzerland. [2]Laboratory of Cell and Molecular Biology, Institute of Biology, University of Neuchâtel, Neuchâtel, Switzerland. [3]Electron Microscopy Facility, University of Lausanne, Lausanne, Switzerland. [4]Vital-IT Competence Center, Swiss Institute of Bioinformatics, Lausanne, Switzerland. [5]Department of Plant and Microbial Biology & Zurich-Basel Plant Science Centre, University of Zurich, Zurich, Switzerland. [6]Genomic Technologies Facility, University of Lausanne, Lausanne, Switzerland. [7]Present address: NGSAI, Epalinges, Switzerland. [8]Present address: Max Planck Institute for Plant Breeding Research, Cologne, Germany. ✉e-mail: Robertas.Ursache@unil.ch; Niko.Geldner@unil.ch; Josephus.Vermeer@unine.ch

SHORT HYPOCOTYL 2 (*SHY2* (also known as *IAA3*))-dependent auxin signalling. SHY2 represses its own transcription in a typical, auxin-induced negative-feedback loop and is thus also an early transcriptional auxin-response marker in the endodermis[10,11]. The targets of SHY2 (direct or indirect) that drive the complex accommodating responses in the endodermis remain unknown. Therefore, we set out to obtain a SHY2-mediated transcriptional response profile in the endodermis. Generating such a dataset comes with particular challenges. First, most endodermal cells at the moment of lateral root emergence are lignified and suberized, making it impossible to use protoplast isolation for single-cell or cell-type-specific sequencing. Second, only a subset of endodermal cells—those overlying an auxin-emitting lateral root primordium from stage I and onwards—will be stimulated in a *SHY2*-dependent fashion[10]. We therefore first compared wild-type and *CASP1pro::shy2-2* seedlings—in which auxin signalling is suppressed specifically in the differentiated endodermis—after auxin treatment to obtain an endodermis-specific set of auxin-responsive genes. In the wild type, the auxin-reporter *SHY2pro::NLS-3xmVenus* fluorescence peaks in the endodermis at about 16 h after treatment with the membrane-permeable auxin analogue NAA and is blocked in the *CASP1pro::shy2-2* line (Fig. 1a,d and Extended Data Fig. 1). However, since the *CASP1pro::shy2-2* transgene also indirectly impairs the auxin-mediated induction of lateral roots[10], a simple comparison of the auxin-induced transcriptomes of *CASP1pro::shy2-2* roots and wild-type roots after auxin treatment would be dominated by pericycle and cell cycle-related responses, preventing identification of endodermal auxin responses. Therefore, we added a genetic manipulation that would strongly enrich for auxin-induced transcriptional changes in the endodermis. We combined the dominant *solitary root 1* (*slr-1* (also known as *iaa14*)) mutant with *CASP1pro::shy2-2*. Lateral root formation is impaired in the *Arabidopsis slr-1* mutant[12]. Importantly, *SLR* is expressed in the pericycle, cortex and epidermis, but not in the endodermis, and the *slr-1* mutant should thus specifically block auxin response in the cell layers surrounding the endodermis[12,13](Extended Data Fig. 2a). As predicted, we found that auxin-mediated induction of *SHY2* in the endodermis still occurred in *slr-1* roots (Fig. 1b,d). We further predicted that, in the combined *CASP1pro::shy2-2/slr-1* background, auxin signalling should be largely blocked in all differentiated root cell layers. Indeed, we could not detect induction of *SHY2pro::NLS-3xmVenus* in the endodermis in this background. Based on these results, we predicted that a comparison (subtraction) of the NAA-induced transcriptomes of roots from the *slr-1* single mutant with the *CASP1pro::shy2-2/slr-1* double mutant would enable us to extract a specific endodermal auxin signalling transcriptomic profile, which would otherwise be obscured by the strong, proliferation-inducing auxin responses of the XPPs (Fig. 1a–e).

Differentiated endodermal cells have a distinct transcriptional auxin response. We interrogated the genome-wide transcriptional responses in *slr-1* and *CASP1pro::shy2-2/slr-1* after NAA treatment at multiple time points. We established that around 800–900 genes are differentially expressed at 2, 4, 8 and 16 h after treatment and around 1,000 are significantly changed after 24 h treatment compared with the zero timepoint (Supplementary Table 1). Using non-supervised methods and manual tests, we settled on seven clusters to describe the data (Fig. 1f,g). As expected, the dataset contained a large number of cell wall-related genes and hardly any cell cycle-related genes. Analysing the gene ontology (GO) annotations, we observed terms linked to auxin signalling and lateral root development (clusters 2 and 5), whereas terms related to lipid transport and fatty acid metabolism were enriched in clusters 3 and 5. The fact that we observed few GO terms related solely to auxin signalling and lateral root development is most probably a result of the experimental design, which provides an auxin-response profile focused on a specific, differentiated cell type. To substantiate this proposition, we compared the *slr-1* versus *CASP1pro::shy2-2/slr-1* data with the two previously published datasets from transcriptome analyses dealing either with roots treated with auxin or microdissected root sections after gravistimulation-mediated lateral root induction[14,15]. There appeared to be little correlation between the differentially expressed genes in our dataset and those in the datasets of Lewis et al.[14] or Voß et al.[15] (Extended Data Fig. 2b,c), confirming the distinct and specific nature of this transcriptional profile. To identify genes involved in cell wall modification, as well as to confirm the validity of our transcriptional profile, we selected a wide range of genes possibly related to the observed endodermal responses, including genes linked to lignification or lipid transport, as well as several unknown genes showing particularly strong and high-confidence differential responses. We generated promoter–reporter lines to characterize their expression pattern during root development and lateral root formation. In a strong validation of our approach, 24 out of 27 of the selected genes were found to display auxin-regulated expression in the endodermis (Extended Data Fig. 3 and Supplementary Table 2). A selection of these candidates (with constitutive or induced expression during lateral root formation) is shown in Extended Data Fig. 3c.

Many suberization-associated genes respond to auxin in the endodermis. Since we were interested in possible cell wall modifying enzymes, we searched the list of differentially expressed genes for cell wall-associated functions. We found that many genes with functions attributed to cutin or suberin homeostasis showed highly dynamic, differential expression in our dataset (Extended Data Fig. 3e). Suberin deposition has been shown to be highly plastic and might be continuously turned over, both for adaptation to the soil environment and during lateral root development[6–8]. Because we still lack an understanding of suberin deposition and turnover in the apoplast, we investigated whether some of the cell wall-related differentially expressed genes could be involved in this process. In particular, we were intrigued by the high number of differentially expressed GDSL-type esterase/lipase proteins (GELPs) in our dataset (Extended Data Fig. 3e), since members of this large family have been shown to be involved in cutin polymerization and to be able to degrade both cutin and suberin[16–20]. We therefore focused on the differentially regulated set of GELPs.

Concomitant suberin degradation and lateral root cap cuticle formation during lateral root formation. Fluorol yellow staining reveals dynamic changes during lateral root formation. However, fluorol yellow stains both suberin and cutin[21] (Extended Data Fig. 6a), and it remains unclear if, how and at which stage endodermal suberin is degraded and a cutin-like structure is formed at the surface of the primordium. Therefore, we analysed the dynamics of suberin and cutin during lateral root formation using transmission electron microscopy (TEM) (Fig. 2). Analysing stage II lateral root primordia, which usually form in the unsuberized zone, we could detect suberin lamellae only in the endodermal cell walls facing the lateral root primordia, but not in the cell walls on the opposite side of the root (Fig. 2a). Stage III primordia are found in the patchy suberized zone of the root and, as expected, we detected both suberized and non-suberized endodermal cells. At this stage, we began to distinguish the onset of the lateral root cap cuticle formation, accompanied by the disappearance of suberin in the endodermal cell walls overlying the primordium (Fig. 2b). In stage IV primordia, which are usually found in the fully suberized zone, we detected suberin deposition in all endodermal cells in zones without a primordium. At the same time, it was difficult to observe any suberin in endodermal cells facing the primordia. Indeed, it appeared as if suberin was degraded in coordination with the formation of the root cap cuticle (Fig. 2c). In fully emerged lateral roots, we could

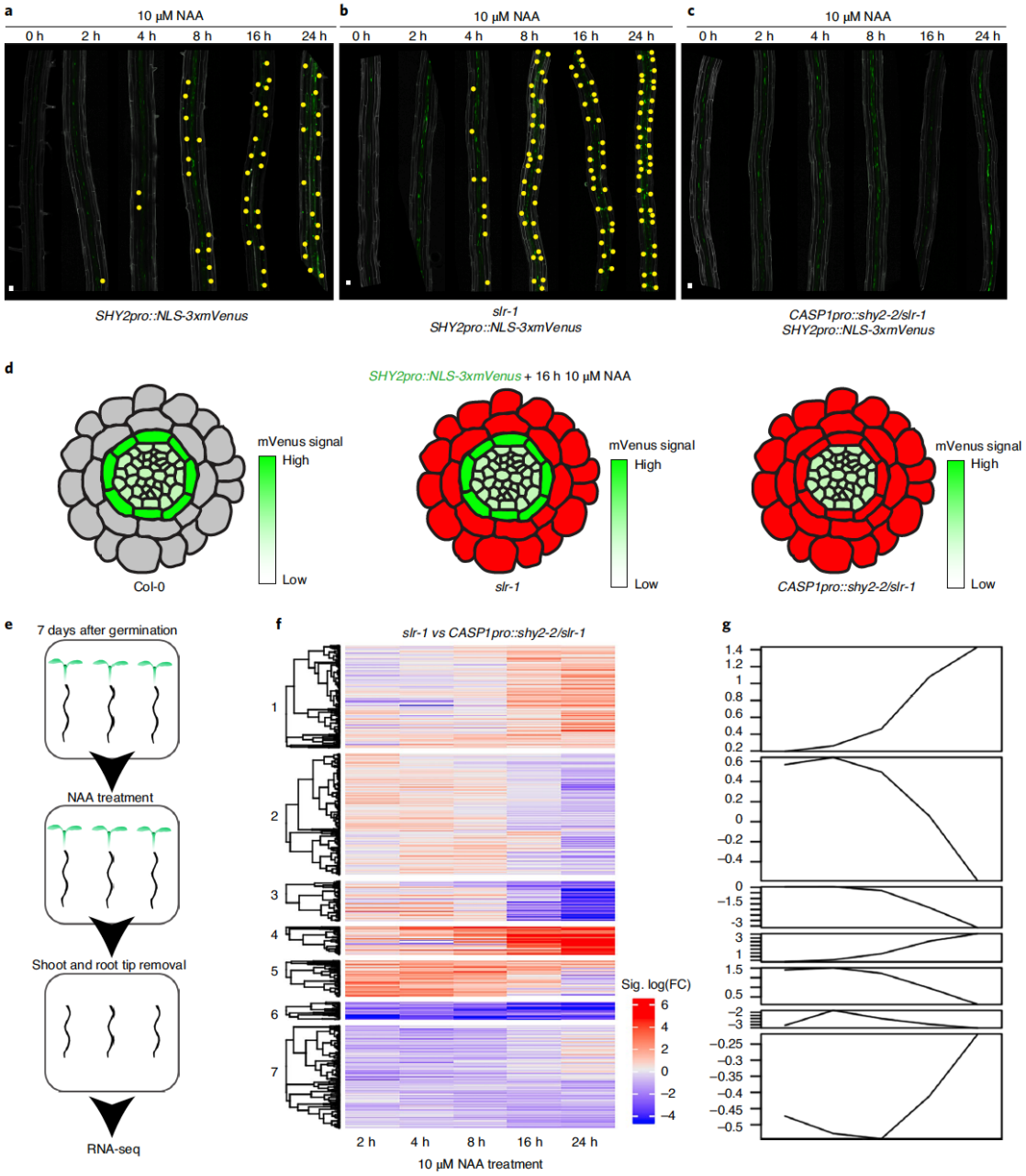

Fig. 1 | Using genetics to map auxin responses in the differentiated endodermis. a–**c**, Maximum intensity projections of roots expressing *SHY2pro::NLS-3xmVenus* treated with 10 µM NAA for 0, 2, 4, 8, 12 and 24 h. **a**, Col-0. **b**, *slr-1*. **c**, *CASP1pro::shy2-2/slr-1*. Yellow dots indicate *SHY2pro::NLS-3xmVenus* signal in the endodermis. Further details are provided in Extended Data Fig. 1. Images are representative of experiments repeated three times. **d**, Schematic representation of *SHY2pro::NLS-3xmVenus* responses in the different genetic backgrounds after treatment with 10 µM NAA for 16 h. *SHY2pro::NLS-3xmVenus* signal is indicated in green and inhibition of auxin signalling by *slr-1* or *CASP1pro::shy2-2* is indicated in red. **e**, Experimental setup of the RNA-seq experiment. **f**, Heat map showing the seven clusters containing the significant differentially expressed genes (cut-off fold change (FC) >2, false discovery rate <0.05) between roots of *slr-1* and *CASP1pro::shy2-2/slr-1* plants during the time course of NAA treatment. **g**, Graphical presentation of the behaviour of the seven clusters during the NAA time course depicted in **e**. Scale bars in **a**–**c**, 50 µm.

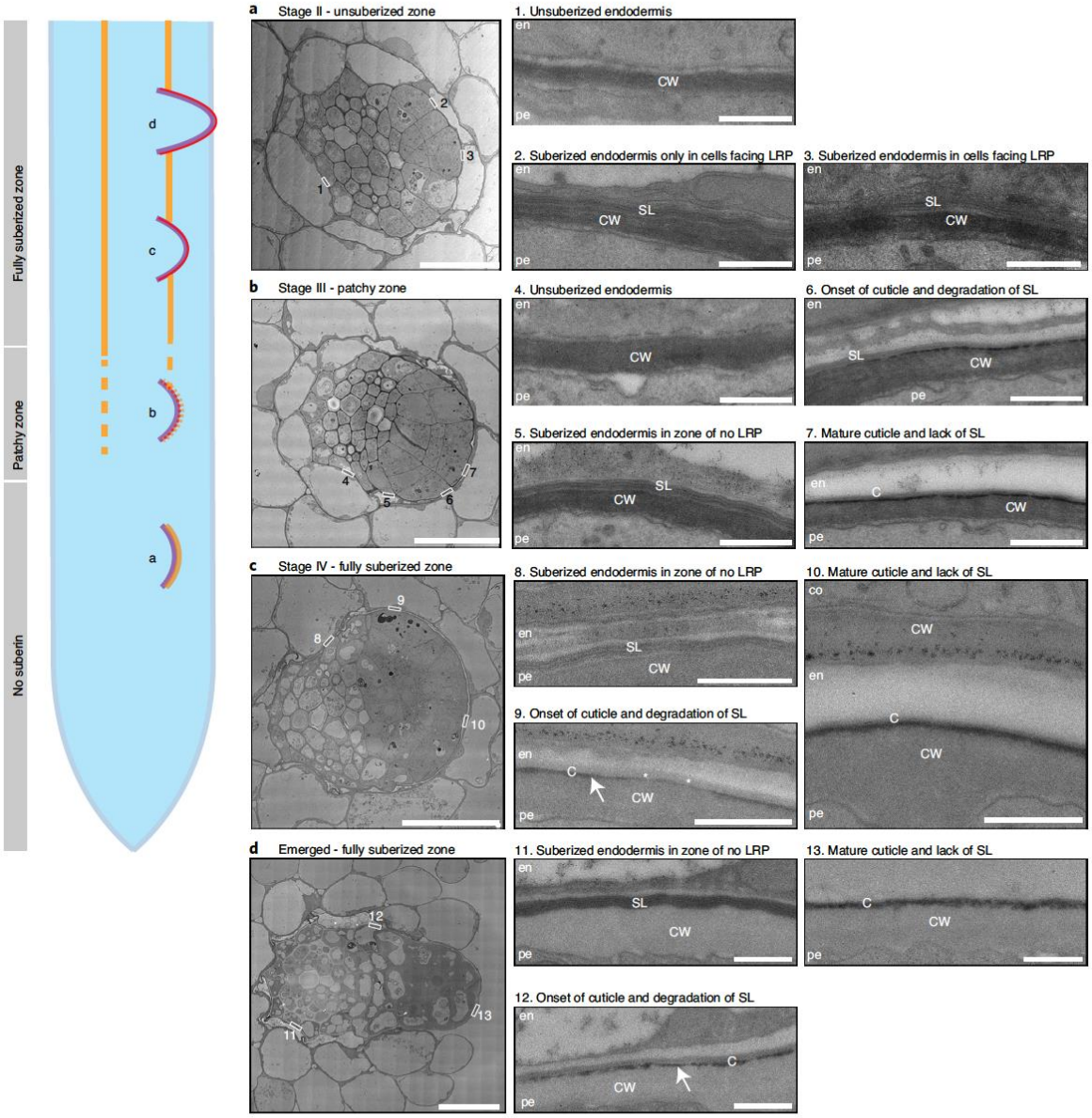

Fig. 2 | Suberin is degraded while the lateral root cap cuticle is established during lateral root formation. a–d, TEM micrographs of root sections containing stage II (**a**), stage III (**b**) and stage IV (**c**) lateral root primordia (LRP) and emerged lateral root (**d**). The numbered boxed regions are magnified on the right. Each experiment was repeated three times. The root schematic indicates the different stages of lateral root development shown in **a–d**. Purple, outline of lateral root primordium; yellow, suberin; red, cutin; en, endodermis; pe, pericycle; co, cortex; SL, suberin lamellae; C, lateral root cap cuticle; CW, cell wall. Arrows in panel 9 and 12 indicate the forming lateral root cap cuticle. Scale bars: 10 µm (**a–d**, main image); 1 µm (**a–d**, magnified images 1–12).

detect only the lateral root cap cuticle, whereas endodermal cells not in contact with the primordium still maintained their suberin lamellae (Fig. 2d). Thus, our analysis reveals that suberin is gradually degraded in cell walls of endodermal cells overlying the lateral root primordium, concomitant with the synthesis of a lateral root cap cuticle in the primordium as a protective coating[21].

Expression of auxin-repressed GELPs strongly correlates with endodermal suberization. To our knowledge, no factors mediating suberin polymerization[22] have been identified. Currently, the strongest available interference with suberin biosynthesis in roots relies on either endodermis-specific interference with abscisic acid (ABA) or cytokinin signalling, artificial overexpression of a cutin-degrading

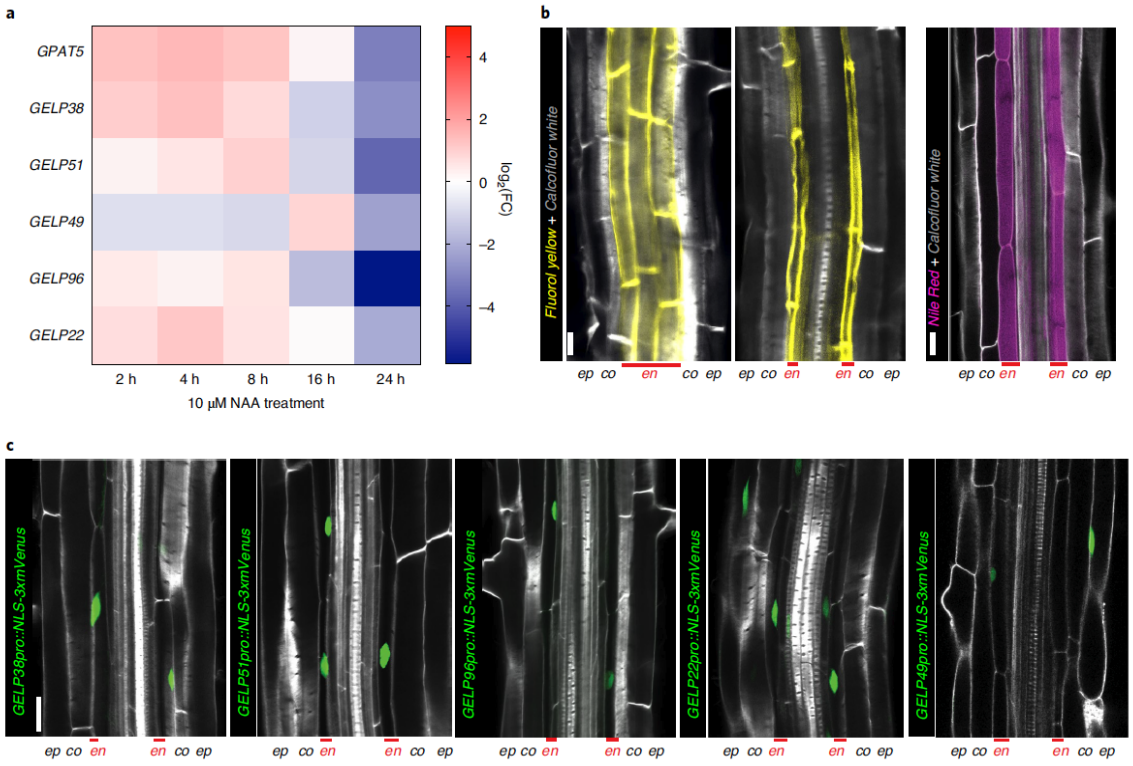

Fig. 3 | A cluster of five auxin-repressed GELPs is expressed in the differentiated endodermis. a, Heat map showing the differential expression of *GPAT5*, *GELP38*, *GELP51*, *GELP49*, *GELP96* and *GELP22* during the time course of NAA treatment (10 µM). **b**, Representative image of staining of suberin lamellae in the endodermis using fluorol yellow (yellow) or Nile red (magenta). ep, epidermis; co, cortex; en, endodermis. **c**, Confocal images of root sections expressing transcriptional reporters for each of the GELPs mentioned in **a**. NLS–3xmVenus is shown in green, calcofluor white staining of cell walls in grey. Each experiment was repeated three times. Scale bars in **b**,**c**, 25 µm.

enzyme or tissue-specific manipulation of phenylpropanoid production[6,7,18,23]. *CUTIN DEFICIENT 1* (*CD1*), a member of the large family of GELP proteins[20], has been shown to have in vitro cutin synthase activity, and CD1 loss-of-function mutants in tomato show partial defects in cuticle formation, but no equivalent evidence exists for suberin synthases. We observed a group of five GELP genes (*GELP22*, *GELP38*, *GELP49*, *GELP51 and GELP96*) to be downregulated after prolonged auxin treatment (Fig. 3a). Since auxin treatment should downregulate suberin-biosynthetic enzymes during lateral root formation[8], we speculated that the five downregulated GELPs might have a role in suberin biosynthesis. This idea was corroborated by the expression of transcriptional reporters for *GELP22*, *GELP38*, *GELP49*, *GELP51* and *GELP96*. *GELPXpro::NLS-3xmVenus* reporter lines revealed endodermis-specific expression for *GELP38*, *GELP51* and *GELP96*, and expression in endodermis and epidermis for *GELP22* and *GELP49* (Fig. 3c). Since treatment of *Arabidopsis* seedlings with ABA and CASPARIAN STRIP INTEGRITY FACTOR 2 (CIF2) peptide results in increased suberin deposition and *GPAT5* marker expression[7,24,25], we further checked whether *GELP22*, *GELP38*, *GELP49*, *GELP51* and *GELP96* would be induced by treatment with ABA and CIF2. All *GELP* reporter lines were induced in response to these treatments and also expanded their expression domain into the cortex, similar to what has been reported for *GPAT5*[7] and (Extended Data Fig. 4a,b). Together, our data establishes a strong correlation between suberin biosynthesis and the expression pattern of these five GELPs.

Suberin deposition requires auxin-repressed GELPs. To establish a function for these GELPs in suberin biosynthesis, we collected available transfer DNA (T-DNA) insertion mutants and characterized them for differences in suberin deposition using fluorol yellow or Nile red, two fluorescent dyes that stain suberin (Fig. 3b). In the absence of T-DNA insertion lines for *GELP38*, we generated two loss-of-function mutants using clustered regularly interspaced short palindromic repeats (CRISPR)–CRISPR-associated protein-9 nuclease (Cas9) (CRISPR–Cas9). None of the single mutants showed any significant difference in suberin occupancy in *Arabidopsis* roots compared to wild-type (Extended Data Fig. 4c–e). Using CRISPR–Cas9, we then generated two different allelic combinations of the five putative suberin biosynthesis-related GELPs: *gelp22-c1/gelp38-c3/gelp49-c1/gelp51-c1/gelp96-c1* and *gelp22-c2/gelp38-c4/gelp49-c2/gelp51-c2/gelp96-c2* (hereafter called $gelp^{quint\text{-}1}$ and $gelp^{quint\text{-}2}$, respectively) (Extended Data Fig. 4f). To test whether suberin levels in roots of the $gelp^{quint\text{-}1}$ and $gelp^{quint\text{-}2}$ mutants were affected, we stained roots of five-day-old plants with fluorol yellow and Nile red. Whereas suberin staining in wild-type plants resulted in the described patterns[18], both quintuple mutants showed a complete absence of suberin staining (Fig. 4a–d and Extended Data Fig. 5a). ABA treatment is known to strongly enhance suberization both in endodermis and cortex[7]. Yet, even after ABA induction, no suberin deposition could be detected using fluorol yellow staining in the roots of $gelp^{quint\text{-}1}$ and $gelp^{quint\text{-}2}$ plants (Fig. 4e,f). CIF2 peptide

did also not enhance suberization in *gelp*$^{quint\text{-}1}$ plants (Extended Data Fig. 5c). Since cutin and suberin can both be stained by fluorol yellow, we investigated whether the lateral root cap cuticle was affected in roots of the *gelp*$^{quint\text{-}1}$ mutant. We found that fluorol yellow still stained the dome of the emerging lateral root, suggesting that the *gelp*^{quint} mutants are specifically affected in suberization, leaving the lateral root cap cuticle intact (Fig. 4g,h). This was confirmed by TEM analysis (Extended Data Fig. 5d). Since endodermal suberin was shown to interfere with uptake from the apoplast, we used the fluorescein diacetate (FDA) penetration assay[7] to test for the presence of functional suberin lamellae in the endodermis of *gelp*^{quint} roots. Whereas FDA could enter only the epidermis and cortex in the suberized zone of wild-type roots, it entered the endodermis of *gelp*^{quint} roots, demonstrating absence or a strong deficiency of the endodermal suberin barrier (Extended Data Fig. 5e). To directly measure suberin levels, we performed a chemical analysis of the suberin content in roots of wild-type and *gelp*^{quint} mutants. This revealed substantial reductions in the amount of aliphatic suberin monomers in both *gelp*$^{quint\text{-}1}$ and *gelp*$^{quint\text{-}2}$ mutants, with nearly identical patterns in both allelic combinations. Dicarboxylic acids were nearly absent (98% reduction), whereas ω-hydroxy acids and fatty alcohols were reduced by about 90% and 50%, respectively (Fig. 4i). Ferulates were reduced by 70%, whereas coumarates showed only minor reductions. This resulted in an overall reductions of about 85% in the amount of suberin monomers compared with wild-type roots (Fig. 4i), correlating well with the fluorol yellow staining. Next, we complemented the suberin phenotype of the *gelp*$^{quint\text{-}1}$ mutant by introducing an inducible *GELP38proXVE>>GELP38-mCITRINE* fusion into the *gelp*$^{quint\text{-}1}$ mutant. This restored the stereotypical fluorol yellow staining in roots, demonstrating functionality of the GELP38–mCITRINE protein (Fig. 4j,k). The complementation was further confirmed using TEM analysis (Extended Data Fig. 5g). Moreover, GELP38–mCITRINE was localized in the apoplast of the endodermis where suberin polymerization takes place (Fig. 4l and Extended Data Fig. 5f). We also tested whether the Casparian strip was unaffected in the *gelp*^{quint} mutants and found both lignin staining with basic fuchsin and uptake of propidium iodide to be unaffected (Extended Data Fig. 5h–j). Thus, a cluster of five auxin-repressed GELPs is essential for normal suberin deposition in the endodermis, but does not affect lateral root cap cuticle formation.

Finally, using TEM, we could readily detect suberin lamellae in endodermal cell walls of wild-type, but did not see any indication of lamellae formation in roots of *gelp*$^{quint\text{-}1}$ (Fig. 4m,n and Extended Data Fig. 5b). Instead, we observed a layer of low electron density in the cell wall of the *gelp*$^{quint\text{-}1}$ mutant (Fig. 4m,n and Extended Data Fig. 5b). This layer appears amorphous with no resemblance to the lamellar structures in the wild-type. We speculate that this layer might be formed due to the accumulation of unpolymerized suberin monomers in the mutant cell wall. Together, our results strongly support an absence of suberin in the endodermis of the *gelp*^{quin1} mutant.

The *gelp*^{quint} mutants show expected defects of a suberin-deficient mutant. Since it has been repeatedly demonstrated that roots with non-functional suberin barriers are more susceptible to elevated salt concentrations, we also subjected 4-day-old seedlings to a mild salt stress (85 mM NaCl) for 8 days. Both *gelp*^{quint} mutants were more affected by the salt stress compared with the wild type (Extended Data Fig. 5k–m). We observed fewer emerged lateral roots and the fresh weight of the shoot was also significantly reduced (Extended Data Fig. 5k–m). These observations again strongly support the absence of a functional suberin barrier in the *gelp*^{quint} mutants. We finally checked whether the expression of known suberin biosynthesis-related genes was altered in the *gelp*^{quint} mutants. None of these genes were differentially expressed in the *gelp*^{quint} mutants (Extended Data Fig. 5n). This excludes the possibility that the observed absence of suberin would be due to an indirect feedback regulation of suberin biosynthesis and supports a direct role for the five GELPs in suberin polymerization in the apoplast.

Some auxin-induced GELPs have the capacity to degrade suberin. We also identified a group of five GELPs (*GELP12*, *GELP55*, *GELP72*, *GELP73* and *GELP81*) that were induced by auxin (Fig. 5a). Our RNA-sequencing (RNA-seq) data revealed that expression of *GELP12*, *GELP55* and *GELP72* peaks after 24 h of NAA treatment, whereas expression of *GELP73* and *GELP81* peaks after about 4 h (Fig. 5a). Expression of GELP12, GELP55 and GELP72 reporters show specific induction in endodermis during lateral root formation, whereas *GELP73* and *GELP81* reporters display endodermal expression already before lateral root formation (Fig. 5e and Extended Data Fig. 6f,g). Since we and others have demonstrated that the endodermal suberin gradually disappears, while a layer of cutin is formed at the primordium[16,21] (Fig. 2 and Extended Data Fig. 6a), we hypothesized that in contrast to the auxin-repressed suberin-biosynthetic GELPs, the five auxin-induced GELPs could regulate removal of suberin. First, we confirmed removal of suberin by other fluorescent staining methods besides fluorol yellow and found that both auramine O and Nile red can be used to visualize suberin in differentiated roots and both confirmed local degradation of suberin in cells overlying the lateral root (Fig. 5b,c). We also assessed suberin staining in the *bodyguard* mutant. BODYGUARD is an α/β-hydrolase that has been implicated in the establishment of the root cap cuticle[21], but it is not clear whether it affects endodermal suberin accumulation. Fluorol yellow staining in *bodyguard* roots confirmed the effect on lateral root cap cuticle, but suberin degradation appears to be normal and even more easily observable in this mutant, due to the lack of cuticle staining (Fig. 5d and Extended Data Fig. 6b,c). When characterizing the expression patterns of the five putatively suberin-degrading

Fig. 4 | Suberin deposition requires a cluster of auxin-repressed GELPs. a, Confocal images of Col-0 seedling roots stained with fluorol yellow. **b**, Confocal images of *gelp*$^{quint\text{-}1}$ and *gelp*$^{quint\text{-}2}$ seedling roots stained with fluorol yellow. Note absence of fluorol yellow staining. **c**,**d**, Close-up image of root sections of Col-0 (**c**) or *gelp*$^{quint\text{-}1}$ and *gelp*$^{quint\text{-}2}$ (**d**) stained with fluorol yellow for suberin and calcofluor white for cell walls. **e**,**f**, ABA-induced increased suberin deposition in Col-0 roots (**e**) but not in roots of *gelp*$^{quint\text{-}1}$ and *gelp*$^{quint\text{-}2}$ mutants (**f**). **g**,**h**, Fluorol yellow staining of Col-0 (**g**) and *gelp*$^{quint\text{-}1}$ (**h**) roots, showing that the cuticle layer protecting emerging lateral roots appears to be unaffected in the *gelp*$^{quint\text{-}1}$ mutant. Each experiment in **a**–**h** was repeated at least three times. **i**, Chemical analysis of the suberin content in roots of wild-type and *gelp*$^{quint\text{-}1}$ or *gelp*$^{quint\text{-}2}$ reveals a decrease of about 85% in total suberin monomers. Quantification of aliphatic and aromatic ester-bond suberin monomers isolated from six-day-old roots of wild-type (Col-0) and *gelp*$^{quint\text{-}1}$ and *gelp*$^{quint\text{-}2}$ mutants. The graph shows the analysis of the principal suberin monomers and the inset shows the total monomers per genotype. Data are mean ± s.e.m.; $n = 4$. Analysis of variance (ANOVA) and Tukey test: ***$P < 0.001$, **$P < 0.01$, *$P < 0.05$, NS, not significant. DCA, dicarboxylic acid; ω, ω-hydroxy acid; FA, fatty alcohol. **j**,**k**, Induction of *GELP38-XVEpro::GELP38-mCITRINE* restores suberin deposition in the roots of *gelp*$^{quint\text{-}1}$. **l**, Confocal image of a root expressing *GELP38-XVEpro::GELP38-mCITRINE* (green) after β-oestradiol treatment (5 µM) stained with Nile red (magenta) for suberin and calcofluor white (grey) for cell walls. **m**,**n**, TEM micrographs of root cross sections showing presence of suberin lamellae in wild-type roots (**m**) and absence of suberin lamellae in cross sections of *gelp*$^{quint\text{-}1}$ roots (**n**). Note that the structure of the endodermis of the *gelp*$^{quint\text{-}1}$ mutant is much better preserved compared to wild-type. Images in **j**–**n** are representatives of experiments that were repeated three times. Scale bars: 500 µm (**a**,**b**,**e**,**f**,**j**); 25 µm (**c**,**d**,**g**,**h**,**k**,**l**); 10 µm (**m**,**n**, whole root sections); 20 nm (**m**,**n**, magnified regions).

GELPs, we observed three different expression patterns. *GELP12* and *GELP55* marker lines showed expression in the cortex or no signal in absence of lateral root formation, but were induced in endodermal cells overlying the lateral root from stages I to IV (Fig. 5e and Extended Data Fig. 6d). *GELP72* was induced in endodermal cells overlying the lateral root primordium and from stage III onwards,

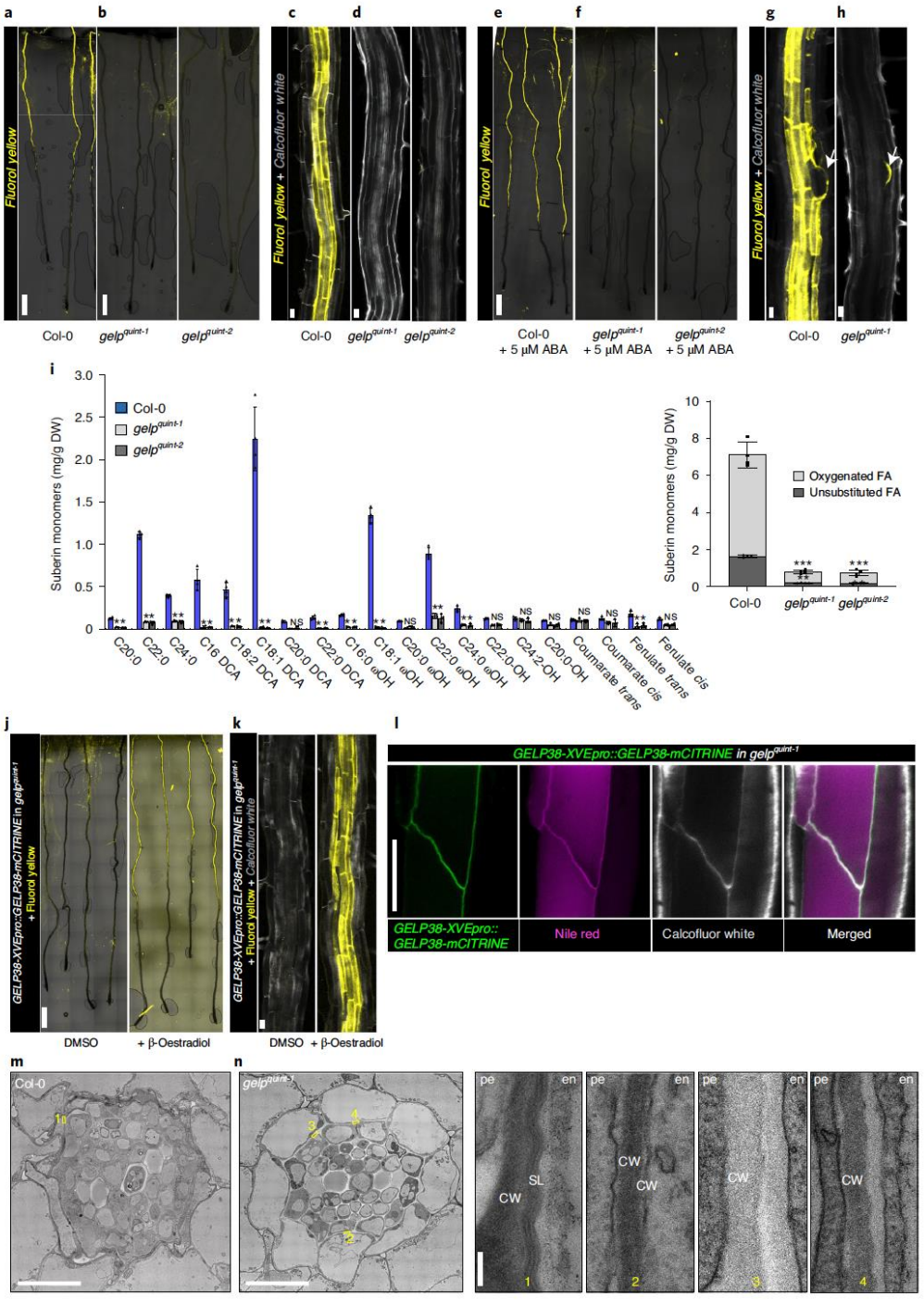

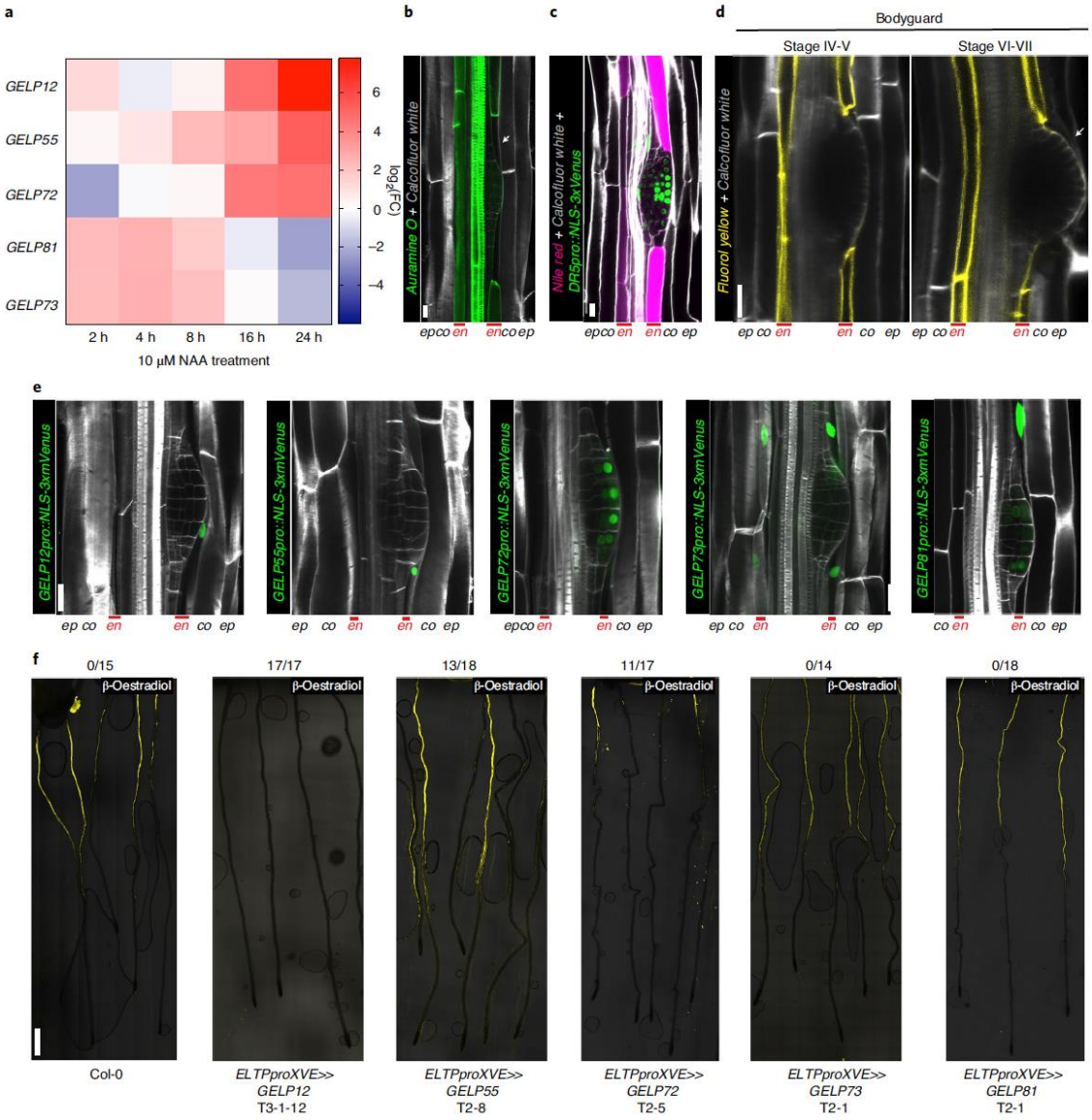

Fig. 5 | A cluster of auxin-induced GELPs is required for suberin degradation. a, Heat map showing the differential expression of *GELP12*, *GELP55*, *GELP72*, *GELP81* and *GELP73* during the 10 µM NAA time course. **b**, Use of auramine O (green) to visualize degradation of suberin in the cell wall of endodermal cells overlying a lateral root primordium. **c**, Use of Nile red staining (magenta) to visualize suberin degradation in the cell wall of endodermal cells overlying a lateral root primordium. Auxin signalling is visualized by *DR5pro::NLS-3xVenus* (green). **d**, Fluorol yellow staining in roots of *bodyguard* mutant, demonstrating normal presence of suberin lamellae, whereas the cuticle layer surrounding the lateral root primordium is discontinuous (arrow). **e**, Confocal images showing the expression patterns of the isolated auxin-upregulated GELPs during lateral root formation. NLS–3xmVenus signal in green and calcofluor white staining of cell walls is in grey. Asterisk indicates endodermal signal. **f**, Fluorol yellow staining on roots of Col-0 treated with oestradiol results in normal suberin pattern, whereas inducible endodermis-specific overexpression of *GELP12*, *GELP55* or *GELP72* results in degradation of suberin highlighted by absence of fluorol yellow signal. The overexpression of *GELP73* and *GELP81* results in a normal suberin pattern similar to untreated wild-type roots. The numbers above the images indicate the number of roots without fluorol yellow staining/total number of imaged roots. Images in **b**–**f** are representative of experiments repeated at least three times. Scale bars: 25 µm (**b**–**e**); 500 µm (**f**).

and was also expressed in the outer layer of the growing primordium (Fig. 5e and Extended Data Fig. 6e). Finally, *GELP73* and *GELP81* were already expressed in the endodermis before lateral root initiation and were induced in the overlying endodermal cells from stages I to IV (Fig. 5e and Extended Data Fig. 6f,g). In addition, from stage IV onwards, *GELP81* was induced in the outer layer of the primordium, similarly to *GELP72* (Extended Data Fig. 6g). Confirming the RNA-seq data, GELP12, GELP55 and GELP72 marker lines were induced by auxin in an endodermis-specific fashion (Extended Data Fig. 6h–j). To characterize a possible role in suberin degradation, we first undertook a gain-of-function approach by inducibly overexpressing each GELP in the endodermis and assessing whether this causes suberin removal using fluorol yellow staining. Indeed, inducible expression of *GELP12*, *GELP55* and *GELP72* in the endodermis caused a disappearance of fluorol yellow staining, whereas no clear effect on fluorol yellow staining was observed when inducing *GELP81* and *GELP73* (Fig. 5f and Extended Data Fig. 7a,c). We also performed a transfer experiment in which we germinated the inducible lines with endodermis-specific expression of GELP12 on normal β-oestradiol-free medium for 4 d to allow suberin formation and then transferred the seedlings to the plates containing oestradiol for 36 h. We observed a clear reduction in root suberin (Extended Data Fig. 7b). We then tested whether single loss-of-function mutants of each individual GELP affects lateral root formation (Extended Data Figs. 7d and 8a–g). We performed root bending assays to synchronously induce lateral roots and to quantify the progression of lateral root development at 18 h and 42 h after gravistimulation[26,27]. Among the three GELPs that can degrade suberin, only one (GELP72) showed a delayed lateral root development in both alleles and time points (Extended Data Fig. 8d–g). However, the single mutants of the *GELP73* and *GELP81* genes—which did not affect fluorol yellow staining when overexpressed in the endodermis—also displayed a delayed lateral root emergence (Extended Data Fig. 8h–k). Thus, some auxin-inducible GELPs are able to degrade suberin when overexpressed and some also display single mutant phenotypes during lateral root emergence. Thus, while our data makes auxin-induced GELPs strong candidates for suberin degradases during lateral root emergence and suggests a need for suberin degradation for proper lateral root emergence, further efforts in generating and analysing multiple mutant combinations of these GELPs will be needed to clearly establish their role and the requirement for suberin degradation during this process.

Discussion

Our data reveal that differentiated endodermal cells have a distinct auxin-mediated transcriptome. Mining this unique auxin-response dataset enabled us to identify the first suberin synthase candidates (Figs. 1 and 3) and a set of candidate suberin degradases (Fig. 5). Together these enzymes appear to form a module for regulating suberin plasticity in roots. Knocking out all five suberin synthases resulted in roots without detectable suberin that are hypersensitive to mild stress conditions. These *gelp*^{quint} mutants provide the plant community with a powerful tool to test the role of suberin and its plasticity during diverse environmental conditions. It will be interesting to test how the loss of suberin affects interactions with microbiome and susceptibility to pathogen attack[1]. The strong quintuple mutant and the identification of suberin degradase candidates will also aid further understanding of the mechanisms and role of suberin plasticity in plant elemental homeostasis[7]. The large GELP family in *Arabidopsis* and other plants provides a rich, but as-yet untapped genetic resource, to better understand how different cell wall modifications affect biological processes and interactions.

Methods

Plant material and construction. For all experiments, *A. thaliana* ecotype Columbia (Col-0; wild-type) was used. Gene numbers, mutants and transgenic lines used and generated in this study are described in the Supplementary Information. The primers used for genotyping and quantitative PRC (qPCR)-based verification of T-DNA lines are indicated in Supplementary Table 5.

The following T-DNA tagged and transgenic lines were used in this study: *gelp49* (SALK_015138C), *gelp51* (SALK_033359C), *gelp96* (SALK056924C) and *gelp96* (SALK056924C) (NASC centre); *SHY2pro::NLS-3xmVenus*, *CASP1pro::shy2-2, DR5::NLS-3xVenus*[10]; *GPAT5pro::NLS-3xmVenus*[28] and *slr-1*[12] were described previously. The corresponding gene numbers are as follows: *SLR*, AT4G14550; *SHY2*, AT1G04240; *ELTP*, At2g48140; *GPAT5*, At3g11430; *SYP122*, At3g52400; BDG, AT1G64670; HORST, At5g58860; *ASFT*, At5g41040; *FAR1*, At5g22500; FAR4, At3g44540; *KCS2*, At1g04220; *GELP12*, AT1G28650; *GELP55*, AT2G30310; *GELP72*, AT3G48460; *GELP81*, AT4G26790; *GELP73*, AT3G50400; *GELP49*, AT2G19050; *GELP51*, AT2G23540; *GELP96*, AT5G37690; *GELP38*, At1G74460; *GELP22*, AT1G54000; *GELP103*, At5g45960; *PER10*, At1g49570; *PER11*, AT1G68850; *PER23*, AT2G38390; *PER28*, At3g03670; *PER55*, AT5G14130, *PER59*, At5g19890; *LAC2*, AT2G29130; *LAC12*, AT5G05390; *LAC13*, AT5G07130; LAC16, AT5G58910; *UCC1*, AT2G32300; *PLIP3*, AT3G62590; *CASPL4B1*, AT2G38480; *CASPL1A1*, AT1G14160; cytochrome b561 and DOMON domain-containing protein At4g17280; cytochrome b561 and DOMON domain-containing protein At5g47530.

Plant growth conditions. For all experiments, plants were germinated on solid half-strength Murashige and Skoog (MS) medium without addition of sucrose. Seeds were surface sterilized, sown on plates, incubated for 2 days at 4 °C for stratification, and grown vertically in growth chambers at 22 °C under continuous light (100 µE). The microscopic analyses (FDA uptake, fluorol yellow staining, propidium iodide uptake and confocal microscopy) were performed on 5- or 7-day-old seedlings.

Bending experiments. Seeds of wild-type Col-0 and *gelp* mutants were plated on half-strength MS containing 120 × 120 × 17 mm square Petri dishes, stratified in the dark at 4 °C for 2 days, and grown at 22 °C under constant light (100 µE). Lateral root stages were determined after plates with 4-day-old seedlings were rotated 90° and grown for 18 h and 42 h for synchronized lateral root induction. After bending for 18 h and 42 h, the roots were cleared as described in ref. [15] and mounted in 50% glycerol. Determination of lateral root stage in the bent region was done using an upright microscope with differential interference contrast optics. Experiments were repeated 3 times and each replicate had at least 15 seedlings.

Generation of transgenic lines. *CASP1pro::shy2-2* was crossed into the *slr-1* mutant to produce the *CASP1pro::shy2-2/slr-1* line. The In-Fusion Advantage PCR Cloning Kit (Clontech) and Gateway Cloning Technology (Invitrogen) were used for generating marker lines and overexpression constructs. All constructs were transformed by heat shock into *Agrobacterium tumefaciens* GV3101 strain and then transformed into plants by floral dipping[28]. At least ten independent transgenic lines were analysed for expression patterns, and one line showing a representative signal and normal segregation was selected for further studies. For transcriptional reporters, the promoter regions were PCR-amplified from Col-0 genomic DNA and cloned into pDONRP4-P1R (Thermo Fisher). The resulting plasmids were recombined together with pDONRL1-NLS-3xmVenus-L2 (ref. [29]) and the destination vector pFR7m24GW or pFG7m24GW, containing the FastRed or FastGreen cassettes for transgenic seed selection respectively, to create the final *PROMOTER::NLS-3xmVenus* expression clones. To be able to induce expression of individual GELPs in the endodermis, the corresponding pDONR221_L1-GELP-L2 clones were created. The resulting clones were recombined with the oestradiol-inducible pDONR_P4-ELTPproXVE-P1R[23] and destination vector pB7m24GW, to produce *ELTPproXVE::GELP* overexpression lines. To generate *GELP38proXVE»GELP38:mCitrine*, the promoter region of GELP38pro was PCR-amplified from Col-0 genomic DNA and cloned into linearized p1R4-ML:XVE[30] with KpnI by Infusion cloning (Takara) to produce the inducible *GELP38proXVE* promoter clone. The resulting clone was recombined together with *pDONR221_L1-GELP38-L2*, *pDONR_R2-mCitrine-L3* and *pFG7m34GW* to produce the *GELP38proXVE»GELP38:mCitrine* construct. Supplementary Tables 3 and 4 shows details about the primers used for cloning. The spacers to customize sgRNA for SpCas9 were cloned using the oligo annealing technique, then ligated into BbsI linearized, Gateway-entry plasmids[31]. For multiplex targeting of GELP genes, the six sgRNAs utilized were cloned into two vectors, each carrying three sgRNAs and co-transformed together into Col-0 ecotype. The primers used for generating single and multiple CRISPR–Cas9 mutants are indicated in the Supplementary Table 7.

Hormonal treatments. ABA was stored as a 50 mM stock solution in methanol. When seedlings were subjected to short-term 10 µM ABA treatment, the transfer was done when the seedlings were four days old. β-oestradiol was prepared as 100 mM stock in DMSO. In the case of β-oestradiol treatment, seedlings were directly germinated on the medium containing 5 µM oestradiol. For salt experiments, the seedlings were grown on half-strength MS medium and transferred to 85 mM NaCl for 10 d. In the case of auxin (NAA) treatment for RNA-seq experiments, the seedlings were first grown on half-strength MS medium

and then transferred to 10 µM NAA for 4, 8, 16 or 24 h. At each time point, the shoots and the root tips were removed.

Chemical analysis of suberin. Chemical analysis of suberin was performed on six-day-old seedlings. Before analysis, we confirmed that the growth conditions did not affect the phenotype of *gelp*$^{mutn-1}$ and *gelp*$^{mutn-2}$ by fluorol yellow staining. We used the protocol for the determination of ester-bond lipids as described by Berhin et al.[21]. In brief, 200 mg of seeds were grown on nylon mesh (200 mm pore size). After 6 d, the roots were shaved off after flash freezing and extracted in isopropanol/0.01% butylated hydroxytoluene. They were then delipidized three times (at 1 h, 16 h and 8 h) in each of the following solvents: chloroform:methanol (2:1), chloroform:methanol (1:1) and methanol with 0.01% butylated hydroxytoluene, under agitation, before being dried for 3 d under vacuum. Depolymerization was performed by base catalysis[32]. In brief, dried plant samples were transesterified in 2 ml of reaction medium. Twenty millilitres of reaction medium was composed of 3 ml methyl acetate, 5 ml of 25% sodium methoxide in dry methanol and 12 ml dry methanol. The equivalents of 5 mg of methyl heptadecanoate and 10 mg of ω-pentadeca-lactone per sample were added as internal standards. After incubation of the samples at 60 °C for 2 h 3.5 ml dichloromethane, 0.7 ml glacial acetic acid and 1 ml 0.9% NaCl (w/v) Tris 100 mM pH 8.0 were added to each sample and subsequently vortexed for 20 s. After centrifugation (1,500*g* for 2 min), the organic phase was collected, washed with 2 ml of 0.9% NaCl, and dried over sodium sulfate. The organic phase was then recovered and concentrated under a stream of nitrogen. The resulting cutin monomer fraction was derivatized with N,O-Bis(trimethylsilyl) trifluoroacetamide:pyridine (1:1) at 70 °C for 1 h and injected out of hexane on a HP-5MS column (J&W Scientific) in a gas chromatograph coupled to a mass spectrometer and a flame ionization detector (Agilent 6890N GC Network systems). The temperature cycle of the oven was the following: 2 min at 50 °C, increment of 20 °C min^{-1} to 160 °C, of 2 °C min^{-1} to 250 °C and 10 °C min^{-1} to 310 °C, and held for 15 min. Three independent experiments were performed with four replicates for each genotype, respectively, and a representative dataset is presented. The amounts of unsubstituted C16 and C18 fatty acids were not evaluated because of their omnipresence in the plant and in the environment.

Fluorescence microscopy. Confocal laser-scanning microscopy images were obtained using either a Zeiss LSM 880 (with Zen 2.1 SP3 Black edition), Leica SP8 (with LasX 3.1.5.16308) or Leica SP8-MP (with LasX 3.5.6.21594) microscopes. For green and red fluorophores, the following excitation and detection windows were used. mVenus, GFP, fluorol yellow and FDA: 488 nm, 500–530 nm; mCITRINE: 496 nm, 505–530 nm; propidium iodide: 520 nm, 590–650 nm; calcofluor white: 405 nm, 430–485 nm; basic fuchsin/Nile red 561 nm, 600–630 nm. For multiphoton microscopy the following excitation and detection settings were used. mVenus, GFP, fluorol yellow and calcofluor white 960 nm, 435–485 nm (calcofluor white) and 500–550 nm (mVenus, GFP and fluorol yellow). Methods for imaging the Casparian strip lignin and propidium iodide penetration were previously described[25,33]. For visualization of FDA transport, chambered cover glasses (Thermo Scientific), were used where the roots were covered with a slice of agar and time-lapse imaging was performed immediately after the application of FDA.

Methanol-based fluorol yellow staining of suberin in combination with calcofluor white. For most experiments suberin lamellae were observed in five- or seven-day-old roots using fluorol yellow (FY 088, Santa Cruz Biotechnology) staining. Seedlings were incubated in methanol at room temperature for at least 3 d, stained with FY 088 (0.01%, methanol) for 1 h at room temperature, rinsed in methanol and counterstained with aniline blue (0.5%, methanol) at room temperature for 1 h in darkness, washed, and visualized using 1-well chambered cover glass (ThermoFisher Scientific, catalogue no. 155361). To combine with calcofluor white for cell wall staining, the seedlings were first incubated in calcofluor white solution (0.1%, in methanol) for 3 d and then stained with fluorol yellow as described above.

Electron microscopy. For chemical fixation, plants were fixed in 2.5% glutaraldehyde solution (Electron Microscopy Services) in 0.1 M phosphate buffer pH 7.4 for 1 h at room temperature and post-fixed in a fresh mixture of osmium tetroxide 1% (Electron Microscopy Services) with 1.5% potassium ferrocyanide (Sigma) in phosphate buffer for 1 h at room temperature. The samples were then washed twice in distilled water and dehydrated in ethanol solution (Sigma) at graded concentrations (30%, 40 min; 50%, 40 min; 70%, 40 min; and 100%, 2× 1 h). This was followed by infiltration in Spurr resin (Electron Microscopy Services) at graded concentrations (Spurr 33% in ethanol, 4 h; Spurr 66% in ethanol, 4 h; Spurr 100%, 2× 8 h) and finally polymerized for 48 h at 60 °C in an oven. For the multiple mutant, 50-nm-thick sections were cut transversally 2 mm below the hypocotyl–root junction, using a Leica Ultracut (Leica Mikrosysteme), picked up on a copper slot grid 2× 1 mm (Electron Microscopy Services) coated with a polystyrene film (Sigma). For lateral roots, 50-nm-thick sections were cut longitudinally (transversally from main root). For high-pressure freezing, plants were fixed in 2.5% glutaraldehyde solution (Electron Microscopy Services) in 0.1 M phosphate buffer pH 7.4 for 1 h at room temperature and post-fixed in a fresh mixture of osmium tetroxide 1% (Electron Microscopy Services) with 1.5% potassium ferrocyanide (Sigma) in phosphate buffer for 1 h at room temperature. The samples were then washed twice in distilled water before a high-pressure freezing step. For the high-pressure freezing, 2-mm-long root pieces were cut below the hypocotyl junction region, and then placed in an aluminium planchet 3 mm in diameter with a 0.2 mm cavity (article 241, Wohlwend) filled with hexadecene (Merck) covered with a tap planchet (article 353, Wohlwend) and directly frozen under high pressure using a HPF Compact 02 (Wohlwend). The samples were then dehydrated and infiltrated with resin at low temperature using the Leica AFS2 freeze-substitution machine (Leica Mikrosysteme) with the following protocol: dehydration in 100% acetone (Sigma) at graded temperature (−90 °C, 10 h; −90 °C to −60 °C, 2 h; −60 °C, 8 h; −60 °C to −30 °C, 2 h; −30 °C, −3 h.) This was followed by infiltration in spurr resin (Electron Microscopy Services) at graded concentration and temperature (30%, −30 °C to 0 °C, 10 h; 66%, 0 °C to 20 °C, 10 h; 100%, 20 °C, 2× 10 h) and finally polymerized for 48 h at 60 °C in an oven. Fifty-nanometre sections were cut transversally to the root, using a Leica Ultracut (Leica Mikrosysteme), picked up on a copper slot grid of 2× 1 mm (Electron Microscopy Services) coated with a polystyrene film (Sigma). Micrographs and panoramic were taken with a transmission electron microscope FEI CM100 (FEI) at an acceleration voltage of 80 kV with a TVIPS TemCamF416 digital camera (TVIPS) using the software EM-MENU 4.0 (TVIPS). Panoramas were aligned with the software IMOD[34].

RNA-seq experiments. Seeds were surface-sterilized, sown on plates, incubated for 2 d at 4 °C for stratification, and grown vertically in growth chambers at 22 °C under continuous light (100 µE) for 6 d. For each biological replicate (3 in total) 60 seedlings from each genotype were transferred to plates (20 seedlings per plate) containing 1/2 MS medium supplemented with 10 µM NAA and transferred back into the growth chamber. After the desired incubation period (2, 4, 8, 16 and 24 h) seedlings were harvested after removal of the root apical meristem (~3 mm) and the shoot including hypocotyl was snap-frozen in liquid nitrogen. RNA was extracted using a Trizol-based method. After RNase-free DNase (QIAGEN) treatment, RNA was cleaned-up using a RNeasy mini-elute kit (QIAGEN http://www.qiagen.com). RNA-seq libraries were prepared as described[35]. In brief, RNA quality was assessed on a Fragment Analyser (Advanced Analytical Technologies). RNA-seq libraries were prepared using 1,000 ng total RNA and the Illumina TruSeq Stranded mRNA reagents (Illumina) on a Sciclone liquid-handling robot (PerkinElmer) using a PerkinElmer-developed automated script. Cluster generation was performed with the resulting libraries using the Illumina TruSeq SR Cluster Kit v4 reagents and sequenced on the Illumina HiSeq 2500 using TruSeq SBS Kit v4 reagents. Sequencing data were processed using the Illumina Pipeline Software v.2.2.

RNA-seq data processing and analysis. Data processing was performed by the Lausanne Genomic Technologies Facility using their in-house RNA-seq pipeline. Data analysis was done using an in-house RNA-seq pipeline that performed the following steps. Quality controls were applied for cleaning data for adapters and trimming of low-quality sequence ends. Cleaned data was aligned and read counts computed using two methods: STAR[36] + HTSeq[37] and STAR + RSEM[38]. The first method generates gene counts and the second method generates isoform counts. TAIR10 genome and Ensembl 21 annotation were used. Additional quality controls were performed using R to inspect the sample counts summary, pairwise sample correlations, clustering and sample PCA. Statistical analysis was performed for genes and isoforms with the Bioconductor package EdgeR (R v.3.4.0) for normalization and limma (R v.3.18.2) for differential expression. Two types of statistical tests were applied depending on the contrast model tested. A moderated *t*-test was used for each pairwise comparison in group t0 and group *slr-1* vs *CASP1pro::shy2-2/slr-1*. A moderated *F*-test was used for each time-course model and their interaction. The result files contain one row per gene or transcript. Adjusted *P*-values were computed for each comparison by the Benjamini–Hochberg method, controlling for false discovery rate. Genes were considered significant in further analysis if the adjusted *P*-value was equal or below 0.05 and the $\log_2$-fold change was ≥ 1. Further analysis has been conducted using R (v.3.4.1). Heat maps were generated using ComplexHeatmap[39] (v.1.14.0) using Pearson distance, and 'average' for clustering. Non-supervised clustering of genes using kmeans (factoextra v.1.0.4; https://github.com/kassambara/factoextra)-suggested 3 clusters as optimal together. This represented a low resolution and we examined into clusters of size 4–8, which contained slightly lower silhouette values. After testing multiple cluster suggestions manually we settled on 7 inferred clusters based on the biologically most sensible separation. GO analysis was conducted using the package topGO v. 2.28.0 (weight01 algorithm[40]). GO annotations were obtained through org.At.tairGO (v.3.4.1). For the comparison with Lewis et al.[14], the published series matrix file was obtained from the Gene Expression Omnibus archive and the differential gene-expression analysis was repeated in order to obtain the expression of all genes. Results were compared with their published table of differentially expressed genes and found to be highly similar. A *z*-score based on the log (fold change) value was calculated for both our datasets and the reanalysed Lewis et al. data[14] to make the different datasets more comparable. For the comparison with Voß et al.[15], we used the published table directly; this table

included all expressed genes and calculated z-scores for the different time points. We kept time points T0, T6, T9, T15 and T24, which resulted in 7,145 differentially regulated genes with similar cut-off of $P < 0.05$ and a fold change of 2.

qPCR analysis. For qPCR quantifications, plants were grown on plates with half-strength MS medium covered with mesh. In the case of quintuple *gelp* mutants, only root parts (around 100 mg) were collected and total RNA was extracted using a Trizol-adapted ReliaPrep RNA Tissue Miniprep Kit (Promega). To verify the transcript level in single T-DNA lines, RNA extraction from whole seedlings was performed. Reverse transcription was carried out with PrimeScript RT Master Mix (Takara). All steps were done as indicated in manufacturer's manual. The qPCR reaction was performed on an Applied Biosystems QuantStudio3 thermocycler using a Mesa Blue SYBR Green kit (Eurogentech). All transcripts were normalized to ADAPTOR PROTEIN-4 MU-ADAPTIN (AP4M) (AT4G24550) expression. All primers used for qPCR are shown in Supplementary Table 6.

High-resolution melting analysis of CRISPR mutants. The high-resolution melting method was used to screen for the mutants generated using the CRISPR–Cas9-based method. Genomic DNA of selected Cas9-free, T2 generation plants, was extracted using the cetyl trimethylammonium bromide DNA extraction method. The qPCR reaction was performed on Applied Biosystems QuantStudio3 thermocycler using a MeltDoctor HRM Master Mix, according to the manufacturer's indications (Applied Biosystems). HPLC-purified primers were used to generate an amplicon of around 200 base pairs. The results were analysed using High Resolution Melt Software v.3.1 (Thermo Fisher Scientific). The selected candidates were verified by sequencing. Primers used for amplification and sequencing the potential mutation sites are indicated in Supplementary Tables 8 and 9.

Quantification and statistical analysis. For quantifying the fluorol yellow occupancy, confocal images were analysed with the Fiji package (v.2.0.0-rc-69/1.52p (build: 269a0ad53f); http://fiji.sc/Fiji)[41]. Contrast and brightness were adjusted in the same manner for all images. The suberized regions of the roots were measured together with total root lengths to determine the percentage of suberin occupancy. All statistical analyses were done with the GraphPad Prism software v.9.0.0 (86) (https://www.graphpad.com/) or using the R package (v.3.5.1) (http://www.r-project.org). One-way ANOVA was performed, and a two-sided t-test was subsequently used as a multiple-comparison procedure. For the analysis of lateral root development using the bending assay, we used a Pearson's χ^2 test. Details about the statistical approaches used can be found in the figure legends. The data are presented as mean ± s.d. or mean ± s.e.m. where indicated, and n represents the number of plant roots. Each experiment was repeated at least three times.

Reporting Summary. Further information on research design is available in the Nature Research Reporting Summary linked to this article.

Data availability

All data to support the conclusions of this manuscript are included in the main text and the supplementary materials. The full RNA-seq dataset was deposited in the NCBI Gene Expression Omnibus under accession GSE153478. Source data are provided with this paper.

Received: 17 July 2020; Accepted: 25 January 2021;
Published online: 8 March 2021

References

1. Castrillo, G. et al. Root microbiota drive direct integration of phosphate stress and immunity. *Nature* **543**, 513–518 (2017).
2. Duran, P. et al. Microbial interkingdom interactions in roots promote *Arabidopsis* survival. *Cell* **175**, 973–983 (2018).
3. Hassani, M. A., Duran, P. & Hacquard, S. Microbial interactions within the plant holobiont. *Microbiome* **6**, 58 (2018).
4. Banda, J. et al. Lateral root formation in *Arabidopsis*: a well-ordered LRexit. *Trends Plant Sci.* **24**, 826–839 (2019).
5. Stoeckle, D., Thellmann, M. & Vermeer, J. E. Breakout-lateral root emergence in *Arabidopsis thaliana*. *Curr. Opin. Plant Biol.* **41**, 67–72 (2018).
6. Andersen, T. G. et al. Tissue-autonomous phenylpropanoid production is essential for establishment of root barriers. *Curr. Biol.* (in the press).
7. Barberon, M. et al. Adaptation of root function by nutrient-induced plasticity of endodermal differentiation. *Cell* **164**, 447–459 (2016).
8. Li, B. et al. Role of LOTR1 in nutrient transport through organization of spatial distribution of root endodermal barriers. *Curr. Biol.* **27**, 758–765 (2017).
9. Yadav, V. et al. ABCG transporters are required for suberin and pollen wall extracellular barriers in *Arabidopsis*. *Plant Cell* **26**, 3569–3588 (2014).
10. Vermeer, J. E. et al. A spatial accommodation by neighboring cells is required for organ initiation in *Arabidopsis*. *Science* **343**, 178–183 (2014).
11. Tian, Q., Uhlir, N. J. & Reed, J. W. *Arabidopsis* SHY2/IAA3 inhibits auxin-regulated gene expression. *Plant Cell* **14**, 301–319 (2002).
12. Fukaki, H., Tameda, S., Masuda, H. & Tasaka, M. Lateral root formation is blocked by a gain-of-function mutation in the SOLITARY-ROOT/IAA14 gene of *Arabidopsis*. *Plant J.* **29**, 153–168 (2002).
13. Swarup, K. et al. The auxin influx carrier LAX3 promotes lateral root emergence. *Nat. Cell Biol.* **10**, 946–954 (2008).
14. Lewis, D. R. et al. A kinetic analysis of the auxin transcriptome reveals cell wall remodeling proteins that modulate lateral root development in *Arabidopsis*. *Plant Cell* **25**, 3329–3346 (2013).
15. Voß, U. et al. The circadian clock rephases during lateral root organ initiation in *Arabidopsis thaliana*. *Nat. Commun.* **6**, 7641 (2015).
16. Bakan, B. & Marion, D. Assembly of the cutin polyester: from cells to extracellular cell walls. *Plants* **6**, 57 (2017).
17. Girard, A. L. et al. Tomato GDSL1 is required for cutin deposition in the fruit cuticle. *Plant Cell* **24**, 3119–3134 (2012).
18. Naseer, S. et al. Casparian strip diffusion barrier in *Arabidopsis* is made of a lignin polymer without suberin. *Proc. Natl Acad. Sci. USA* **109**, 10101–10106 (2012).
19. Philippe, G. et al. Ester cross-link profiling of the cutin polymer of wild-type and cutin synthase tomato mutants highlights different mechanisms of polymerization. *Plant Physiol.* **170**, 807–820 (2016).
20. Yeats, T. H. et al. The identification of cutin synthase: formation of the plant polyester cutin. *Nat. Chem. Biol.* **8**, 609–611 (2012).
21. Berhin, A. et al. The root cap cuticle: a cell wall structure for seedling establishment and lateral root formation. *Cell* **176**, 1367–1378 (2019).
22. Philippe, G. et al. Cutin and suberin: assembly and origins of specialized lipidic cell wall scaffolds. *Curr. Opin. Plant Biol.* **55**, 11–20 (2020).
23. Andersen, T. G. et al. Diffusible repression of cytokinin signalling produces endodermal symmetry and passage cells. *Nature* **555**, 529–533 (2018).
24. Doblas, V. G. et al. Root diffusion barrier control by a vasculature-derived peptide binding to the SGN3 receptor. *Science* **355**, 280–284 (2017).
25. Fujita, S. et al. SCHENGEN receptor module drives localized ROS production and lignification in plant roots. *EMBO J.* **39**, e103894 (2020).
26. Lucas, M., Godin, C., Jay-Allemand, C. & Laplaze, L. Auxin fluxes in the root apex co-regulate gravitropism and lateral root initiation. *J. Exp. Bot.* **59**, 55–66 (2008).
27. Péret, B. et al. Auxin regulates aquaporin function to facilitate lateral root emergence. *Nat. Cell Biol.* **14**, 991–998 (2012).
28. Clough, S. J. & Bent, A. F. Floral dip: a simplified method for *Agrobacterium*-mediated transformation of *Arabidopsis thaliana*. *Plant J.* **16**, 735–743 (1998).
29. Gasperini, D. et al. Multilayered organization of jasmonate signalling in the regulation of root growth. *PLoS Genet.* **11**, e1005300 (2015).
30. Siligato, R. et al. MultiSite Gateway-compatible cell type-specific gene-inducible system for plants. *Plant Physiol.* **170**, 627–641 (2016).
31. Fauser, F., Schiml, S. & Puchta, H. Both CRISPR–Cas-based nucleases and nickases can be used efficiently for genome engineering in *Arabidopsis thaliana*. *Plant J.* **79**, 348–359 (2014).
32. Li-Beisson, Y. et al. Acyl-lipid metabolism. *Arabidopsis Book* **11**, e0161 (2013).
33. Ursache, R., Andersen, T. G., Marhavy, P. & Geldner, N. A protocol for combining fluorescent proteins with histological stains for diverse cell wall components. *Plant J.* **93**, 399–412 (2018).
34. Kremer, J. R., Mastronarde, D. N. & McIntosh, J. R. Computer visualization of three-dimensional image data using IMOD. *J. Struct. Biol.* **116**, 71–76 (1996).
35. Jan, M., Gobet, N., Diessler, S., Franken, P. & Xenarios, I. A multi-omics digital research object for the genetics of sleep regulation. *Sci. Data* **6**, 258 (2019).
36. Dobin, A. et al. STAR: ultrafast universal RNA-seq aligner. *Bioinformatics* **29**, 15–21 (2013).
37. Anders, S., Pyl, P. T. & Huber, W. HTSeq—a Python framework to work with high-throughput sequencing data. *Bioinformatics* **31**, 166–169 (2015).
38. Li, B. & Dewey, C. N. RSEM: accurate transcript quantification from RNA-seq data with or without a reference genome. *BMC Bioinformatics* **12**, 323 (2011).
39. Gu, Z., Eils, R. & Schlesner, M. Complex heatmaps reveal patterns and correlations in multidimensional genomic data. *Bioinformatics* **32**, 2847–2849 (2016).
40. Alexa, A. & Rahnenfuhrer, J. topGO: enrichment analysis for gene ontology. R package version 2.38.1 (2019).
41. Schindelin, J. et al. Fiji: an open-source platform for biological-image analysis. *Nat. Methods* **9**, 676–682 (2012).

Acknowledgements

We thank C. Grefen and M. Barberon for insightful discussions about GDSL-domain-containing proteins, experimental approaches and stimulating discussions; and the Electron Microscopy Facility and Imaging Facility of the University of Lausanne and the Center of Microcopy and Image Analysis of the University of

Zurich for excellent service and support. Work in the Geldner laboratory was supported by an ERC Consolidator Grant (GA-N: 616228-ENDOFUN) and two consecutive SNSF grants (CRSII3_136278 and 31003A-156261). R.U. was supported by an EMBO Long-Term Fellowship (EMBO ALTF 1046-2015). Work in the Nawrath laboratory was supported by a Swiss National Science Foundation grant (no. 310030_188672/1). Work in the Vermeer laboratory was supported by grants from the Swiss National Science Foundation (Schweizerischer Nationalfonds zur Förderung der Wissenschaftlichen Forschung; PP00P3_157524 and 316030_164086), the Netherlands Organization for Scientific Research (Nederlandse Organisatie voor Wetenschappelijk Onderzoek; NWO 864.13.008) and support from the University of Neuchâtel.

Author contributions

R.U., N.G. and J.E.M.V. conceived, designed and coordinated the project. R.U., C.D.J.V.T., V.D.T., D.D.B., K.G., V.S., T.G.A. and J.E.M.V. performed all experimental work. E.S.-S., S.C. and S.P. analysed RNA-seq data. J.E.M.V. wrote the first draft of the manuscript. R.U., T.G.A., C.N., N.G. and J.E.M.V. revised the manuscript and all authors were involved in the discussion of the work.

Competing interests

The authors declare no competing interests.

Additional information

Extended data is available for this paper at https://doi.org/10.1038/s41477-021-00862-9.

Supplementary information The online version contains supplementary material available at https://doi.org/10.1038/s41477-021-00862-9.

Correspondence and requests for materials should be addressed to R.U., N.G. or J.E.M.V.

Peer review information *Nature Plants* thanks Owen Rowland and the other, anonymous, reviewer(s) for their contribution to the peer review of this work.

Reprints and permissions information is available at www.nature.com/reprints.

Publisher's note Springer Nature remains neutral with regard to jurisdictional claims in published maps and institutional affiliations.

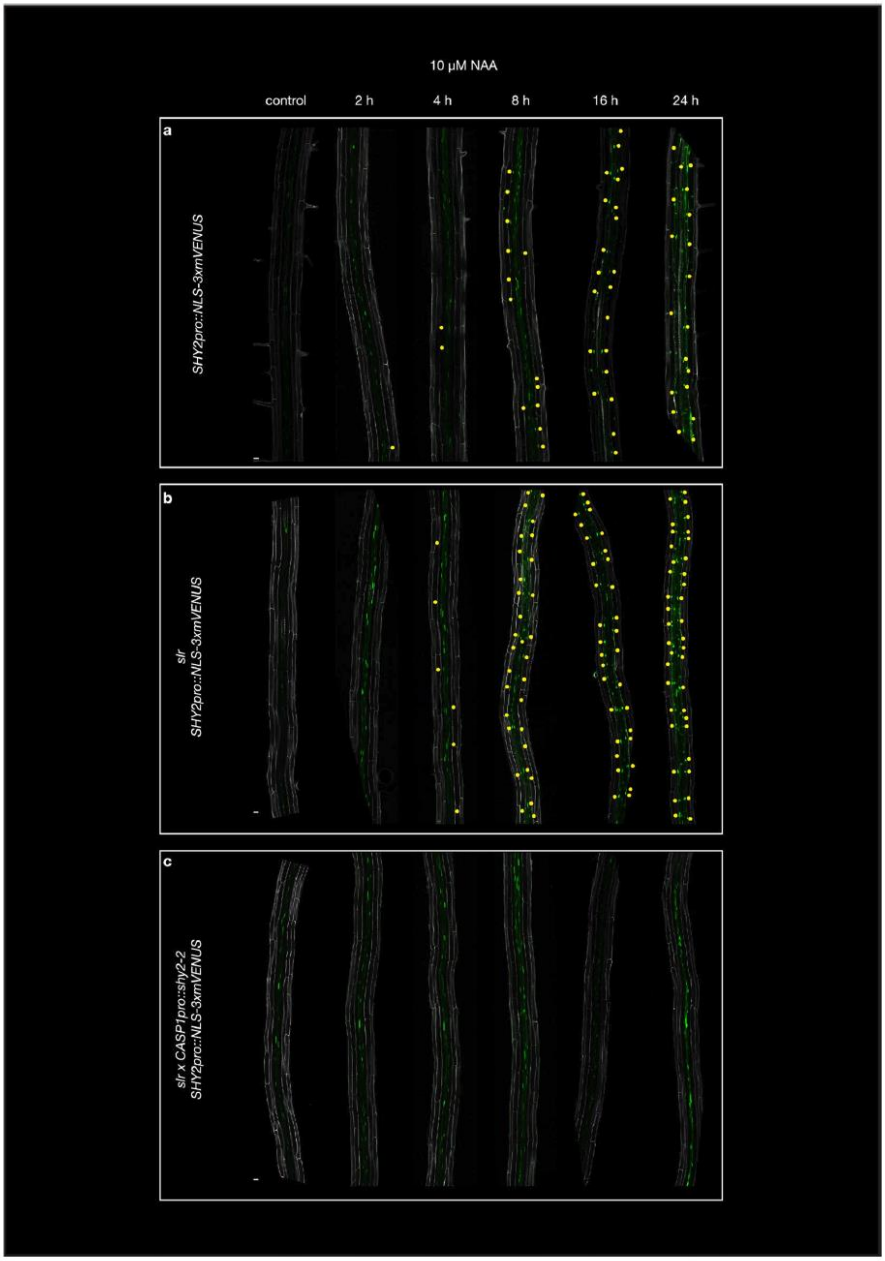

Extended Data Fig. 1 | *SHY2pro::NLS-3xmVENUS* dynamics in Col-0 (a), *slr-1* (b) and *CASP1pro::shy2-2/slr-1* treated with NAA. a. Maximum image projections of roots expressing *SHY2pro::NLS-3xmVENUS* in Col-0 **(a)**, *slr-1* **(b)** and *CASP1pro::shy2-2/slr-1* **(c)** after 2, 4, 8, 16 and 24 hours of NAA treatment. Yellow dots indicate *SHY2pro::NLS-3xmVENUS* signal in the endodermis. The images in are representatives of each experiment repeated 3 times. Scale bar in (**a**) = 50 µm.

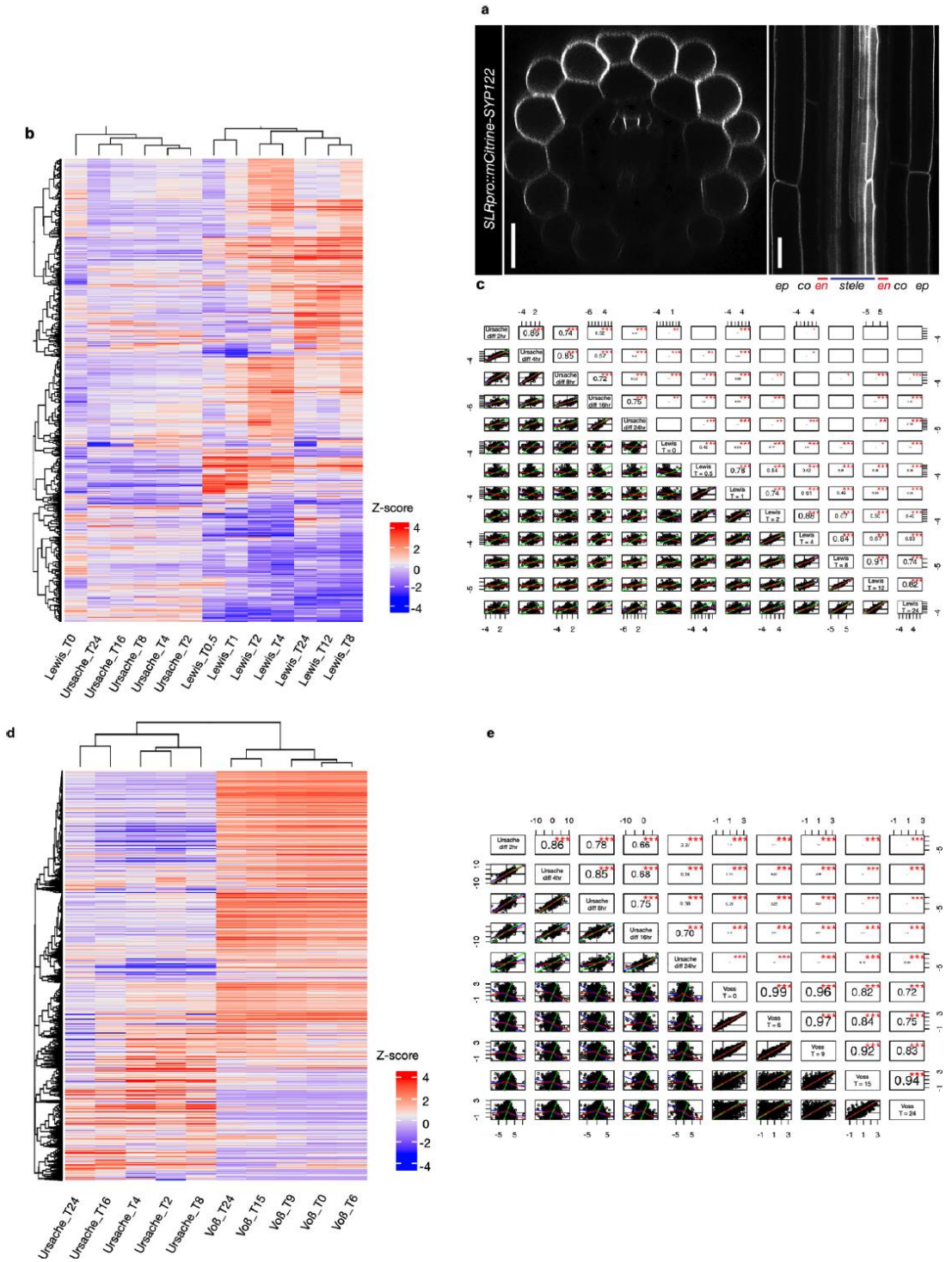

Extended Data Fig. 2 | Differentiated endodermal cells have a distinct transcriptional response to auxin. a, Confocal images of a root expressing *SLRpro::CITRINE:SYP122* confirming that *SLR* is expressed in the epidermis, cortex, pericycle and weakly in the stele, but not in the endodermis (indicated by asterisks). The images are representatives of the experiment repeated 3 times. **b** and **c**, Comparison of the current dataset (Ursache) with the data set of Lewis et al.[14]. **b**, Heatmap showing that both datasets cluster separately and do not have significant overlap, which is confirmed by the analysis of correlation between the two data sets (**c**). **d** and **e**, Comparison of the current dataset (Ursache) with the data set of Voß et al.[15]. **d**, Heatmap showing that both datasets cluster separately and do not have significant overlap, which is confirmed by the analysis of correlation between the two data sets (**e**). *p* values in **c** and **e** are derived from a Pearson correlation test, are two-sided t-test values and not corrected for multiple testing. The corresponding cut-points (*/**/***) represent here $p < 0.05$, $p < 0.01$ and $p < 0.001$. The r value measures the correlation between 2 sets of data. The p-value states whether there are enough observations to believe that an observed correlation is not appearing by chance. Scale bar = 25 µm.

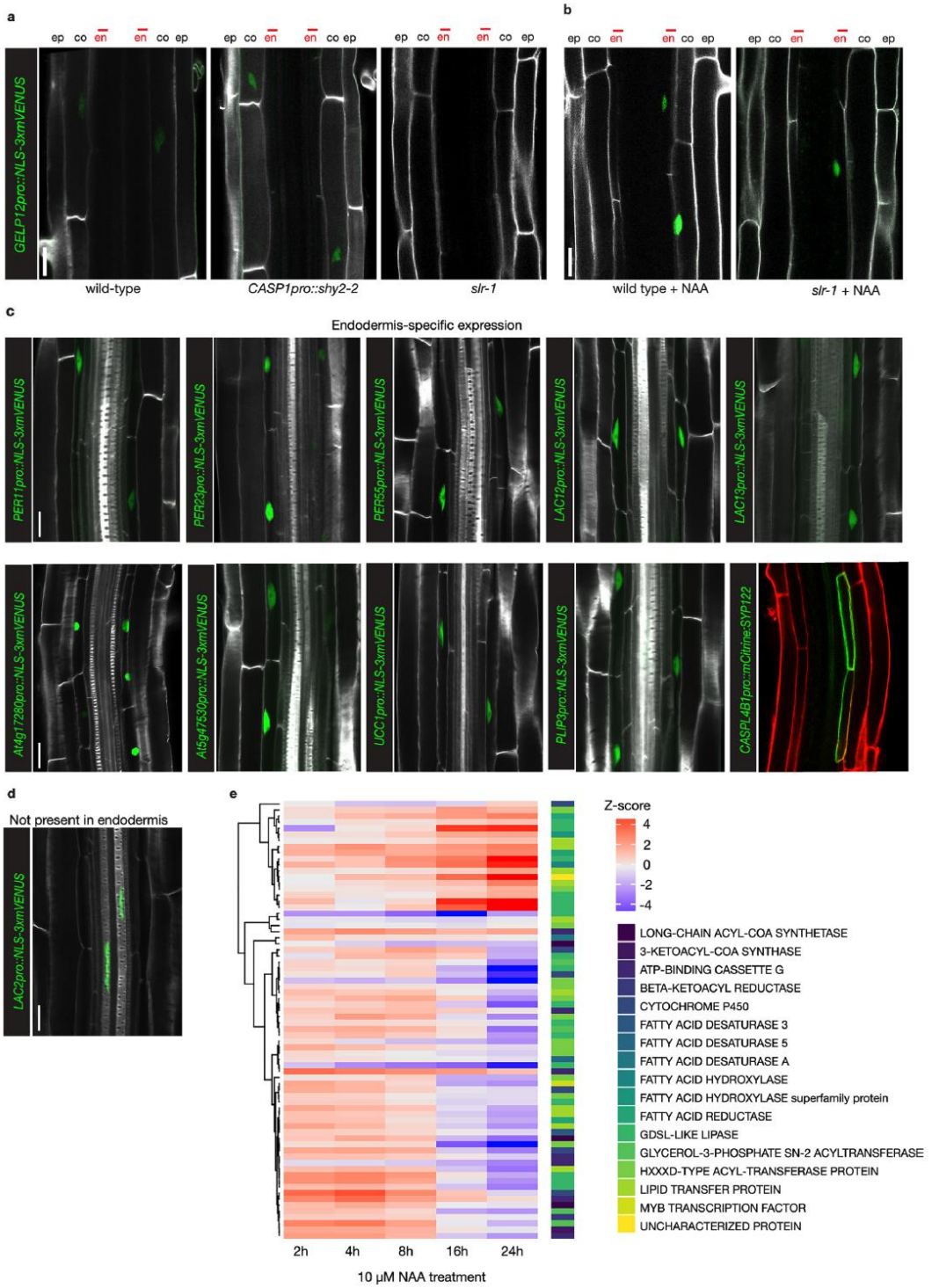

Extended Data Fig. 3 | A high number of differentially regulated genes are expressed in the endodermis. a, Confocal images of *GELP12pro::NLS-3xmVENUS* expression in different genetic backgrounds, showing repression in *slr-1* under control conditions. **b**, Auxin treatment (10 µM NAA, 16hrs) results in induction of *GELP12pro::NLS-3xmVENUS* expression in the endodermis of *slr-1* roots. NLS-3xmVENUS signal is shown in green and CFW staining of cell walls is shown in grey. **c**, Confocal images of roots expressing transcriptional markers of candidate genes differentially expressed between *slr-1* and *CASP1pro::shy2-2/slr-1* roots and showing specific expression in the endodermis. **d**, Confocal images showing xylem-specific expression of *LAC2pro::NLS-3xmVENUS*. **e**, Heatmap showing the expression dynamics of suberin-related genes significant differentially expressed. NLS-3xmVENUS signal is shown ir green, CFW staining of cell walls in gray and cell wall staining by PI in red. The images in **(a-d)** are representatives of each experiment repeated at least 3 times. Scale bars = 20 µm.

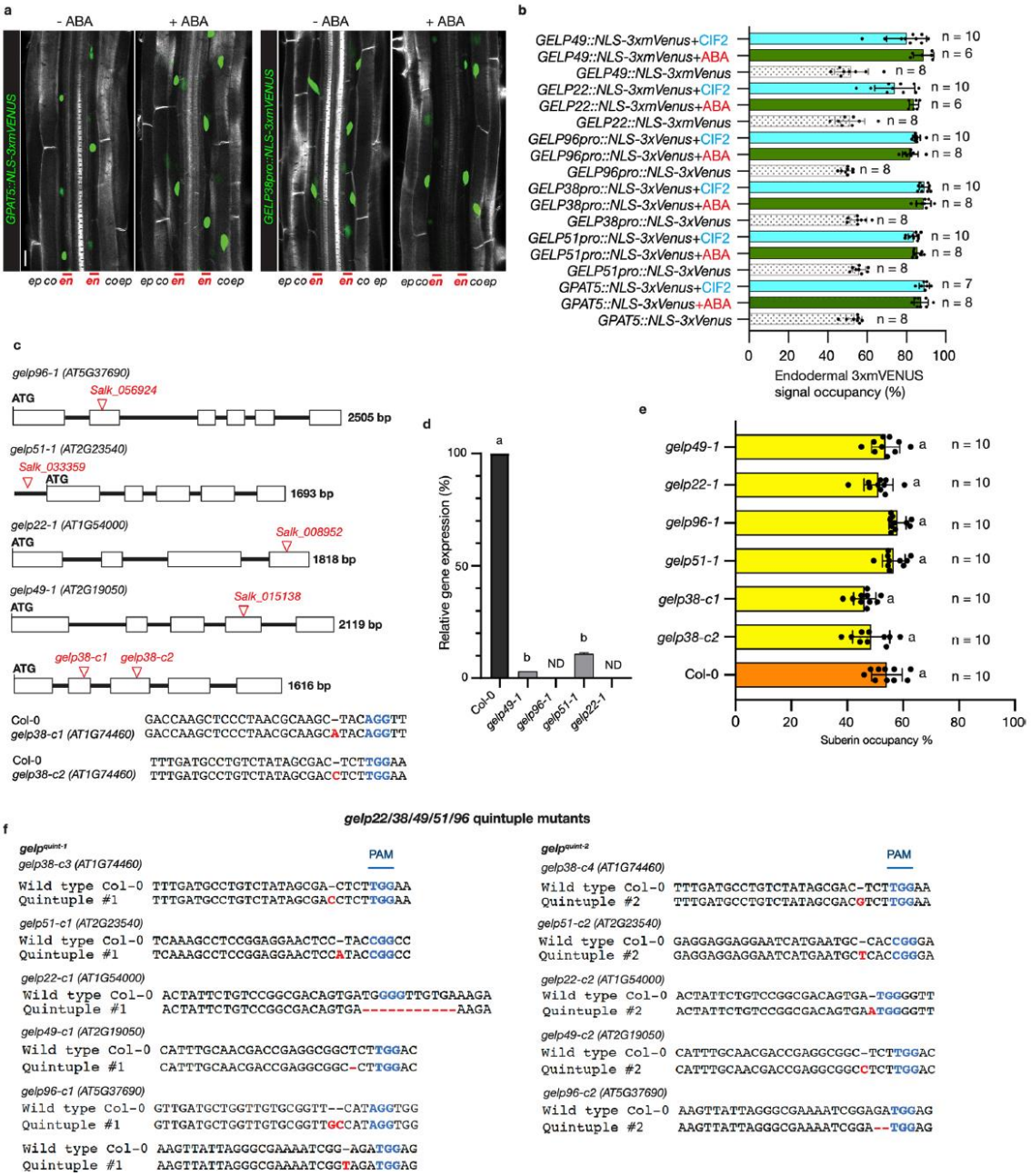

Extended Data Fig. 4 | Expression of suberin biosynthesis-related GELPs is induced by ABA and CIF2 treatment. a, Confocal images showing effect of ABA treatment (1 µM, 24hr) on the expression domain of *GPAT5pro::NLS-3xmVENUS* and *GELP38pro::NLS-3xmVENUS* in Arabidopsis roots. The images are representatives of the experiment repeated 3 times. **b**, Quantification of the effect of ABA (1 µM, 24hr) and CIF2 peptide (500 nM, 24h) treatment on the expression of suberin biosynthesis-related GELPs identified as being repressed by auxin treatment. **c**, Schematic representation of the different single mutants of the suberin biosynthesis-related GELPs used in this study. **d**, qPCR results showing the relative gene expression in Col-0 control (100%) and T-DNA insertion lines of the suberin synthesis-related GELPs used in this study. The results are based on three biological replicates. The *p* value versus the Col-0 control for *gelp49-1* is <0.000001 and for *gelp51-1* is < 0.000001. ND, not detected. **e**, Quantification of suberin occupancy in the endodermis of the single mutants of the suberin biosynthesis-related GELPs using FY staining (n = 10 biologically independent samples). The *p* value versus the Col-0 control for *gelp38-c1* is 0.1269, for *gelp38-c2* is 0.2616, for *gelp51-1* is > 0.9999, for *gelp96-1* is 0.9385, for *gelp22-1* is > 0.9999 and for *gelp49-1* is > 0.9999. Different letters in **(d)** and **(e)** ($p < 0.05$) indicate statistically significant differences between means by ANOVA and two-sided t-test analysis. **f**, Schematic representation of the mutations in the *gelp*$^{quint-1}$ and *gelp*$^{quint-2}$ mutants. The mutations are indicated in red and the PAM sites in blue. Error bars in **(b)**, **(d)** and **(e)** are SD. Scale bar in (**a**) = 25 µm.

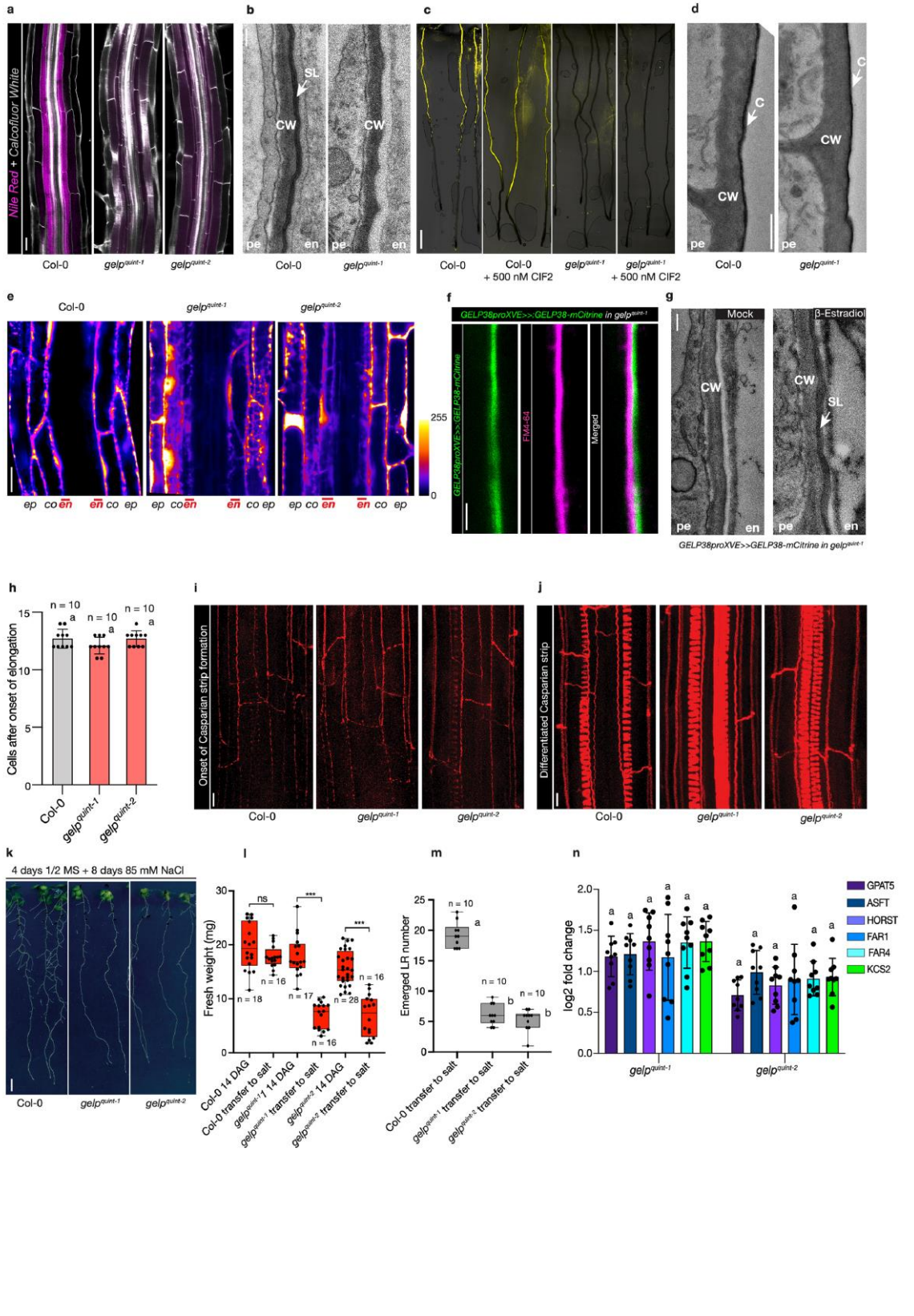
a
Nile Red + Calcofluor White
Col-0
gelp quint-1
gelp quint-2
b
SL
CW
pe
en
c
+ 500 nM CIF2
d
C
e
ep co en en co ep
255
0
f
GELP38proXVE>>GELP38-mCitrine in gelp quint-1
FM4-64
Merged
g
Mock
β-Estradiol
h
Cells after onset of elongation
n = 10
i
Onset of Casparian strip formation
j
Differentiated Casparian strip
k
4 days 1/2 MS + 8 days 85 mM NaCl
l
Fresh weight (mg)
ns
n = 18
n = 16
n = 17
n = 28
Col-0 14 DAG
Col-0 transfer to salt
gelp quint-1 14 DAG
gelp quint-1 transfer to salt
gelp quint-2 14 DAG
gelp quint-2 transfer to salt
m
Emerged LR number
n
log2 fold change
GPAT5
ASFT
HORST
FAR1
FAR4
KCS2

Extended Data Fig. 5 | Extended characterization of the phenotype of *gelp*^{quint} mutants. a, Nile Red staining of wild-type and *gelp*$^{quint-1}$ and *gelp*$^{quint-2}$ roots confirms the absence of suberin in the mutants. **b**, TEM micrographs of high-pressure frozen roots of wild-type and *gelp*$^{quint-1}$ showing the absence of suberin lamella in the mutant. A region without lateral root primordia has been chosen to highlight the absence of suberin lamella. **c**, FY staining of CIF2 peptide treated Col-0 and *gelp*$^{quint-1}$ seedlings showing absence of CIF2-mediated suberin deposition in *gelp*$^{quint-1}$. **d**, TEM micrograph of high-pressure frozen roots of wild-type and *gelp*$^{quint-1}$ showing that the lateral root cap cuticle is not affected in the *gelp*$^{quint-1}$ mutant. **e**, Fluorescein di-acetate (FDA) uptake assay in wild-type roots showing a suberin mediated block of uptake at the level of the endodermis. **f**, Confocal image of a root expressing *GELP38-XVEpro::GELP38- mCITRINE* (green) in *gelp*$^{quint-1}$ after β-Estradiol treatment (5 µM) stained with FM4-64 dye. **g**, TEM micrographs of roots of *gelp*$^{quint-1}$ and the complementation by *GELP38-XVEpro::GELP38- mCITRINE* showing the complete recovery of endodermis suberin lamella. The images in **(a-g)** are representatives of each experiment repeated at least 3 times. **h**, Counting of PI-stained cells as a proxy for Casparian strip barrier in the roots of wild-type and *gelp*$^{quint-1}$ and *gelp*$^{quint-2}$ seedlings. All individual data points are plotted. No statistically significant difference was detected in using ANOVA and Bonferroni-adjusted paired two-sided t-test. The *p* value versus the Col-0 control for *gelp*$^{quint-1}$ is 0.1680 and for *gelp*$^{quint-2}$ is > 0.9999. **i-j**, Basic Fuchsin staining of the Casparian strip in early and differentiated endodermal cells of wild-type and *gelp*$^{quint-1}$ and *gelp*$^{quint-2}$ roots. **k**, Salt stress assay showing that *gelp*$^{quint-1}$ and *gelp*$^{quint-2}$ mutant seedlings are more sensitive to mild salt stress (85 mM NaCl) compared to wild-type. The images in **(i-k)** are representatives of each experiment repeated at least 3 times. **l**, Quantification of the effect of prolonged salt stress on the fresh weight of wild-type and *gelp*$^{quint-1}$ and *gelp*$^{quint-2}$ seedlings. All individual data points are plotted. The *p* value versus the Col-0 control for Col-0 transferred to salt is 0.7857, for *gelp*^{quint1} versus *gelp*^{quint1} transferred to salt is < 0.000001 and for *gelp*$^{quint-2}$ versus *gelp*$^{quint-2}$ transferred to salt is < 0.000001. **m**, Quantification of emerged lateral roots in wild-type and *gelp*$^{quint-1}$ and *gelp*$^{quint-2}$ mutants after 8 days of exposure to salt. All individual data points are plotted (n = 10). **n**, Quantification of the expression of known suberin biosynthesis-related genes in *gelp*$^{quint-1}$ and *gelp*$^{quint-2}$ mutants. Results are presented as fold-change compared to their expression levels in Col-0 (n = 9). No statistically significant difference was detected in using ANOVA and Bonferroni-adjusted paired two-sided t-test. For GPAT5, the *p* value versus Col-0 for *gelp*$^{quint-1}$ is > 0.9999 and for *gelp*$^{quint-2}$ is 0.4546, for ASFT the *p* values are > 0.9999 and > 0.9999; for HORST the *p* values are 0.1122 and > 0.9999; for FAR1 the *p* values are > 0.9999 and > 0.9999; for FAR4 the *p* values are 0.1467 and > 0.9999; for KSC2 the *p* values are 0.1136 and > 0.9999 correspondingly. Different letters in **(m)** ($p < 0.001$) and asterisks in **(l)** ($p < 0.001$) indicate statistically significant differences between means by ANOVA and two-sided t-test analysis. ns, not significant. For the boxplots in **(l)** and **(m)** the center depicts the median while the lower and upper box limits depict the 25th and 75th percentile respectively. Whiskers represent minima and maxima. Closed dots depict individual samples. Data in **(h)** and **(n)** are presented as mean +/- SD. Scale bars for **(a), (d), (e), (f), (g), (h-j)** = 25 µm. Scale bars for **(b)** and **(c)** = 1 µm, for **(k)** = 5 mm.

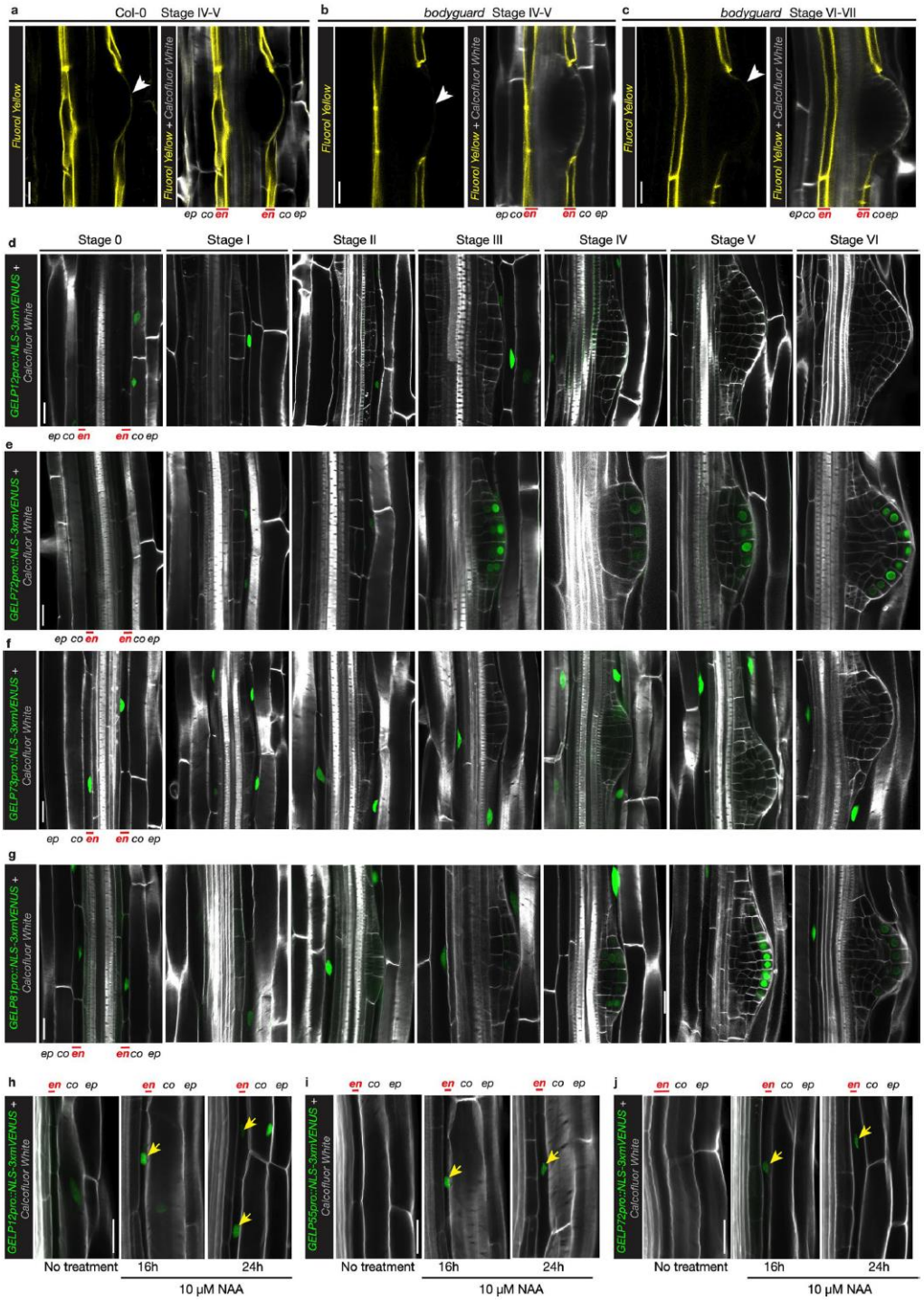

Extended Data Fig. 6 | See next page for caption.

Extended Data Fig. 6 | Auxin-upregulated GELPs show three distinct expression patterns. a, FY staining of a Col-0 root at the site of lateral root emergence highlighting the presence of cuticle (indicated by arrow). **b-c**, FY staining of *bodyguard* mutant root at the site lateral root emergence. The absence of a proper cuticle is highlighted by the gap in FY staining. **d-g**, Confocal images showing the expression patterns of *GELP12* **(d)**, *GELP72* **(e)**, *GELP73* **(f)** and *GELP81* **(g)** during lateral root emergence. **h-j**, Confocal images showing the expression of *GELP12* **(h)**, *GELP55* **(i)** and *GELP72* **(j)** after 10 µM NAA treatment. NLS-3xmVENUS signal is in green and Calcofluor White staining of cell walls is in gray. The images are representatives of each experiment repeated at least 3 times. Scale bars = 25 µm.

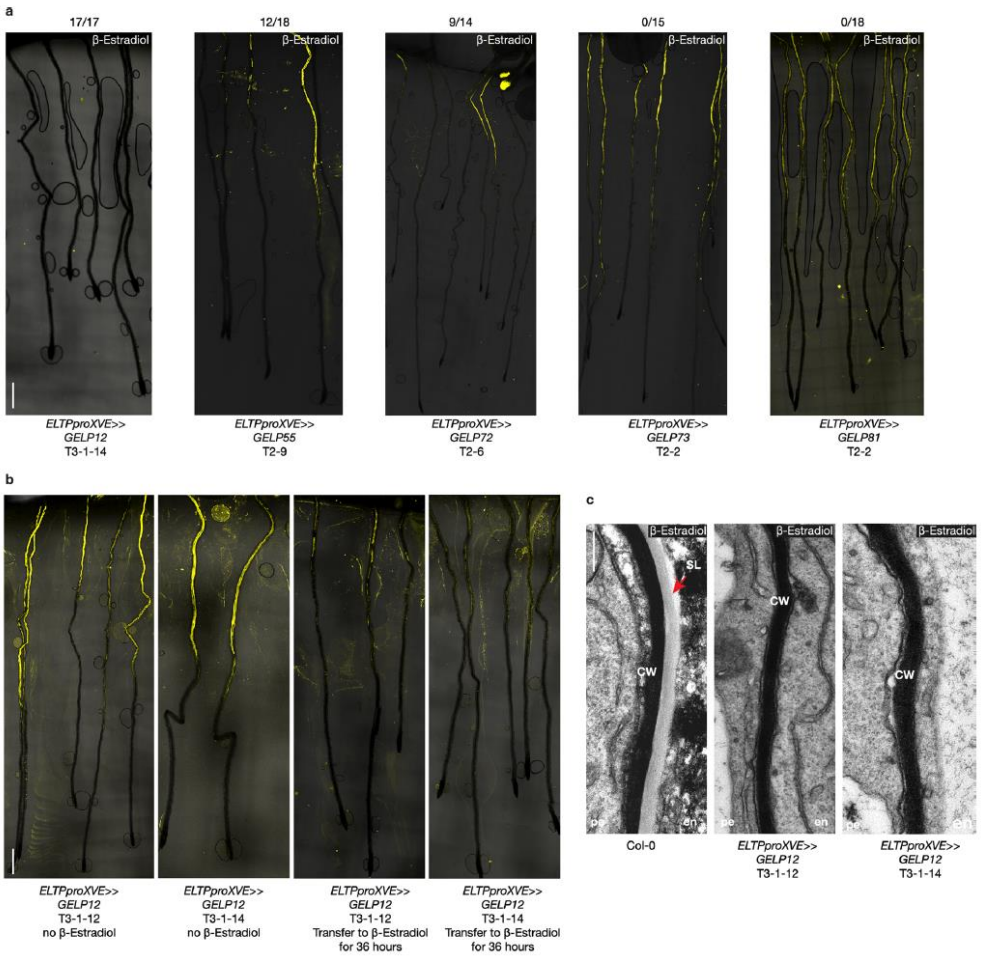

d

Single CRISPR mutants for auxin-upregulated GELPs:

	gRNA1 PAM	gRNA2 PAM
Col-0	AAGCTTACGATGAGCGAAGCC-ATGAGGAGA	GTTTTACAAGAAAGGCACGAT-CCAAGGCGG
gelp12-c1 (AT1G28650)	AAGCTTACGATGAGCGAAGCCCATGAGGAGA	GTTTTACAAGAAAGGCACGATTCCAAGGCGG
Col-0	AAGCTTACGATGAGCGAAGCCATGAGGAGA	GTTTTACAAGAAAGGCACGAT-CCAAGGCGG
gelp12-c2 (AT1G28650)	AAGCTTACGATGA--------CATGAGGAGA	GTTTTACAAGAAAGGCACGATTCCAAGGCGG
Col-0	GGTTGCCGAAATATTGTGGTC-GGAGGGTTA	
gelp55-c1 (AT2G30310)	GGTTGCCGAAATATTGTGGTCCGGAGGGTTA	
Col-0	GGTTGCCGAAATATTGTGGTC-GGAGGGTTA	CAATGTAATTGTAGGCAGC-TTCCGAGGGAT
gelp55-c2 (AT2G30310)	GGTTGCCGAAATATTGTGGTCAGGAGGGTTA	CAATGTAATTGTAGGCAGCTTTCCGAGGGAT
Col-0	TGCTAACGTTAAGCATCCAGTTGCTGGATG	
gelp72-c1(AT3G48460)	TGCTAACGTTAAGCATCCAGT-GCTGGATG	
Col-0	ACAATTACCTAGTCCCTTTTGTCGCGGCTC	
gelp73-c1 (AT3G50400)	ACAATTACCTAGTCCCTTTT-TCGCGGCTC	
Col-0	CCATCTCGTGGAAATCCAACC-GGCCGGTTT	TATGGACGCTCGGAAATTTGT-GGTGGGAAA
gelp73-c2 (AT3G50400)	CCATCTCGTGGAAATCCAACCTGGCCGGTTT	TATGGACGCTCGGAAATTTGTTGGTGGGAAA
Col-0	TCAAAGTAATCCCGGCCATATGGCTGGAAA	
gelp81-c1 (AT4G26790)	TCAAAGTAATCCCGGT--------TGGAAA	
	14bp insertion+334bp deletion	
gelp81-c2 (AT4G26790)	GTTCTGAAGAGCAATTTCCAGCCCAGGCTACTACAAA-334bp deletion-GAATACTACAAAGAATACC	

Extended Data Fig. 7 | Overexpression of three auxin-induced GELPs leads to suberin degradation. a, FY staining on roots of Col-0 treated with b-Estradiol results in normal suberin pattern, whereas inducible endodermis-specific overexpression of *GELP12*, *GELP55* or *GELP72* results in degradation of suberin highlighted by absence of FY signal. The overexpression of GELP73 and GELP81 results in a normal suberin pattern similar to wild-type. **b**, FY staining of *ELTPproXVE>>GELP12* lines germinated on normal 1/2MS medium for 4 days and transferred to the plates supplemented with 5 µM β-estradiol for 36 hours to observe the suberin degradation. **c**, TEM micrographs of *ELTPproXVE>>GELP12* grown on plates with and without β-estradiol to highlight the absence of suberin lamella upon induction of GELP12 expression in endodermis. **d**, Schematic representation of the mutations in the auxin-upregulated single GELP mutants. The mutations are indicated in red and the PAM sites in blue. The images in **(a-c)** are representatives of each experiment repeated at least 3 times. Scale bars in **(a)** and **(b)** = 500 µm. Scale bars in **(c)** = 1 µm.

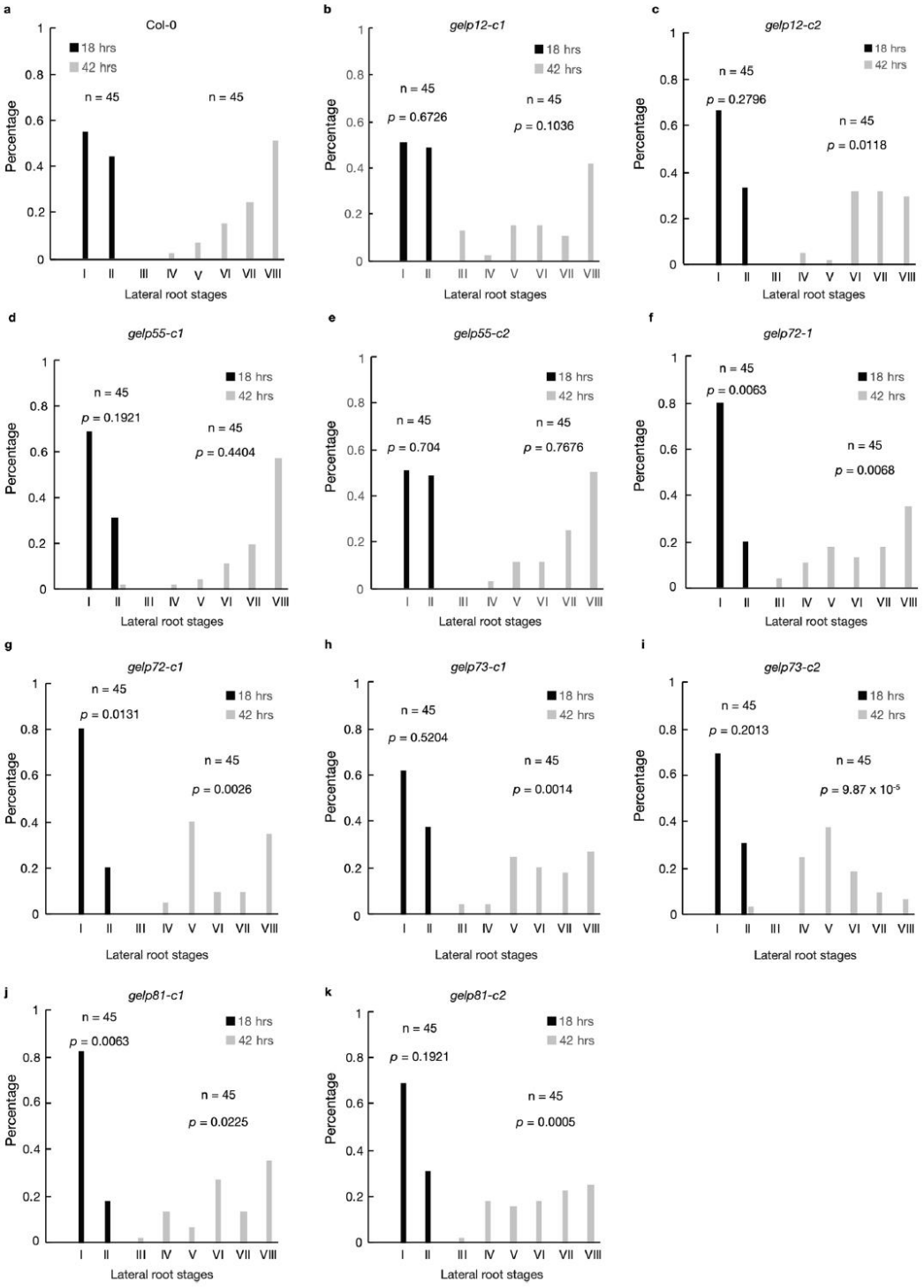

Extended Data Fig. 8 | Some auxin-inducible GELPs facilitate lateral root emergence. a-k, Gravistimulation-mediated induction of lateral root formation to functionally characterize the role of auxin-induced *GELPs* during lateral root formation. Staging of lateral root development was performed at 18hr and 42hr after gravistimulation. **a**, Col-0. **b** and **c**, *gelp12-c1* and *gelp12-c2*. **d** and **e**, *gelp55-c1* and *gelp55-c2*. **f** and **g**, *gelp72-1* and *gelp72-c1*. **h** and **i**, *gelp73-c1* and *gelp73-c2*. **j** and **k**, *p* values are indicated. A *p* value below 0.05 indicates a statistically significant difference as determined using a Pearson's χ^2 test. Experiments were repeated three times with a minimal of 15 seedlings per genotype and time point.

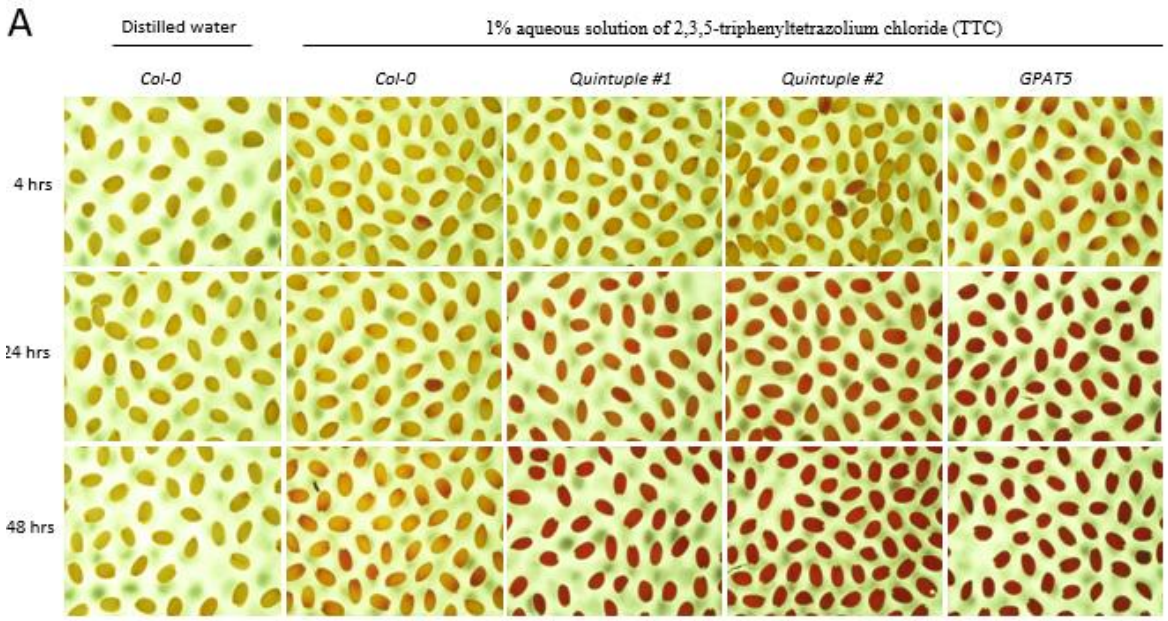

Extended Data Fig. 9 (not published – see more in the Chapter 5). Tetrazolium penetration assay indicates that the GELP quintuple mutation likely affects the synthesis of polymers involved in sealing the seed coat. GPAT5 was used as a positive control.

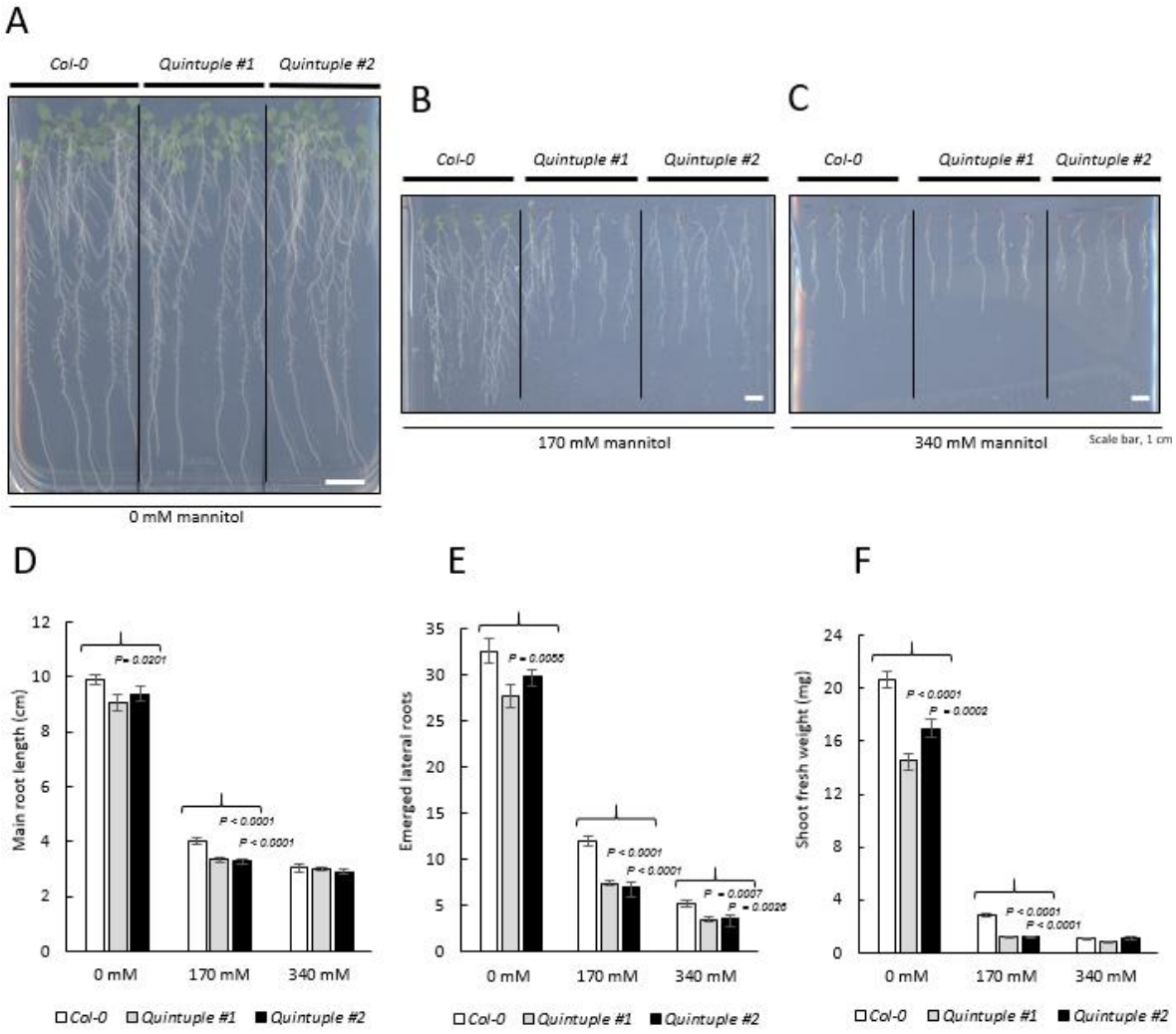

Extended data Fig. 10 (not published). GELP quintuple mutants show decreased lateral root development under mannitol treatments.

CHAPTER 3

2. An updated toolset for observing lateral root development in *Brachypodium distachyon*

Cristovão De Jesus Vieira Teixeira[1] *and Joop E.M. Vermeer*[1]

[1] Laboratory of Molecular and Cellular Biology, Institute of Biology, University of Neuchâtel, Rue Emile Argand 11, CH-2000, Neuchâtel, Switzerland.

Author contributions:

Chapter 3 was fully written by *Cristovão De Jesus Vieira Teixeira* with suggestions and corrections by *Prof Dr. Joop E.M. Vermeer*. All experiments were performedand analysed by *Cristovão De Jesus Vieira Teixeira*

3.1 Abstract

The study of plant organogenesis presents significant challenges due to the small number of cells involved in their initial stages. Observing the initial cell divisions becomes increasingly challenging when transitioning from *Arabidopsis thaliana* (Arabidopsis) to other species. Lateral root (LR) initiation is an essential process for enhancing a plant's ability to access water and nutrients. LR formation starts in the pericycle of the parent root, giving rise to a new meristem. Understanding the mechanisms coordinating LR development is important for improving plant resilience to biotic and abiotic stresses. The prediction of the precise timing and location of LR initiation along the root axis remains challenging, even in Arabidopsis. This is magnified when attempting to observe LR development in crops. *Brachypodium distachyon* (Brachypodium) has emerged as a versatile model for cereal crops. However, studying Brachypodium LR development requires a revision of protocols and methodologies to be applied from seedling growth to root imaging. Here, we present updated protocols for seed preparation for in vitro growth and tissue clearing. Whereas ClearSee is unsuitable for rendering Brachypodium root tissues transparent in a reasonable incubation period, the DEEP-Clear method showed improved efficiency in tissue clearing and is compatible with major fluorescence proteins and dyes. Finally, we introduce a simple and straightforward approach to locally synchronizes LR development. These tools and methodologies are crucial for advancing our knowledge of plant root system architecture, transitioning from a model plant to agronomically important species.

3.2 Introduction

Plant roots consist of various cell types arranged in concentric layers around the vascular tissues (Kenrick and Strullu-Derrien, 2014). In Arabidopsis, this vasculature is diarch, featuring two xylem and phloem poles (Dolan and Roberts, 1995; Malamy and Benfey, 1997). In contrast, plants like maize and rice have a polyarch vascular structure, containing multiple alternating xylem and phloem elements (Yu, Hochholdinger and Li, 2019). The vascular tissues are enclosed by the pericycle, which is itself surrounded by the endodermal, cortical, and epidermal cell layers. Lateral root (LR) formation in angiosperms starts with a distinct group of pericycle cells known as founder cells (Beeckman and Eshel, 2024). In Arabidopsis, as well as in onion, radish, and sunflower, these founder cells are situated at the xylem poles, while in maize, rice, and carrot, pericycle cells at the phloem poles are especially prone to initiating LRs (Casero, Casimiro and Lloret, 1995). The initial step in LR formation is an asymmetric anticlinal division that occurs simultaneously in three or more adjacent pericycle founder cells (Malamy and Benfey, 1997). Further periclinal and anticlinal divisions lead to the creation of a dome-shaped primordium that eventually emerges from the parent root (Stoeckle, Thellmann and Vermeer, 2018; Amtmann, Bennett and Henry, 2022). However, the timing and location of these initial divisions are challenging to predict. The limited number of cells involved makes studying LR initiation particularly difficult (Péret, Larrieu and Bennett, 2009). This challenge increases when moving from Arabidopsis to larger plant species.

Brachypodium was suggested as a plant model more than 20 years ago (Garvin, 2007; Vogel, 2008; Raissig and Woods, 2021). Its versatility makes it an excellent choice for a wide range of plant biology research areas. It serves as a robust foundation for studying aspects such as plant diversity, molecular-level genome organization, plant responses to environmental stimuli and cell wall structures and their modification (Raissig and Woods, 2021). These characteristics are particularly relevant for gaining insights into major developmental processes that can be applied to agricultural species. However, working with Brachypodium presents significant challenges compared to Arabidopsis, particularly in the context of LR formation. In this chapter, we present a detailed set of tools and updated protocols that are aimed to speed up and optimize the visualization of LR development in Brachypodium and likely other monocot species. Approaches such as improved growth conditions, seed preparation, LR synchronization and histological methods are presented as tools to enhance our understanding of LR development in Brachypodium.

3.3 RESULTS

3.3.1 Brachypodium from seed to seed

The initial step in establishing Brachypodium for in vitro growth involves ensuring that the seeds can grow uniformly and free from contamination. Brachypodium seeds (including Bd21 and Bd21-3) are encased in a husk which must be removed to expose the embryo (**Figure 1A**). This process is crucial for reducing contamination risks and enhancing germination rates. The seed husks can be efficiently removed using forceps taking care not to damage the embryo (**Figure 1A**). Viable seeds are typically darker and stiffer, whereas non-viable seeds are lighter and softer (**Figure 1A**). This allows for a pre-selection of seeds to ensure homogeneous germination.

After husk removal, seeds require sterilization. We observed that gas sterilization, often used for Arabidopsis (Weigel & Glazebrook, 2002; Lindsey III et al., 2017), significantly reduces germination rates do not recommended this for Brachypodium seeds. Sterilization with ethanol also proved less effective under our conditions as it slightly reduced germination and many seeds still showed contamination. The most effective method that we tested was a 6% bleach and 0.1% Tween solution (Sauer and Burroughs, 1986). For this, we advise to use a Falcon tube of at least 15 ml to ensure the seeds are fully submerged (tubes can be re-used multiple times). Filling the tube to a maximum of 50% capacity with seeds is suggested to enhance sterilization efficiency. The tubes should be vigorously shaken to ensure each seed contacts the solution for at least 1 minute. After sterilization, remove the solution using a sterile 2 ml pipette (or similar) and wash the seeds at least five times with sterilized distilled water. A complete removal of the bleach solution is essential to ensure standard germination. for plating (**Figure 1A**). Before plating, rinse the seeds to remove any residual bleach. The seeds generally germinate and grow well on 12x12 cm plates using a 0.8 to 1% plant agar medium supplemented with ½ Murashige and Skoog (MS) basal medium. Although some protocols recommend adding 0.3% sucrose, we opted not to use it in this study as the plants demonstrated satisfactory growth without it (reference to chemical specifications in the appendix).

For root phenotyping, we recommend placing one row of no more than 15 seeds, positioned 2 cm from the top of the plate to allow proper shoot growth. When placing seeds, ensure the embryo faces upward and is not in contact with the medium to promote the correct growth direction (see **Figure 1C**). Afterwards, transfer the plates to growth chambers (continuous light and 22°C). Note that the plates should be angled approximately 20° angle to prevent roots from growing into or out of the medium. (Note: most Arabidopsis growth cabinets typically only accommodate a 15° angle).

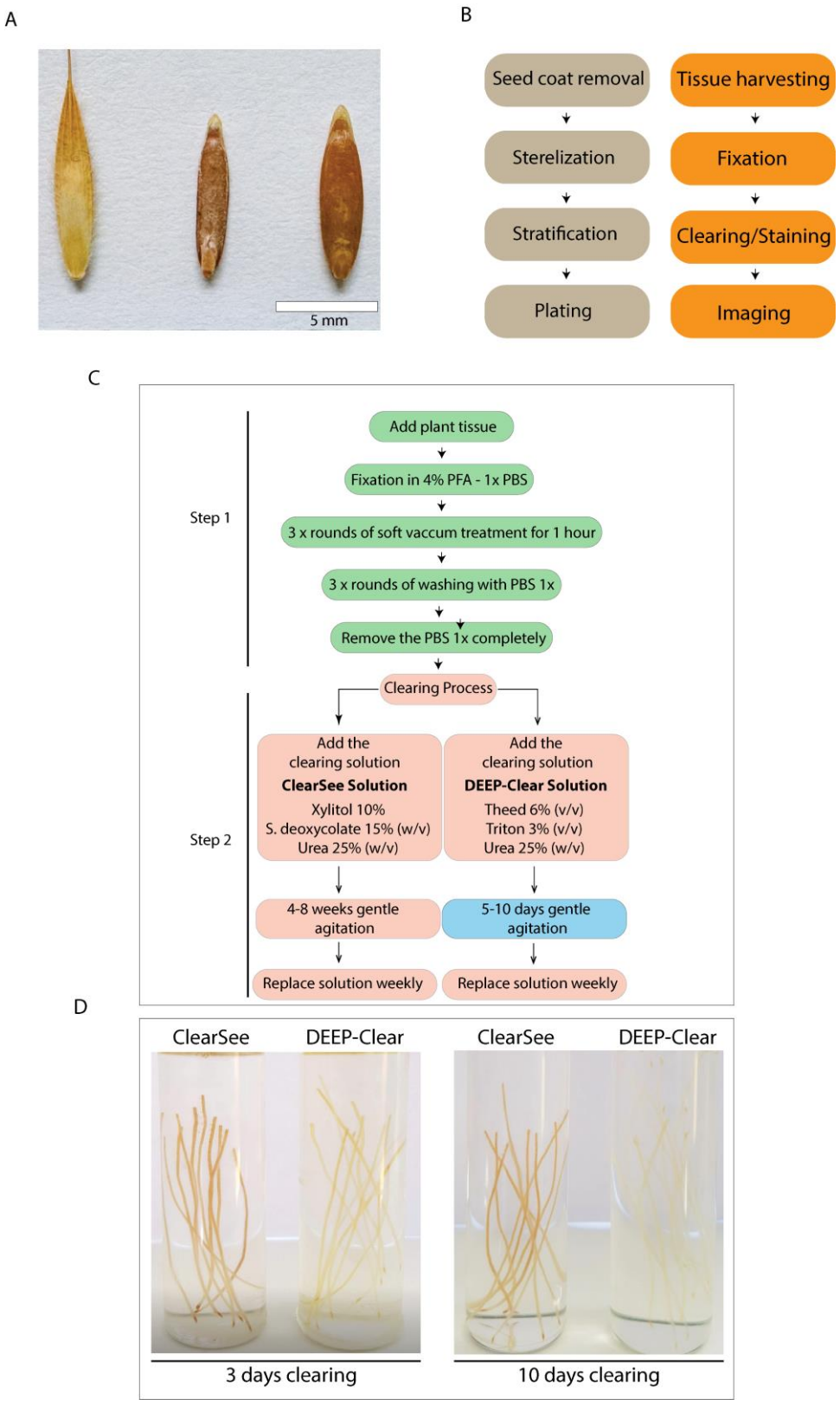

Figure 1. Workflow from seed to imaging of Brachypodium LR development: **A**) Seed preparation is essential for growing Brachypodium in vitro: untreated seed (left), seed with husk removed (middle), and seed after 3 days at 4°C, ready for plating (right). **B**) Overview of the major steps in the protocol for *Brachypodium* root tissue preparation. **C**) Comparison of the ClearSee and DEEP-Clear protocols: root tissue transparency can be achieved in 5 to 10 days (highlighted in blue). **D**) Brachypodium root tissue treated with ClearSee and DEEP-Clear after 3 and 10 days of incubation: DEEP-Clear achieves quicker tissue transparency compared to ClearSee.

Interestingly, Bd21-3 roots grow well parallel to the medium surface at a 15° angle while Bd21 seedlings frequently grow out of the medium at this angle. Therefore, special attention should be paid to the angle of inclination for Bd21 and likely to other genotypes.

Following sterilization, leave the seeds in water in the dark for 2 to 4 days at 4°C. After this period, seeds are typically enlarged and the embryos become clearly visible indicating readiness Brachypodium seedlings can usually be grown up to 7 days before reaching the bottom of the 12x12cm squared plates. For longer experiments, larger plates are recommended (see appendix for details). Seeds can be also transferred directly to soil after sterilization. In this case, plants also grow well at 22°C with a 20-hour photoperiod in a growth room or greenhouse. To prolong the vegetative phase, plants can be grown under a 16-hour photoperiod. This will require more growth space as the plants grow taller and produce more seeds. For faster seed settling, we suggest storing plates with 7-day-old seedlings in dark conditions at 4°C for about 10 days. Although this method reduces flowering time and accelerates seed production, it also decreases seed quantity.

Brachypodium grows well in soil conditions like those for Arabidopsis but using a 4:1 vermiculite mixture is advisable for better water retention. Brachypodium needs frequent watering especially during flowering necessitating daily monitoring at this stage. Fertilizing weekly starting from the fourth week is also recommended (See appendix). The growth cycle typically lasts 16 weeks, although a shorter 12-week cycle is possible with the above vernalization step. Plants need to be watered until they appear completely dry. Seeds should be harvested about two weeks after stopping watering; harvesting green or not fully dried seeds can reduce germination rates and increase chances of contamination. (Note: Remove seeds carefully from the spikelet and wear gloves, as the seeds can be sharp). After harvesting, place the seeds in paper bags at 37°C for at least two days to reduce humidity. Seeds can be stored in room conditions after being completely dried. Based on our results, 5-year-old seeds still germinated well.

3.3.2 CleaSee is unsuitable for clearing of Brachypodium root tissue

High-resolution microscopy facilitates insights into numerous biological developmental processes (Keller, 2013). However, when applied to tissues or whole organisms, light microscopy often encounters limitations due to molecules and pigments that refract or absorb light. Clearing methods are known to render tissues transparent and enable the examination of cells in situ (Richardson et al., 2021). These methods strive to preserve fluorescent proteins and be compatible with histological stains (Kurihara et al., 2015; Piccinini, Nirina Ramamonjy and Ursache, 2024). In plants, challenges are heightened by the presence of chloroplasts, thick cell walls, and multiple cell layers depending on the organ

to be observed. Most plant (root) clearing methods were optimized for Arabidopsis, which has a relatively simple structure that allows a rather straightforward deep tissue imaging. On the other hand, Brachypodium presents up to five cortex cell layers at the LR primordia (LRP) initiation sites and exhibits strong autofluorescence (Van Der Schuren, 2019). This complexity makes live cell imaging of Brachypodium inner root tissues particularly challenging, underscoring the need for an effective clearing method to study LRs without resorting to laborious fixation and sectioning techniques.

To characterize LRP development in Brachypodium, we first used the well-established ClearSee protocol, adapted from (Kurihara et al., 2022), combined with histological stains as described by (Ursache et al., 2018a). For this study, we used 5-7 days old seedlings of genotypes Bd-21 and Bd-3. Intriguingly, Brachypodium roots (mainly Bd21-3) begin to get brown upon exposure to air likely due to oxidation already mentioned above (Van Der Schuren, 2019). Consequently, roots needed to be immediately immersed in a fixative solution to prevent browning that can compromise the clearing efficacy. Here, we used a solution of 4% PFA in 1x PBS + 0.1% Tween for tissue fixation as in (Ursache et al., 2018b). It is strongly recommended to use vacuum infiltration (3 to 5 rounds + max of total 2 hours) to make sure the fixative reaches most of inner tissues. For clearing lines with fluorescent proteins (FPs), we recommend performing fixation in a cold room (4°C). Whenever possible, we recommend performing fixation in a cold room (4°C) for clearing lines expressing fluorescent proteins (FPs) to partially mitigate tissue browning and preserve the FP signal.

Subsequently, samples were washed in 1x PBS for at least five times. The complete removal of the fixative is essential, especially for maintaining the integrity of FPs. One round of vacuum infiltration with 1x PBS is also recommended for this step. Afterwards, samples were transferred to the ClearSee solution. To enhance solution penetration, three rounds of soft vacuum were applied, and samples were agitated gently at room temperature for four weeks. The ClearSee solution required weekly replacement although it is also recommended to change the solution after 3 days in case of leaf tissue clearing. Finally, samples were stained with 0.1% Calcofluor White (dissolved in ClearSee solution) and examined using two-photon excitation microscopy.

Tissue clearing with ClearSee is particularly suitable for analyzing thin roots, embryos, and leaves (Kurihara et al., 2015). However, despite repeated efforts, we were unable to establish a ClearSee-compatible procedure for investigating LR development in Brachypodium (**Figure 2**). Although ClearSee efficiently cleared the root tip and part of the root meristem, LRs in later developmental stages could not be consistently visualized

(**Figure 2**). Moreover, we observed significant shrinkage of the root tissue likely due to the high osmotic potential of the ClearSee solution and multiple vacuum steps. This issue was partially mitigated by preconditioning the root samples first in 25% ClearSee (diluted in 1x PBS) followed by a gradual increase to full strength. Nonetheless, this did not enhance tissue transparency in the LR emergence zone. A more recent version of the CleaSee (ClearSee + 50 mM sodium sulfite), named as ClearSeeAlpha, was shown to be efficient in removing the browning of the roots tissue in many plant species (Kurihara et al., 2021).

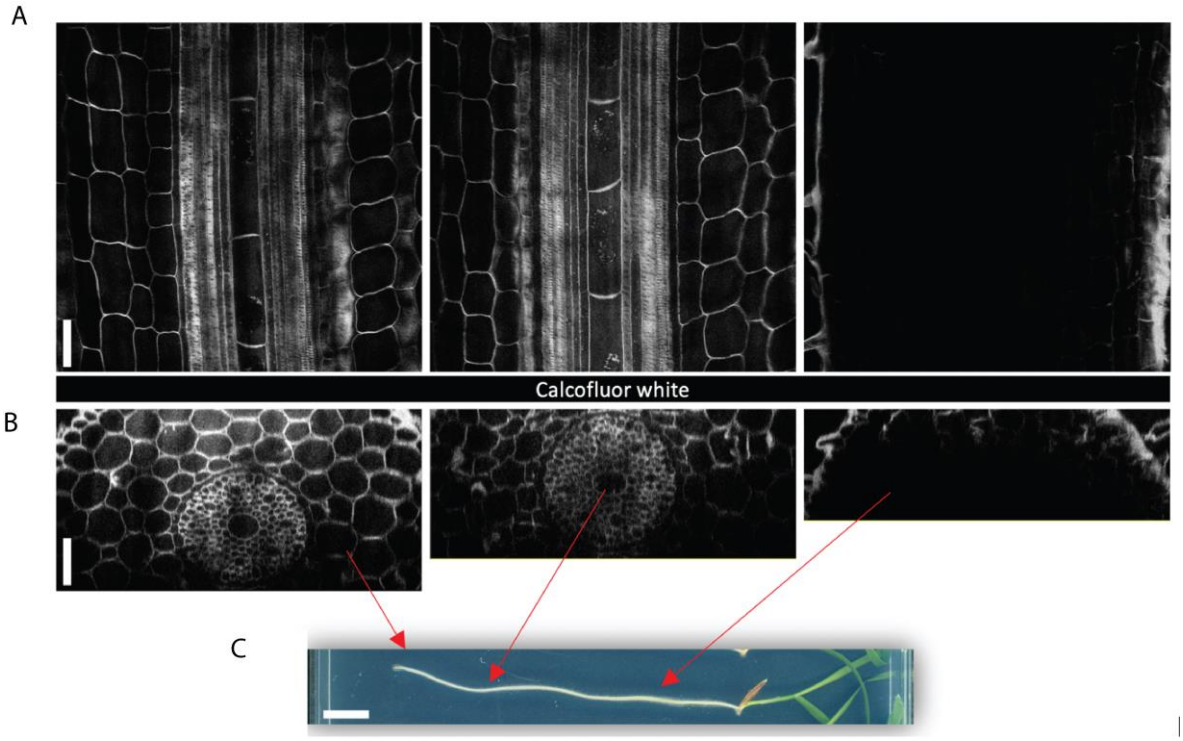

Figure 2. Ineffectiveness of ClearSee for rapid clearing of Brachypodium roots. Brachypodium roots were cleared using the standard ClearSee protocol. Optical sectioning provided longitudinal (**A**) and orthogonal (**B**) views. The clearing efficiency varied along the root axis not allowing for consistent localization of LRPs in various developmental stages. The roots were stained with 0.1% Calcofluor white and examined using two-photon excitation microscopy. Scale bars: (**A**-**B**) 100 µm, (**C**) 1 cm.

However, we observed that the ClearSeeAlpha protocol is incompatible with Basic Fuchsin (staining for labeling lignin) likely due to the adding of 50 mM sodium sulfite. These results suggest that the current ClearSee, and ClearSeeAlpha protocols are not effective to allow deep tissue imaging of Brachypodium roots while preserving tissue integrity and keeping compatibility to a range of fluorescent stains.

3.3.3 Deep-Clear is compatible with fluorescent proteins and -dyes

Recently, chemical mixtures have been developed to reduce autofluorescence in mammalian tissue while preserving FPs (Hou et al., 2015; Ueda et al., 2020) . The ClearSee protocol, originally designed for mouse brain samples, serves as the basis for these methods. Although ClearSee has shown to provide satisfactory tissue transparency in many plant organs, we found it challenging to apply to *Brachypodium* root tissues. We have tested other methods (Warner et al., 2014; Richardson and Lichtman, 2015; Du et al., 2018; Kurihara et al., 2021) but most of them proved too laborious or incompatible with FPs and/or dyes.

While searching for a suitable clearing method for Brachypodium roots, the DEpigmEntation-Plus-Clearing (DEEP-Clear) method stood out for its simplicity and reported efficiency in clearing animal tissues (Pende et al., 2018). The study showed optimal results for depigmenting tissue in small marine species and enabled deep tissue imaging of labeled structures, from whole-body light-sheet microscopy to high-resolution confocal microscopy. The full protocol is quite extensive but the core clearing steps resemble the ClearSee protocol (**Figure 1C**). Therefore, we decided to test an adapted version of the DEEP-Clear method on plant tissues. DEEP-Clear is a urea-based aqueous reagent similar to ClearSee that incorporates an aminoalcohol, N,N,N',N'-tetrakis (2-hydroxypropyl-ethylenediamine (THEED), which decolorizes and solubilizes samples for increased transparency (Muntifering *et al*., 2018; Pende *et al*., 2018). We adapted DEEP-Clear protocol by replacing the ClearSee solution while keeping the same fixation and staining steps from (Ursache et al., 2018b; Kurihara et al., 2021) with minor modifications (**Figure 1C**).

We first tested the DEEP-Clear on Arabidopsis to confirm its capacity to clear to visualize root structures in 3D, assess FPs stability after clearing, and verify its compatibility with fluorescent dyes. We also applied the standard ClearSee protocol for comparison. DEEP-Clear produced similar clearing power compared to ClearSee achieving surprising tissue transparency already within the first 24 hours.

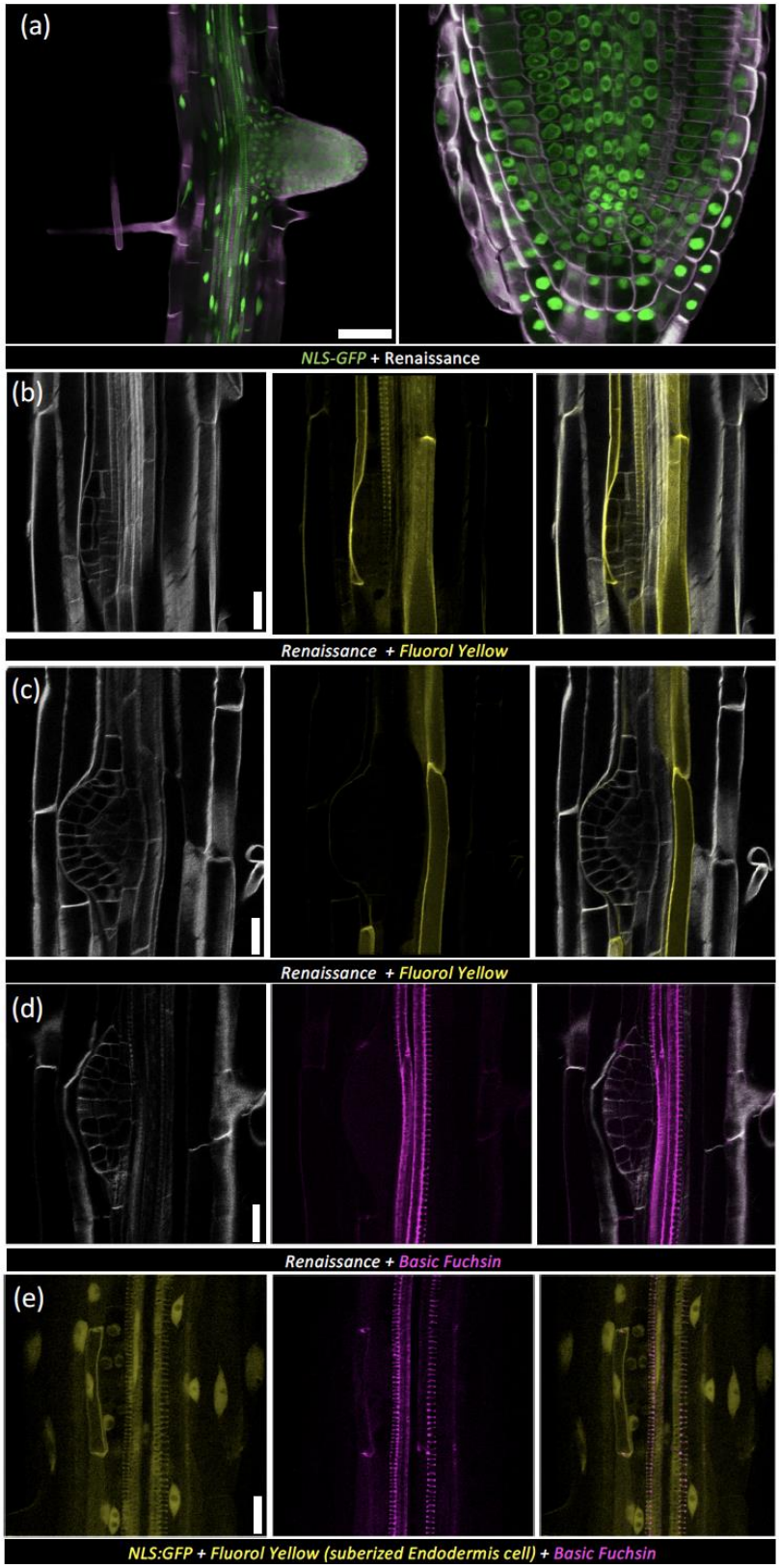

Figure 3. The Deep-Clear method is compatible with fluorescent proteins and -dyes. (**A**) Arabidopsis fully emerged LRP (left) and root tip expressing *NLS::GFP* with cell walls stained by Renaissance for cellulose (grey). (**B**) LRP at stage 4 and (**C**) stage 7, both stained sequentially with Renaissance (grey) and Fluorol Yellow (yellow) to highlight endodermal suberization. (**D**) LRP region stained sequentially with Basic Fuchsin for lignin (magenta) and Renaissance (grey). (**E**) *NLS::GFP* combined with Basic Fuchsin and Fluorol Yellow, illustrating Casparian strips as dot-like structures near a suberized endodermal cell covering a young LRP (arrowheads). Scale bars: 20 µm.

By day three, both solutions produced similar clarity, with leaves fully depigmented and roots transparent (**Figure 1D**).

Fluorescent protein stability and staining compatibility were confirmed through 3D imaging of Arabidopsis roots expressing a nuclear-localized reporter, *NLS::GFP* (**Figure 3E**) (Decaestecker et al., 2019). FP signals and fluorescent stains remained consistently visible throughout the root in tissues treated with either ClearSee or DEEP-Clear (**Figure 3E**). Surprisingly, Fluorol Yellow, which is not soluble in ClearSee, was compatible with DEEP-Clear, providing consistent staining of endodermal suberization (**Figures 3B, 3C**). These findings suggest that DEEP-Clear enables sufficient transparency for two-photon microscopy and is compatible multicolor imaging with various FPs and dyes.

3.3.4 DEEP-Clear facilitates Brachypodium root tissue clearing

Deep tissue imaging is challenging due to the complex and multi-layered structure of the specimens. However, DEEP-Clear has demonstrated impressive results in clearing entire marine animals (Pende et al., 2018), and in our conditions, it proved compatible with plant tissues. Therefore, we aimed to determine if DEEP-Clear could improve deep imaging in Brachypodium roots. For this, we collected 7-day-old seedlings (Bd-21-3) and used our adapted DEEP-Clear protocol. Brachypodium roots often show damage during prolonged incubation in 6-well cell culture plates, which are commonly used in such protocols. Instead, we incubated the roots (3-4 cm long) in screw-cap glass tubes placed in a shaking incubator at 28°C (only recommended for samples with no FPs). This setup allowed vigorous shaking without damaging the roots. After 3 days of incubation, roots treated with ClearSee retained their usual brown pigment (**Figure 1D**), with no significant improvement even after seven more days of incubation (**Figure 1D**).

Surprisingly, DEEP-Clear-treated roots showed a significant reduction in brown pigmentation within the first three days (**Figure 1D**). After ten days, they reached a level of transparency never observed in ClearSee-treated roots (**Figure 1D**). We then stained the cell walls of both samples using Renaissance (for cellulose) in ClearSee and DEEP-Clear solutions for three days. After staining, we washed the samples in their respective clearing agents for two days. Using two-photon microscopy, we found that ClearSee-treated samples allowed observation of the inner layers of the root tip, but only the DEEP-Clear treatment enabled precise identification of early LR primordia (LRP) sites and vascular development at later LRP stages (**Figure 5**). Surprisingly, DEEP-Clear was compatible with propidium iodide, allowing the tracking of early LRP development using a fluorescence microscope without needing a confocal apparatus for quick visualization (**Figure 5**). These findings suggest that DEEP-Clear enhances the transparency of Brachypodium roots and facilitates

detailed imaging of critical developmental stages without solely relying on confocal microscopy.

3.3.5 LR synchronization in Brachypodium

Understanding LR development is challenging due to the small number of cells involved in initiation and the lack of synchrony across different sites (Lavenus et al., 2013). Various LR Inducible Systems (LRIS) have been developed to address this challenge (Ditengou et al., 2008; Voß et al., 2015; Crombez et al., 2016). In Arabidopsis, LR initiation can be mechanically induced through gravitropic curvature or manually bending of the root (Ditengou et al., 2008). This mechanical bending causes auxin accumulation at the induction site leading to LR primordium formation within 42 hours. However, the method yields limited tissue, and we could not observe a clear LRP induction in the bending zone of Brachypodium roots. Another system uses seed germination in presence of the polar auxin transport inhibitor naphthylphthalamic acid (NPA), followed by growth on naphthalene acetic acid (NAA) containing medium (Crombez et al., 2016). This method efficiently first represses and subsequently induces LRP development, but the effect of early hormone treatments on many auxin induced or repressed genes is so far uncertain. Additionally, seeds are reported to not germinate well in presence of NPA (Crombez et al., 2016). Therefore, the need of pre-growth without hormone treatment leads to an increasing variability in LRP stages.

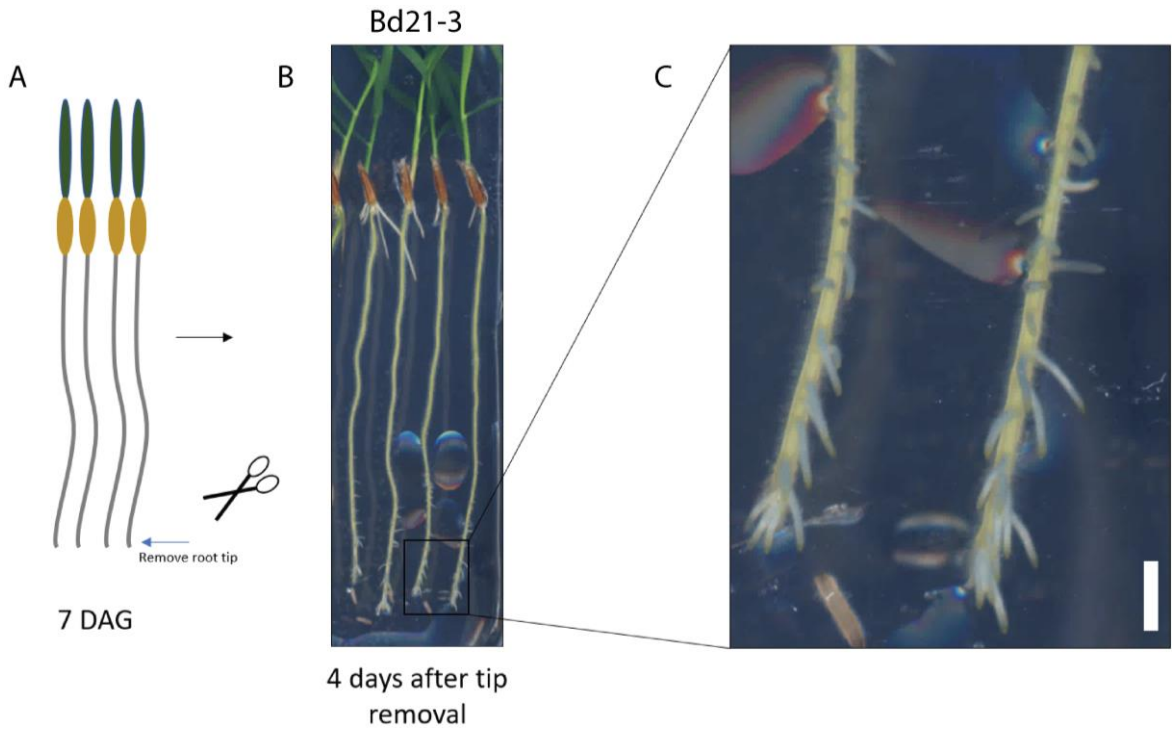

Figure 4. Compensatory LR growth following root tip excision as an LR Induction System (LRIs). (**A**) Representation of plants were grown on ½ MS medium for 7 days before the root tip was excised. (**B**, **C**) After 4 days, LRs near the excision site showed visually homogeneous emergence. This observation prompted us to explore this method as a potential system for inducing lateral root formation. Scale bar: 3 mm.

A different method involves root tip excision (RTE) to stimulate compensatory LR growth. For instance, cutting the main root tip in rice promotes LR development and branching in the proximal sections (Sasaki *et al*., 1984; Kawai *et al*., 2017; Kawai *et al*., 2022). Kawai *et al*. (2022) used this approach to analyze compensatory root growth in rice through RTE, but the authors did not perform any LRP morphological staging. The first question, therefore, is when to remove the root tip after germination. To investigate this, Bd21 and Bd21-3 plants were grown for 2, 3, 4, 5, 6, and 7 days. We then removed the root tip after each respective period of growth and plants were incubated an additional five days under standard growth conditions. Plants with shorter growth periods (2, 3, and 4 days) did not present emerged LRs but instead promoted the growth of adventitious roots. In contrast, plants that grew for at least five days produced LRs after RTE (**Figure 4**).

Additionally, LR with similar sizes were observed in an area about 5 mm from the root tip (**Figure 4C**). This finding suggests that Brachypodium seedlings need to grow at least 5 to 7 days for optimal application of RTE as a LRIS and LRs formed closer to the root excision are more likely to exhibit a similar developmental stage.

Next, the timing of LR initiation following root tip excision in Bd21-3 seedlings grown for six days was investigated. 15 seedlings per timepoints (0h, 1h, 2h, 4h, 6h, 8h, 12h, 16h, 24h, and 32h) were grown and each experiment was repeated 3 times. After excising the root tips, seedlings were returned to the growth chamber, and 5 mm of root tissue above the cut was harvested at specified time points.

The samples were fixed and cleared using the DEEP-Clear protocol and stained with propidium iodine to visualize nuclei. Notably, despite root tip removal, 100% of LRPs in Brachypodium develop predominantly from the phloem associated pericycle cells in contact with the growth medium. A LR staging system is described in detail in Chapter 4 and based on (Malamy and Benfey, 1997), was applied for classifying the developmental staging of LRPs. Brachypodium LRP staging was performed consistently within the first 3 mm after RTE, with one LRP staged per segment of 1 mm. Most LRPs were fully emerged at 32 hours after root tip removal (**Figure 5**), while initial cell divisions in the pericycle were already observed after 1 hour (**Figure 5**). Cell divisions in the endodermis occurred after 2 hours (**Figure 5**), and by the 4-hour mark, divisions were also noted in the cortex near the LRP (**Figure 5**). Root cap formation typically occurred between 12 and 16 hours (**Figure 5**). Intriguingly, although many LRPs reached Stage 9 (approaching the exodermis) by earlier time points, crossing the exodermis was only accomplished at 32 hours after RTE. These results suggest that this approach offers a degree of synchronization of LR development in Brachypodium.

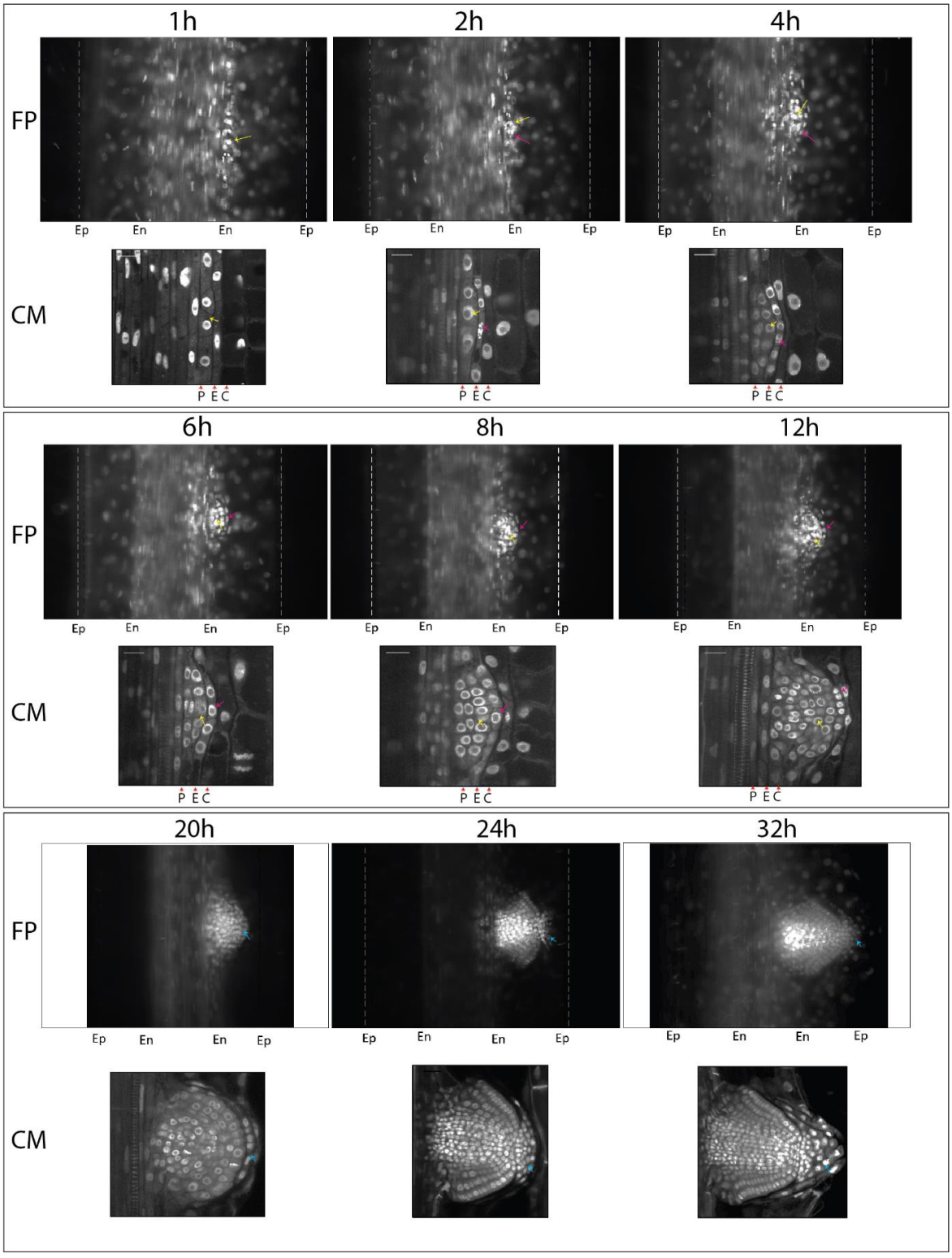

Figure 5: Root tip excision triggers cell divisions in the pericycle within 1 hour and LR emergence after approximately 32 hours. Root tip excision synchronizes LRP development at predefined time intervals following the removal of the root tip. Clearing with DEEP-Clear and staining with propidium iodide enables visualization of LRPs from the initial cell divisions in the pericycle, employing both fluorescence microscopy (**FP**) and confocal microscopy (**CM**). Yellow arrowheads indicate cell divisions in the pericycle; purple arrowheads denote cell divisions in the endodermis; blue arrowheads highlight the formation of the columella and root cap. Ep: Epidermis, En, E: Endodermis, P: Pericycle. Scale bars: 100 µm in **FP** and 100 µm **CM**.

4 Discussion and applications

The advancement of plant transformation techniques has enabled the construction of a variety of mutants and reporter lines in Arabidopsis (Yaschenko, Alonso and Stepanova, 2024). Despite initial challenges, mutants are gradually becoming available in the model plant Brachypodium (O'Connor et al., 2017; Raissig and Woods, 2021). In this chapter, we demonstrate that systematic preparation and sterilization of Brachypodium seeds are essential for standard growth and preventing contamination on agar plates. Similar approaches have been used for rice and barley (Inukai et al., 2005; Lou et al., 2022); however, adaptations are necessary to ensure Brachypodium roots grow parallel to the agar, such as careful attention to the angle of the plates. This is crucial to allow seedlings to grow on plates long enough to start producing LRs. Despite showing features that make it an excellent plant model for LR studies in lab-controlled conditions, *Brachypodium* roots have a more complex structure compared to Arabidopsis, which complicates live cell imaging of deep tissues such as the pericycle. We initially tested Clear-See (Kurihara et al., 2015) on Brachypodium roots. However, this was unsuccessful due to increased oxidation causing brown pigmentation in the roots, likely caused by the presence of sodium carboxylate in the original ClearSee protocol, as suggested by Richardson et al. (2021). Although ClearSee is compatible with a wide range of plant species, tissue browning has also been reported in tobacco and tomato (Kurihara et al., 2021). The authors of the original ClearSee protocol subsequently developed an adapted protocol named ClearSeeAlpha (Kurihara et al., 2021); however, we observed that this was incompatible with Basic Fuchsin (staining lignin). Although still being compatible with many FPs, the adding of sodium sulfite to the new protocol might have changed the compatibility of ClearSee with many fluorescence dyes as shown by (Ursache et al., 2018b) for the original protocol.

An adapted version of the DEEP-Clear protocol was used here yielding superior clearing compared to ClearSee and ClearSeeAlpha, while still being compatible with many fluorescent dyes, including Fluorol Yellow. The original DEEP-Clear protocol (Pende et al., 2018) integrates specific elements for in-situ hybridization, although the core urea-based mixture is rather basic and we could show its compatibility with other steps in the ClearSee Protocol with minor changes. Despite the success in clearing Brachypodium roots, it still needs to be tested with a wider range of fluorescent proteins (FPs) and dyes, as well as in other plant species as in (Affaticati *et al.*, 2018; Du *et al.*, 2018; Muntifering *et al.*, 2018; Ursache *et al.*, 2018b; Kurihara *et al.*, 2021).

Finally, we presented a quick and simple method for synchronizing LR development that relies on root tip excision to stimulate compensatory LR growth with root tissue

harvested after predetermined time points based on (Kawai *et al.*, 2022). We observed that phloem pole pericycle cells facing the half MS medium started to divide within the first hour after the root tip excision. Full emergence of the LRP was observed approximately 32 hours later. Compensatory LR growth induced by surgical excision of the main root tip has been reported in various plant species (Torrey 1950; Crossett *et al*. 1975; Biddington and Dearman 1984; Sasaki *et al*. 1984; Van Staden and Ntingane 1996; Vysotskaya *et al*.2001; Xu et al. 2017). In rice, root tip excision of the crown root tip promoted the development of L-type LRs (Sasaki *et al*. 1984), which are thick and long, and capable of producing higher-order LR. However, to this date, an anatomical description of different stages of LRP was not performed using this method. Root bending (Ditengou *et al.*, 2008) was also tested; however, no clear LRP induction in the bending region was observed as shown in *Arabidopsis*. The combination of NPA and NAA (Crombez *et al.*, 2016) was tested for its effects on inhibiting and inducing LR development; although the approach is presented to be successful in maize, the impact of this manipulation on major auxin-responsive genes (Vermeer *et al.*, 2014; Stöckle *et al.*, 2021; Ursache *et al.*, 2021) requires further exploration. In conclusion, improved growth conditions and histological approaches are essential for monitoring the expression patterns of specific genes during LR formation and for elucidating their roles in the process. The described LRI approach could be instrumental for high-resolution transcriptome analysis of cells competent for LRP and subsequent developmental stages.

3.5 APPENDIX: Step by step protocols and chemical references.

Materials Required:

Brachypodium seeds (Bd21, Bd21-3)

- Forceps
- 15 ml Falcon tubes
- 6% bleach solution (with 0.1% Tween)
- Sterile distilled water
- 0.8 - 1% plant agar medium
- ½ Murashige and Skoog (MS) basal medium
- Growth chambers (continuous light, 22°C)
- Growth plates (12x12 cm)
- Paper bags

Husk Removal :

- Carefully remove the husks using forceps, avoiding embryo damage (see **Figure 1a**).
- Pre-select viable seeds by checking for darker and stiffer appearance (non-viable seeds are lighter and softer).

Seed Sterilization :

- Place seeds in a 15 ml Falcon tube filled to 50% capacity – (Tubes can be reused without the need of sterilization).
- Add a 6% bleach solution with 0.1% Tween to fully submerge the seeds.
- Vigorously shake the tube for at least 1 minute to ensure complete seed contact with the solution.
- Remove the solution using a sterile 2 ml pipette (or similar) and wash seeds five times with autoclaved distilled water.
- Ensure complete removal of the bleach solution for optimal germination.

Stratification :

- After sterilization, leave seeds in water in the dark at 4°C for 2-4 days.
- Seeds should enlarge, and embryos become visible, indicating readiness for plating.

Seed Plating :

- Rinse seeds to remove residual bleach.
- Prepare 12x12 cm plates with a 0.8-1% plant agar medium and ½ MS basal medium (no sucrose required).
- For root phenotyping, position one row of no more than 15 seeds, 2 cm from the top of the plate.
- Ensure the embryo faces upward and is not in contact with the medium (see Fig. 1C).

Incubation and Growth :

- Transfer plates to growth chambers with continuous light at 22°C.
- Angle the plates at approximately 20 degrees to prevent root growth into or out of the medium – 15° angle is enough for Bd21-3.
- For Bd21 seeds, increase the angle to prevent roots from growing out of the medium.
- For longer growth (up to 7 days), use larger plates (see appendix for details).
- Alternatively, transfer sterilized seeds directly to soil for greenhouse growth (22°C, 20-hour photoperiod).

Growth in Soil :

- Use a 4:1 vermiculite mixture for soil growth.

- Water frequently during flowering and fertilize weekly from the fourth week.
- Extend the vegetative phase using a 16-hour photoperiod.

Harvesting and Seed Storage :

- Water plants until they appear completely dry and harvest seeds after two weeks.
- Place seeds in paper bags at 37°C for at least two days to reduce humidity.
- Store seeds at room temperature after complete drying.
  Notes: The growth cycle typically lasts 16 weeks but can be shortened to 12 weeks using vernalization. Proper seed handling and storage (e.g., wearing gloves during harvesting) can prolong seed viability for up to 5 years (as per my experience).

Step-by-step summary for the adapted DEEP-Clear Protocol for plant tissues:

Chemicals :

- Urea (Sigma, CAS-No: 57-13-6)
- Triton™ X-100 (Merck CAS-No: 9036-19-5)
- Theed (Sigma, CAS-No.: 140-07-8, Ref: 87600-100ML)
- Sodium sulfite (Sigma, CAS-No: 7757-83-7)
- Calcofluor White M2R (Fluorescent brightener 28) (Polysciences, CAT#4359)
- Rennaissance
- Fluorol Yellow
- Basic Fucsin
- Propdium iodine
- Paraformaldehyde (Merck, CAS-No: 30525-89-4)

Other required materials :

- Vacuum chamber and vacuum pump (for vacuum treatment, mostly for roots)
- Soft brushes (for handling delicate samples)
- Microscope slides chambers and coverslips
- Parafilm or sealing film.

DEEP-Clear solution preparation

Combine the following chemicals in a suitable container:

- 25% Urea (w/v)
- 3% Triton™ X-100 (v/v)
- 6% Theed (v/v)
- Sodium sulfite (final concentration: 50 mM)

Note: Do not use Sodium sulfite in case you intend to stain your samples with Basic Fuchsin.

- Add deionized water to reach the final volume.
- Mix well on a magnetic stirrer for 30 minutes to 1 hour until all chemicals are completely dissolved.

4% PFA (paraformaldehyde) solution preparation.

- Weigh out 4g of paraformaldehyde powder and add to 100 mL of 1X PBS to achieve a final concentration of 4%.
- Place the solution on a magnetic stirrer and heat to approximately 60°C while stirring. Note: Do not exceed 70°C and avoid boiling.
- Gradually increase the pH by adding KOH dropwise until the solution clears.
- Recheck the pH and adjust to approximately 6.9 using HCl.
- Cool the solution before use. Aliquot and store at +4°C for up to a week, or freeze at -20°C for up to two weeks. For best results, use fresh PFA.

Fixation

- Submerge samples in 4% PFA (paraformaldehyde) in 1X PBS for max 2 hour at room temperature with gentle agitation.
- Apply vacuum infiltration: 3 to 5 rounds with slow release of the vaccum. For samples with fluorescent proteins (FPs), perform fixation in a cold room (4°C).
  Notes: Use a soft brush to push the samples into the fixative (in case they float) every vacuum round.

Washing :

- Wash fixed tissues at least 3 times for 1 minute each in 1X PBS. Removal of the fixative is crucial for effective clearing.
- Apply one round of vacuum infiltration with 1x PBS in the last washing step.

Clearing :

- Transfer seedlings to DEEP-Clear solution and incubate at room temperature with gentle agitation. Apply again 3 rounds of gentle vacuum infiltration.
  Note: tissue clearing efficiency is optimized by incubating the samples at 28C at 100 RPM. Use screw-cap glass tubes in a shaking incubator to avoid sample damage. This step is not recommended for samples with FPs.
- Change the DEEP-Clear solution if it turns yellow or brown.

Staining cell walls (Calcofluor White or Renaissance)

- Prepare a 0.1% Calcofluor White or Renaissance solution directly in DEEP-Clear.

- Incubate samples in the stain for 2 hours (Apply 1 round of gentle vacuum infiltration for thicker root tissues).
- Remove the staining solution and rinse once in DEEP-Clear.
- Wash samples overnight in DEEP-Clear.
  Note: Both Calcofluor White or Renaissance are very stable and prolonged washing tend to reduce background noise during imaging acquisition.

Mounting and Imaging :

- Mount seedlings on chambered cover glasses with DEEP-Clear solution for imaging (only for inverted microscopes).
  Note: Chamber cover glasses are helpful to ensure tissue integrity during the mounting. Use slide spacers in case these chambers are not available.
- Image Calcofluor White with a 405 nm excitation and detect at 425-475 nm.
  Note: The DEEP-Clear protocol is compatible with various staining methods. For more details on staining protocols.

Step-by-step summary for RTE-LRIs

Sample material :

- Prepare at least double the number of *Brachypodium* seeds you estimate will be needed for your experiment, to accommodate variability in root growth.
- Allow the seeds to germinate and grow for at least 6 days, ensuring they do not reach the bottom of the plates.

Removing the root tip :

- Open the plates inside a sterile flow hood.
- Using a sterile scalpel, quickly cut the root tip at the point where root hairs begin to grow. Be careful not to push the root into the medium. Use back-and-forth movements with the scalpel to gently make the cut.
- Seal the plate immediately.

Sectioning, collecting root samples, and clearing:

- After the respective time interval, carefully harvest approximately 5 mm of root tissue starting from the cut section.
  Note: Select the seedlings, align them so the root tips are even, and make a single cut across up to 10 seedlings at once. This method reduces exposure to air and speeds up handling time.

- Immediately after sectioning, transfer the root samples to a fixative solution.
- Proceed to clear the samples as previously described to prepare them for microscopic examination.

Image acquisition :

- Mount the samples in DEEP-Clear using slide chambers or spacers to avoid damaging the samples. If using a confocal microscope, start imaging in an orthogonal view to localize the lateral root primordia (LRPs).

  Note: Begin examining samples from later time points to familiarize yourself with the localization of LRPs. Once comfortable, proceed to earlier time points to observe developmental stages. Lower resolution image acquisition can also be performed using a standard fluorescence microscope.

REFERENCE LIST

Affaticati, P. *et al.* (2018) 'X-fact: Xenopus-fast clearing technique', in *Methods in Molecular Biology*. Humana Press Inc., pp. 233–241. Available at: https://doi.org/10.1007/978-1-4939-8784-9_16.

Amtmann, A., Bennett, M.J. and Henry, A. (2022) 'Root Phenotypes for the Future', *Plant, Cell & Environment* [Preprint]. Available at: https://doi.org/10.1111/PCE.14269.

Beeckman, T. and Eshel, A. (2024) *Plant Roots: The Hidden Half, Fifth Edition*. CRC Press. Available at: https://books.google.ch/books?id=FmVx0AEACAAJ.

Casero, P.J., Casimiro, I. and Lloret, P.G. (1995) 'Lateral root initiation by asymmetrical transverse divisions of pericycle cells in four plant species:Raphanus sativus, Helianthus annuus, Zea mays, andDaucus carota', *Protoplasma*, 188(1), pp. 49–58. Available at: https://doi.org/10.1007/BF01276795.

Crombez, H. *et al.* (2016) 'Lateral Root Inducible System in Arabidopsis and Maize', *J. Vis. Exp*, 107, p. 53481. Available at: https://doi.org/10.3791/53481.

Decaestecker, W. *et al.* (2019) 'CRISPR-Tsko: A technique for efficient mutagenesis in specific cell types, tissues, or organs in Arabidopsis[open]', *Plant Cell*, 31(12), pp. 2868–2887. Available at: https://doi.org/10.1105/tpc.19.00454.

Ditengou, F.A. *et al.* (2008) 'Mechanical induction of lateral root initiation in Arabidopsis thaliana', *Proceedings of the National Academy of Sciences of the United States of America*, 105(48), pp. 18818–18823. Available at: https://doi.org/10.1073/pnas.0807814105.

Dolan, L. and Roberts, K. (1995) 'The Development of Cell Pattern in the Root Epidermis', *Philosophical Transactions: Biological Sciences*, 350(1331), pp. 95–99. Available at: http://www.jstor.org/stable/56258.

Du, H. *et al.* (2018) 'Advances in CLARITY-based tissue clearing and imaging (Review)', *Experimental and Therapeutic Medicine* [Preprint]. Available at: https://doi.org/10.3892/etm.2018.6374.

Garvin, D.F. (2007) 'Brachypodium: a new monocot model plant system emerges', *Journal of the Science of Food and Agriculture*, 87(7), pp. 1177–1179. Available at: https://doi.org/10.1002/jsfa.2868.

Hou, B. *et al.* (2015) 'Scalable and DiI-compatible optical clearance of the mammalian brain', *Frontiers in neuroanatomy*, 9, p. 19. Available at: https://doi.org/10.3389/fnana.2015.00019.

Inukai, Y. *et al.* (2005) 'Crown rootless1, which is essential for crown root formation in rice, is a target of an Auxin Response Factor in auxin signaling', *Plant Cell*, 17(5), pp. 1387–1396. Available at: https://doi.org/10.1105/tpc.105.030981.

Kawai, T. *et al.* (2022) 'WUSCHEL-related homeobox family genes in rice control lateral root primordium size', *Proceedings of the National Academy of Sciences of the United States of America*, 119(1). Available at: https://doi.org/10.1073/PNAS.2101846119/-/DCSUPPLEMENTAL.

Keller, P.J. (2013) 'Imaging Morphogenesis: Technological Advances and Biological Insights', *Science*, 340(6137). Available at: https://doi.org/10.1126/science.1234168.

Kenrick, P. and Strullu-Derrien, C. (2014) 'The Origin and Early Evolution of Roots', *PLANT PHYSIOLOGY*, 166(2), pp. 570–580. Available at: https://doi.org/10.1104/pp.114.244517.

Kurihara, D. *et al.* (2015) 'ClearSee: a rapid optical clearing reagent for whole-plant fluorescence imaging.', *Development (Cambridge, England)*, 142(23), pp. 4168–79. Available at: https://doi.org/10.1242/dev.127613.

Kurihara, D. *et al.* (2021) 'ClearSeeAlpha: Advanced Optical Clearing for Whole-Plant Imaging', *Plant and Cell Physiology* [Preprint]. Available at: https://doi.org/10.1093/pcp/pcab033.

Kurihara, D. *et al.* (2022) 'Optical Clearing of Plant Tissues for Fluorescence Imaging', *JoVE (Journal of Visualized Experiments)*, 2021(179), p. e63428. Available at: https://doi.org/10.3791/63428.

Lavenus, J. *et al.* (2013) 'Lateral root development in Arabidopsis: Fifty shades of auxin', *Trends in Plant Science*, 18(8), pp. 1360–1385. Available at: https://doi.org/10.1016/j.tplants.2013.04.006.

Lindsey III, B.E. *et al.* (2017) 'Standardized Method for High-throughput Sterilization of Arabidopsis Seeds', *Journal of Visualized Experiments* [Preprint], (128). Available at: https://doi.org/10.3791/56587.

Lou, H. *et al.* (2022) 'The cellulose synthase-like F3 (CslF3) gene mediates cell wall polysaccharide synthesis and affects root growth and differentiation in barley', *The Plant Journal*, 110(6), pp. 1681–1699. Available at: https://doi.org/10.1111/TPJ.15764.

Malamy, J.E. and Benfey, P.N. (1997) 'Organization and cell differentiation in lateral roots of Arabidopsis thaliana', *Development*, 124(1), pp. 33 LP – 44. Available at: http://dev.biologists.org/content/124/1/33.abstract.

Muntifering, M. *et al.* (2018) 'Clearing for Deep Tissue Imaging', *Current Protocols in Cytometry*, 86(1), pp. 1–33. Available at: https://doi.org/10.1002/cpcy.38.

O'Connor, D.L. *et al.* (2017) 'Cross-species functional diversity within the PIN auxin efflux protein family', *eLife*, 6. Available at: https://doi.org/10.7554/eLife.31804.

Pende, M. *et al.* (2018) 'High-resolution ultramicroscopy of the developing and adult nervous system in optically cleared Drosophila melanogaster', *Nature Communications*, 9(1), pp. 1–12. Available at: https://doi.org/10.1038/s41467-018-07192-z.

Péret, B., Larrieu, A. and Bennett, M.J. (2009) 'Lateral root emergence: A difficult birth', *Journal of Experimental Botany*, 60(13), pp. 3637–3643. Available at: https://doi.org/10.1093/jxb/erp232.

Piccinini, L., Nirina Ramamonjy, F. and Ursache, R. (2024) 'Imaging plant cell walls using fluorescent stains: The beauty is in the details', *Journal of Microscopy* [Preprint]. John Wiley and Sons Inc. Available at: https://doi.org/10.1111/jmi.13289.

Raissig, M.T. and Woods, D.P. (2021) 'The wild grass Brachypodium distachyon as a developmental model system'. Available at: https://zenodo.org/record/5548408.

Richardson, D.S. *et al.* (2021) 'Tissue clearing', *Nature Reviews Methods Primers*, 1(1), p. 84. Available at: https://doi.org/10.1038/s43586-021-00080-9.

Richardson, D.S. and Lichtman, J.W. (2015) 'Clarifying Tissue Clearing', *Cell*, 162(2), pp. 246–257. Available at: https://doi.org/10.1016/j.cell.2015.06.067.

Sauer and Burroughs (1986) 'Disinfection of Seed Surfaces with Sodium Hypochlorite ', *Journal of Plant Tech*, 6(1986), pp. 1–6.

Van Der Schuren (2019) *Characterization of Brachypodium distachyon Root Development*. Available at: http://serval.unil.chhttp://serval.unil.ch.

Stöckle, D. *et al.* (2021) 'Microtubule-based perception of mechanical conflicts controls plant organ morphogenesis', *bioRxiv*, p. 2021.09.09.459674. Available at: https://doi.org/10.1101/2021.09.09.459674.

Stoeckle, D., Thellmann, M. and Vermeer, J.E. (2018) 'Breakout — lateral root emergence in Arabidopsis thaliana', *Current Opinion in Plant Biology*. Elsevier Ltd, pp. 67–72. Available at: https://doi.org/10.1016/j.pbi.2017.09.005.

Ueda, H.R. *et al.* (2020) 'Tissue clearing and its applications in neuroscience', *Nature Reviews Neuroscience*. Nature Research, pp. 61–79. Available at: https://doi.org/10.1038/s41583-019-0250-1.

Ursache, R. *et al.* (2018a) 'A protocol for combining fluorescent proteins with histological stains for diverse cell wall components', *Plant Journal*, 93(2), pp. 399–412. Available at: https://doi.org/10.1111/tpj.13784.

Ursache, R. *et al.* (2018b) 'A protocol for combining fluorescent proteins with histological stains for diverse cell wall components', *The Plant Journal*, 93(2), pp. 399–412. Available at: https://doi.org/10.1111/tpj.13784.

Ursache, R. *et al.* (2021) 'GDSL-domain proteins have key roles in suberin polymerization and degradation', *Nature Plants*, 7(3), pp. 353–364. Available at: https://doi.org/10.1038/s41477-021-00862-9.

Vermeer, J.E.M. *et al.* (2014) 'A spatial accommodation by neighboring cells is required for organ initiation in arabidopsis', *Science*, 343(6167), pp. 178–183. Available at: https://doi.org/10.1126/SCIENCE.1245871.

Vogel, J. (2008) 'Unique aspects of the grass cell wall', *Current Opinion in Plant Biology*, 11(3), pp. 301–307. Available at: https://doi.org/10.1016/j.pbi.2008.03.002.

Voß, U. *et al.* (2015) 'The circadian clock rephases during lateral root organ initiation in Arabidopsis thaliana', *Nature Communications*, 6(1), p. 7641. Available at: https://doi.org/10.1038/ncomms8641.

Warner, C.A. *et al.* (2014) 'An optical clearing technique for plant tissues allowing deep imaging and compatible with fluorescence microscopy', *Plant Physiology*, 166(4), pp. 1684–1687. Available at: https://doi.org/10.1104/pp.114.244673.

Weigel & Glazebrook (2002) 'Arabidopsis: A Laboratory Manual. D. WEIGEL & J. GLAZEBROOK Cold Spring Harbor Laboratory Press. 2002. 354 pages. ISBN 0 87969 573 0.', *Genetical Research*, 80(1), pp. 77–77. Available at: https://doi.org/10.1017/S0016672302215852.

Yaschenko, A.E., Alonso, J.M. and Stepanova, A.N. (2024) ‘Arabidopsis as a model for translational research’, *The Plant Cell* [Preprint]. Available at: https://doi.org/10.1093/plcell/koae065.

Yu, P., Hochholdinger, F. and Li, C. (2019) ‘Plasticity of Lateral Root Branching in Maize’, *Frontiers in Plant Science*, 10. Available at: https://doi.org/10.3389/fpls.2019.00363.

CHAPTER 4

3. An atlas of *Brachypodium distachyon* lateral root development.

Cristovao De Jesus Vieira Teixeira[1], Kevin Bellande[1,3], Alja van der Schuren[2], Devin O'Connor[4#], Christian S. Hardtke[2] and Joop EM Vermeer[1*].

1. Laboratory of Molecular and Cell Biology, Institute of Biology, University of Neuchâtel, Switzerland.

2. Department of Plant Molecular Biology, University of Lausanne, Lausanne, Switzerland.

3. IPSiM, University of Montpellier, CNRS, INRAE, Institut Agro, Montpellier, France

4. Sainsbury Lab, University of Cambridge, Cambridge, U.K.

* Corresponding author: Joop.Vermeer@unine.ch

[#] current address: Pairwise, Durham, North-Carolina, USA.

Author contributions:

Cristovao De Jesus Vieira Teixeira conducted the experiments, image processing, figure assembly, and wrote the chapter, with the exception of Fig. S5, where the images were acquired by *Dr. Kevin Bellande*. The other authors provided biological material and valuable suggestions and corrections throughout.

*This work has been published in Biology Open (https://doi.org/10.1242/bio.060531)

4.1 Abstract

The root system of plants is a vital part for successful development and adaptation to different soil types and environments. A major determinant of the shape of a plant root system is the formation of lateral roots, allowing for expansion of the root system. *Arabidopsis thaliana*, with its simple root anatomy, has been extensively studied to reveal the genetic program underlying root branching. However, to get a more general understanding of lateral root development, comparative studies in species with a more complex root anatomy are required. Here, by combining optimized clearing methods and histology, we describe an atlas of lateral root development in *Brachypodium distachyon*, a wild, temperate grass species. We show that lateral roots initiate from enlarged phloem pole pericycle cells and that the overlying endodermis reactivates its cell cycle and eventually forms the root cap. In addition, auxin signaling reported by the DR5 reporter was not detected in the phloem pole pericycle cells or young primordia. In contrast, auxin signaling was activated in the overlying cell cortical layers, including the exodermis. Thus, Brachypodium is a valuable model to investigate how signaling pathways and cellular responses have been repurposed to facilitate lateral root organogenesis.

Key words: *Brachypodium distachyon*, lateral roots, endodermis, exodermis, organogenesis.

4.2 Introduction

Root branching is vital for plant survival as it facilitates the uptake of water and nutrients (Orosa-Puente *et al.*, 2018). Root system architecture (RSA) consists of structural features like root length, spread, number, and length of lateral roots (LRs), among others (Bao *et al.*, 2014; Morris *et al.*, 2017; Kumar *et al.*, 2019). RSA exhibits great plasticity in response to environmental changes and it is a desirable trait to breed more resilient crops (Ye *et al.*, 2017; Yu, Hochholdinger and Li, 2019; Schäfer *et al.*, 2022). In both monocots and dicots, the growth angle and number of LRs are the central components of the overall RSA (Atkinson *et al.*, 2014; Roychoudhry *et al.*, 2017). However, the molecular and cell biological program underlying root branching are less described for major crops due to the difficulty of observing the root system throughout the plant's life cycle (Hochholdinger and Zimmermann, 2008).

Due to the relatively simple organization of its root system, tissue transparency and extensive genetic tool box, *Arabidopsis thaliana* (Arabidopsis) has been the most characterized experimental system for dissecting the molecular mechanisms underlying LR development (Banda *et al.*, 2019). In Arabidopsis, LRs initiate from Lateral Root Founder Cells (LRFCs), and a series of highly coordinated cell divisions leads to the development of a new LR primordium (LRP) (Casimiro *et al.*, 2001; Ditengou *et al.*, 2008; Stoeckle, Thellmann and Vermeer, 2018; Gala *et al.*, 2021). In this case, LRFCs are patterned along the primary root axis with a regulated spacing, beginning from the basal root meristem (Lavenus *et al.*, 2015; Chen *et al.*, 2018; Kircher and Schopfer, 2018; Torres-Martínez *et al.*, 2020). Early stage LRP are more likely initiated closer to the root tip. The first morphological event of LR initiation takes place in the differentiation zone where LRFC founders cells divide asymmetrically and anticlinal (Malamy and Benfey, 1997). In addition, auxin signaling in the neighboring endodermis plays a major role during LRP formation as blocking auxin responses in this tissue abolishes LR formation (Vermeer, et al., 2014). Subsequent periclinal and anticlinal divisions give rise to an organized dome shaped LRP (Malamy and Benfey, 1997).

In monocots, LR studies have mostly been conducted on rice and maize (Wang *et al.*, 2002; Hochholdinger and Zimmermann, 2008; Jansen *et al.*, 2012; Uga *et al.*, 2013). Notably, LR initiation in monocots predominantly occurs in the phloem-associated pericycle (Jansen et al., 2013; Hardtke and Pacheco-Villalobos, 2015) and the underlying mechanisms governing the patterning of LR formation in these agriculturally important crops are not well described. In contrast to Arabidopsis, in monocots and many other plant species, during LR development both the pericycle and endodermis undergo cell divisions,

thereby contributing to the formation of the new organ (Casero, Casimiro and Lloret, 1995; Rebouillat *et al.*, 2009; Banda *et al.*, 2019; Xiao *et al.*, 2019). However, only few studies have investigated the auxin-mediated transcriptome changes underlying LRP formation in monocots (Stelpflug *et al.*, 2016; Kortz, Hochholdinger and Yu, 2019). Moreover, it is still unknown which signal is regulating the cell divisions in the endodermis overlying the newly formed LR.

The endodermis is the innermost cortical cell layer surrounding the vasculature (Geldner, 2013). Casparian strips (CS) and suberin lamellae (SL) formed in this layer were shown to be crucial in regulating the uptake of nutrients, in the response to osmotic stress and protection against pathogens (Ranathunge *et al.*, 2008; Barberon *et al.*, 2016). Additionally, a wide range of plant species have an extra apoplastic diffusion barrier localized just beneath the epidermis, known as the hypodermis or exodermis (Enstone, Peterson and Ma, 2002). The term exodermis is used when the hypodermis contains a localized lignification and suberin deposition in its cell walls, serving a similar barrier function as the endodermis (Enstone, Peterson and Ma, 2002; Kajala *et al.*, 2021; Manzano *et al.*, 2022). The exodermis differs from the endodermis in its pattern of differentiation. In maize roots for instance, the CS follows a synchronous development pattern, as ring-like structures, within the entire endodermis. In later stages of development, the CS increase in width, thereby enclosing the entire central cylinder (Enstone, Peterson and Ma, 2002). The SLs are deposited later, but less synchronously, starting from a patchy zone that will develop in a fully suberized endodermis (with exception from the passage cells), depending on the growth conditions (Enstone, Peterson and Ma, 2002; Kreszies *et al.*, 2020; Andersen *et al.*, 2021; Sexauer *et al.*, 2021). In contrast, the development of the exodermis in maize is rather irregular in both radial and longitudinal directions (Líška *et al.*, 2016). A recent study has also shown that suberization in the exodermis is essential for survival of tomato under drought conditions, revealing an important physiological function for this cell type (Cantó-Pastor *et al.*, 2024). However, we still lack insights on how these two layers are involved in the emergence of the LRP.

Using crop plants for conducting LR studies is a challenging task due to their demanding growth requirements (Garvin, 2007; Scholthof *et al.*, 2018). Instead, the wild grass *Brachypodium distachyon* (Brachypodium), possesses several characteristics that make it an excellent monocot model for studying LR development (Raissig and Woods, 2021). Brachypodium has a relatively small genome size, simple growth requirements, fast regeneration time, and exhibits self-pollination. Its embryonic root anatomy consists of a single axial primary root with seminal and leaf node roots developing later depending on the growth conditions. The general radial organization of the primary root consists of an

epidermis, five cortex layers, and a single endodermis (Hardtke and Pacheco-Villalobos, 2015). The stele is surrounded by a single pericycle, and the vasculature is arranged with alternating xylem and phloem poles. Most of the above features are closely similar to root anatomy described in major cereal crops (Chochois, Vogel and Watt, 2012; Hardtke and Pacheco-Villalobos, 2015; Raissig and Woods, 2021) including the site of LR initiation (Yu *et al.*, 2016). For instance, in rice, maize and barley LRs initiate from cell divisions in pericycle cells associated to the protophloem, so-called phloem pole pericycle cells (Jansen *et al.*, 2013; Ni *et al.*, 2014; Xiao *et al.*, 2019). Thus, the Brachypodium root system exhibits a high degree of developmental and anatomical similarity to important cereal crops, but with less complexity.

In this study, we present a developmental atlas describing the developmental stages of LR development in Brachypodium. We show that the endodermis reactivates its cell cycle and appears to contribute to the formation of the root cap and the formation of columella cells of the emerged LRs. Furthermore, our results indicate the auxin signaling as reported by DR5 promoter activity is not evident in the phloem pole pericycle and during the early stages of LR development. Instead, auxin responses rather appear to be correlated with cell wall modifications during the emergence of the LRP. We show that early suberin deposition in roots appear to be controlled by water and nutrient availability and LRPs emerge towards the growth medium. Finally, we show that the lignification pattern in the exodermis suggests a possible role in the timing of LRP emergence.

RESULTS

4.3.1 Lateral roots initiate from phloem pole pericycle cells in Brachypodium

To characterize the sequential developmental stages during LR development in the Brachypodium accession Bd21-3, we adapted the DEEP-CLEAR (Pende *et al.*, 2020) protocol for plant tissue to clear roots and used propidium iodide (PI) to visualize the nuclei of the cleared roots via multiphoton microscopy (Fig. 1, Fig. S1). To categorize the LRP development in Brachypodium, we used the model described for Arabidopsis (Malamy and Benfey, 1997) with a few adaptations in the later developmental stages:

Stage I: Cell divisions occurring in pericycle cells adjacent to the phloem poles (between two xylem poles) are the first anatomical signs of LR initiation (Fig. 1B, C, Fig. S1B).

Stage II: This stage is marked by the initiation of the first anticlinal cell divisions in the endodermal cells overlying a stage I LRP. Subsequently, the cells within the LRP undergo periclinal while endodermal cells continue to divide anticlinal (Fig. 1D, Fig. S1C).

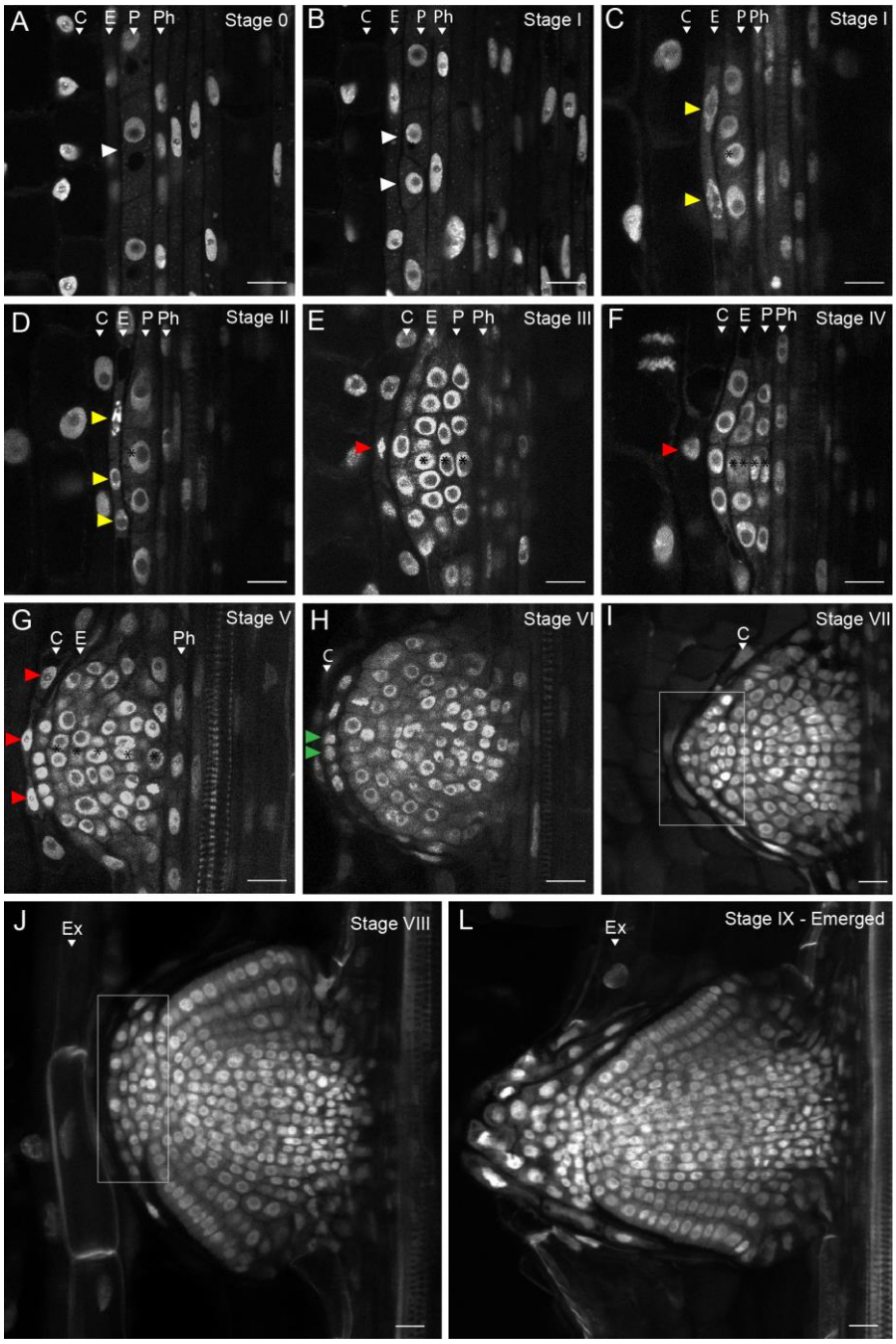

Fig. 1. Different stages of LRP development in Brachypodium. (**A**) Stage **0**: No discernible cell divisions in the pericycle cells. (**B**) Stage **I**: White arrows indicate the first anticlinal cell division in the pericycle. (**C**) Stage **I**: Yellow arrows indicate the flattening of the endodermal cells preceding the cell divisions in the next stage. (**D**) Stage II: The endodermis starts to divide anticlinal (yellow arrows). (**E**) Stage **III**: Periclinal divisions take place at the center of the LRP resulting in three layers of cells. The red arrow indicates cell divisions in the overlying cortex. (**F**) Stage **IV**: The LRP undergoes radial expansion through constant anticlinal and periclinal cell divisions in the center of the LRP. Four pericycle cell layers can be observed. (**G**) Stage **V**: Five to six pericycle cell layers can still be distinguished. LRP boundaries are established, and the endodermis appears to become integrated in the LRP. Red arrows indicate more cell divisions in the cortex layer in the vicinity of the LRP. (**H**) Stage **VI**: The endodermal cells on the apex of the LRP start to divide again (green arrows). Pericycle cell layer counting is no longer used from this stage. (**I**) Stage **VII**: Formation of the root cap (white rectangular area. (**J**) Stage **VIII**: The LRP reaches the root exodermis. (**K**) Stage **IX**: Emerged: The LRP is fully formed and traverses the exodermis and epidermis. (**Ex**) Exodermis, (**C**) Cortex, (**E**) Endodermis, (**P**) Pericycle (**Ph**) Phloem. Representative images were obtained from 45 seedling roots from three independent replicates each consisting of at least 15 plants of Bd21-3. Samples were cleared with DEEP-Clear and stained with 0.01% propidium iodide. Scale bar = 20 μm.

Stage III: Periclinal divisions occur in the center of the LRP resulting in the formation of three layers of cells. In parallel, the endodermis continues to divide anticlinal forming a boundary that span the entire LRP. Additionally, the innermost cortex cell layer, in contact with the endodermis, appears to flatten (Fig. 1E, Fig. S1D).

Stage IV: This stage is characterized by ongoing radial expansion of the LRP through additional anticlinal and periclinal divisions in its central region (Fig. 1F).

As a result, the canonical dome shape begins to become apparent, and four layers of cells can be counted. Furthermore, ongoing anticlinal cell divisions in the first cortex cell layer were observed, although these cells did not appear to become incorporated in the LRP (Fig. 1F).

Stage V: Five distinct cortex cell layers remain discernible. The LRP boundaries become well-defined, and the cell divisions patterns indicate that the endodermis-derived cells are integrated within the LRP (Fig. 1G, Fig. S1E).

Stage VI: In this stage the first periclinal endodermal cell divisions occur at the apex of the LRP suggesting the initiation of the lateral root cap formation (Fig. 1H, Fig. S1E). On average, LRP still have six to seven layers of cells. However, due to the increasing number of cell divisions in the central part of the LRP, it is impossible to apply the cell layer counting system for the remaining LRP developmental stages.

Stage VII: The LRP resembles a mature root tip containing an early developmental stage of the lateral root cap that continues to divide anticlinal (Fig. 1I, Fig. S1F)

Stage VIII: At this stage the LRP reaches the exodermis.

Stage IX: The LRP crosses the exodermis and epidermis characterizing its full emergence towards the root surface. Fig. S2 shows an illustration for the LRP developmental stages in Brachypodium.

4.3.2 *DR5pro::ER-mRFP* does not detect transcriptional auxin responses during early stages of LR development

The phytohormone auxin plays a crucial role during all stages of LRP development in many plant species including important cereal crops such as rice (Lin and Sauter, 2019), maize (Yu, Hochholdinger and Li, 2019) and barley (Kirschner *et al.*, 2017). However, most of the insights on how auxin signaling coordinates LR development comes from studies in Arabidopsis (Fukaki and Tasaka, 2009; Vermeer *et al.*, 2014; Guseman *et al.*, 2015; Cavallari, Artner and Benkova, 2021), and much less is known whether discrete auxin-driven developmental modules have a similar role in monocots. To characterize transcriptional responses to auxin during LR development, we utilized a *DR5pro::ER-mRFP* marker line

(van der Schuren *et al.*, 2018). In contrast to what was described for LR initiation in maize (Jansen *et al.*, 2013) we were unable to observe a clear *DR5pro::ER-mRFP* signal in phloem pole pericycle cells and in **Stages I**-**II** LRP (Fig. 2A, B); thus, making it challenging to correlate tissue specific changes in auxin responses with LRFC specification and LR initiation. We did observe a weak *DR5pro::ER-mRFP* signal in the endodermis and most inner cortex cells overlying stage I-II LRP (Fig. 2A, B). The earliest detectable *DR5pro::ER-mRFP* signal in the LRP was only observed at **Stage III**, when the endodermis is already actively dividing (Fig. 2C). In later stages, the *DR5pro::ER-mRFP* signal was no longer detected in the endodermis but it gradually intensified at the apex of the growing LRP (Fig. 2D). As the LRP developed (Stages **IV** to **VIII**), we observed an increased *DR5pro::ER-mRFP* signal in the cortical cell layers overlying the developing LRP (Fig. 2D, E). Prior to and after to emergence, the DR5pro::ER-mRFP signal in the newly-formed LR exhibited an expression pattern comparable to the tip of the main root (Fig. 2E-G and Fig. S4). Notably, we also observed a clear *DR5pro::ER-mRFP* signal in the exodermis cells overlying the LRP (Fig. S4). Although we have observed that Brachypodium LR development is induced under auxin treatment (Fig. S6), we failed to detect a *DR5pro::ER-mRFP* signal in **stage I** LRP.

Based on these observations, we characterized whether SISTER of PIN-FORMED 1 (SoPIN1) and AUXIN RESISTANT 1 (AUX1), known transporters involved in auxin efflux and import, respectively, were expressed in early stage LRP (Marchant *et al.*, 2002; Reinhardt *et al.*, 2003; O'Connor *et al.*, 2017). Although we were unable to detect *DR5pro::ER-mRFP* during LR initiation, the presence of SoPIN1-Citrine was evident as early as **Stage I** (Fig. S5A). Later, signal was observed in the endodermis coinciding with its initial cell divisions in the endodermis **Stage II** (Fig. S5A). Subsequently, in later stages, SoPIN1-Citrine expression became predominantly localized in the central region of the LRP (Fig. S5A). Conversely, AUX1-sGFP exhibited expression within the LRP starting from **Stage I** initially in the phloem-pole pericycle and in the flanking regions with its intensity increasing subsequently in both the vasculature and endodermis (**Stages III** to **V**). Robust expression within the vasculature was also observed in **Stage V** and **VI** (Fig. S5B).

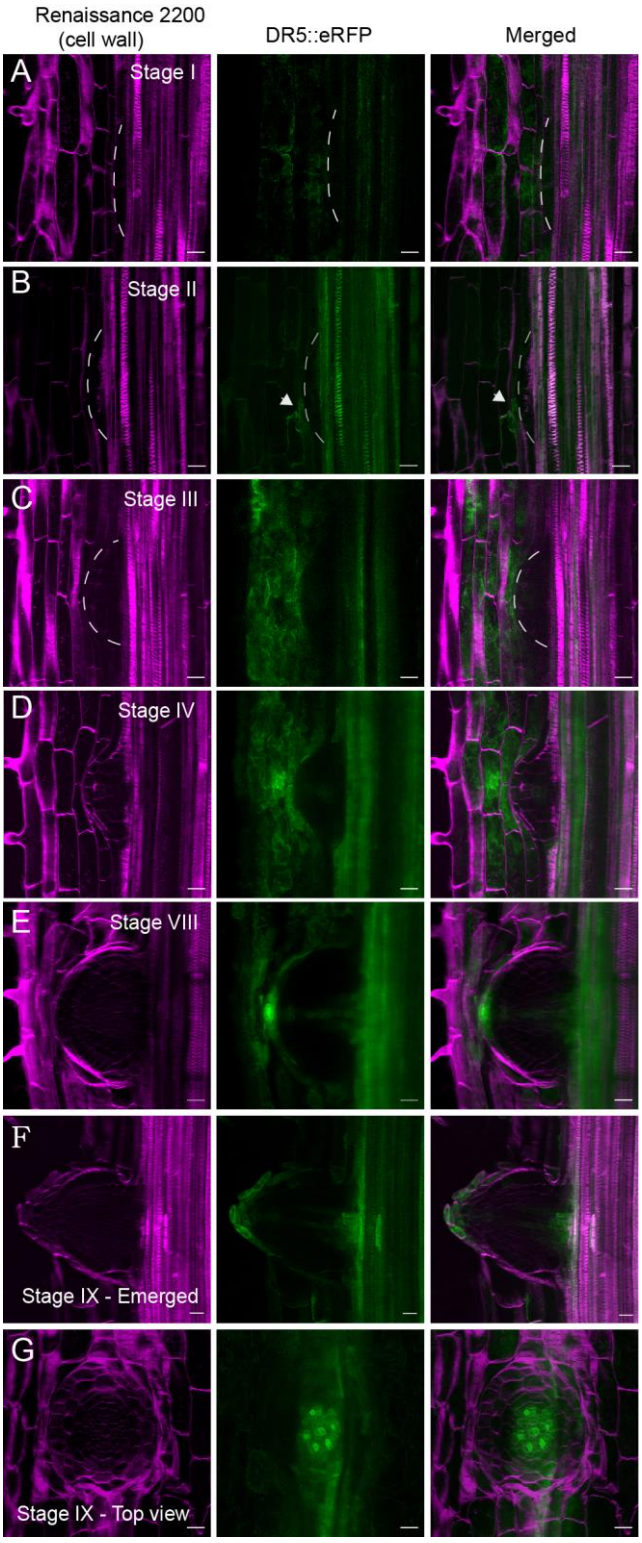

Fig. 2. *DR5pro::ER-mRFP* activity during LR development in Brachypodium. (**A**) The DR5 signal is not evident in Stage I during the first pericycle cell divisions. (**B**) The DR5 signal could be observed in Stage II when the endodermis starts to divide (white arrowheads). (**C**, **D**) The DR5 signal is no longer observed in the endodermis but in the cortex cell layer in the vicinity of the LRP and in the central part of the LRP resembling vasculature. (**E**) The DR5 signal is intensified at the apex of the LRP, in the vasculature, and in the last cortex cell layer. (**F, G**) A fully emerged LR shows a similar DR5 pattern as usually observed in the primary root. Representative images were obtained from 45 seedlings from three independent replicates each consisting of at least 15 plants of Bd21-3. *DR5pro::ER-mRFP* (green) and cell walls stained with SCRI Renaissance (magenta) for cellulose. Scale = 50 μm.

4.3.3 Endodermal-derived cells form the root cap of new LRs.

Next, we investigated whether the endodermal cells that reactivated their cell cycle and underwent anticlinal and periclinal divisions contribute to the formation of the columella of the LRP. Starch granule formation serves as a marker for differentiation of the columella cells (Guyomarc'h *et al.*, 2012; Roychoudhry *et al.*, 2023).

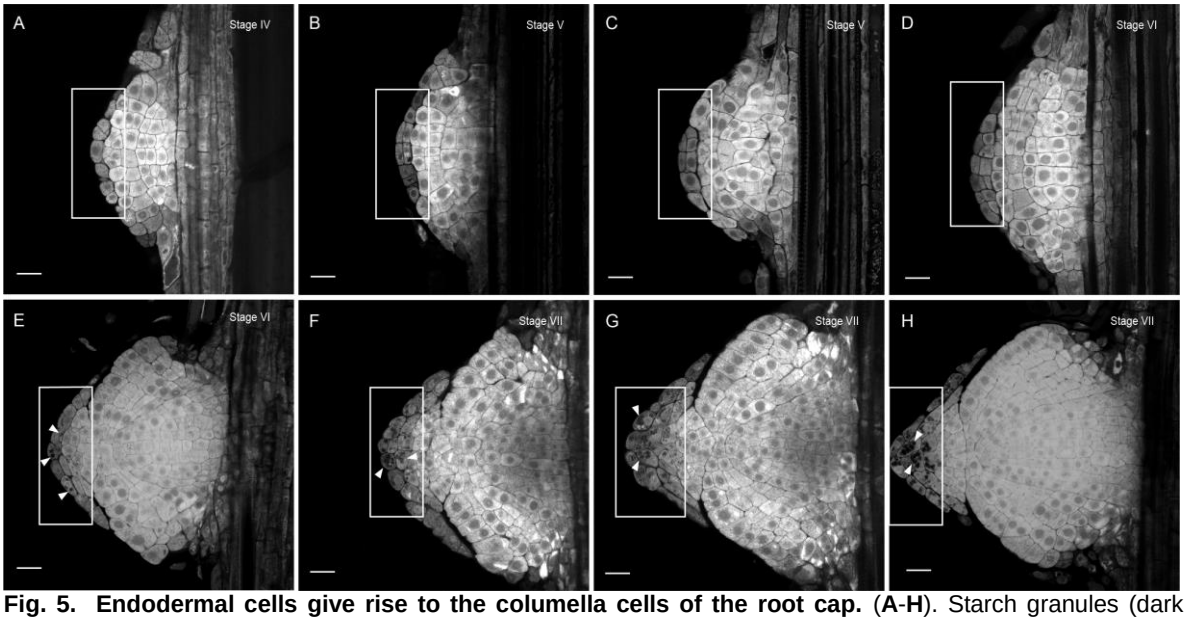

Fig. 5. Endodermal cells give rise to the columella cells of the root cap. (**A**-**H**). Starch granules (dark structures in boxed area) were detected using Lugol staining. The boxed area shows cell divisions in the endodermis and its progression in differentiating into columella cells from Stage VI (**E**) to Stage VII (**H**) marked by the sediments of starch granules (arrowheads) in the first cell layer on the apex of the LRP in Stage VI. Representative images were obtained from 30 seedlings from three independent replicates, each consisting of at least 10 plants of Bd21-3. The root cortex was mechanically removed with forceps preserving the LRPs integrity. Samples were cleared with DEEP-Clear and stained with Lugol. Scale = 50 µm.

To assess columella formation, we utilized Lugol's staining in conjunction with our histological clearing approach. Columella cells (Boxed area in Fig. 5) were characterised by the presence of sediments of amyloplasts. Even though the endodermis starts to undergo periclinal divisions from **Stage V** (Fig. 5B, C), starch accumulation was only observed in the first cell layer of the columella during late **Stage VI-VII** (Fig. 5E, F), following numerous rounds of periclinal cell divisions. The intensity of Lugol's staining gradually intensified from **Stage VII** to the fully emerged LRP (Fig. 5H).

4.3.4 Suberin deposition in the exodermis of Brachypodium roots is delayed compared to the endodermis.

During the growth of Brachypodium seedlings on plate, we observed a very strong hydropatterning effect (Fig. S3) (Orosa-Puente *et al.*, 2018). Basically, all LRs emerged on the side of the root in contact with the growth medium. It is proposed that hydropatterning serves to ensure roots have access with to water and nutrients (Möller, Xuan and Beeckman, 2017).

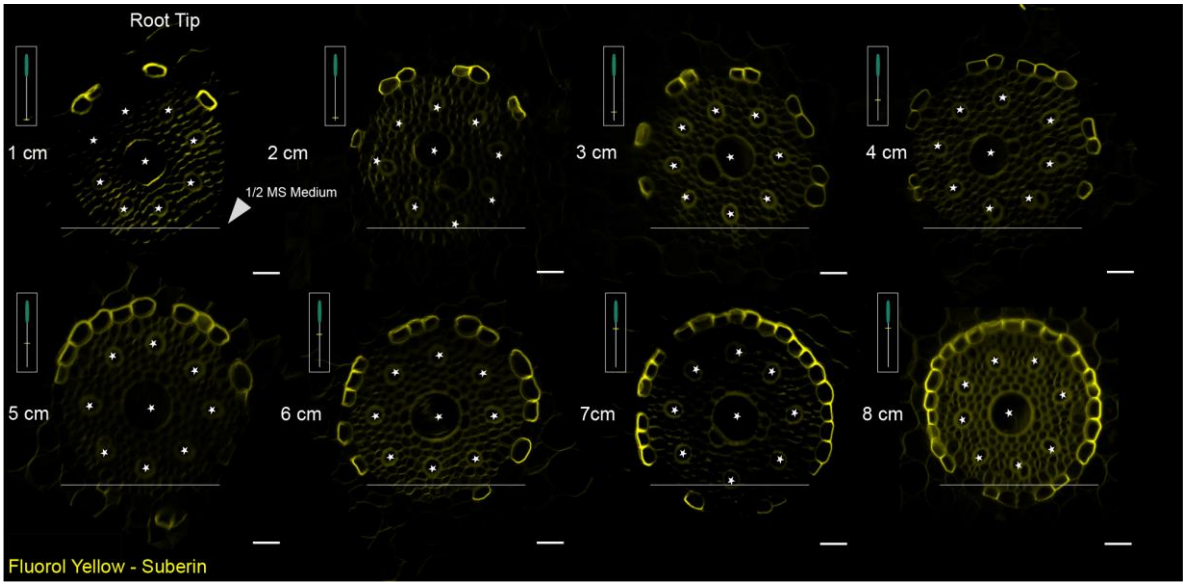

Fig. 3. Pattern of endodermal suberization along the Brachypodium root axis adjacent to the nutrient medium growth. Cross-sections of Brachypodium primary root showing asymmetric suberization. Suberin lamellae (SL) developed unilaterally on the side of the root exposed to the air from the root apex, but not on the side exposed to nutrient medium. Representative images were obtained from 30 seedlings of Bd21-3 from three independent replicates, each consisting of at least 10 plants. Roots of similar length were positioned in parallel for consistency, and regions of interest of approximately 1 cm were sectioned. Scale = 20 *µm*.

Brachypodium, like many monocots, has an additional cell layer that undergoes localized suberin deposition, the exodermis (Sexauer *et al.*, 2021). Using Fluorol Yellow (FY) staining of cleared roots, we confirmed that the pattern of endodermal and exodermal suberization in Brachypodium also occurs after CS establishment initially with patchy zones for both the endodermis and exodermis (Fig. 3, Fig. S7B). This observation is consistent with the findings reported in rice, barley and tomato (Cai *et al.*, 2011; Líška *et al.*, 2016; Cantó-Pastor *et al.*, 2024). Interestingly, suberization in the exodermis appeared delayed compared to suberin deposition in the endodermis (Fig. S7B). As previously reported in maize, Brachypodium, when grown vertically on agar plates, shows that endodermis and exodermis cells closest to the growth medium are the last to deposit suberin (Fig. 3).

4.3.5 Dividing endodermal cells overlying the LRP appear not to establish a Casparian strip.

The participation of the endodermis during LR organogenesis in Brachypodium is not unique, as it has been demonstrated already for a range of plant species (Xiao *et al.*, 2019). Although we could not observe suberin deposition in the endodermis overlying the LRP under our growth conditions, the Casparian strip domain (CSD) and CS are already present in the overlying endodermis prior to LR initiation. However, little is known regarding the cell fate of the endodermis cells that reactivate their cell cycle and eventually become a part of the LRP.

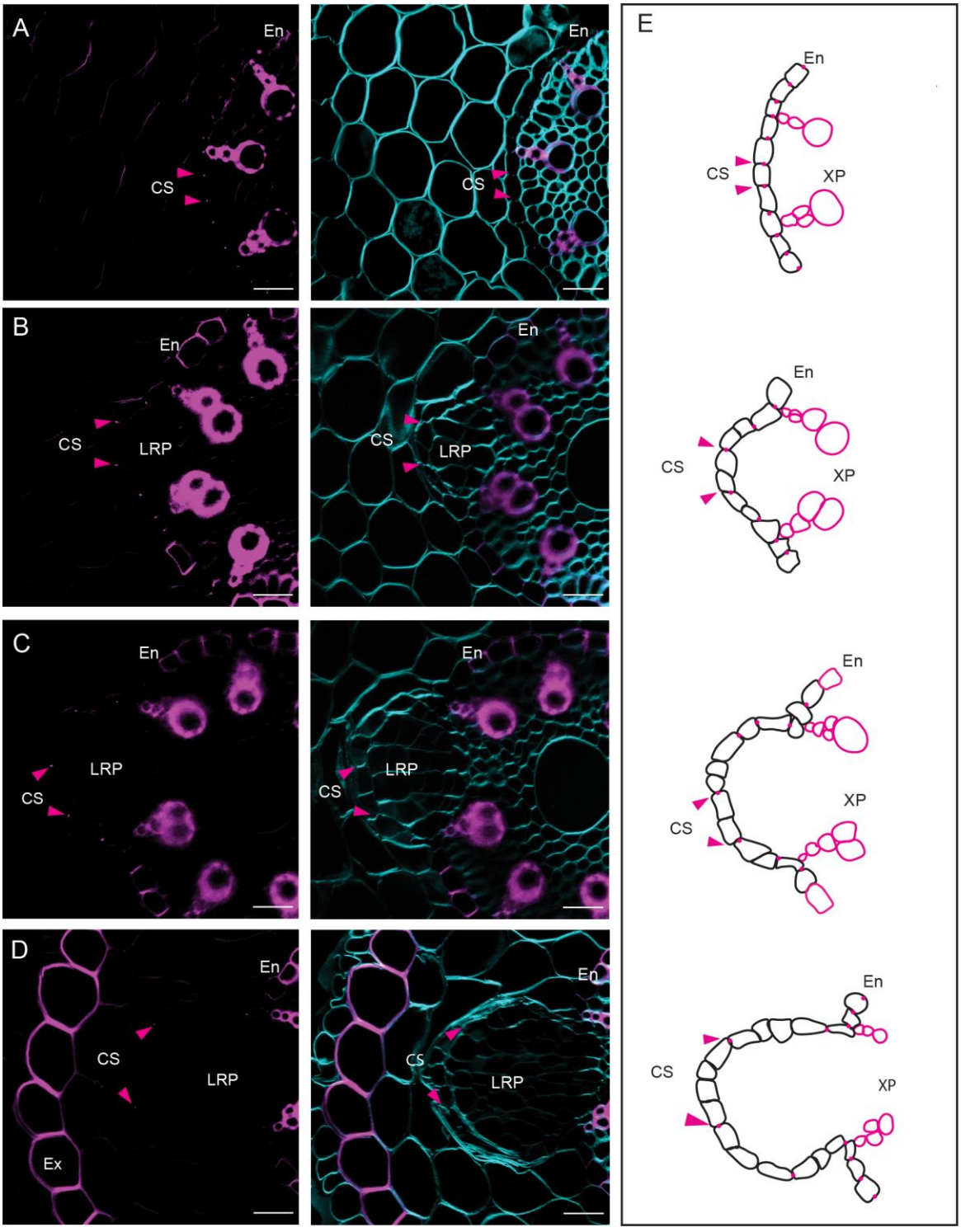

Fig. 4. Recently divided endodermal cells do not establish Casparian strips. (**A**-**D**) Cross-sections stained with BF (lignin) in magenta and Renaissance SR2200 (cellulose) in cyan. The images illustrate the progression of cell divisions in the endodermis and the distancing of the previously formed CS. (left) A graphical representation depicting the cell divisions in the endodermis and the separation of the CS is shown on the left. The arrows indicate the position of the CS. Roots of seedlings (6 DAG) with similar length were positioned in parallel for consistency, and regions of interest of approximately 1 cm from the root tip were sectioned. Representative images were obtained from 30 seedlings of Bd21-3 from three independent replicates, each consisting of at least 10 plants. Scale = 50 µm.

Do these cells after division establish a CSD that is attached to the CS? To address this, we used a histochemical staining for lignin (Basic Fuchsin) and cellulose (Calcofluor White) to counterstain cell walls. In root sections containing LRP, we observed that endodermal cells that underwent anticlinal divisions appear not to establish a CSD, similar to endodermal cells undergoing periclinal divisions, based on the absence of the characteristic lignified spot in the endodermal cross wall (Roppolo *et al.*, 2011) (Fig. 4). From surface projections of root sections containing LRP in which the endodermis already underwent a few rounds of divisions, it appeared that no newly established CS were present in these endodermis cells (Fig. 4B-D). We observed that the CS appeared to undergo a regulated breaking like what was observed during Arabidopsis LR formation (Vermeer *et al.*, 2014). In addition, we observed that the CS appears to undergo a lateral detachment ("sliding") to facilitate the outgrowth of the LRP (Fig. S8).

4.4 Discussion

In this study, we present an atlas describing the consecutive stages of LR development in Brachypodium based on the model utilized for Arabidopsis (Malamy and Benfey, 1997; Péret, Larrieu and Bennett, 2009; Van Norman *et al.*, 2013; Vermeer and Geldner, 2015; Wachsman and Benfey, 2020). We show that in Brachypodium, like other monocots, pericycle cells adjacent to phloem are competent for LR organogenesis. However, to really map the origin and contribution of pericycle cells, a clonal analysis would be required. This approach was recently used to show that also phloem pole pericycle cells can contribute to LRP in Arabidopsis (Torres-Martínez *et al.*, 2020). Thus, it would be interesting to use clonal analysis to determine whether the XPP could contribute to LR formation in Brachypodium, especially during later developmental stages. Furthermore, the endodermis undergoes mitotic activation soon after the initial pericycle cell divisions and overlying endodermal cells will become an integral part of the LRP in later developmental stages, as they will form the root cap (Fig. 1 and 5). While the inner-most cortex layer appears to undergo cell divisions, we could not confirm whether these cells become part of the LRP itself, like the overlying endodermal cells. In both cases, usage of clonal analysis would be very useful to trace the cell fate of the endodermis-derived cells during LR development. Alternatively, we hypothesize these divisions are required to accommodate the expansion growth of the LRP, thereby facilitating emergence. Although most of textbook knowledge regarding LR development is based on Arabidopsis studies, the mitotic reactivation and participation of the endodermis and derived cells are observed in a large number of plants species including barrel clover (Herrbach *et al.*, 2014), maize (Jansen *et al.*, 2013) barley (Orman-Ligeza *et al.*, 2013) and many others (Xiao *et al.*, 2019). It appears that absence of the incorporation of the endodermis during LRP growth could be specific for

the Brassicaceae (Xiao *et al.*, 2019). Alternatively, we hypothesize that these divisions are necessary to accommodate the expansion growth of the LRP, potentially aiding in its emergence by facilitating growth through the overlying both the endodermis and adjacent cortex cell layers (Bell and McCully, 1970; Torres-Martínez *et al.*, 2020). The mitotic reactivation of the endodermis raises important questions: What triggers this process and do the dividing endodermal cell change their identity and if so at what stage? At which stage do they obtain columella identity? To address these questions follow-up studies employing sectorial (mosaic) analyses and high-resolution expression analysis (single cell/ nuclei sequencing, spatial transcriptomics) (Birnbaum, 2018; Torres-Martínez *et al.*, 2020; Liu *et al.*, 2023) would be a logical step to track cell lineages and changes of cell identity during the LRP developmental process.

Auxin serves as a crucial regulator of LR patterning, development and the DR5 reporter is commonly employed to visualize auxin responses (Ulmasov *et al.*, 1997; Liao *et al.*, 2015). In this study, we could not detect the *DR5pro::ER-mRFP* (DR5) signal in phloem pole pericycle cells during the formative cell divisions leading to a stage I LRP. However, there was induction of DR5 signal in the overlying endodermis and even more so in the cortex cells overlying the LRP. Interestingly, we also observed during later stages of LRP development, clear induction of the DR5 signal in the exodermis overlying the LRP. This suggests for a similar role of auxin signaling to regulate cell wall modifications to facilitate the emergence of the LRP (Swarup *et al.*, 2008; Meng *et al.*, 2019). The observed induction of the DR5 reporter in the overlying exodermis suggest for a possible role for auxin signaling to regulate cellular responses, such as modification of the lignin barrier, to accommodate emergence (Nakayama *et al.*, 2017).

Previous studies have reported the absence or presence of a weak DR5 signal during the first cell divisions in the pericycle of rice (Ni *et al.*, 2014) barley (Kirschner *et al.*, 2017) and maize (Jansen *et al.*, 2012) opposite to what is commonly observed in Arabidopsis (Dubrovsky *et al.*, 2000; Vanneste *et al.*, 2005; Marhavý *et al.*, 2013). Similarly, during many stages of Brachypodium embryo development, the DR5 signal was not or barely detected (Hao *et al.*, 2021) counterintuitive compared to the observations during Arabidopsis embryogenesis (Mo and Weijers, 2009). The synthetic DR5 promoter contains direct repeats of a medium-affinity biding site for the AUXIN RESPONSE FACTORs (ARF) transcriptional regulators (Ulmasov *et al.*, 1997; Boer *et al.*, 2014). Therefore, it is likely that only part of the transcriptional response to auxin is reported. The use of higher affinity binding sites could provide a solution to better address the role of auxin during early developmental processes in Brachypodium (Liao *et al.*, 2015; Hao *et al.*, 2021). The same DR5 reporter has been used to monitor changes in auxin signaling during Brachypodium spikelet formation in the shoot

(O'Connor *et al.*, 2017). In addition, we observed a clear DR5 signal during later stages of LRP development, including in the cortex and exodermis. A plausible explanation would be that a set of ARFs with reduced affinity for the DR5 promoter are regulating auxin responses during early stages of LR development in Brachypodium. It would also be important to test brighter and/or triple-fluorescent protein fusions that are targeted to the nucleus, or radiometric reporters such as R2D2 to might be better suited at reporting auxin signaling (Liao *et al.*, 2015). It is clear that auxin can induce LR formation in Brachypodium (Pacheco-Villalobos *et al.*, 2013) and important regulators of auxin import and efflux are already expressed in stage I LRP (Fig. S5).

The root endodermis serves as apoplastic barrier for the radial transport of water and nutrients to the plant's vascular system (Barberon *et al.*, 2016). To fulfil this role, the endodermis relies on the formation of the lignified Casparian strips. Subsequently, suberin lamellae are deposited as a secondary cell wall modification surrounding the plasma membrane (Barbosa, Rojas-Murcia and Geldner, 2019). Moreover, many plant species have an extra barrier called the exodermis, which also exhibits lignin and suberin deposition (Kajala *et al.*, 2021; Liu and Kreszies, 2023). Recent studies have reported that the exodermis functions in the tolerance to abiotic stresses (Cai *et al.*, 2011; Kajala *et al.*, 2021; Manzano *et al.*, 2022; Cantó-Pastor *et al.*, 2024). Here, we demonstrate that the daughter cells of divided endodermal cells do not appear to form a CSD in their cross walls (Fig. 4). Similar to what was described for Arabidopsis, the CS appears to be detached longitudinally and local breaks appear, likely facilitating the emergence of the LRP. While there is increasing interest in studying the function and formation of the CS in monocots such as rice and maize (Karahara *et al.*, 2004; Wang *et al.*, 2022), little is known whether the CASPARIAN STRIP DOMAIN PROTEINs (CASP) are degraded during LR development as described for Arabidopsis (Vermeer *et al.*, 2014) to facilitate the reported "sliding" of the CS. In addition, it would be interesting to test whether Brachypodium has orthologs of the GAPLESS proteins that were identified in rice. These secreted proteins interact with OsCASP1 and are required for the tethering of the CS to the cell wall (Song *et al.*, 2023). It will be interesting to test whether CASP/CSD degradation could be a general mechanism to break the GAPLESS-mediated tethering of the CS to the cell wall to allows for loosening and/or local breaking of the CS in plants during LR emergence. Moreover, Brachypodium has a lignified exodermis (Sexauer *et al.*, 2021). However, under our experimental conditions, the exodermis in many cases showed still little lignification at the time of LR emergence.

4.5 CONCLUDING REMARKS

Here we provide an atlas describing the various developmental stages of LRP development in Brachypodium and shed light on the potential roles of different cell types and molecular mechanisms involved to facilitate their development. This now provides a perfect starting point to dissect the trajectories of cell types and if there are regulatory mechanisms that could be part of conserved modules for root branching in general. Brachypodium LRP formation provides a beautiful (non-domesticated) plant model to investigate how the endodermis and cortex re-activate their cell cycle and contribute to organogenesis and emergence. In addition, it allows the investigation which (hormonal) signaling pathways are re-wired and which are conserved during developmental processes.

4.6 MATERIALS AND METHODS

Plant Materials and Growth Conditions

Brachypodium distachyon seedlings (Bd-21-3) (Vogel and Hill, 2008) were grown vertically on 0.8% agar supplemented with half strength Murashige-Skoog (MS) pH 5.8 at 22° C under long day or constant light. 5 DAG seedlings were collected for analysis. After removal of the seed husk, seeds were surface sterilized using sodium hypochlorite 5% and 0.01% Triton for 4 min and rinsed at least four times in autoclaved desilted water. Seeds were placed on medium (prepared as described above) with embryo towards the bottom of the and facing the lid of the 120mm square plate to prevent shoots and roots growing into the media or in the wrong direction. Plates were placed into growth conditions at an angle of about 20° to ensure that roots grow on the medium and not into the air as described by (van der Schuren *et al.*, 2018). After a maximum of 7 days in 22 C under long day or constant light, seedlings were harvested for clearing and analysis. The description of the Brachypodium LR developmental stages was based on representative images obtained from 45 seedlings from three independent replicates each consisting of at least 15 plants.

Auxin Treatment

A total of 45 seedlings (three independent biological replicates) of Brachypodium Bd-21-3 were grown vertically under long day conditions for 5 days on standard ½ MS plates with 0.8% agar. The seedlings were then transferred to plates treated with 10 µM Indole-3-Acetic Acid (IAA) (I0901, Duchefa Biochemie) from a 10mM stock in DMSO. Images were taken at 0, 3, and 7 days after the seedlings were transferred to auxin.

Chemicals for clearing and staining solutions

The following chemicals were used in the DEEP-Clear (Pende *et al.*, 2020) adapted version to plant tissues: PFA (paraformaldehyde) (CAS no. 30525-89-4, Merck, http://www.merck.com/), xylitol (CAS no. 87-99-0, Sigma, http://www.sigmaaldrich.com/), urea (CAS no. 57-13-6, Sigma), SR2200 (Renaissance Chemicals), Basic Fuchsin (CAS no. 58969-01-0, Sigma), THEED (Sigma-Aldrich, 87600-100ML), 5% (v/v) Triton X-100 (Roth, 3051.2).

Preparation of hand-sectioned root samples

For sectioning, seedlings roots (6 DAG) of similar length were placed in parallel and fragments of 1 cm with the region of interest were partitioned and embedded in 4% agarose. After solidified, agarose blocks containing the region of interest were glued on a hand microtome (www.daigger.com/hand-microtome) and sections of approximately 50 µm were prepared for clearing or immediate visualization. Representative images were obtained from at least 30 seedlings from three independent replicates

Clearing and staining

Clearing steps using DEEP-Clear were performed as described for ClearSee in (Kurihara *et al.*, 2015) and adapted from (van der Schurenet al., 2018) for *Brachypodium* samples. DEEP-clear solution consists in 5 to 8% (v/v) THEED, 5% (v/v) Triton X-100, and 25% (w/v) urea in water. Heating the solution is not recommended. 7 DAG old root seedlings were collected for clearing for full root treatment and/or for semi-thin sectioning. Samples were fixed for 1 hour in 4% (w/v) paraformaldehyde in 1× phosphate-buffered saline (PBS) with 3 rounds of soft vacuum infiltration. After, roots were washed five times in 1x PBS with another round vacuum to ensure the removal of PFA. Samples were then transferred to DEEP-Clear solution for clearing. Fixed root tissue was incubated at room temperature with gentle shaking and solution for 7-10 days and solution replaced twice. For staining of the fixed and cleared tissue, 1% stock solution of Basic Fuchsin (for lignin staining), Fluorol Yellow (for suberin staining), Renaissance and/or Calcofluor (for cell wall staining) were separately prepared directly in DEEP-Clear and stored at 4°C. Working solutions were prepared as in (Ursache *et al.*, 2018). In order to combine multiple dyes, samples were incubated first in Basic F (0,1% in DEEP-Clear) for one 1 hour and washed in DEEP-Clear overnight. After, several rounds of washings, samples were transferred to Renaissance (0,1% in DEEP-Clear) for 2 days and washed overnight in DEEP-Clear. Finally, samples were transferred to Fluorol Yellow (FY) (0,01% in DEEP-Clear) for 1 hour and counterstained in aniline blue (0,5% in water) for 1 hour in the darkness. Samples prior FY staining can be stored in 50% glycerol at 4%. FY solutions and FY-stained samples were kept in darkness to prevent bleaching.

Starch staining

To observe starch granules in the LRPs of Brachypodium, the root cortex of a total of 30 seedlings (three independent biological replicates) was mechanically removed without damaging the LRPs. Roots were then cleared for 3 days in DEEP-Clear. After, roots were dipped in Lugol's staining solution (Sigma-Aldrich) for 5 minutes, washed with distilled water, and observed under 2-photon microscopy.

Microscopy

Roots were observed using Leica TCS SP8-MP equipped with a resonant scanner (8 kHz) using 25x, 40x and 63x water immersion objectives. Figures were arranged in Adobe Illustrator (Adobe Systems Inc., http://www.adobe.com/) or in PowerPoint (Microsoft Corporation) and the brightness was increased equally, without further modifications. The 3D reconstruction was done using the Fiji package (Schindelin *et al.*, 2012).

ACKNOWLEDGEMENTS

We like to thank Dr. Anne Roulin (Agroscope, Switzerland) and Dr. Michael T. Raissig (University of Bern, Switzerland) for sharing their Brachypodium knowledge and enthusiasm. We thank the members of the Vermeer lab for critical feedback on the manuscript.

COMPETING INTERESTS

The authors declare no competing or financial interests.

FUNDING

Work in the Vermeer lab was supported by a Swiss National Science Foundation (project 197568 awarded to JEMV) and the University of Neuchâtel. KB was supported by a Marie Curie Global Fellowship (PLANT-ID, grant agreement: 101106663). Work in the Hardtke lab was supported by a Swiss National Science Foundation grant CR32I3_156724 awarded to CSH.

DATA AVAILABILITY

All data will be made available upon request.

REFERENCE LIST

Andersen, T.G. *et al.* (2021) 'Tissue-Autonomous Phenylpropanoid Production Is Essential for Establishment of Root Barriers', *Current Biology*, 31(5), pp. 965-977.e5. Available at: https://doi.org/https://doi.org/10.1016/j.cub.2020.11.070.

Atkinson, J.A. *et al.* (2014) 'Branching Out in Roots: Uncovering Form, Function, and Regulation', *Plant Physiology*, 166(2), pp. 538–550. Available at: https://doi.org/10.1104/pp.114.245423.

Banda, J. *et al.* (2019) 'Lateral Root Formation in Arabidopsis: A Well-Ordered LRexit', *Trends in Plant Science*, 24(9), pp. 826–839. Available at: https://doi.org/10.1016/j.tplants.2019.06.015.

Bao, Y. *et al.* (2014) 'Plant roots use a patterning mechanism to position lateral root branches toward available water', *Proceedings of the National Academy of Sciences*, 111(25), pp. 9319 LP – 9324. Available at: https://doi.org/10.1073/pnas.1400966111.

Barberon, M. *et al.* (2016) 'Adaptation of Root Function by Nutrient-Induced Plasticity of Endodermal Differentiation', *Cell*, 164(3), pp. 447–459. Available at: https://doi.org/10.1016/j.cell.2015.12.021.

Barbosa, I.C.R., Rojas-Murcia, N. and Geldner, N. (2019) 'The Casparian strip—one ring to bring cell biology to lignification?', *Current Opinion in Biotechnology*. Elsevier Ltd, pp. 121–129. Available at: https://doi.org/10.1016/j.copbio.2018.10.004.

Bell, J. and McCully, M. (1970) 'A histological study of lateral root initiation and development inZea mays', *Protoplasma*, 205, pp. 179–205. Available at: http://www.springerlink.com/index/H534X7JN67X81711.pdf.

Birnbaum, K.D. (2018) 'Power in Numbers: Single-Cell RNA-Seq Strategies to Dissect Complex Tissues', *Annual Review of Genetics*, 52(1), pp. 203–221. Available at: https://doi.org/10.1146/annurev-genet-120417-031247.

Boer, D.R. *et al.* (2014) 'Structural Basis for DNA Binding Specificity by the Auxin-Dependent ARF Transcription Factors', *Cell*, 156(3), pp. 577–589. Available at: https://doi.org/10.1016/J.CELL.2013.12.027.

Cai, X. *et al.* (2011) 'Development of Casparian strip in rice cultivars', *Plant Signaling & Behavior*, 6(1), pp. 59–65. Available at: https://doi.org/10.4161/psb.6.1.13545.

Cantó-Pastor, A. *et al.* (2024) 'A suberized exodermis is required for tomato drought tolerance', *Nature Plants*, 10(1), pp. 118–130. Available at: https://doi.org/10.1038/s41477-023-01567-x.

Casero, P.J., Casimiro, I. and Lloret, P.G. (1995) 'Lateral root initiation by asymmetrical transverse divisions of pericycle cells in four plant species:Raphanus sativus, Helianthus annuus, Zea mays, andDaucus carota', *Protoplasma*, 188(1), pp. 49–58. Available at: https://doi.org/10.1007/BF01276795.

Casimiro, I. *et al.* (2001) 'Auxin Transport Promotes Arabidopsis Lateral Root Initiation', *The Plant Cell*, 13(4), p. 843. Available at: https://doi.org/10.2307/3871344.

Cavallari, N., Artner, C. and Benkova, E. (2021) 'Auxin-regulated lateral root organogenesis', *Cold Spring Harbor Perspectives in Biology*, 13(7). Available at: https://doi.org/10.1101/cshperspect.a039941.

Chen, Y. *et al.* (2018) 'A comparison of lateral root patterning among dicot and monocot plants', *Plant Science*, 274, pp. 201–211. Available at: https://doi.org/10.1016/j.plantsci.2018.05.018.

Chochois, V., Vogel, J.P. and Watt, M. (2012) 'Application of Brachypodium to the genetic improvement of wheat roots', *Journal of Experimental Botany*, 63(9), pp. 3467–3474. Available at: https://doi.org/10.1093/jxb/ers044.

Ditengou, F.A. *et al.* (2008) 'Mechanical induction of lateral root initiation in Arabidopsis thaliana', *Proceedings of the National Academy of Sciences of the United States of America*, 105(48), pp. 18818–18823. Available at: https://doi.org/10.1073/pnas.0807814105.

Dubrovsky, J.G. *et al.* (2000) 'Pericycle cell proliferation and lateral root initiation in Arabidopsis.', *Plant physiology*, 124(4), pp. 1648–1657. Available at: https://doi.org/10.1104/pp.124.4.1648.

Enstone, D.E., Peterson, C.A. and Ma, F. (2002) 'Root Endodermis and Exodermis: Structure, Function, and Responses to the Environment', *Journal of Plant Growth Regulation*, 21(4), pp. 335–351. Available at: https://doi.org/10.1007/s00344-003-0002-2.

Fukaki, H. and Tasaka, M. (2009) 'Hormone interactions during lateral root formation', *Plant Molecular Biology*, 69(4), pp. 437–449. Available at: https://doi.org/10.1007/s11103-008-9417-2.

Gala, H.P. *et al.* (2021) 'A single-cell view of the transcriptome during lateral root initiation in Arabidopsis thaliana', *The Plant cell*, 33(7), pp. 2197–2220. Available at: https://doi.org/10.1093/PLCELL/KOAB101.

Garvin, D.F. (2007) 'Brachypodium: a new monocot model plant system emerges', *Journal of the Science of Food and Agriculture*, 87(7), pp. 1177–1179. Available at: https://doi.org/10.1002/jsfa.2868.

Geldner, N. (2013) 'The endodermis', *Annual Review of Plant Biology*, pp. 531–558. Available at: https://doi.org/10.1146/annurev-arplant-050312-120050.

Guseman, J.M. *et al.* (2015) 'Auxin-induced degradation dynamics set the pace for lateral root development', *Development (Cambridge)*, 142(5), pp. 905–909. Available at: https://doi.org/10.1242/DEV.117234/258638/AM/AUXIN-INDUCED-DEGRADATION-DYNAMICS-SET-THE-PACE.

Guyomarc'h, S. *et al.* (2012) 'Early development and gravitropic response of lateral roots in Arabidopsis thaliana', *Philosophical Transactions of the Royal Society B: Biological Sciences*, 367(1595), pp. 1509–1516. Available at: https://doi.org/10.1098/rstb.2011.0231.

Hao, Z. *et al.* (2021) 'Conserved, divergent and heterochronic gene expression during Brachypodium and Arabidopsis embryo development', *Plant Reproduction*, 34(3), pp. 207–224. Available at: https://doi.org/10.1007/S00497-021-00413-4/FIGURES/7.

Hardtke, C.S. and Pacheco-Villalobos, D. (2015) 'The Brachypodium distachyon Root System: A Tractable Model to Investigate Grass Roots', pp. 245–258. Available at: https://doi.org/10.1007/7397_2015_6.

Herrbach, V. *et al.* (2014) 'Lateral root formation and patterning in Medicago truncatula', *Journal of Plant Physiology*, 171(3–4), pp. 301–310. Available at: https://doi.org/10.1016/j.jplph.2013.09.006.

Hochholdinger, F. and Zimmermann, R. (2008) 'Conserved and diverse mechanisms in root development', *Current Opinion in Plant Biology*, pp. 70–74. Available at: https://doi.org/10.1016/j.pbi.2007.10.002.

Jansen, L. *et al.* (2012) 'Phloem-associated auxin response maxima determine radial positioning of lateral roots in maize'. Available at: https://doi.org/10.1098/rstb.2011.0239.

Jansen, L. *et al.* (2013) 'Comparative transcriptomics as a tool for the identification of root branching genes in maize', *Plant Biotechnology Journal*, 11(9), pp. 1092–1102. Available at: https://doi.org/10.1111/pbi.12104.

Kajala, K. *et al.* (2021) 'Innovation, conservation, and repurposing of gene function in root cell type development', *Cell*, 184(12), pp. 3333-3348.e19. Available at: https://doi.org/10.1016/J.CELL.2021.04.024.

Karahara, I. *et al.* (2004) 'Development of the Casparian strip in primary roots of maize under salt stress', *Planta*, 219(1), pp. 41–47. Available at: https://doi.org/10.1007/s00425-004-1208-7.

Kircher, S. and Schopfer, P. (2018) 'The plant hormone auxin beats the time for oscillating light-regulated lateral root induction', *Development (Cambridge)*, 145(23). Available at: https://doi.org/10.1242/DEV.169839/VIDEO-1.

Kirschner, G.K. *et al.* (2017) 'Unique and Conserved Features of the Barley Root Meristem', *Frontiers in Plant Science*, 8, p. 1240. Available at: https://doi.org/10.3389/fpls.2017.01240.

Kortz, A., Hochholdinger, F. and Yu, P. (2019) 'Cell Type-Specific Transcriptomics of Lateral Root Formation and Plasticity', *Frontiers in Plant Science*, 10.

Kreszies, T. *et al.* (2020) 'Seminal roots of wild and cultivated barley differentially respond to osmotic stress in gene expression, suberization, and hydraulic conductivity', *Plant Cell and Environment*, 43(2), pp. 344–357. Available at: https://doi.org/10.1111/pce.13675.

Kumar, J. *et al.* (2019) 'Towards Exploitation of Adaptive Traits for Climate-Resilient Smart Pulses', *International journal of molecular sciences*, 20(12), p. 2971. Available at: https://doi.org/10.3390/ijms20122971.

Kurihara, D. *et al.* (2015) 'ClearSee: a rapid optical clearing reagent for whole-plant fluorescence imaging.', *Development (Cambridge, England)*, 142(23), pp. 4168–79. Available at: https://doi.org/10.1242/dev.127613.

Lavenus, J. *et al.* (2015) 'Inference of the Arabidopsis Lateral Root Gene Regulatory Network Suggests a Bifurcation Mechanism That Defines Primordia Flanking and Central Zones', *The Plant Cell*, 27(5), pp. 1368 LP – 1388. Available at: https://doi.org/10.1105/tpc.114.132993.

Liao, C.Y. *et al.* (2015) 'Reporters for sensitive and quantitative measurement of auxin response', *Nature Methods*, 12(3), pp. 207–210. Available at: https://doi.org/10.1038/nmeth.3279.

Lin, C. and Sauter, M. (2019) 'Polar auxin transport determines adventitious root emergence and growth in rice', *Frontiers in Plant Science*, 10, p. 444. Available at: https://doi.org/10.3389/FPLS.2019.00444/BIBTEX.

Líška, D. *et al.* (2016) 'Líška, D. et al. (2016) "Asymmetrical development of root endodermis and exodermis in reaction to abiotic stresses", Annals of Botany, 118(4), pp. 667–674. doi: https://doi.org/10.1093/aob/mcw047.

Liu, T. and Kreszies, T. (2023) 'The exodermis: A forgotten but promising apoplastic barrier', *Journal of Plant Physiology*, 290, p. 154118. Available at: https://doi.org/https://doi.org/10.1016/j.jplph.2023.154118.

Liu, Z. *et al.* (2023) 'Integrated single-nucleus and spatial transcriptomics captures transitional states in soybean nodule maturation', *Nature Plants*, 9(4), pp. 515–524. Available at: https://doi.org/10.1038/s41477-023-01387-z.

Malamy, J.E. and Benfey, P.N. (1997) 'Organization and cell differentiation in lateral roots of Arabidopsis thaliana', *Development*, 124(1), pp. 33 LP – 44. Available at: http://dev.biologists.org/content/124/1/33.abstract.

Manzano, C. *et al.* (2022) 'Regulation and Function of a Polarly Localized Lignin Barrier in the Exodermis', *bioRxiv*, p. 2022.10.20.513117. Available at: https://doi.org/10.1101/2022.10.20.513117.

Marchant, A. *et al.* (2002) 'AUX1 Promotes Lateral Root Formation by Facilitating Indole-3-Acetic Acid Distribution between Sink and Source Tissues in the Arabidopsis Seedling', *The Plant Cell*, 14(3), pp. 589–597. Available at: https://doi.org/10.1105/tpc.010354.

Marhavý, P. *et al.* (2013) 'Auxin reflux between the endodermis and pericycle promotes lateral root initiation', *EMBO Journal*, 32(1), pp. 149–158. Available at: https://doi.org/10.1038/emboj.2012.303.

Meng, F. *et al.* (2019) 'Molecular Mechanisms of Root Development in Rice', *Rice (New York, N.Y.)*, 12(1), p. 1. Available at: https://doi.org/10.1186/s12284-018-0262-x.

Mo, B. and Weijers, D. (2009) 'Auxin Control of Embryo Patterning', pp. 1–13.

Möller, B.K., Xuan, W. and Beeckman, T. (2017) 'Dynamic control of lateral root positioning', *Current Opinion in Plant Biology*, 35, pp. 1–7. Available at: https://doi.org/10.1016/j.pbi.2016.09.001.

Morris, E.C. *et al.* (2017) 'Shaping 3D Root System Architecture', *Current Biology*, 27(17), pp. R919–R930. Available at: https://doi.org/10.1016/j.cub.2017.06.043.

Nakayama, T. *et al.* (2017) 'A peptide hormone required for Casparian strip diffusion barrier formation in Arabidopsis roots', *Science*, 355(6322), pp. 284–286. Available at: https://doi.org/10.1126/science.aai9057.

Ni, J. *et al.* (2014) 'Histological characterization of the lateral root primordium development in rice', *Botanical Studies*, 55(1), pp. 1–6. Available at: https://doi.org/10.1186/s40529-014-0042-x.

Van Norman, J.M. *et al.* (2013) 'To branch or not to branch: the role of pre-patterning in lateral root formation', *Development*, 140(21), pp. 4301–4310. Available at: https://doi.org/10.1242/DEV.090548.

O'Connor, D.L. *et al.* (2017) 'Cross-species functional diversity within the PIN auxin efflux protein family', *eLife*, 6. Available at: https://doi.org/10.7554/eLife.31804.

Orman-Ligeza, B. *et al.* (2013) 'Post-embryonic root organogenesis in cereals: branching out from model plants', *Trends in Plant Science*, 18(8), pp. 459–467. Available at: https://doi.org/10.1016/J.TPLANTS.2013.04.010.

Orosa-Puente, B. *et al.* (2018) 'Root branching toward water involves posttranslational modification of transcription factor ARF7', *Science*, 362(6421), pp. 1407–1410. Available at: https://doi.org/10.1126/science.aau3956.

Pacheco-Villalobos, D. *et al.* (2013) 'Disturbed Local Auxin Homeostasis Enhances Cellular Anisotropy and Reveals Alternative Wiring of Auxin-ethylene Crosstalk in Brachypodium distachyon Seminal Roots', *PLoS Genetics*. Edited by H. Yu, 9(6), p. e1003564. Available at: https://doi.org/10.1371/journal.pgen.1003564.

Pende, M. *et al.* (2020) 'A versatile depigmentation, clearing, and labeling method for exploring nervous system diversity', *Science Advances*, 6(22). Available at: https://doi.org/10.1126/sciadv.aba0365.

Péret, B., Larrieu, A. and Bennett, M.J. (2009) 'Lateral root emergence: A difficult birth', *Journal of Experimental Botany*, 60(13), pp. 3637–3643. Available at: https://doi.org/10.1093/jxb/erp232.

Raissig, M.T. and Woods, D.P. (2021) 'The wild grass Brachypodium distachyon as a developmental model system'. Available at: https://zenodo.org/record/5548408.

Ranathunge, K. *et al.* (2008) 'Soybean root suberin and partial resistance to root rot caused by Phytophthora sojae', *Phytopathology*, 98(11). Available at: https://doi.org/10.1094/PHYTO-98-11-1179.

Rebouillat, J. *et al.* (2009) 'Molecular genetics of rice root development', *Rice*, 2(1), pp. 15–34. Available at: https://doi.org/10.1007/s12284-008-9016-5.

Reinhardt, D. *et al.* (2003) 'Regulation of phyllotaxis by polar auxin transport', *Nature*, 426(6964), pp. 255–260. Available at: https://doi.org/10.1038/nature02081.

Roppolo, D. *et al.* (2011) 'A novel protein family mediates Casparian strip formation in the endodermis', *Nature*, 473(7347), pp. 380–383. Available at: https://doi.org/10.1038/nature10070.

Roychoudhry, S. *et al.* (2017) 'The developmental and environmental regulation of gravitropic setpoint angle in Arabidopsis and bean', *Scientific reports*, 7, p. 42664. Available at: https://doi.org/10.1038/srep42664.

Roychoudhry, S. *et al.* (2023) 'Antigravitropic PIN polarization maintains non-vertical growth in lateral roots', *Nature Plants*, 9(9), pp. 1500–1513. Available at: https://doi.org/10.1038/s41477-023-01478-x.

Schäfer, E.D. *et al.* (2022) 'Modeling root loss reveals impacts on nutrient uptake and crop development', *Plant Physiology*, 190(4), pp. 2260–2278. Available at: https://doi.org/10.1093/plphys/kiac405.

Schindelin, J. *et al.* (2012) 'Fiji: An open-source platform for biological-image analysis', *Nature Methods*, pp. 676–682. Available at: https://doi.org/10.1038/nmeth.2019.

Scholthof, K.-B.G. *et al.* (2018) 'Brachypodium: A monocot grass model system for plant biology', *The Plant Cell*, 30(August), p. tpc.00083.2018. Available at: https://doi.org/10.1105/tpc.18.00083.

van der Schuren, A. *et al.* (2018) 'Broad spectrum developmental role of Brachypodium AUX1', *New Phytologist*, 219(4), pp. 1216–1223. Available at: https://doi.org/10.1111/nph.15332.

Sexauer, M. *et al.* (2021) 'Visualizing polymeric components that define distinct root barriers across plant lineages', *Development (Cambridge)*, 148(23). Available at: https://doi.org/10.1242/DEV.199820/273645.

Song, T. *et al.* (2023) 'A new family of proteins is required for tethering of Casparian strip membrane domain and nutrient homoeostasis in rice', *Nature Plants* [Preprint]. Available at: https://doi.org/10.1038/s41477-023-01503-z.

Stelpflug, S.C. *et al.* (2016) 'An Expanded Maize Gene Expression Atlas based on RNA Sequencing and its Use to Explore Root Development', *The Plant Genome*, 9(1), p. plantgenome2015.04.0025. Available at: https://doi.org/10.3835/plantgenome2015.04.0025.

Stoeckle, D., Thellmann, M. and Vermeer, J.E. (2018) 'Breakout — lateral root emergence in Arabidopsis thaliana', *Current Opinion in Plant Biology*. Elsevier Ltd, pp. 67–72. Available at: https://doi.org/10.1016/j.pbi.2017.09.005.

Swarup, K. *et al.* (2008) 'The auxin influx carrier LAX3 promotes lateral root emergence', *Nature Cell Biology*, 10(8), pp. 946–954. Available at: https://doi.org/10.1038/ncb1754.

Torres-Martínez, H.H. *et al.* (2020) 'From one cell to many: Morphogenetic field of lateral root founder cells in Arabidopsis thaliana is built by gradual recruitment', *Proceedings of the National Academy of Sciences*, 117(34), pp. 20943–20949. Available at: https://doi.org/10.1073/pnas.2006387117.

Uga, Y. *et al.* (2013) 'Control of root system architecture by DEEPER ROOTING 1 increases rice yield under drought conditions', *Nature Genetics*, 45(9), pp. 1097–1102. Available at: https://doi.org/10.1038/ng.2725.

Ulmasov, T. *et al.* (1997) 'Aux/IAA proteins repress expression of reporter genes containing natural and highly active synthetic auxin response elements.', *The Plant Cell*, 9(11), pp. 1963–1971. Available at: https://doi.org/10.1105/tpc.9.11.1963.

Ursache, R. *et al.* (2018) 'A protocol for combining fluorescent proteins with histological stains for diverse cell wall components', *The Plant Journal*, 93(2), pp. 399–412. Available at: https://doi.org/10.1111/tpj.13784.

Vanneste, S. *et al.* (2005) 'Cell cycle progression in the pericycle is not sufficient for SOLITARY ROOT/IAA14-mediated lateral root initiation in Arabidopsis thaliana', *Plant Cell*, 17(11), pp. 3035–3050. Available at: https://doi.org/10.1105/tpc.105.035493.

Vermeer, J.E.M. *et al.* (2014) 'A spatial accommodation by neighboring cells is required for organ initiation in arabidopsis', *Science*, 343(6167), pp. 178–183. Available at: https://doi.org/10.1126/SCIENCE.1245871.

Vermeer, J.E.M. and Geldner, N. (2015) 'Lateral root initiation in Arabidopsis thaliana: a force awakens', *F1000Prime Reports*, 7. Available at: https://doi.org/10.12703/P7-32.

Vogel, J. and Hill, T. (2008) 'High-efficiency Agrobacterium-mediated transformation of Brachypodium distachyon inbred line Bd21-3', *Plant Cell Reports*, 27(3), pp. 471–478. Available at: https://doi.org/10.1007/s00299-007-0472-y.

Wachsman, G. and Benfey, P.N. (2020) 'Lateral Root Initiation: The Emergence of New Primordia Following Cell Death', *Current Biology*, 30(3), pp. R121–R122. Available at: https://doi.org/10.1016/j.cub.2019.12.032.

Wang, S. *et al.* (2002) 'Lateral root formation in rice (Oryza sativa): promotion effect of jasmonic acid', *Journal of Plant Physiology*, 159(8), pp. 827–832. Available at: https://doi.org/https://doi.org/10.1078/0176-1617-00825.

Wang, Y. *et al.* (2022) 'A dirigent family protein confers variation of Casparian strip thickness and salt tolerance in maize', *Nature Communications*, 13(1), p. 2222. Available at: https://doi.org/10.1038/s41467-022-29809-0.

Xiao, T.T. *et al.* (2019) 'Lateral root formation involving cell division in both pericycle, cortex and endodermis is a common and ancestral trait in seed plants', *Development (Cambridge)*, 146(20). Available at: https://doi.org/10.1242/dev.182592.

Ye, Y.J. *et al.* (2017) 'A Novel Chemical Inhibitor of ABA Signaling Targets All ABA Receptors', *Plant physiology*, 173(4), pp. 2356–2369. Available at: https://doi.org/10.1104/PP.16.01862.

Yu, P. *et al.* (2016) 'Genetic Control of Lateral Root Formation in Cereals', *Trends in Plant Science*. Elsevier Ltd, pp. 951–961. Available at: https://doi.org/10.1016/j.tplants.2016.07.011.

Yu, P., Hochholdinger, F. and Li, C. (2019) 'Plasticity of Lateral Root Branching in Maize', *Frontiers in Plant Science*, 10. Available at: https://doi.org/10.3389/fpls.2019.00363.

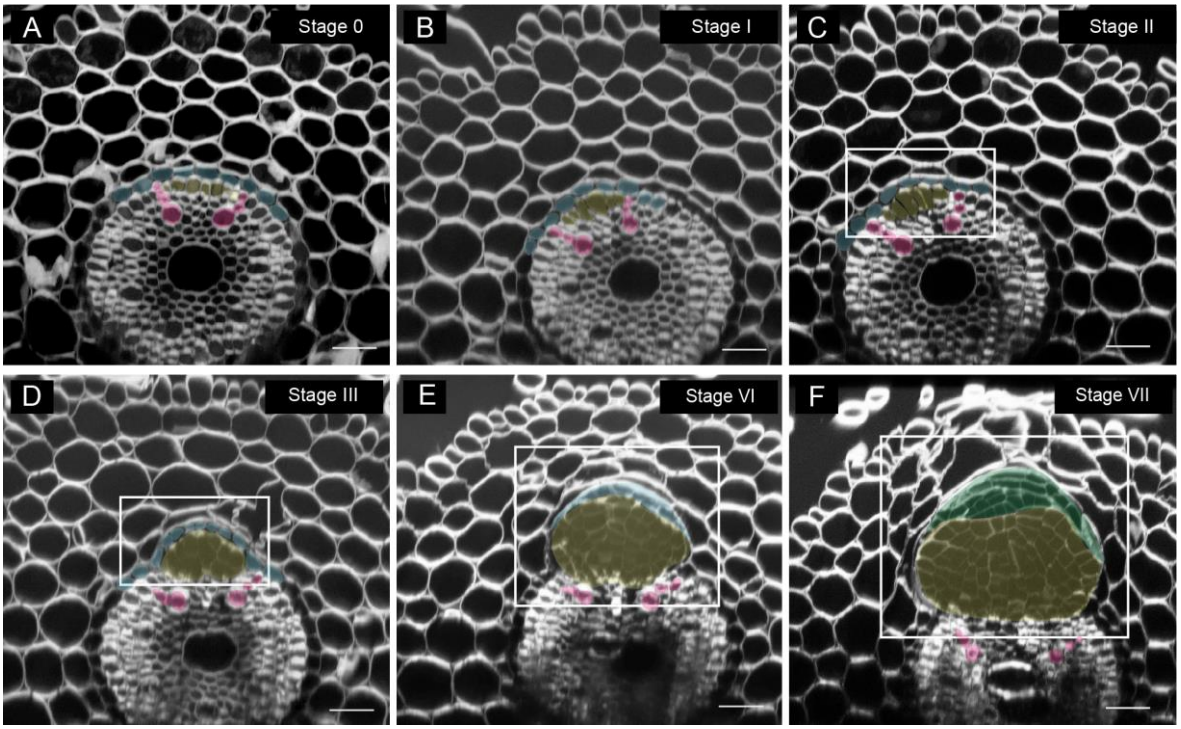

Fig. S1. Orthogonal view of developmental stages of LRP formation in Brachypodium. (**A**) Stage **0**: No evident swelling of the pericycle cells (white arrows). (**B**) Stage **II**: Recently divided pericycle cells promote the displacement of the endodermis. In (**C** and **D**) Stage **II** and **III** pericycle divides anticlinal and periclinal (rectangular area). (**E** and **F**) - Periclinal and anticlinal cell divisions are observed at the apex of the LRP (Stage **V**) following the establishment of the lateral root cap (Stage **VII**). Representative images were obtained from 30 seedlings from three independent replicates, each consisting of at least 10 plants. Magenta: Xylem, Cyan: Endodermis, Yellow: Pericycle, Green: Root Cap. Scale: 50 µm.

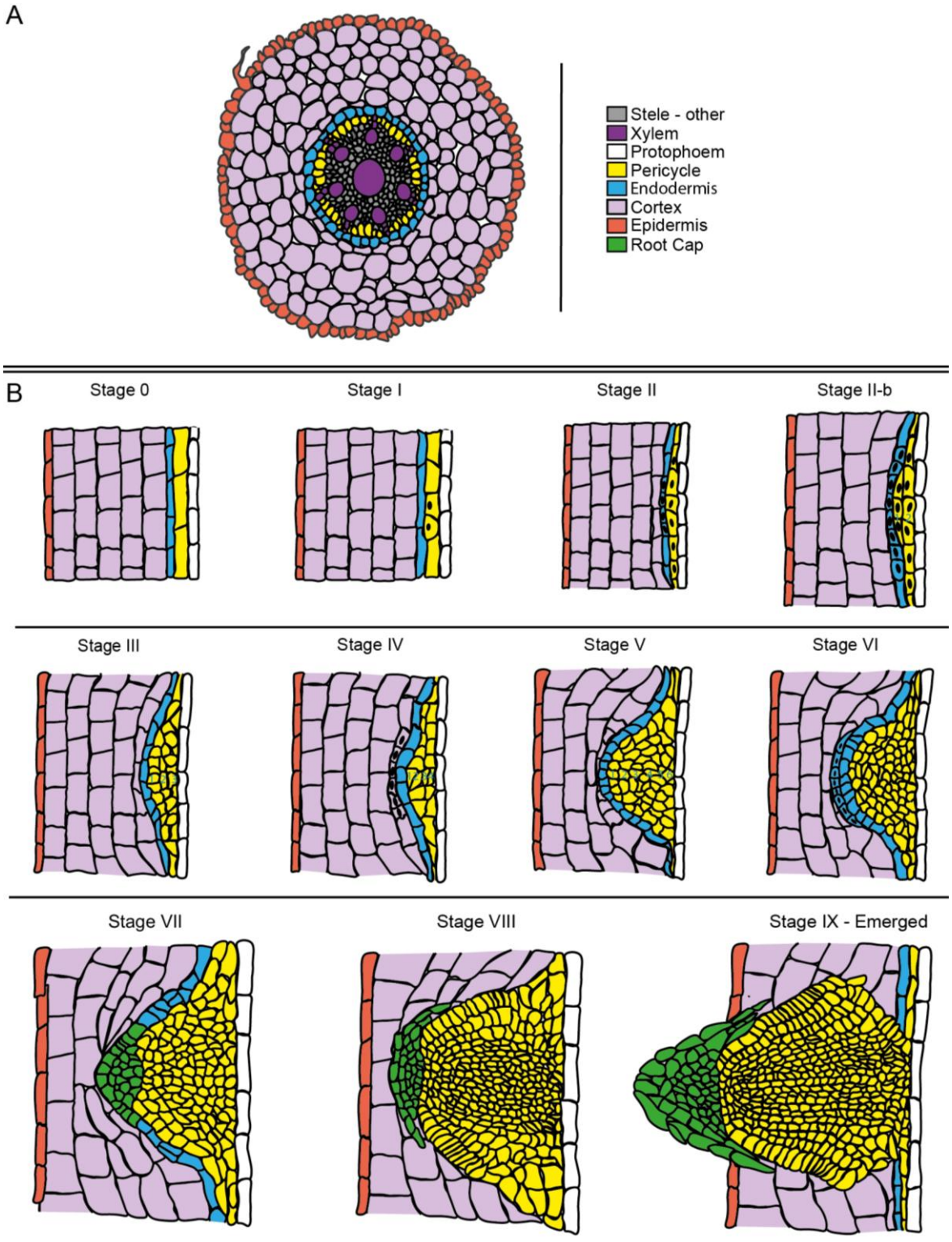

Fig. S2. Schematic representation of LRP development in Brachypodium. (**A**) Representation of root cross section of Brachypodium. (**B**) Successive stages of LRP formation are illustrated.

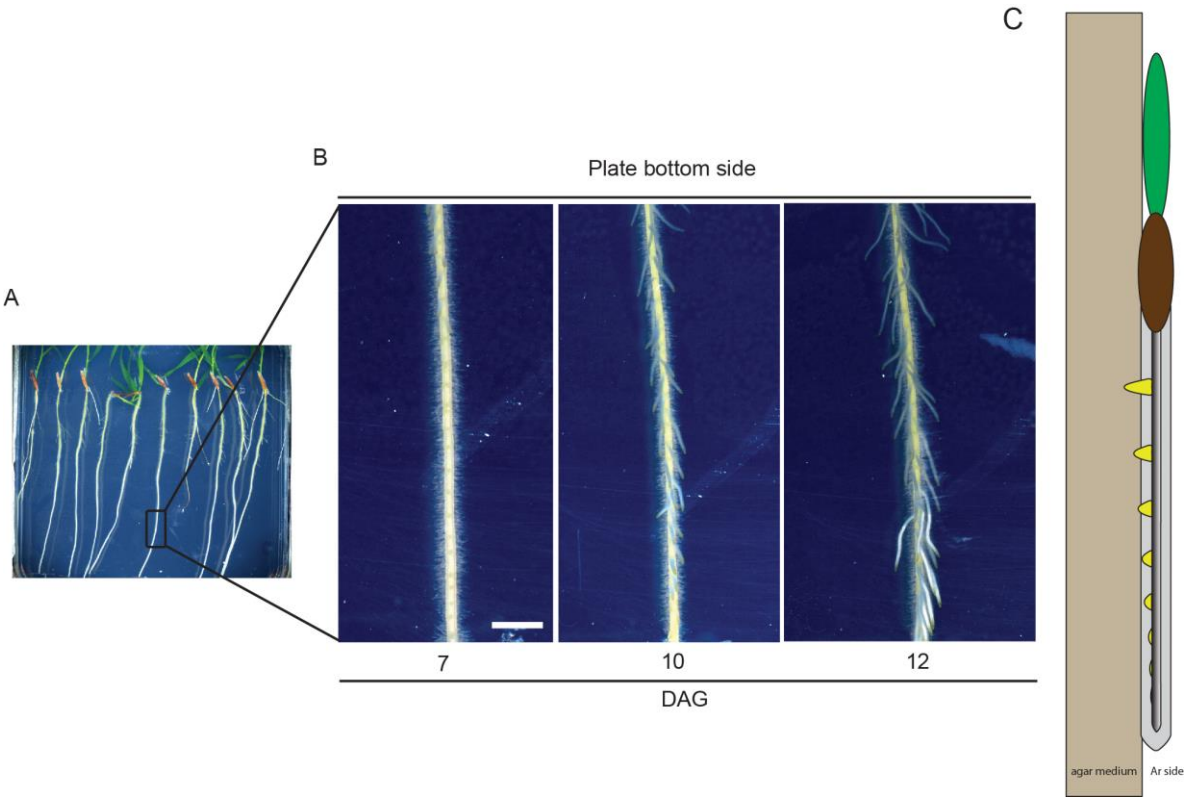

Fig. S3. Brachypodium LRs emerge towards the agar medium. (**A**) Brachypodium seedlings grown on 12x12 cm plates supplemented with half-strength MS solution. (**B**) Progression of lateral root emergence towards the agar after 7, 10, and 12 days after germination (DAG). (**C**) Side view illustration of lateral roots growing towards the agar medium. Representative images were obtained from 45 seedlings from three independent replicates, each consisting of at least 15 plants. Scale : (**B**) 3 mm.

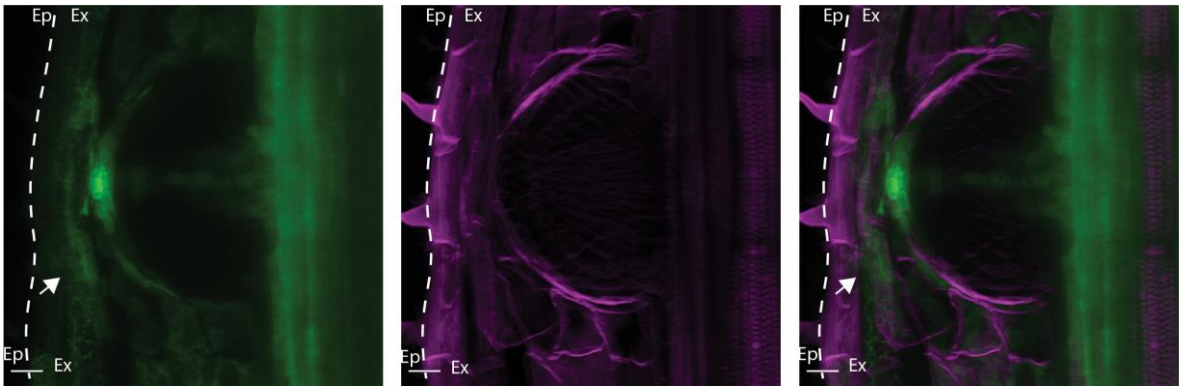

Fig. S4. *DR5pro::ER-mRFP* is induced in the apex of the LRP and in the overlying exodermis. The white arrow indicates presence of the DR5 signal (green) confined to the overlying exodermis. Representative images were obtained from 15 seedlings from three independent replicates, each consisting of at least 5 plants. *DR5pro::ER-mRFP* (green) and cells walls stained with SCRI Renaissance (magenta) for cellulose. Ep: Epidermis, Ex: Exodermis. Scale bar = 20 µm.

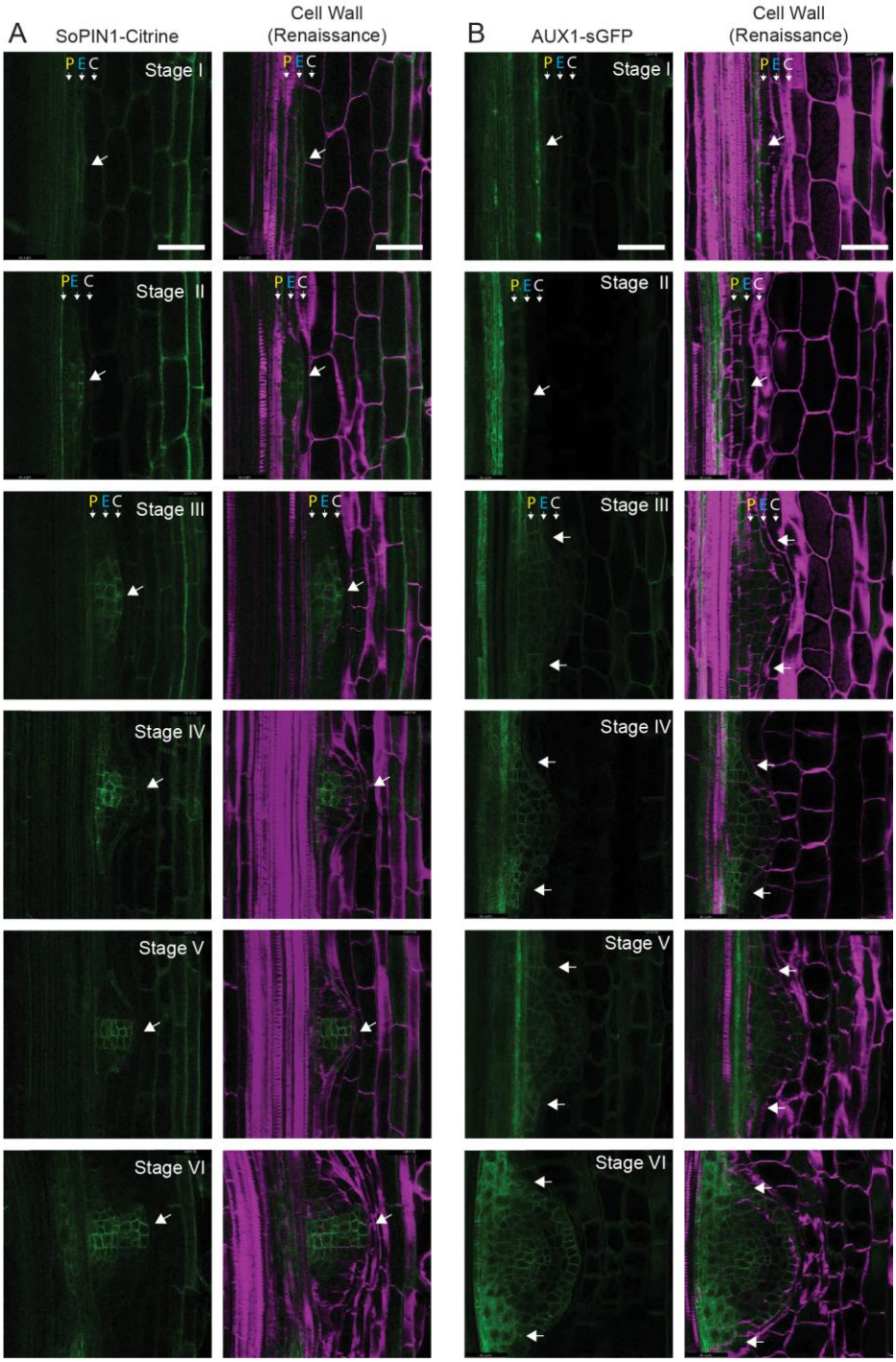

Fig. S5. Localization of *SoPIN1-Citrine* and *BdAUX1-sGFP* during LR formation in Brachypodium. (**A**) SoPIN1-Citrine is observed from Stage I (white arrowhead) during the initial cell divisions in the endodermis. Later, expression is localized in the central region of the LRP. (**B**) Expression of AUX1-sGFP is observed in the vasculature of the primary root and in the LRP from Stage I (white arrowheads). During later stages of LR development, AUX1-sGFP signal is observed in the flanking regions of the LRP with its intensity increasing subsequently in both the vasculature and endodermis in Stage VI. Representative images were obtained from 30 seedlings from three independent replicates, each consisting of at least 10 plants. SoPIN1-Citrine and BdAUX1-sGFP (green) and cells walls stained with SCRI Renaissance (magenta) for cellulose. Scale bar = 50 μm.

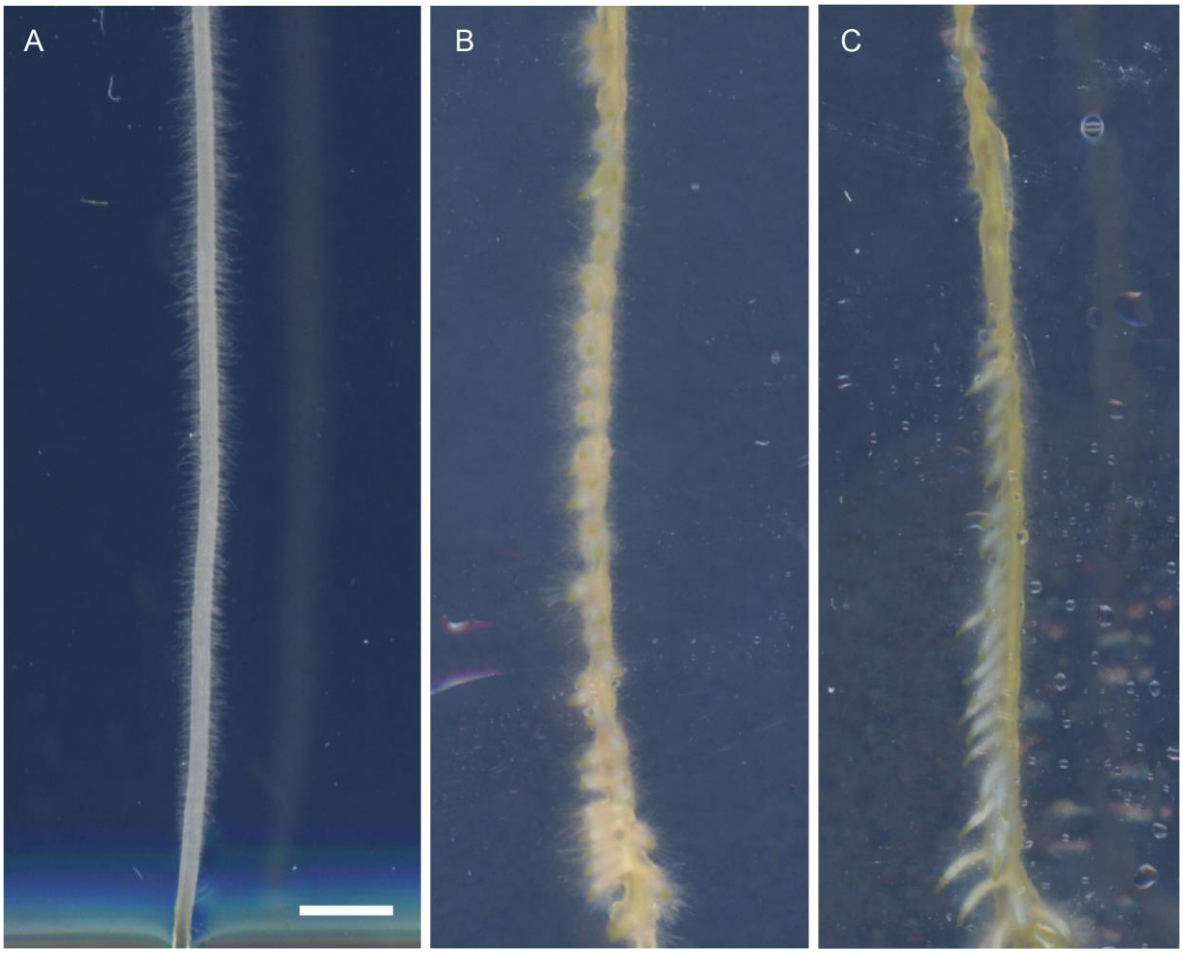

Fig. S6. Exogenous auxin addition induces lateral root formation in Brachypodium. Seedlings were grown on standard ½ MS plates for 6 days and transferred to auxin treatment (10 µM IAA) for 0 (A), 3 (B), and 7 days (C). Scale bar: 0.3 cm. Representative images were obtained from 45 seedlings from three independent replicates, each consisting of at least 15 plants of Bd21-3. Scale bar = 3 mm.

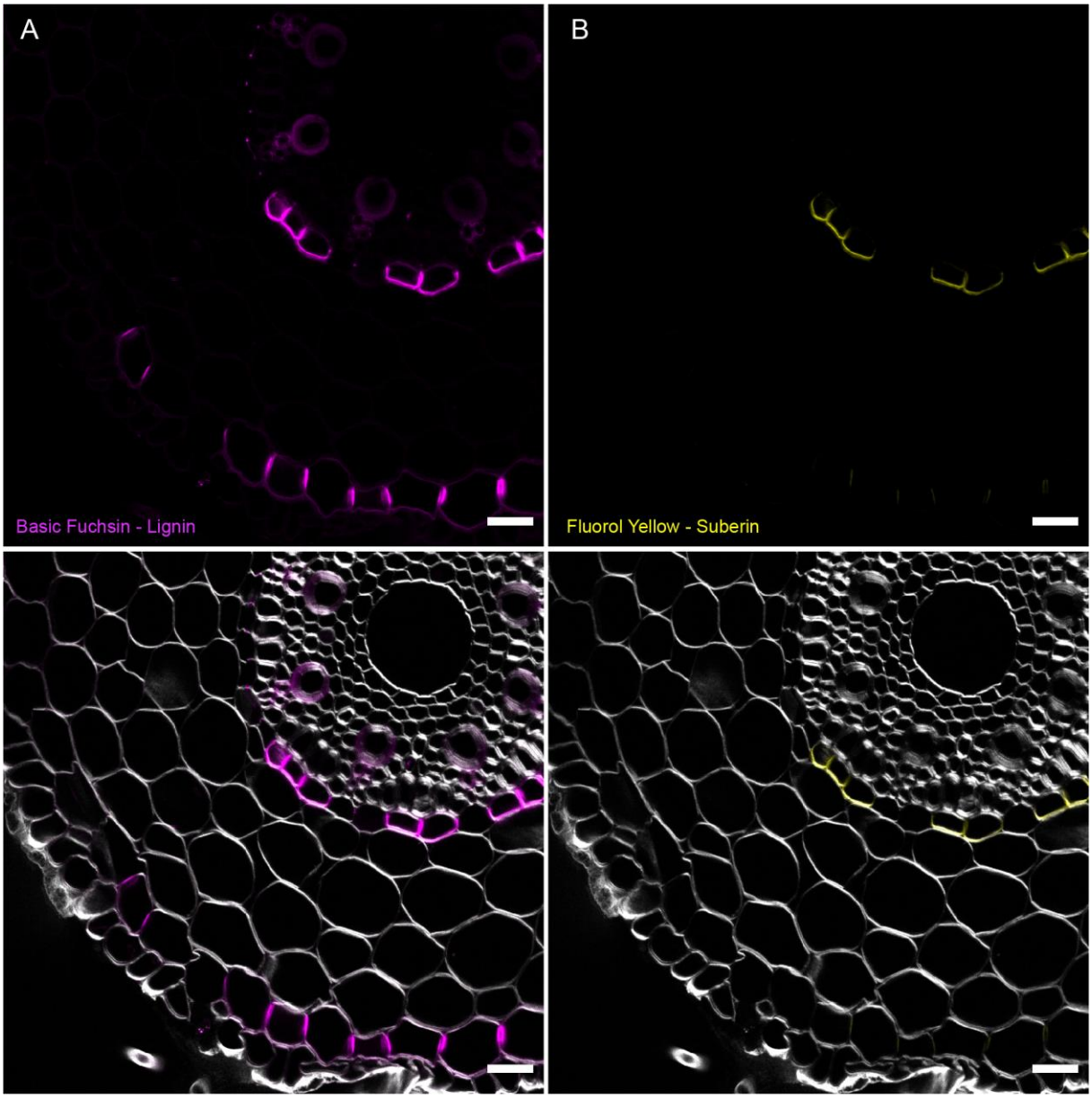

Fig. S7. **The exodermis shows delayed suberization compared to the endodermis.** Cross-sections of Brachypodium primary roots double stained for (**A**) lignin (BF) (**B**) suberin (FY) counter stained with Renaissance SR2200 (cellulose). Roots of seedlings (6 DAG) with similar length were positioned in parallel for consistency, and regions of interest of approximately 1 cm from the root tip were sectioned. Representative images were obtained from 30 seedlings of Bd21-3 from three independent replicates, each consisting of at least 10 plants. Magenta = BF/lignin, Yellow = FY/suberin and gray = SR2200/cellulose. Scale bar: 50 µm.

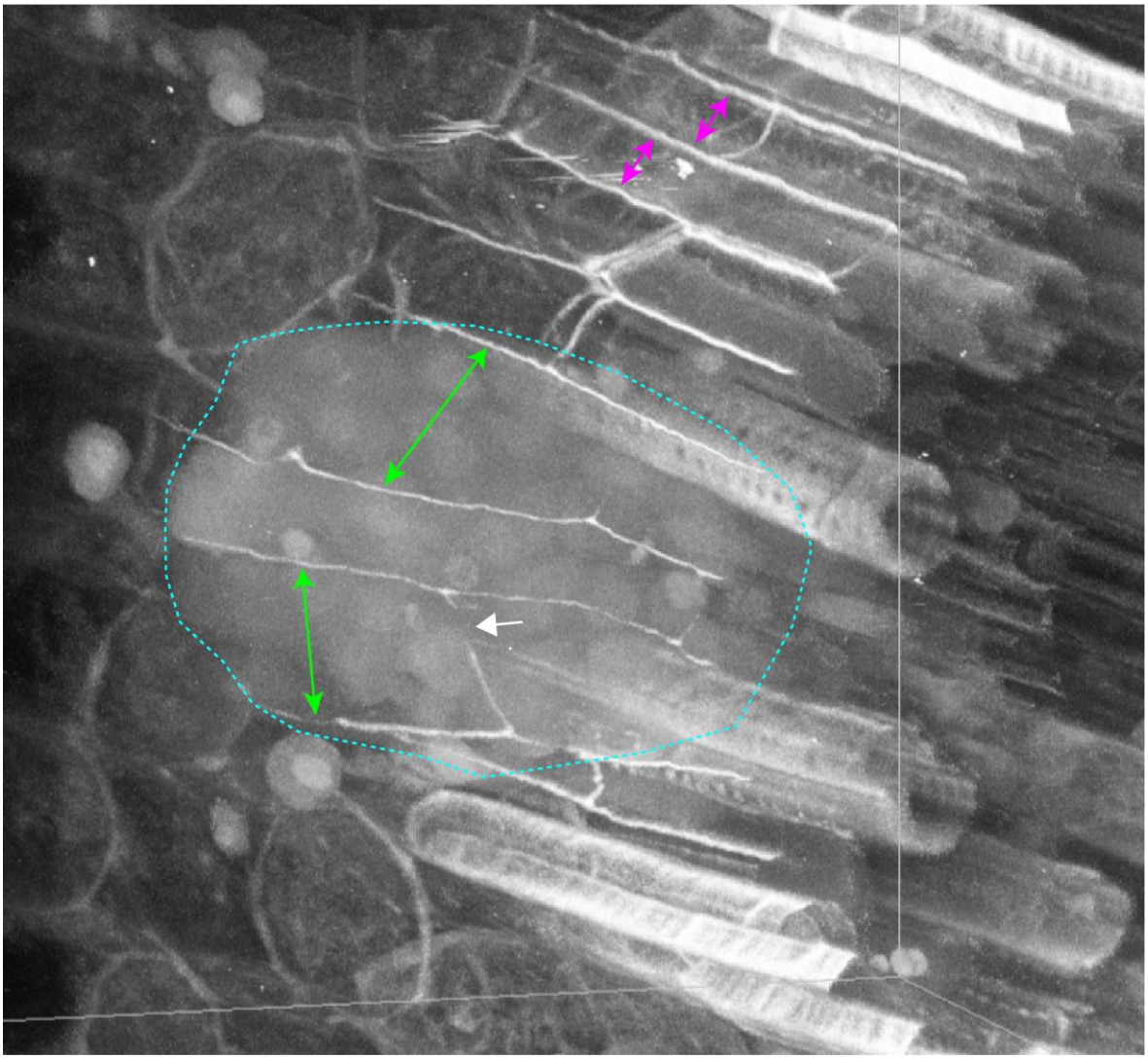

Fig. S8. The CS undergoes lateral detachment during LRP development in Brachypodium. Maximum image projection of a cleared root stained with Basic Fuchsin. The CS breaks locally (white arrow) and appears to be laterally displaced (compare spacing between CS indicated overlying a LRP (green double arrow) and without the presence of a LRP (magenta double arrow) during the emergence of the LRP, outlined by dotted cyan line. Representative images were obtained from 15 seedlings of Bd21-3 from three independent replicates, each consisting of at least 5 plants. BF/lignin = gray. Scale bars = 20 µm.

CHAPTER 5

5. Root Tip Excision (RTE) uncovers differences in lateral root emergence in Brachypodium accessions

Cristovão De Jesus Vieira Teixeira[1]; Kevin Bellande[1], Joop E.M. Vermeer[1] and Thomas Badet[1*]*

Laboratory of Molecular and Cellular Biology, Institute of Biology, University of Neuchâtel, Rue Emile Argand 11, CH-2000, Neuchâtel, Switzerland.

* Corresponding authors: Joop.Vermeer@unine.ch; Thomas.Badet@unine.ch

Author contributions: Chapter 5 was fully written by Cristovão De Jesus Vieira Teixeira with valuable suggestions and corrections by Prof Dr. Joop E.M. Vermeer and Dr Kevin Bellande. All experiments and figures, except some elements from Figure 4 (designed by Dr Thomas Badet) were performed by Cristovão De Jesus Vieira Teixeira.

5.1 ABSTRACT

Root System Architecture (RSA) is vital for plant growth and development, especially under challenging environmental conditions. RSA encompasses structural characteristics such as root length, spread, and the number and length of lateral roots (LRs), which are essential for efficient water and nutrient uptake. RSA's adaptability, known as phenotypic plasticity, enables root systems to respond dynamically to soil resource availability, enhancing plant survival and productivity. This trait is particularly significant given the increasing water scarcity due to climate change and is crucial for developing resilient crop varieties. Despite its importance, the detailed molecular and cellular mechanisms governing RSA, particularly in major crops, are not well understood due to monitoring challenges. In monocotyledons, LR initiation occurs in phloem-associated pericycle cells. We employed the root tip excision (RTE) method to synchronize LR development in Brachypodium, thereby revealing distinct responses between accessions Bd21 and Bd21-3. In Bd21-3, LRs displayed delayed emergence along the root axis compared to Bd21. Additionally, osmotic stresses and hormonal treatments significantly reduced LR number and size in Bd21-3. Histological analyses suggested challenges in LRP emergence imposed by a lignified exodermis in Bd21-3, unlike Bd21, where delayed lignification was associated with facilitated LRP emergence. Integrating RTE with RNA-seq analysis of selected time points revealed a rapid induction of genes encoding for cell-wall remodelling enzymes following LR formation synchronization.

5.2 INTRODUCTION

Root System Architecture (RSA) is essential for plant growth and development, particularly in challenging environmental conditions (Pandey and Bennett, 2024). RSA encompasses various structural characteristics including root length, spread, and the number and length of lateral roots (LRs), which are critical for efficient uptake of water and nutrients (Lynch, 1995). The adaptability of RSA, known as phenotypic plasticity, allows root systems to respond dynamically to spatiotemporal variations in soil resource availability (Uga et al., 2013; Leftley et al., 2021). This plasticity is crucial for enhancing the absorption capabilities of plants, thereby supporting their survival and productivity (Santos Teixeira and ten Tusscher, 2019; Ober et al., 2021). Phenotypic plasticity in roots is particularly significant in the context of increasing water scarcity as a direct consequence of climate change (Morris et al., 2017; Lombardi, De Gara and Loreto, 2021). It is a genetically regulated trait and is considered key to developing more resilient crop varieties (Zhang et al., 2019). Root branching, a major component of RSA, plays a vital role in this process by maximizing the efficiency of water and nutrient acquisition (Moreno-risueno et al., 2010; Atkinson et al., 2014; Yu, Hochholdinger and Li, 2019). The number of LRs and their growth angle are important traits in both monocotyledonous (monocots) and dicotyledonous (dicots) plants that determine the effectiveness of the root system (Waidmann, Sarkel and Kleine-Vehn, 2020). Despite its critical importance, the detailed molecular and cellular mechanisms governing RSA are not well understood, especially in major crops (Yu, Hochholdinger and Li, 2019; Mehra et al., 2023). This gap in knowledge is primarily due to the difficulties associated with monitoring root systems throughout a plant's lifespan (Atkinson et al., 2014). Therefore, the importance of the use of plant models to help us to enhance our understanding of root system development as an important step towards crop improvement.

Arabidopsis thaliana (Arabidopsis) is a well-studied model for understanding the molecular mechanisms underlying LR development due to its simple root system, tissue transparency, and extensive genetic tools (Aceves-García et al., 2016; Tofanelli, Vijayan and Schneitz, 2019; Pardal and Heidstra, 2021). Lateral root primordia (LRP) in Arabidopsis initiate from LR Founder Cells (LRFCs) in the pericycle (Malamy and Benfey, 1997; Vermeer et al., 2014; Stoeckle, Thellmann and Vermeer, 2018). The pericycle is presented as a heterogeneous tissue with diarch symmetry with two distinct cell types positioned opposite to the xylem poles showing different cytological abilities (Beeckman, Burssens and Inzé, 2001; Casimiro et al., 2001; Guyomarc'h et al., 2012; Pandey and Bennett, 2024). In this case, different from quiescent phloem-pole-pericycle (PPP) cells, xylem-pole-pericycle (XPP) cells are competent for LRP formation (Parizot et al., 2008). LRFCs are spatially patterned along the primary root axis with regulated spacing, beginning from the basal root

meristem. The first morphological event in LR initiation occurs in the differentiation zone where LRFCs divide asymmetrically and anticlinal (Malamy and Benfey, 1997). The first developmental stages are strongly influenced by auxin signalling in adjacent tissues (Guseman et al., 2015; Cavallari, Artner and Benkova, 2021; Perianez-Rodriguez et al., 2021). For instance, the presence of a lignified Casparian strip network (CS) and other cell wall modifications, division and expansion of pericycle cells are strictly controlled by the endodermis responses (Vermeer et al., 2014; Ötvös and Benková, 2017; Barbosa, Rojas-Murcia and Geldner, 2019). After several rounds of periclinal and anticlinal cell divisions the LRP advances through the overlying layers to emergence. Despite significant findings on pericycle-endodermis interactions during LR emergence in Arabidopsis, little is known about whether this interaction has similar important roles during LR development in other plant species.

In monocotyledons, LR initiation typically occurs in the phloem-associated pericycle (Pacheco-Villalobos and Hardtke, 2012; Jansen et al., 2013; Crombez et al., 2016; Yu, Hochholdinger and Li, 2019). We previously showed (Chapter 3) that, unlike in Arabidopsis, LR development in Brachypodium involves cell divisions in both the pericycle and the endodermis, contributing to the formation of the new organ. This was also consistent with what is reported for other plant species (Jansen et al., 2012; Xiao et al., 2019). We demonstrated that the Casparian strip (CS) in the endodermis appears to become detached from the cell wall during the LR emergence. However, Brachypodium and many other plant species exhibit one or more additional barriers, functionally similar to the CS, called the exodermis (Enstone, Peterson and Ma, 2003; Sexauer et al., 2021; Liu and Kreszies, 2023). However, the contribution of the exodermis has been often overlooked in the context of LR development. A plausible explanation could be that the endodermis is ubiquitous for angiosperms, whereas the exodermis is absent in several species (Enstone, Peterson and Ma, 2003), particularly in the model plant Arabidopsis. Although the endodermis is found in almost all vascular plants, certain significant species such as Arabidopsis and crops including cultivated barley, soybean, and wheat lack an exodermis (Kreszies, Schreiber and Ranathunge, 2018; Liu and Kreszies, 2023). In Brachypodium, the exodermis becomes both lignified and suberized (Sexauer et al., 2021), and its response likely varies, depending on nutrient availability, as has been demonstrated in the exodermis of maize (Hose et al., 2001). However, we still lack a clear characterization of its function during the emergence of the LRP.

In this study, we applied the root tip excision (RTE) method (Kawai, Shibata, et al., 2022) as a system to synchronize LR development in Brachypodium. We observed that the RTE approach elicited distinct developmental responses between the Brachypodium

accessions Bd21 and Bd21-3. Although both accessions exhibit similar LR development near the RTE site, LRPs in Bd21-3 fail to progress in their growth along the root axis. Intriguingly, we also observed that the RTE-induced LR phenotype in Bd21-3 is not maintained when plants are transferred from one growth plate to another. Furthermore, both abiotic stresses and hormonal treatments result in a marked reduction in LR number and size in Bd21-3 when compared to Bd21. Histological analyses suggest that LRPs in Bd21-3 likely face challenges in traversing a fully lignified exodermis; whereas in Bd21, LRP emergence appears to be facilitated by a significant delay in lignification. Additionally, by integrating RTE as a LR induction system (LRIS) with RNA-seq analysis, we demonstrated that genes related to cell-wall processes are rapidly induced following synchronization of LR formation.

5. RESULTS

5.3.1 Bd21 and Bd21-3 show distinct LR developmental responses after RTE

Phenotypic plasticity is defined as the ability of an organism to alter its phenotype in response to environmental conditions (McCleery, Mohd-Radzman and Grieneisen, 2017). One notable example is root plasticity, which enables plants to explore soils for water and nutrients (Amtmann, Bennett and Henry, 2022). This capability heavily relies on the development of primary roots and LR growth (Kawai, 2022). Among many other factors, LR development is promoted when the elongation of the parent root is inhibited. In Chapter 2, we demonstrated that compensatory LR growth following RTE could serve as an alternative method for synchronizing early LR development in Brachypodium Bd21-3. We then questioned how this approach would function in other *Brachypodium* accessions. To further explore and better visualize LR development after RTE in Brachypodium, we selected the accessions Bd21 and Bd21-3 for detailed analyses. In the Bd21 accession, excision of the primary root tip resulted in consistent emergence of LRs along the root axis, with a marked decline in LR density near the root-shoot junction (**Figures 1B** and **1D**). In contrast, plants of the Bd21-3 accession showed similar LR development in the first 1 cm of the root axis near the RTE site (**Figure 1B-D**); however, at 72hrs after RTE, LRs in the upper part of the primary root either failed to emerge or did not continue to grow towards the nutrient medium (**Figure 1B**-**C** – white arrows). We previously observed that it takes approximately 32-36 hours for an LRP to fully emerge in Bd21-3 within the first 5 mm past the RTE region. High-resolution images enabled us to identify a zone of LR formation where LRPs were either fully emerged or in early stages prior to emergence. Interestingly, there was no significant difference in the number of visible LRPs within 24 hours post-RTE between Bd21 and Bd21-3 (**Figure 1E**).

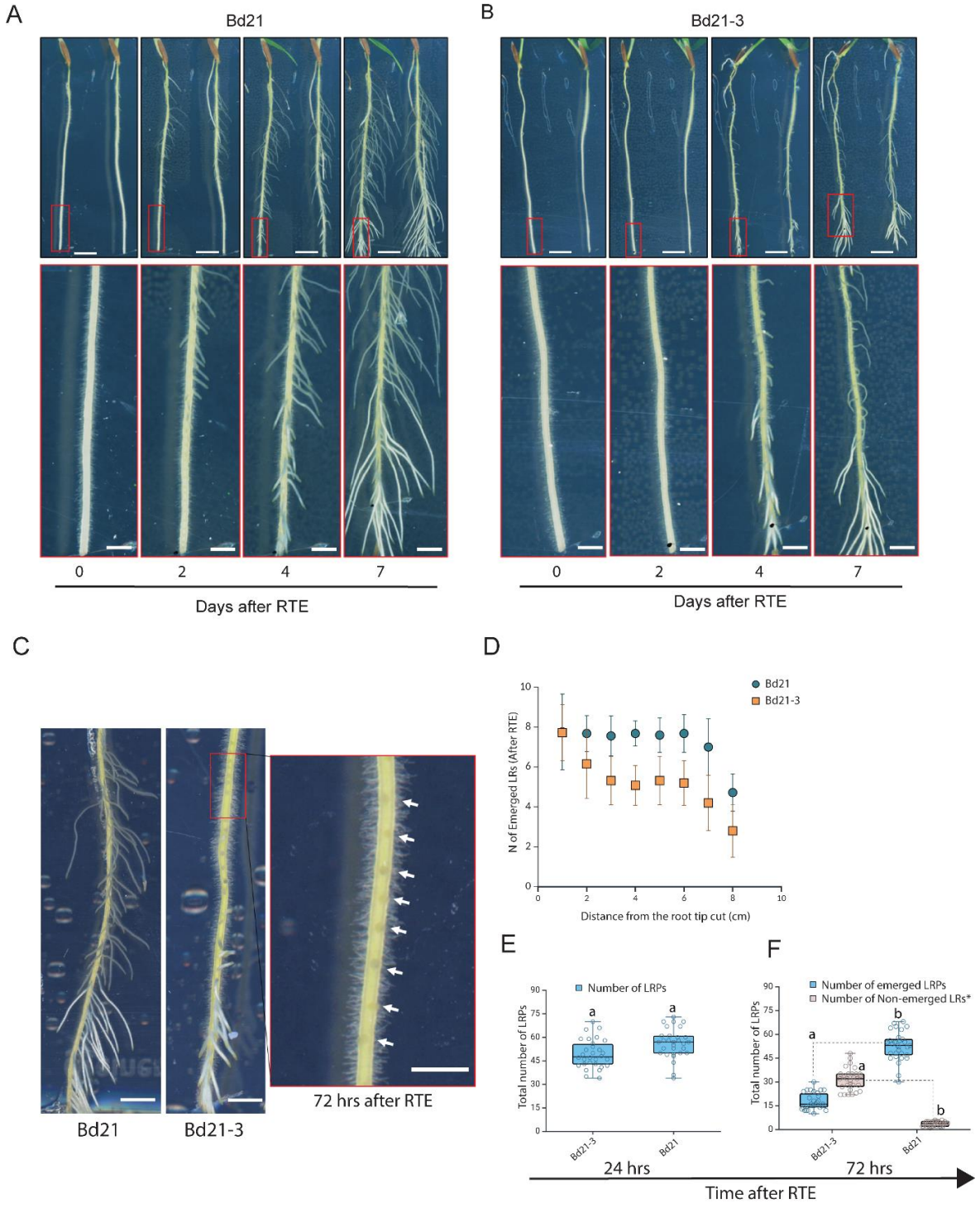

Figure 1. **Impaired LR development in Bd21-3 compared to Bd21 following root tip excision.** (**A**, **B**) Comparison of LR emergence at 0, 2, 4, and 7 days post root tip excision (**RTE**). Red rectangles in the first row of images highlight the corresponding root regions shown in the second row. (**C**) Bd21 and Bd21-3 accessions 72 hours after RTE. The magnification shows that LRPs are visible in Bd21-3 but fail to develop further approximately 1 cm from the RTE region. (**D**) Graph showing the density of fully emerged LRs along the root axis of Bd21 and Bd21-3. (**E**) Graph showing the total number of LRPs observed 24 hours after RTE. (**F**) Graph showing the total number of fully emerged and non-emerged LRs 72 hours post-RTE. (*****) LRPs that crossed the exodermis but failed to continue growth were counted as non-emerged for Bd21 and Bd21-3. Scale bars: (**A**-**B**, upper panel: 5 mm; lower panel: 3 mm), (C: 3 mm). Values represent mean ± SD (n = 3 independent biological replicates). Different letters indicate significant differences among groups ($P < 0.05$).

Nevertheless, 72 hours after RTE, the majority of LRPs in Bd21-3 fail to continue their growth towards the medium (**Figure 1F**). This suggests that although RTE triggers LR initiation in both accessions, they display differential regulation of LR emergence.

5.3.2 Brachypodium Bd21-3 shows delayed LR emergence under abiotic stresses and hormonal treatments.

The development of lateral roots has been shown to be significantly affected by different abiotic stresses (Amtmann, Bennett and Henry, 2022; Pandey and Bennett, 2024). These stresses can significantly RSA and function, primarily through hormonal regulation (Khan, Gemenet and Villordon, 2016). Among the key hormones involved, auxin and abscisic acid play pivotal roles in mediating plant responses to environmental conditions (Signora et al., 2001; Cavallari, Artner and Benkova, 2021). Drought and osmotic stresses have also been reported to modulate LR development (Xiong et al., 2006; Uga et al., 2013). We hypothesized that exposing Bd21 and Bd21-3 to a diversity of hormonal and stress treatments would result in similar diferences in LR development. To investigate the effects of indole-3-acetic acid (IAA) and abscisic acid (ABA) treatment on Brachypodium LR development following RTE, seedlings (6 DAG) were transferred to plates supplemented with either 1 µM or 10 µM IAA, or 1 µM or 10 µM ABA.

To simulate salt and osmotic stresses, another set of seedlings was transferred to plates containing 85 mM or 170 mM NaCl, and 170 mM or 340 mM mannitol, respectively. After 72 hours, LR number and size were quantified. Interestingly, differential LR emergence of Bd21-3 is lost after the plate transfer transfer (**Figure 1**). In this case, LR number and size were similar in both Bd21 and Bd21-3, displaying comparable LR densities (**Figure 1**). IAA treatments reduced the size of LRs in Bd21 but did not dramatically affect their density along the root axis (**Figure 1A** and **1C**). Conversely, Bd21-3 exhibited a significant reduction in LR emergence and length at both 1 µM and 10 µM IAA concentrations (**Figure 1A** and **1C**). ABA treatments strongly inhibited LRP development in both Bd21 and Bd21-3 at a concentration of 1 µM, with a more pronounced effect observed in Bd21-3 (**Figure 1B** and 1D). At 10 µM ABA, both Bd21 and Bd21-3 showed a dramatic decrease in LRP emergence (**Figure 1B** and **1D**). Exposure to NaCl resulted in reduced overall LR size and density at both 85 mM and 170 mM concentrations in both accessions (**Figure 1D** and **1E**

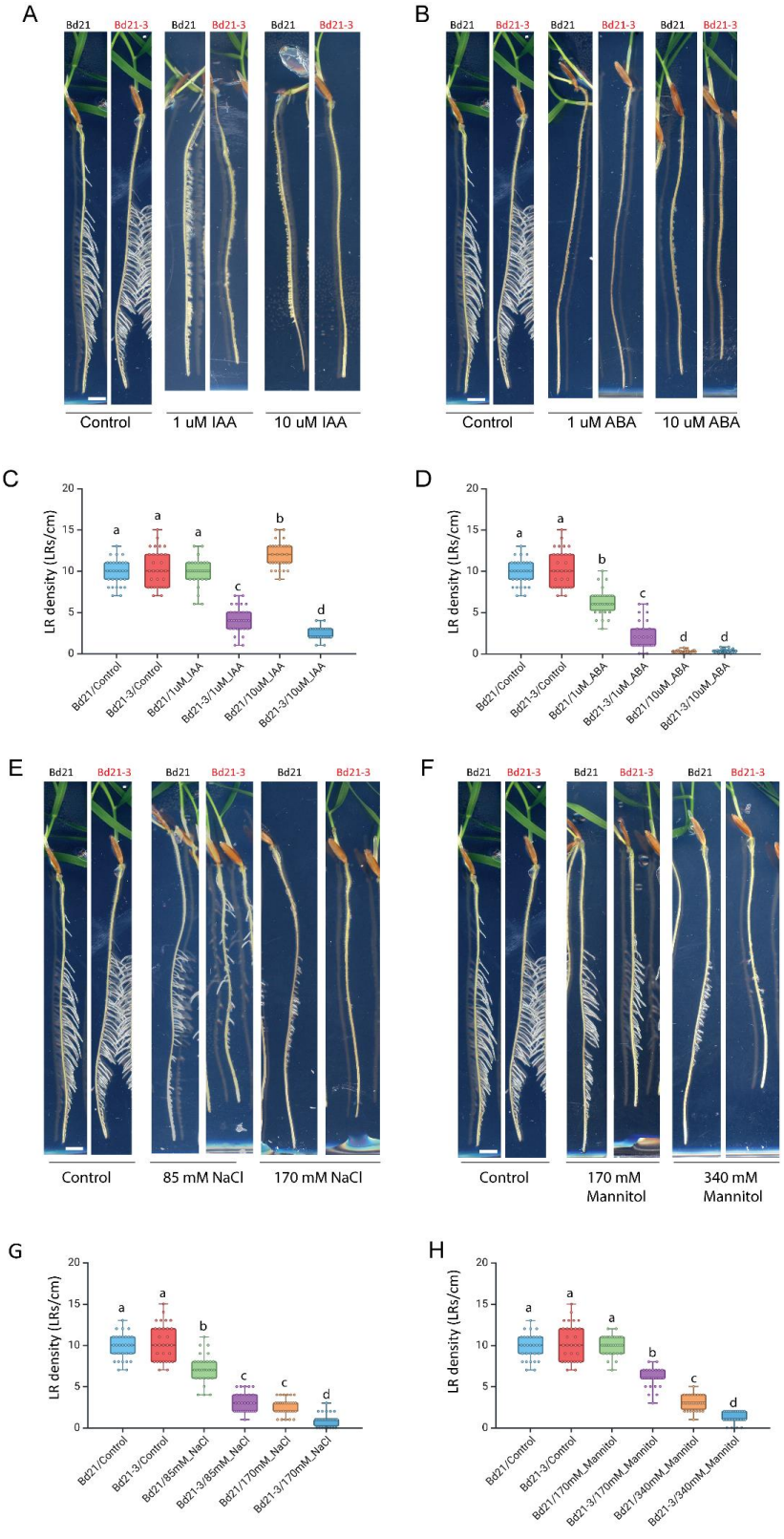

Figure 2: **Bd21-3 exhibits inhibition of LR development under hormonal and osmotic stress conditions.** Six-day-old Bd21 and Bd21-3 seedlings, previously grown on regular ½ MS plates, were transferred to plates treated with (**A**) 1 µM and 10 µM IAA, (**B**) 1 µM and 10 µM ABA, (**E**) 85 mM and 170 mM NaCl, and (**F**) 170 mM and 340 mM mannitol and RTE was applied. Panels (**C**), (**D**), (**G**), and (**H**) display graphs showing LR density (fully emerged LRs/cm) along the root axis, comparing treatments to controls. Scale bars: (**A**-**B**, **E**-**F**: 5 mm). Values represent mean ± SD (n = 3 independent biological replicates). Different letters indicate significant differences among groups ($P < 0.05$).

Notably, Bd21 maintained a number of fully developed LRs at 85 mM NaCl, and many LRs still emerged at 170 mM NaCl (**Figure 1E** and **1G**).

However, no LRPs were detected in Bd21-3 at 170 mM NaCl (**Figure 1E** and **1G**). For the mannitol treatments, there was a decrease in LR size but not in LR density for Bd21 at 170 mM, and a mild decrease in LR density and LR emergence for Bd21-3 (Figure 1F and 1G). While Bd21 exhibited some LR emergence at 340 mM mannitol, this treatment dramatically reduced the number of emerged LRs in Bd21-3 (**Figure 1F** and **1H**). These results suggest that although the RTE-LR phenotype observed in Bd21-3 in (**Figure 1**) is lost when transferring plants to new plates, both hormonal and abiotic treatments trigger a more pronounced decrease in LR number and size in Bd21-3 partially recovering the original RTE-LR phenotype.

5.3.3 Exodermal lignification correlates with delayed LR emergence

The exodermis and endodermis represent the outermost and innermost layers of the root cortex, respectively (Peterson & Cholewa, 1998; Steudle & Peterson, 1998). Previous studies have documented that structural features of the root exodermis and endodermis, such as Casparian strips, suberin lamellae, lignin deposition, and tertiary walls, are finely regulated in response to osmotic stress and tissue damage (Enstone et al., 2002; Henry et al., 2012; Geldner, 2013; Tylová et al., 2017). Therefore, lignin, a highly rigid compound less plastic than suberin, could potentially restrict the emergence of LRP upon reaching the exodermis in Brachypodium. We hypothesized that the lignification of root cell layers, especially the exodermis, along with other anatomical features, influences the ability of LRPs to emerge and continue their developmental process in Brachypodium Bd21-3. To test this hypothesis, we applied the RTE method and analysed plants 24 hours after RTE. To assess lignification, roots from Bd21 and Bd21-3 were stained with phloroglucinol-HCl. This staining reacts with coniferaldehyde residues in lignin in the presence of acid, generating a red condensation product known as the Wiesner reaction (Davidson et al., 1995). Phloroglucinol-HCl treated roots of Bd21 exhibited consistent clear, light red staining, slightly darker in the central vasculature (**Figure 3A**).

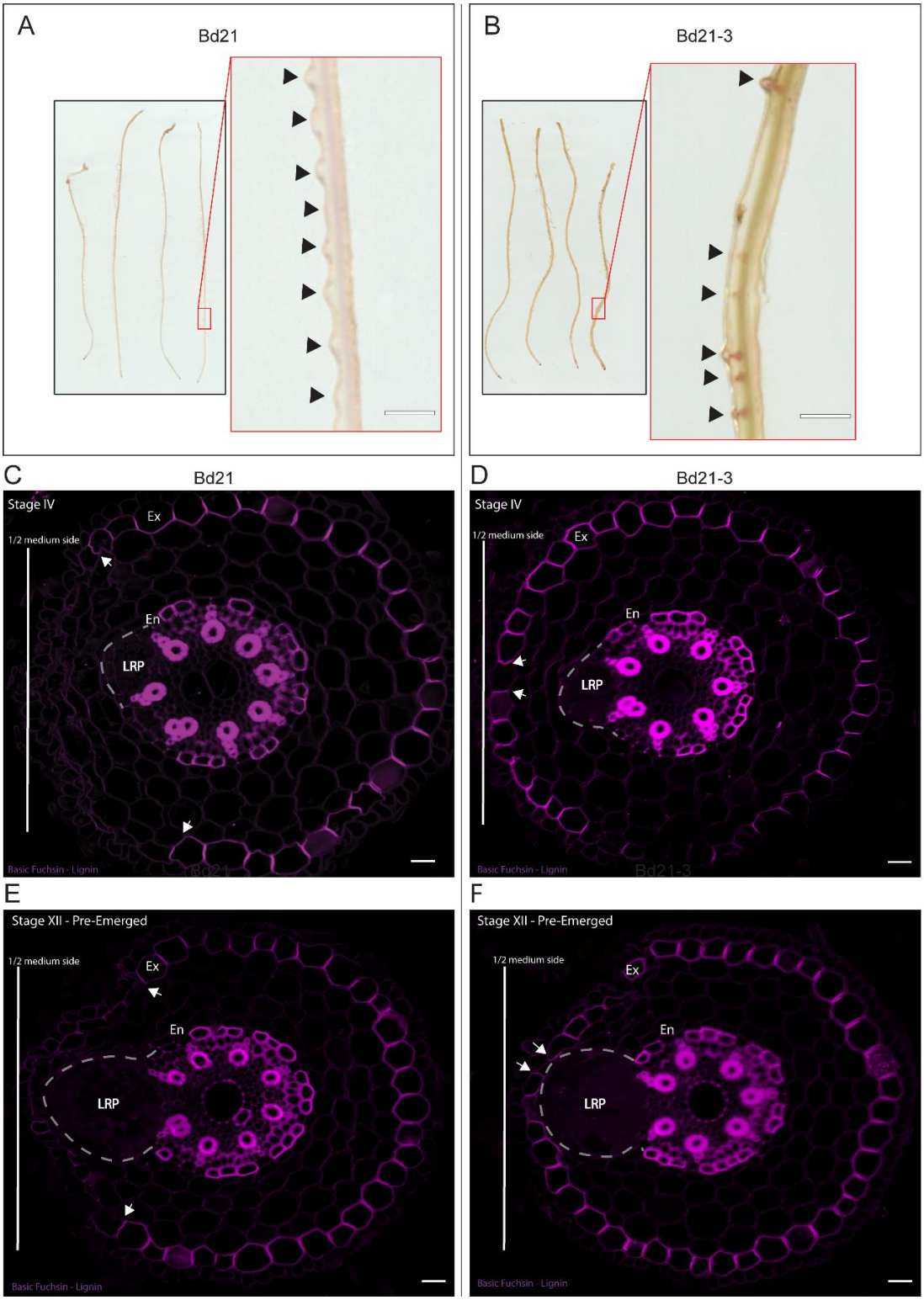

Figure 3. Bd21-3 displays earlier lignification in the exodermis. (**A**, **B**) Roots of Bd21 and Bd21-3 stained with Phloroglucinol-HCl exhibit a red-brown color. A red rectangle in the left images highlights the area magnified in the right panel. Black arrows indicate LRPs 36 hours post-RTE. Light brown-red staining is observed in the LRPs of Bd21, with enhanced color intensity in Bd21-3, especially in the LRPs and exodermis. (**C**, **D**, **E**, **F**) Basic Fuchsin-stained sections of Bd21 and Bd21-3 roots show lignin deposition in the vasculature and exodermis at distinct developmental stages of LRPs. The exodermis in Bd21-3 shows lignification before LRP emergence. A white vertical bar on the left side of each image marks the side facing the ½ MS medium. White arrowheads indicate the limits of exodermal lignification opposite to the LRP emergence side. Scale bars: (**A**-**B**: 2 mm, **C**-**F**: 50 µm). (45 seedlings were analysed with 3 independent biological replicates for each staining approach).

In contrast, roots from Bd21-3 showed a darker red color throughout the root axis and vasculature (**Figure 3B**). Interestingly, the LRPs appeared transparent in color in Bd21 (**Figure 3A**, dark arrows), while an intense red color was observed in LRPs and the overlying exodermis of Bd21-3. These results suggest a more pronounced overall lignification in Bd21-3 roots.

To further investigate endodermal and exodermal lignification in the LR emergence region of Bd21 and Bd21-3, we conducted an additional experiment using a second set of roots grown under the same conditions. Cross-sections of these roots were stained with Basic Fuchsin, a fluorescent dye that indicates the presence of lignin, and observed using confocal microscopy. Firstly, we observed that exodermal lignification in Brachypodium initiates similarly to Casparian strips and spans nearly the entire dimension of an anticlinal wall for both Bd21 and Bd21-3 (**Figure S1**). In Bd21, lignification was reported in the area where LRP emergence was anticipated by Stage IV (**Figure 3c**). By Stage XII, lignification was confined to the vicinity of the emergence zone. LRPs in Bd21 exhibited an elongated bell shape as typically observed in monocots such as rice and maize (Jansen et al., 2012; Ni et al., 2014). On the other hand, in Bd21-3, exodermal lignification was observed much earlier evident in the LRP emergence region. The exodermis was already fully lignified around Stage IV primordia with a likely passage cell opposite the LRP (**Figure 3D, F**). The shape of LRPs in Bd21-3 was rounded and less elongated compared to those in Bd21 (**Figure 3D, F**). These results suggest that LRPs in Bd21-3 likely encounter difficulties in penetrating through a fully lignified exodermis, whereas LRP emergence is likely facilitated in Bd21 due to the absence of evident lignification. Although these observations strongly support our hypothesis regarding the LR phenotype observed in Bd21-3 following RTE, further insights into the molecular mechanisms underlying these changes, as well as the roles of other cell wall components in the emergence of LRPs in Brachypodium, are still needed.

5.3.4 Cell-wall-related genes are rapidly induced after RTE

The early steps in LR development require significant cell wall modifications to allow the new organ to emerge through the overlying tissues. To investigate whether difference in gene expression after RTE in Bd21 and Bd21-2 could explain the observed emergence phenotype, we performed transcriptome profiling of root sections collected at selected time points following RTE. Analysis of the results revealed significant differences in gene expression between Bd21 and Bd21-3 (**Figure 4**).

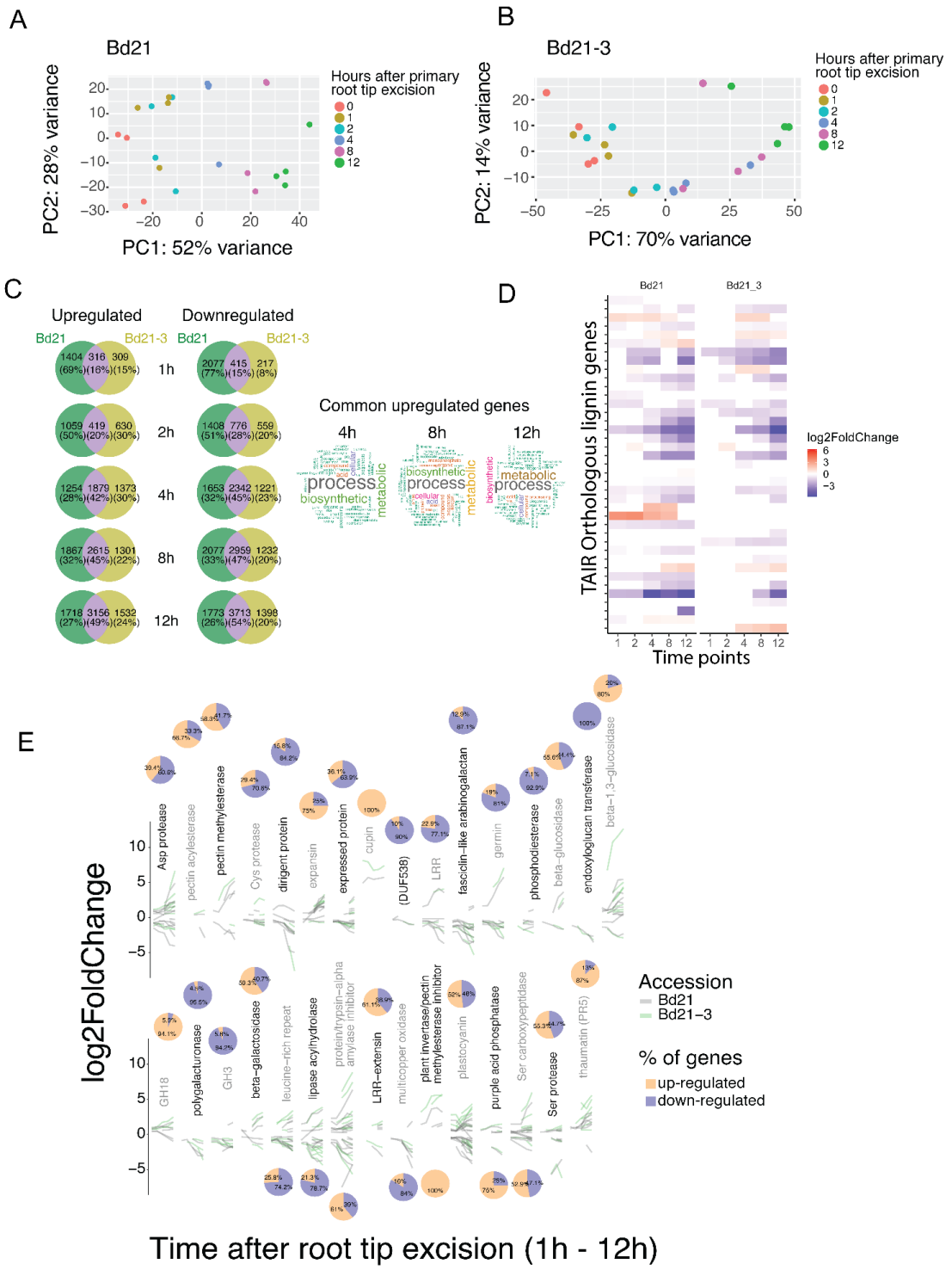

Figure 4. Overview of Differential Gene Expression (DGE) analysis in Brachypodium Bd21 and Bd21-3 after root tip excision (RTE). (**A**-**B**) The scatter plot shows the first two principal components (PC1 and PC2) of RNA-seq data, with RNA extracted from root tissue collected at different time points (0h, 1h, 2h, 4h, 8h, and 12h) after RTE, with four replicates per time point. Plots highlight the temporal changes in gene expression following RTE in both Brachypodium accessions.(**C**) Overlap between upregulated and downregulated genes at timepoints 1h, 2h, 4h, 8h, and 12h after RTE. Common upregulated genes are shown in the right panel for 4h, 8h, and 12h. (**D**) Heatmap of TAIR orthologous lignin gene expression in Brachypodium Bd21 and Bd21-3 across different timepoints after RTE. (**E**) Representation of the main cell wall-related compounds and the percentage of upregulated and downregulated genes for Brachypodium Bd21 and Bd21-3. Log2FoldChange from timepoints 1h and 12h after RTE. At least 30 seedlings per timepoint in 4 independent biological replicates.

A comprehensive analysis identified 13,214 and 14,093 differentially expressed genes (DEGs) in Bd21-3 and Bd21, respectively, with the majority of these genes (86% in Bd21-3 and 83% in Bd21) being differentially expressed at 12 hours post-RTE (**Figure 4C**). Principal component analysis (PCA) distinguished two major transcriptomic clusters corresponding to early (0-2 hours) and late (8-12 hours) time points, indicating distinct temporal responses **(Figure 4A** and **B**). The number of upregulated and downregulated genes increased progressively over time, with significant overlap observed at 4, 8, and 12-hour time points (**Figure 4C**). Functional categorization revealed that genes associated with transcriptional regulation, hormone signaling, and cell-wall remodeling were prominently represented among the top 100 upregulated and downregulated genes (**Figure S4**). Notably, cell-wall remodeling enzymes, such as cellulases, pectinases, and peroxidases, which are crucial for loosening the primary root cell wall to allow new root emergence, showed significant differential expression (**Figure 4E**). Comparative analysis with Arabidopsis orthologous lignin biosynthesis genes revealed upregulation in Brachypodium at early time points of Bd21, whereas no corresponding expression was detected in Bd21-3 (**Figure 4D**). This suggests species-specific regulatory mechanisms to one of the Brachypodium accessions. Overall, the data suggest a rapid activation of cell-wall-related genes following RTE, particularly at early and late time points, underscoring their role in LR development. However, further studies are needed to directly associate these gene expression changes with specific processes in LR formation.

5.4 DISCUSSION

Compensatory root growth might induce changes in Brachypodium LRP morphology

Compensatory root growth is crucial for maintaining total root length and thus water and nutrient uptake in compacted soils (Kawai, Shibata, et al., 2022). In this study, we investigated LR development in Brachypodium using this principle. Our findings from the LR-RTE synchronization system show distinct LR developmental responses between Brachypodium accessions Bd21 and Bd21-3 (**Figure 1** and **2**). Bd21 demonstrates strong LR regenerative capabilities, while Bd21-3 displays altered LR emergence and elongation when grown vertically on plates. A similar method was used in rice identifying QHB/OsWOX5 as a key regulator of root development (Kawai, Chen, et al., 2022; Kawai, Shibata, et al., 2022). Rice genotypes exhibited compensatory root growth with altered LR distributions in response to RTE. This approach was also shown to increase the diameter of first-order LRs by enhancing the number of ground-tissue layers and the stele diameter, promoting elongation and higher-order LR emergence in proximal regions to RTE (Kawai, Chen, et al., 2022). LRP morphology may also change in Brachypodium likely varying with the distance

from the cut site. More studies will be required to quantify the degree of change in LRP shape pre/post RTE along the root axis after RTE.

LR formation in Bd21-3 is more sensitive to stress and hormone treatments compared to Bd21.

We investigated the RTE-LR phenotype in Brachypodium Bd21 and Bd21-3 roots in response to osmotic stress and hormonal treatments. We identified the inhibition of LR number and growth in both Bd21 and Bd21-3 accessions. Our preliminary studies indicated that these treatments had a stronger overall effect on the Bd21-3 accession, in which LRs either failed to emerge or to continue their development. ABA is a prime mediator of drought and plays an important role in regulating plant growth, development, and responses to several environmental stresses (Zhu, 2002; Boominathan et al., 2004). Drought-mediated inhibition of LR development appears to be partly mediated by ABA (Xiong et al., 2006). In our results, exogenous ABA had similar inhibitory effects on LR development as salt or osmotic stress (NaCl and mannitol) (**Figure 1**). The inhibitory effect of ABA on LR development has been reported (Signora et al., 2001). The hormone auxin (IAA) is known to inhibit root elongation and promote the initiation of LRs (Dharmasiri et al., 2005; De Smet, 2012; Du and Scheres, 2018; Javed et al., 2023). We observed that IAA treatment reduced LR emergence in Bd21-3 compared to Bd21. The RTE approach was expected to decrease cell elongation since the root meristem is removed. If auxin also increased LR induction simultaneously, too many LRs could form on roots with decreased emergence. It may be that the levels of endogenous auxin in Bd21-3 are higher than in Bd21 and to some extent limit the emergence of elongation of the LRPs in combination with external auxin stimulus. Thus, ABA may have a general regulatory role in controlling LR development in Brachypodium. However, the complex hormone signaling regulating the cell-to-cell communication between LRP emergence and the overlying cell layers still remains unclear or unexplored in monocots. It would be useful to have reporters for auxin responses, such as DR5 or R2D2 to really compare the endogenous levels of auxin signalling in these two accessions (Ulmasov *et al.*, 1997; Liao *et al.*, 2015).

Brachypodium natural accessions as a potential source to study genetic variability in LR emergence after RTE

The present study reveals an unexpected root phenotype in Brachypodium Bd21-3. Interestingly, Bd21-3 was originally collected from the same location as the accession used to create the first reference genome, Bd21 (Vogel, 2008; Chochois, Vogel and Watt, 2012). However, Bd21-3 is not a descendant of Bd21, despite their close relationship (Bevan, Garvin and Vogel, 2010). Notably, they showed major differences in root phenotype after

RTE treatment. A large number of Brachypodium accessions have been collected throughout its native growth range in the Mediterranean and the Middle East (Garvin, 2007; Bourgeois *et al.*, 2018; Mur, 2022). Our results suggest that the combination of the straightforward LR-RTE approach with the analysis of natural phenotypic variation in Brachypodium accessions could be a major tool for identifying single nucleotide polymorphisms (SNPs) linked with LR development through a genome wide association (GWAs) methodology (Huang and Han, 2014).

Timing of exodermal lignification is associated with LR emergence

The exodermis (hypodermis with Casparian bands) of plant roots represents a barrier of variable resistance to the radial flow of both water and solutes and may contribute significantly to overall resistance (Hose *et al.*, 2001; Enstone, Peterson and Ma, 2003). A recent study suggests that in tomato, polymerized lignin impregnates the primary cell wall and serves as an apoplastic barrier dependent on its lignin composition unlike Casparian strips which are centrally localized (Manzano *et al.*, 2022). Conversely, our results show that Brachypodium exodermis exhibits lignification similar to Casparian bands (**Figure S1**). One possible outcome is that the position of the initial lignin impregnation in the exodermis might confer different properties to the cell layer, such as altered rigidity (Enstone, Peterson and Ma, 2003). Similarly, our observations suggest that increased exodermal lignification in Bd21-3 likely acts as a mechanical barrier to LRP emergence; a feature less evident in Bd21. These results are, to some extent, consistent with a previously proposed framework (Enstone, Peterson and Ma, 2003) that discusses the functional adaptations of root cell walls in environmental interactions, but does not specifically address the role of the exodermis the LRP emergence background. Lignification is found in the secondary cell wall of all vascular plants and some red algae, imbuing cell walls with properties of rigidity and hydrophobicity and in some species in multiple exodermis can be formed (Barros *et al.*, 2015). For instance, onions often lack LRs and have a dimorphic exodermis (Enstone, Peterson and Ma, 2003). Potentially, the extra exodermal layer could also limit the development of LRPs in a much earlier developmental stage in the root development. In the case of Brachypodium, it has been observed that although the exodermis shows earlier lignification in Bd21-3, the plants appear to be more sensitive to stress. However, more studies are necessary to confirm whether the Bd21-3 plants are not well developed because the exodermis is failing to block toxic compounds from the roots, or if the early lignification is mechanically repressing the emergence of the LRP and potentially limiting the transport of water and nutrients to the vasculature.

Transcriptome profiling of root sections after RTE aligns with an important role for cell wall modification during LR emergence

Cell wall remodeling enzymes facilitates the process of LR emergence (Somssich, Khan and Persson, 2016). Enzymes such as cellulases, pectinases, and lipases play a pivotal role in modifying the composition and/or properties of cell walls, making them more flexible and extensible (Cheung *et al.*, 2021). Here, we showed that early (0 to 2 hours) and late time points (4 to 12 hours) formed two major transcriptomic clusters. Although a significant number of genes were differentially expressed later in the time course, with the majority showing differential expression at 12 hours post-RTE, we were unable to directly associate function with specific LR developmental processes. However, the fact that a number of up- and down-regulated genes progressively increased over the time course suggests that it might be an association to the CW modifications usually observed during the emergence of the LRP. This is consistent to observations that genes related to transcriptional regulation, hormone signaling, and cell-wall remodeling, as well as many genes with unknown functions were observed among the top 100 up- and downregulated DEGs. However, the finding that many genes with a predicted role in ligninification were upregulated at early time points in Bd21 but not in Bd21-3 is a bit counterintuitive with the increased exodermal lignification observed in this accession. It might well be that we are simply lacking the resolution to pick up genes that regulate exodermal lignification and that we are rather looking at general regulators of lignification in the xylem. Furthermore, the RTE approach also triggers a cascade of wound-responsive genes (Matosevich and Efroni, 2021). Despite our efforts to expedite the tissue collection and RNA extraction procedure, the early time points likely highlight numerous wound-induced genes. These processes are associated with local cell differentiation, focusing on protecting the root from any threats. Consequently, pinpointing gene expression associated with the initial cell divisions in the LRP in Brachypodium presents significant challenges. In this case, utilizing single-cell RNA sequencing (scRNAseq) on root tissues post-RTE would be an appropriate method to investigate the genetic programs underlying cell wall modifications and spatial accommodation changes during LRP emergence.

5.5 MATERIAL AND METHODS

Plant Materials

Brachypodium distachyon accessions Bd21 and Bd21-3 were used for all experiments (Vogel and Hill, 2008).

Germination and Growth Conditions

Seeds were germinated on solid half-strength Murashige and Skoog (MS) medium without sucrose. For microscopic analyses with histological staining, 6-day-old seedlings were used. Both Bd21 and Bd21-3 seeds were peeled and surface sterilized for 1 minute in a 6% bleaching solution, rinsed with water, and then sown on plates. The seeds were stratified by incubating the plates for 2 days at 4°C and then grown vertically (20 degrees) in growth chambers set at 22°C under continuous light (100 µE).

Root tissue sampling for RNA-seq.

For the RNA sequencing (RNAseq) experiment, root tips from 7-day-old seedlings were excised. After excision, the ½ MS square dishes were resealed and returned to the growth chambers. Root portions (3 mm) above the cut site were collected at intervals of 0, 1, 2, 4, 8, and 12 hours post-excision to synchronize lateral root development. These samples were then immediately frozen in liquid nitrogen.

Abiotic stresses and hormonal treatment

A total of 45 seedlings (three independent biological replicates) of *Brachypodium distachyon* Bd-21-3 and Bd21 were grown vertically under long day conditions for 6 days on standard ½ MS plates with 0.8% agar. The seedlings were then transferred to media containing either 1 µM or 10 µM indole-3-acetic acid (IAA), 1 µM or 10 µM abscisic acid (ABA), 85 mM or 170 mM NaCl, or 170 mM or 340 mM mannitol. Afterwards, the plates were returned to growth conditions for 72 hours. LR number and size were quantified.

Chemicals for clearing and staining solutions

The following chemicals were used in the DEEP-Clear (Pende *et al.*, 2020) adapted version to plant tissues: PFA (paraformaldehyde) (CAS no. 30525-89-4, Merck, http://www.merck.com/), xylitol (CAS no. 87-99-0, Sigma, http://www.sigmaaldrich.com/), urea (CAS no. 57-13-6, Sigma), SR2200 (Renaissance Chemicals), Basic Fuchsin (CAS no. 58969-01-0, Sigma), THEED (Sigma-Aldrich, 87600-100ML), 5% (v/v) Triton X-100 (Roth, 3051.2).

Preparation of hand-sectioned root samples.

For sectioning, 6-day-old (DAG) root seedlings of similar length were placed in parallel, and 1 cm fragments containing the region of interest were partitioned and embedded in 4% agarose. After solidification, the agarose blocks containing the region of interest were glued to a hand microtome (www.daigger.com/hand-microtome), and sections of approximately 50 µm were prepared for clearing or immediate visualization. Representative images were obtained from at least 30 seedlings from three independent replicates.

Clearing and staining

Clearing steps using DEEP-Clear were performed as described for ClearSee in (Kurihara *et al.*, 2015) and adapted from (van der Schuren *et al.*, 2018) for Brachypodium samples. DEEP-Clear solution consists of 5 to 8% (v/v) THEED, 5% (v/v) Triton X-100, and 25% (w/v) urea in water. Heating the solution is not recommended. Root seedlings that were 7 days after germination (DAG) were collected for clearing for full root treatment and/or for semi-thin sectioning. Samples were fixed for 1 hour in 4% (w/v) paraformaldehyde in 1× phosphate-buffered saline (PBS) with 3 rounds of soft vacuum infiltration. Afterwards, roots were washed five times in 1× PBS with another round of vacuum to ensure the removal of paraformaldehyde. Samples were then transferred to DEEP-Clear solution for clearing. Fixed root tissue was incubated at room temperature with gentle shaking in the solution for 7-10 days, with the solution replaced twice. For staining of the fixed and cleared tissue, 1% stock solutions of Basic Fuchsin (for lignin staining), Renaissance, and/or Calcofluor (for cell wall staining) were separately prepared directly in DEEP-Clear and stored at 4°C. Working solutions were prepared as described in (Ursache *et al.*, 2018). To combine multiple dyes, samples were incubated first in Basic Fuchsin (0.1% in DEEP-Clear) for 1 hour and washed in DEEP-Clear overnight. After several rounds of washing, samples were transferred to Renaissance (0.1% in DEEP-Clear) for 2 days and washed overnight in DEEP-Clear.

Microscopy

Roots were observed using Leica TCS SP8-MP equipped with a resonant scanner (8 kHz) using 25x, 40x and 63x water immersion objectives. Figures were arranged in Adobe Illustrator (Adobe Systems Inc., http://www.adobe.com/) or in PowerPoint (Microsoft Corporation) and the brightness was increased equally, without further modifications. The 3D reconstruction was done using the Fiji package (Schindelin *et al.*, 2012).

RNA extraction, library preparation, sequencing, and quantification

Total RNA was extracted from the root tips of Bd21 and Bd21-3 accessions using the SV Total RNA Isolation System (Promega), following the manufacturer's instructions. The RNA samples were sent to Agilent Technologies for sequencing. The raw reads were filtered for polyA and TruSeq adapters using BBduk (BBMap suite version 38.96). The trimmed reads were aligned to the respective genome assemblies (BdistachyonBd21_3_537_v1.0 for Bd21-3, and Bdistachyon_314_v3 for Bd21) using STAR aligner version 2.7.10a. The genome index was built with strings of 12 bases, and reads were aligned allowing for multiple matches. The sorted BAM files were indexed with samtools version 1.15.1, and read counts were calculated using the union method with htseq-count (HTSeq suite version 2.0.2), using version 1.2 of the Bd21-3 genome annotation (BdistachyonBd21_3_537_v1.2.gene.gff3).

Differential expression analysis

Differential expression analysis was performed using R version 4.1.2 and the DESeq2 package version 1.32.0. Genes with null expression in more than 20% of the samples were filtered out. The data dispersion was estimated using the *vst* function implemented in DESeq2 package using a sample of 20,000 genes (nsub=20000). Differential expression across time-points was calculated on genes expressed in at least 20% of the samples and with a total read count >= 10. We used the likelihood ratio test to estimate changes in gene expression across the kinetic and extracted results for each comparison using the Wald test implemented in DESeq2.

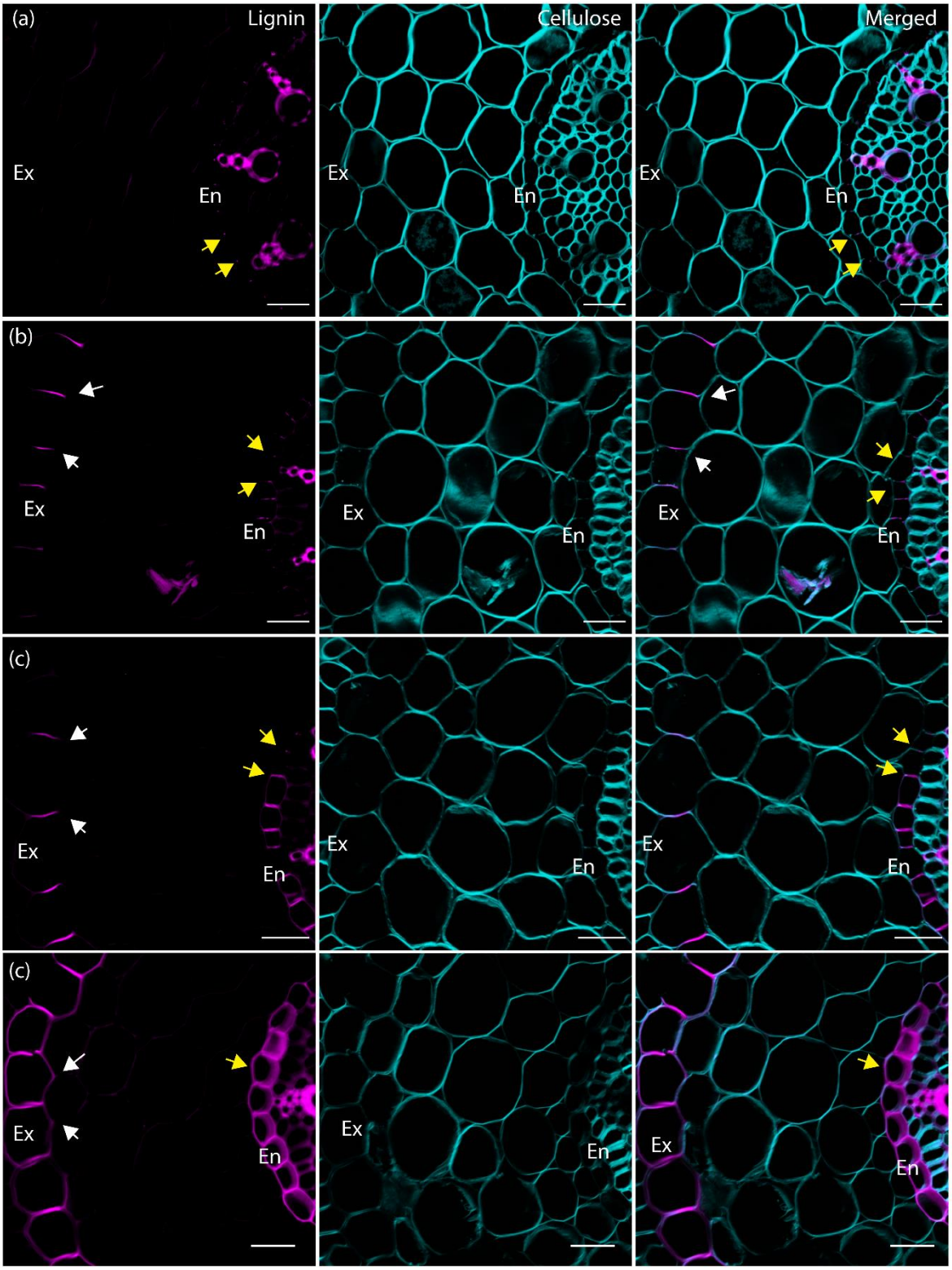

Supplemental Figure S1: Characterization of endodermal and exodermal Lignification in Brachypodium. Brachypodium root cross-sections (6 DAG) stained with basic fuchsin (purple) and Renaissance (cyan) for lignin and cellulose, respectively. Yellow arrows indicate lignification in the Casparian strips (CS), and white arrows indicate lignification in the exodermis. Images from confocal microscopy. En: Endodermis, Ex: Exodermis. Scale bar: 20 µm. Representative images from 45 seedlings from 3 independent biological replicates.

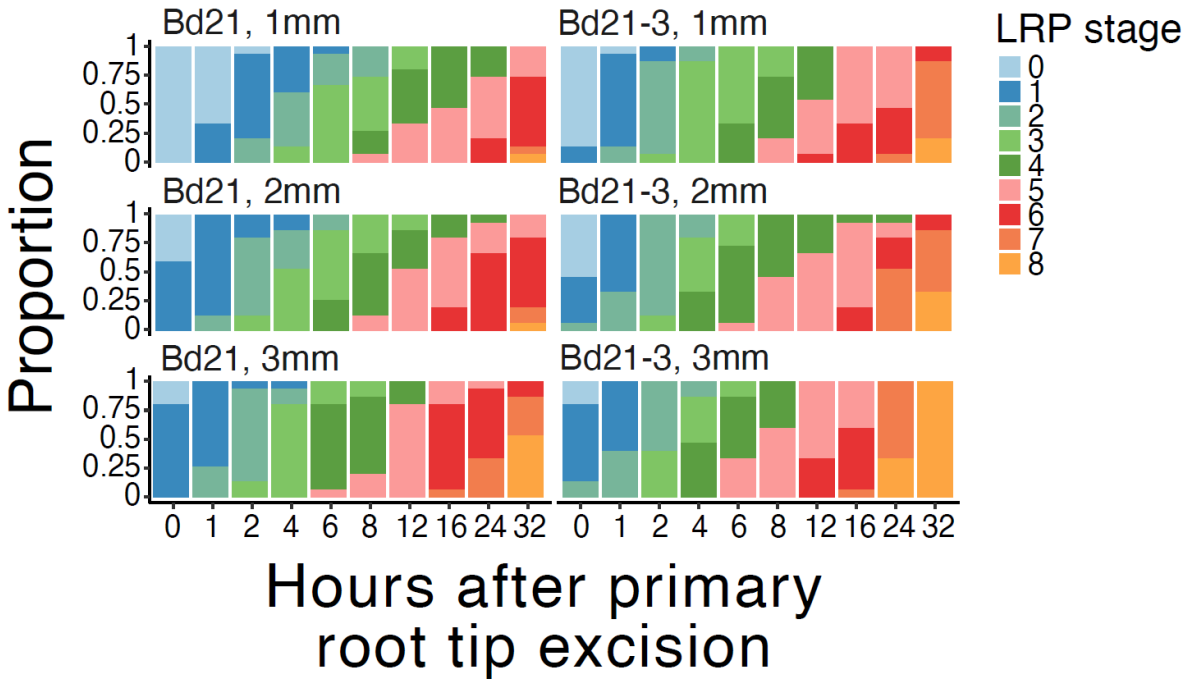

Supplementary Figure S2. RTE-mediated LR development in Bd21 and Bd21-3. LRPs present in the first 1 mm, 2 mm, and 3 mm after the RTE excision were classified into stages for comparison. The proportion of stages per mm in both Bd21 and Bd21-3 did not differ in the analysed total root segment (3 mm). Staging performed in at least 45 seedlings from 3 independent biological replicates.

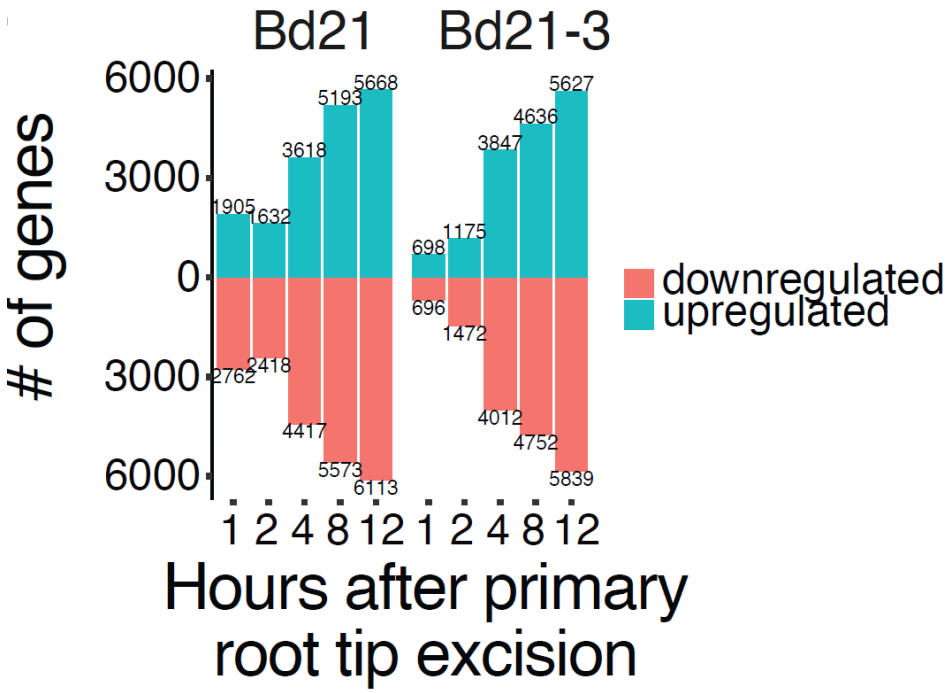

Supplementary Figure S3. Most of the genes showing differential expression compared to the time 0 after root tip excision are found at late times of the kinetic.

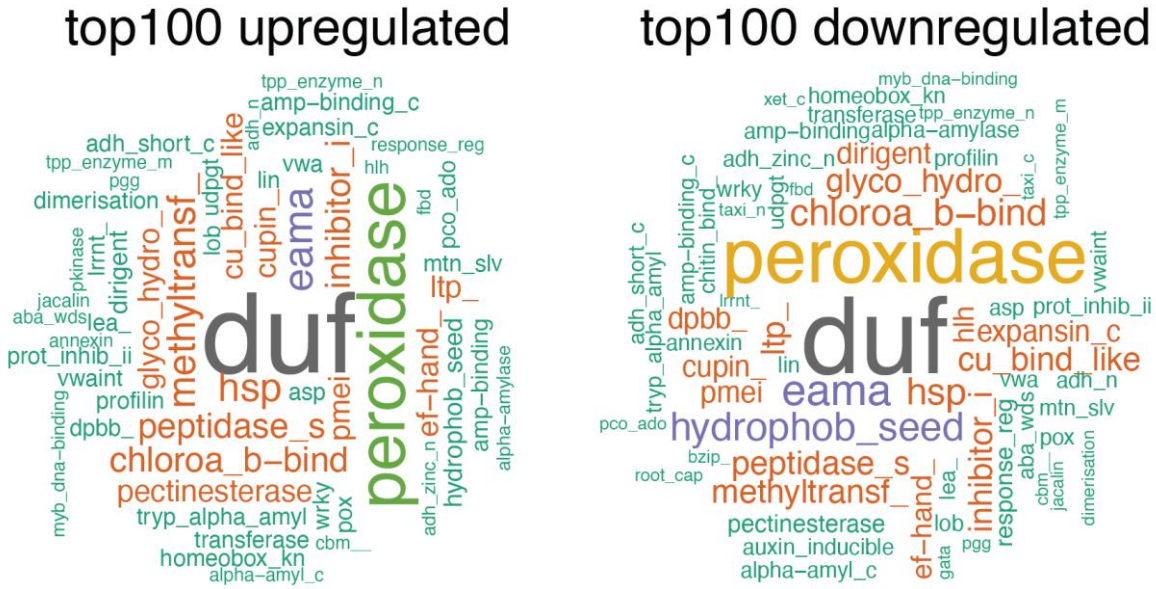

Supplementary Figure S4. Gene families with predicted functions related to transcriptional regulation, hormone signaling, and cell-wall remodeling are among the top 100 upregulated and downregulated.

REFERENCE LIST

Affaticati, P. *et al.* (2018) 'X-fact: Xenopus-fast clearing technique', in *Methods in Molecular Biology*. Humana Press Inc., pp. 233–241. Available at: https://doi.org/10.1007/978-1-4939-8784-9_16.

Amtmann, A., Bennett, M.J. and Henry, A. (2022) 'Root Phenotypes for the Future', *Plant, Cell & Environment* [Preprint]. Available at: https://doi.org/10.1111/PCE.14269.

Beeckman, T. and Eshel, A. (2024) *Plant Roots: The Hidden Half, Fifth Edition*. CRC Press. Available at: https://books.google.ch/books?id=FmVx0AEACAAJ.

Casero, P.J., Casimiro, I. and Lloret, P.G. (1995) 'Lateral root initiation by asymmetrical transverse divisions of pericycle cells in four plant species:Raphanus sativus, Helianthus annuus, Zea mays, andDaucus carota', *Protoplasma*, 188(1), pp. 49–58. Available at: https://doi.org/10.1007/BF01276795.

Crombez, H. *et al.* (2016) 'Lateral Root Inducible System in Arabidopsis and Maize', *J. Vis. Exp*, 107, p. 53481. Available at: https://doi.org/10.3791/53481.

Decaestecker, W. *et al.* (2019) 'CRISPR-Tsko: A technique for efficient mutagenesis in specific cell types, tissues, or organs in Arabidopsis[open]', *Plant Cell*, 31(12), pp. 2868–2887. Available at: https://doi.org/10.1105/tpc.19.00454.

Ditengou, F.A. *et al.* (2008) 'Mechanical induction of lateral root initiation in Arabidopsis thaliana', *Proceedings of the National Academy of Sciences of the United States of America*, 105(48), pp. 18818–18823. Available at: https://doi.org/10.1073/pnas.0807814105.

Dolan, L. and Roberts, K. (1995) 'The Development of Cell Pattern in the Root Epidermis', *Philosophical Transactions: Biological Sciences*, 350(1331), pp. 95–99. Available at: http://www.jstor.org/stable/56258.

Du, H. *et al.* (2018) 'Advances in CLARITY-based tissue clearing and imaging (Review)', *Experimental and Therapeutic Medicine* [Preprint]. Available at: https://doi.org/10.3892/etm.2018.6374.

Garvin, D.F. (2007) 'Brachypodium: a new monocot model plant system emerges', *Journal of the Science of Food and Agriculture*, 87(7), pp. 1177–1179. Available at: https://doi.org/10.1002/jsfa.2868.

Hou, B. *et al.* (2015) 'Scalable and DiI-compatible optical clearance of the mammalian brain', *Frontiers in neuroanatomy*, 9, p. 19. Available at: https://doi.org/10.3389/fnana.2015.00019.

Inukai, Y. *et al.* (2005) 'Crown rootless1, which is essential for crown root formation in rice, is a target of an Auxin Response Factor in auxin signaling', *Plant Cell*, 17(5), pp. 1387–1396. Available at: https://doi.org/10.1105/tpc.105.030981.

Kawai, T. *et al.* (2022) 'WUSCHEL-related homeobox family genes in rice control lateral root primordium size', *Proceedings of the National Academy of Sciences of the United States of America*, 119(1). Available at: https://doi.org/10.1073/PNAS.2101846119/-/DCSUPPLEMENTAL.

Keller, P.J. (2013) 'Imaging Morphogenesis: Technological Advances and Biological Insights', *Science*, 340(6137). Available at: https://doi.org/10.1126/science.1234168.

Kenrick, P. and Strullu-Derrien, C. (2014) 'The Origin and Early Evolution of Roots', *PLANT PHYSIOLOGY*, 166(2), pp. 570–580. Available at: https://doi.org/10.1104/pp.114.244517.

Kurihara, D. *et al.* (2015) 'ClearSee: a rapid optical clearing reagent for whole-plant fluorescence imaging.', *Development (Cambridge, England)*, 142(23), pp. 4168–79. Available at: https://doi.org/10.1242/dev.127613.

Kurihara, D. *et al.* (2021) 'ClearSeeAlpha: Advanced Optical Clearing for Whole-Plant Imaging', *Plant and Cell Physiology* [Preprint]. Available at: https://doi.org/10.1093/pcp/pcab033.

Kurihara, D. *et al.* (2022) 'Optical Clearing of Plant Tissues for Fluorescence Imaging', *JoVE (Journal of Visualized Experiments)*, 2021(179), p. e63428. Available at: https://doi.org/10.3791/63428.

Lavenus, J. *et al.* (2013) 'Lateral root development in Arabidopsis: Fifty shades of auxin', *Trends in Plant Science*, 18(8), pp. 1360–1385. Available at: https://doi.org/10.1016/j.tplants.2013.04.006.

Lindsey III, B.E. *et al.* (2017) 'Standardized Method for High-throughput Sterilization of Arabidopsis Seeds', *Journal of Visualized Experiments* [Preprint], (128). Available at: https://doi.org/10.3791/56587.

Lou, H. *et al.* (2022) 'The cellulose synthase-like F3 (CslF3) gene mediates cell wall polysaccharide synthesis and affects root growth and differentiation in barley', *The Plant Journal*, 110(6), pp. 1681–1699. Available at: https://doi.org/10.1111/TPJ.15764.

Malamy, J.E. and Benfey, P.N. (1997) 'Organization and cell differentiation in lateral roots of Arabidopsis thaliana', *Development*, 124(1), pp. 33 LP – 44. Available at: http://dev.biologists.org/content/124/1/33.abstract.

Muntifering, M. *et al.* (2018) 'Clearing for Deep Tissue Imaging', *Current Protocols in Cytometry*, 86(1), pp. 1–33. Available at: https://doi.org/10.1002/cpcy.38.

O'Connor, D.L. *et al.* (2017) 'Cross-species functional diversity within the PIN auxin efflux protein family', *eLife*, 6. Available at: https://doi.org/10.7554/eLife.31804.

Pende, M. *et al.* (2018) 'High-resolution ultramicroscopy of the developing and adult nervous system in optically cleared Drosophila melanogaster', *Nature Communications*, 9(1), pp. 1–12. Available at: https://doi.org/10.1038/s41467-018-07192-z.

Péret, B., Larrieu, A. and Bennett, M.J. (2009) 'Lateral root emergence: A difficult birth', *Journal of Experimental Botany*, 60(13), pp. 3637–3643. Available at: https://doi.org/10.1093/jxb/erp232.

Piccinini, L., Nirina Ramamonjy, F. and Ursache, R. (2024) 'Imaging plant cell walls using fluorescent stains: The beauty is in the details', *Journal of Microscopy* [Preprint]. John Wiley and Sons Inc. Available at: https://doi.org/10.1111/jmi.13289.

Raissig, M.T. and Woods, D.P. (2021) 'The wild grass Brachypodium distachyon as a developmental model system'. Available at: https://zenodo.org/record/5548408.

Richardson, D.S. *et al.* (2021) 'Tissue clearing', *Nature Reviews Methods Primers*, 1(1), p. 84. Available at: https://doi.org/10.1038/s43586-021-00080-9.

Richardson, D.S. and Lichtman, J.W. (2015) 'Clarifying Tissue Clearing', *Cell*, 162(2), pp. 246–257. Available at: https://doi.org/10.1016/j.cell.2015.06.067.

Sauer and Burroughs (1986) 'Disinfection of Seed Surfaces with Sodium Hypochlorite ', *Journal of Plant Tech*, 6(1986), pp. 1–6.

Van Der Schuren (2019) *Characterization of Brachypodium distachyon Root Development*. Available at: http://serval.unil.chhttp://serval.unil.ch.

Stöckle, D. *et al.* (2021) 'Microtubule-based perception of mechanical conflicts controls plant organ morphogenesis', *bioRxiv*, p. 2021.09.09.459674. Available at: https://doi.org/10.1101/2021.09.09.459674.

Stoeckle, D., Thellmann, M. and Vermeer, J.E. (2018) 'Breakout — lateral root emergence in Arabidopsis thaliana', *Current Opinion in Plant Biology*. Elsevier Ltd, pp. 67–72. Available at: https://doi.org/10.1016/j.pbi.2017.09.005.

Ueda, H.R. *et al.* (2020) 'Tissue clearing and its applications in neuroscience', *Nature Reviews Neuroscience*. Nature Research, pp. 61–79. Available at: https://doi.org/10.1038/s41583-019-0250-1.

Ursache, R. *et al.* (2018a) 'A protocol for combining fluorescent proteins with histological stains for diverse cell wall components', *Plant Journal*, 93(2), pp. 399–412. Available at: https://doi.org/10.1111/tpj.13784.

Ursache, R. *et al.* (2018b) 'A protocol for combining fluorescent proteins with histological stains for diverse cell wall components', *The Plant Journal*, 93(2), pp. 399–412. Available at: https://doi.org/10.1111/tpj.13784.

Ursache, R. *et al.* (2021) 'GDSL-domain proteins have key roles in suberin polymerization and degradation', *Nature Plants*, 7(3), pp. 353–364. Available at: https://doi.org/10.1038/s41477-021-00862-9.

Vermeer, J.E.M. *et al.* (2014) 'A spatial accommodation by neighboring cells is required for organ initiation in arabidopsis', *Science*, 343(6167), pp. 178–183. Available at: https://doi.org/10.1126/SCIENCE.1245871.

Vogel, J. (2008) 'Unique aspects of the grass cell wall', *Current Opinion in Plant Biology*, 11(3), pp. 301–307. Available at: https://doi.org/10.1016/j.pbi.2008.03.002.

Voß, U. *et al.* (2015) 'The circadian clock rephases during lateral root organ initiation in Arabidopsis thaliana', *Nature Communications*, 6(1), p. 7641. Available at: https://doi.org/10.1038/ncomms8641.

Warner, C.A. *et al.* (2014) ‘An optical clearing technique for plant tissues allowing deep imaging and compatible with fluorescence microscopy’, *Plant Physiology*, 166(4), pp. 1684–1687. Available at: https://doi.org/10.1104/pp.114.244673.

Weigel & Glazebrook (2002) ‘Arabidopsis: A Laboratory Manual. D. WEIGEL & J. GLAZEBROOK Cold Spring Harbor Laboratory Press. 2002. 354 pages. ISBN 0 87969 573 0.’, *Genetical Research*, 80(1), pp. 77–77. Available at: https://doi.org/10.1017/S0016672302215852.

Yaschenko, A.E., Alonso, J.M. and Stepanova, A.N. (2024) ‘Arabidopsis as a model for translational research’, *The Plant Cell* [Preprint]. Available at: https://doi.org/10.1093/plcell/koae065.

Yu, P., Hochholdinger, F. and Li, C. (2019) ‘Plasticity of Lateral Root Branching in Maize’, *Frontiers in Plant Science*, 10. Available at: https://doi.org/10.3389/fpls.2019.00363.

CHAPTER 6

6. GENERAL DISCUSSION

Cristovão De Jesus Vieira Teixeira[1] ; Joop E.M. Vermeer[1]

Laboratory of Molecular and Cellular Biology, Institute of Biology, University of Neuchâtel, Rue Emile Argand 11, CH-2000, Neuchâtel, Switzerland.

Chapter 6 was fully written by *Cristovão De Jesus Vieira* Teixeira with suggestions and corrections by Prof *Dr. Joop E.M. Vermeer.*

6.1 INTRODUCTION

In this study, we used the plant models Arabidopsis and Brachypodium to better understand cell-to-cell communication, cell wall (CW) modifications, and other processes related to lateral root primordia (LRP) development. Although Brachypodium has gained acceptance as a versatile research tool for studying plant development, substantial challenges remain in performing cell biological experiments coupled to functional genetics, especially related to the time required for stable transformation, histological approaches, and deep tissue (live) imaging in roots. This section is divided into two parts that discuss our findings obtained from studies in Arabidopsis and Brachypodium.

Distinct auxin response profiles of differentiated endodermal cells revealed by tissue-specific manipulation of signaling in Arabidopsis

Auxin triggers different responses observed in organs or differentiated tissues (Mo and Weijers, 2009; Vermeer *et al.*, 2014; Cavallari, Artner and Benkova, 2021; Das, Weijers and Borst, 2021). We demonstrated that differentiated endodermis cells are responsive to auxin treatment. We obtained a strong enrichment for auxin responsive genes in our target cell type, the endodermis, by employing and combining various auxin signaling mutants. This approach was also applied by (Schlereth *et al.*, 2010) to better understand auxin signaling during Arabidopsis embryogenesis. Comparison of our present data set with other auxin induced transcriptomes derived either from sections or whole roots showed very little overlap between these datasets (Lewis *et al.*, 2013; Voß *et al.*, 2015). This represents the significance of obtaining auxin response profiles at a cell type specific resolution. Additionally, despite being qualitatively different from other auxin response profiles, including those in meristematic tissues, our endodermis-focused profile in differentiated root sections revealed significant differential expression of nearly a thousand genes, suggesting that auxin responses are not strongly attenuated in differentiated tissues.

GDSL-domain containing genes are required for suberin homeostasis

In the extensively studied Arabidopsis root endodermis, suberin is deposited as a hydrophobic layer between the plasma membrane and the primary cell wall(De Bellis *et al.*, 2022). Developmentally, suberin biosynthesis and deposition occur as the second step in endodermal differentiation, following the synthesis and deposition of the lignified Casparian strip (Shukla and Barberon, 2021). Suberin acts as both an apoplastic and transcellular barrier, thereby regulating the movement of water and solutes to the vascular cylinder (Barberon et al., 2016). The Arabidopsis genome contains over 100 GDSL-domain genes,

but only a small portion have been functionally linked to cell wall modification or demonstrated their ability to synthesize or degrade cell wall polymers (Naseer *et al.*, 2012; Yeats *et al.*, 2012). Recently, studies have identified several genes involved in suberin biosynthesis, as well as their transcriptional regulators (Belsson *et al.*, 2007; Cohen *et al.*, 2020). Although suberin shares chemical similarities with cutin, significant differences exist in their composition and deposition within the cell wall (Mustroph and Bailey-Serres, 2010). Overall, the understanding of the genetic programming underlying suberin polymerization and degradation remains limited. The discovery that the GDSL-domain-containing protein CUTICLE DESTRUCTION FACTOR 1 (CDEF1) can degrade suberin when overexpressed in the endodermis suggested the potential of these genes to regulate suberin homeostasis (Naseer *et al.*, 2012). However, to this date, no GDSL-domain-containing genes responsible for suberin polymerization in the endodermis had been identified. Our study now indicates that this was due to a high degree of functional redundancy. Only when five auxin-repressed GELPs were knocked out, roots without detectable suberin, based on Fluorol Yellow staining, were obtained. All five identified GELPs are predicted to be expressed in the endodermis and secreted, supporting a role in cell wall modification.

GELPs are required for endodermal suberization and induced by ABA.

Endodermal suberization has demonstrated a high degree of plasticity in response to various nutritional stress conditions (Andersen, Barberon and Geldner, 2015; Barberon *et al.*, 2016). These conditions influence suberin through multiple phytohormones, notably including ABA signalling (Barberon *et al.*, 2016; Lu *et al.*, 2019; Friero *et al.*, 2022). The finding that GELPs are required for suberin polymerization and induced by ABA treatment further support their specific role in suberization. Although an approximately 85% reduction in suberin monomers was revealed by the chemical analysis, we could not detect potential substrates for the suberin biosynthesis catalyzed by GELPs. Furthermore, the ultrastructural studies on the roots of the *gelp*$^{quint-1}$ mutant also did not show evident agglomerations of unpolymerized material. Rather, a distinct, homogenous zone of low electron density was observed in place of the suberin lamellae. Whether this zone is composed of the remnant, non-polymerized lipidic suberin components (possibly becoming extracted during TEM processing) or whether this is matrix material of unknown, potentially polysaccharide nature remains to be investigated. Nevertheless, our findings clearly show that the five auxin-repressed GELPs are required for forming endodermal suberin. Additionally, by using a functional GELP38 fusion, we demonstrated that the GELP38 localization and activity is in the apoplast surrounding the endodermis. Given the in vitro activity of CUTIN DEFICIENT 1 (CD1), a tomato GELP involved in cutin polymerization, we hypothesize that the five identified Arabidopsis GELPs act as suberin synthases, facilitating the polymerization of

suberin precursors in the cell wall. It has been shown that the seed coats of *GPAT5* mutants exhibit a significantly increased permeability to tetrazolium salts compared to wild-type seed coats (Belsson *et al.*, 2007). Similarly, our results from tetrazolium red assays with the *gelp*$^{quint-1}$ mutant revealed heightened seed permeability (**Figure 1**). These findings suggest that these GELPs are expressed in the seed coat, indicating their potential general roles in suberin synthesis in diverse plant tissues.

Impaired suberin degradation could affect spatial accommodation responses in the endodermis.

From the same dataset where we identified the GELPs involved in suberin polymerization, we also found five GELPs that behaved oppositely; these 5 GELPs were induced by auxin treatment. Our gain- and loss-of-function experiments indicate that the relationship between suberin degradation and LR emergence might be quite complex. Indeed, we demonstrated that suberin is degraded for three of the five auxin-induced GELPs, but only GELP72 seemed to play a role in LR emergence on its own (**Figure 1** – Chapter 2). The hypothesis that suberin degradation is necessary to facilitate LR emergence is supported by the observation of a reduced number of LRs in the *abcg2/abcg6/abcg20* mutant, which exhibits higher levels of suberin in its roots (Yadav *et al.*, 2014). A defect in suberin degradation could potentially disrupt the spatial accommodation responses in the endodermis, leading to delayed LRP emergence. Interestingly, both of the auxin-induced GELPs for which we could not show a direct role in suberin degradation (*GELP73* and *GELP81*) displayed strong effects on LR emergence. Although the phenotypes clearly suggest that they are involved in LR emergence, follow-up studies are required to reveal if and how they modify suberin. Given that the expression of both genes peaks early during LR formation, it is plausible that they contribute to the remodeling of suberin to allow for the establishment of the cuticle on the LRP. This hypothesis is supported by findings that defects in this structure lead to altered LR emergence but differences in the phenotype (Berhin *et al.*, 2019). Additionally, we found that several auxin-inducible GELPs were not only expressed in the endodermis but also induced in the outer layer of the LRP. This suggests that both the primordium and the endodermis require cell wall modifications leading to the formation of the LRC. The observation that overexpression of a single GELP can effectively degrade suberin supports the idea that regulating GELP expression is crucial for coordinating suberin lamellae degradation and the synthesis of a new cuticle structure. It would be interesting to investigate whether there is a functional hierarchy among the suberin-degrading GELPs.

Proanthocyanidin derivatives may cause brown pigmentation in Brachypodium roots after ClearSee treatment.

The initial challenge of this project was to adapt a clearing method suitable for Brachypodium. ClearSee has proven effective for clearing various tissues in a range of plant species, including Arabidopsis (Nagaki, Yamaji and Murata, 2017), soybean (Okuda *et al.*, 2017), Eucalyptus (Eliyahu *et al.*, 2020), rice (Chu *et al.*, 2018), maize (Kelliher *et al.*, 2017), Marchantia (Aki *et al.*, 2019), barley (Ho *et al.*, 2020), and many others (Kurihara *et al.*, 2021). Therefore, it was our first-choice method. Our results show that Brachypodium root samples treated with ClearSee exhibited oxidation of the root epidermis, leading to the formation of brown pigmentation. Fluorescent signals from FPs or fluorescent dyes were not detected in the regions of brown coloration, which instead appeared dark. Brown pigmentation after ClearSee treatment was also reported in siliques and seed coats (Debeaujon *et al.*, 2003). The brown pigment on Brachypodium roots was similar to that obtained with vanillin staining in seed coats (Debeaujon *et al.*, 2003). Vanillin staining can result in the visualization of proanthocyanidins as brown pigment due to oxidation. Proanthocyanidin derivatives accumulate in the seed coat during seed maturation after fertilization (Debeaujon *et al.*, 2003). Therefore, it is likely that for some species, ClearSee treatment can induce the accumulation of proanthocyanidin derivatives causing the brown pigmentation. (Kurihara *et al.*, 2021) also suggests that the quality of sodium deoxycholate may interfere with the clearing process. Some manufacturers' products have a pale-yellow color when dissolved, which interferes with optical clearing and fluorescence microscopy. Reducing agents such as sodium sulfite can suppress tissue oxidation (Kurihara *et al.*, 2021). In our conditions, the addition of sodium sulfite reduced the pigmentation caused by ClearSee. However, Brachypodium roots oxidized rapidly after the opening of plates. This prolonged the clearing process, taking up still to 3 months to complete tissue clearing for imaging and very often compromising tissue integrity.

DEEP-Clear enables combined depigmentation and clearing of Brachypodium roots

In this study we used an adapted version of the DEEP-Clear protocol (Pende *et al.*, 2020) that provided superior clearing of Brachypodium roots compared to ClearSee (Kurihara *et al.*, 2015) and ClearSeeAlpha (Kurihara *et al.*, 2021). Brachypodium roots achieved satisfactory tissue transparency after just 7 days. The original DEEP-Clear protocol includes elements for in-situ hybridization, but its core urea-based mixture is straightforward and compatible with other steps in the ClearSee protocol with minor modifications (Ursache *et al.*, 2018; Kurihara *et al.*, 2021). We show that DEEP-Clear is also compatible with many FPs and cell component dyes, including Fluorol Yellow used for

visualizing suberin and cutin. Despite its success in clearing Brachypodium roots, there are currently no references citing DEEP-Clear as a clearing agent for plant tissues. DEEP-Clear is reported to offer a novel, tailored clearing method that utilizes various strategies to remove different classes of poorly soluble pigments (including pterins, heme, ommochromes, carotenoids, and melanin) that are abundant in many animal tissues and across phyla (Pende *et al.*, 2018). However, more tests as described by others are necessary to confirm its compatibility with a wider range of FPs, fluorescent dyes, plant tissues, as well as other plant species (Ursache *et al.*, 2018; Sexauer *et al.*, 2021).

The polyarch organization structure of vascular tissues in Brachypodium may not allow gravitropic stimulation of LR formation.

Predicting the localization and timing of the formation of the LRP is a challenging task (Van Norman *et al.*, 2013). Some studies aimed to develop a LR inducing system (LRIS) in order to compare and correlate gene expression profiles during LR formation in different species (Ditengou *et al.*, 2008; Crombez *et al.*, 2016). Gravitropic stimulation is often used to synchronize the initiation of LRP at the site of root bending (Voß *et al.*, 2015; Leftley *et al.*, 2021). In Arabidopsis, tissue can be harvested at different timepoints after gravistimulation up to 42 hours prior to the emergence of the LRP (Ditengou *et al.*, 2008). However, we were unable to observe induction of LRP at bending sites in Brachypodium. LRs of dicotyledonous plants originate from a subset of pericycle cells next to the xylem pole (Kircher and Schopfer, 2016). The roots of plants such as Arabidopsis are characterized by a bilaterally symmetric (diarch) organization of the vascular tissues (Ohashi-Ito and Bergmann, 2007). For instance, two xylem poles are localized in opposite sides of the stele and thus two opposite positions of xylem-adjoining pericycle cell files. In contrast, polyarch vascular bundles generally occur in monocots, with typically 6 to 8 xylem poles and one central metaxylem (Parizot *et al.*, 2008). Therefore, it might be that the rigidity and organization of the vasculature of Brachypodium do not allow the roots to make a sharp bend after gravistimulation, which is required to create an auxin gradient to induce the formation of localized LRs as shown in Arabidopsis (Ditengou et al., 2008; Voß et al., 2015). An alternative method involves germinating seedlings on medium supplemented with NPA (an inhibitor of polar auxin transport) followed by a transfer to growth medium supplemented with IAA to induce massive LR development. Although synchronized LR induction was elegantly demonstrated in maize and Arabidopsis (Crombez *et al.*, 2016), we chose not to adhere to this approach. Our concern was that these hormonal treatments might not provide a natural perspective on the developmental process of LRP.

Root tip excision (RTE) effectively induces LRP in Brachypodium.

Compensatory LR formation can be induced in various plant species through root tip excision (RTE) (Torrey, 1950; Van Staden and Ntingane, 1996; Vysotskaya *et al.*, 2001; Xu *et al.*, 2017; Kawai, Shibata, *et al.*, 2022). Here, we demonstrated that RTE is a simple and effective method for synchronizing LR development in Brachypodium. The development of LRP was predominantly synchronized within the first 5 mm after the RTE region. This approach also reduced extensive handling of seedlings, thereby decreasing root tissue oxidation when plates are opened. Although this method does not involve the addition of exogenous hormone treatments, the secondary effects of removing the meristematic zone of the primary root remain unclear for Brachypodium. For example, monocot plants produce two types of LRs: The S-type (short and thin) and the L-type (long, thick, and capable of further branching (Kawa and Brady, 2022). Due to their ability to produce higher-order branches, the formation of L-type LRs significantly contributes to efficient root system expansion (Kawai, Chen, *et al.*, 2022). In rice, RTE induced L-type LR development in the remaining proximal portions and promoted elongation of first-order LRs and higher-order branching (Robin and Saha, 2015; Wu, Pagès and Wu, 2016). Additionally, this approach increased the diameter of first-order LRs by enhancing the number of ground-tissue layers and the stele diameter, further promoting elongation and higher-order LR emergence in proximal regions to the RTE (Kawai, Chen, *et al.*, 2022). Transcriptome analysis suggested the upregulation of auxin signaling in L-type LRPs compared to S-types, possibly inducing the expression of OsWOX10 (a positive regulator of LR diameter) (Kawai, Shibata, *et al.*, 2022). Furthermore, observations of auxin signaling using the auxin-responsive promoter DR5 revealed upregulation on the convex side of curvature where L-type LRs develop after RTE (Lucob-Agustin *et al.*, 2021). Therefore, besides being a useful tool as LRIs for studying LRs, the application of RTE may induce distinct auxin responses in Brachypodium leading to changes in the LRP morphology. More studies using auxin reporter lines after RTE, as in (Kawai, 2022), will be necessary to verify if these features are also conserved in Brachypodium.

Pre-initiation events leading up to LR initiation are still unclear in Brachypodium.

A major goal of this thesis was to characterize the early stages of LR development in Brachypodium. Using the DEEP-Clear adapted clearing protocol, we built an LR developmental atlas describing the consecutive LR developmental stages in Brachypodium based on the model suggested for Arabidopsis (Malamy and Benfey, 1997; Péret, Larrieu and Bennett, 2009; Van Norman *et al.*, 2013; Vermeer and Geldner, 2015; Wachsman and Benfey, 2020). Brachypodium pericycle cells adjacent to the phloem initiate the first cell

divisions leading to the formation of the LRP as observed in many other plant species, including major cereal crops (Hochholdinger and Zimmermann, 2008; Yu, Hochholdinger and Li, 2019). Two types of LRP initiation have been described in Arabidopsis: longitudinal unicellular and longitudinal bi-cellular, in which a single or two adjacent pericycle founder cells in the longitudinal plane, respectively, participate in LRP initiation (Dubrovsky *et al.*, 2008). However, the most common type of initiation is considered to be longitudinal bi-cellular (Casero *et al.*, 1993; Casero, Casimiro and Lloret, 1995; De Rybel *et al.*, 2010; Von Wangenheim *et al.*, 2016). In the transverse plane, we observed that four to six phloem-pericycle adjacent files seem to participate in the early stages of LRP formation in Brachypodium. Similar observations were also made in wheat, barley, and maize (Yu, Hochholdinger and Li, 2019). The most detailed analysis of pericycle participation in LRP morphogenesis has been performed in Arabidopsis (De Smet and Beeckman, 2011). For instance, clonal and anatomical analyses suggested that a single founder cell gradually recruits neighboring pericycle cells to become founder cells (Torres-Martínez *et al.*, 2020). However, to date, little to nothing is known about the specification of pericycle founder cells or other pre-initiation processes before LRP initiation in other species, including monocots.

The endodermis appears to dedifferentiate concomitantly or soon after the formative divisions in the pericycle

We observed that the endodermis appears to dedifferentiates and reactivates the cell cycle after the first cell divisions in the pericycle. Cell divisions were also observed in the most inner cortex layer in the vicinity of the LRP; although we could not address a direct role of these cell divisions to formation of the LRP. In later stages, we observed that the endodermis divides periclinal, most likely to form the columella and root cap. LR formation involving cell divisions in both the pericycle and endodermis is presented as a common feature across a range of species (Xiao *et al.*, 2019). Interestingly, in Brachypodium, Casparian strips (CS) are already present during the emergence of the LRP, and we could even observe the CS impregnations at late LRP stages. However, the new endodermal cell divisions do not present the formation of CS domain (CSD) that would tether the CS to the endodermal cell wall. A major study highlights the importance of the mechanism that allows pericycle-derived primordia to pass through the endodermis were done in Arabidopsis (Vermeer *et al.*, 2014), where the endodermis does dedifferentiate during LRP formation. It is likely that other Brassicaceae species show the same mechanism (Beeckman and Eshel, 2024). Divisions in the endodermis and cortex are likely to affect LRP formation in two directions: They could facilitate the passage of the LRP through the overlying tissues of the parental root by affecting the tethering of the CS to the cell wall or potentially provide an extra protection during the rise of the LRP. In maize, the epidermis and root cap of LR are

both derived from endodermis-derived cells (Jansen *et al.*, 2012; Kiryushkin *et al.*, 2019). The participation of cortex cell divisions in the formation of new organs, such in LRs, is less frequently observed, as seen in *M. truncatula* (Herrbach, Maillet and Bensmihen, 2018; Xiao *et al.*, 2019). Approaches for assessing the involvement of other tissues in the development of LR have mostly relied on anatomical observations or, in rare cases, on cell type identity markers (Torres-Martínez *et al.*, 2019; Xiao *et al.*, 2019). Follow-up studies employing sectorial (mosaic) analyses and high-resolution expression analysis methods such as single-cell/nuclei sequencing and spatial transcriptomics (Birnbaum, 2018; Torres-Martínez *et al.*, 2020) would be the rational strategies to track cell lineages and identity changes during the LRP developmental process in Brachypodium.

Diversity in auxin reporters are key to understanding LRP development in monocots.

A range of pre-initiation events occur before LRP formation (Babé *et al.*, 2012; Van Norman *et al.*, 2013; Du and Scheres, 2017). Molecular markers are crucial in characterizing LR organogenesis from its earliest stages (Calloni *et al.*, 2013). The steps in LR formation are often associated with transcriptional changes from auxin signaling pathways (Du and Scheres, 2017). Degradation of Aux/IAA proteins, regulated by their polyubiquitylation and targeting to the 26S proteasome, is essential for auxin-mediated transcriptional regulation (Figueiredo and Strader, 2022). The Aux/IAA family of transcriptional repressors modulates the activity of the AUXIN RESPONSIVE FACTOR (ARF) family of transcription factors (Figueiredo and Strader, 2022). A common reporter of ARF activity and LR formation is the DR5 promoter and its variants (Ulmasov *et al.*, 1997; Liao *et al.*, 2015). In this study, the *DR5pro::ER-mRFP* (DR5) signal was not detected in phloem pole pericycle cells during formative cell divisions leading to a stage I LRP in Brachypodium. However, DR5 signal induction was observed in the overlying endodermis and cortex cells. During later stages of LRP development, clear DR5 signal induction in the exodermis overlying the LRP suggested auxin signaling regulates cell wall modifications to likely facilitate LRP emergence (Swarup *et al.*, 2008; Meng *et al.*, 2019). This suggests auxin signaling regulates responses like lignin barrier modification to accommodate the LRP emergence (Nakayama *et al.*, 2017). Weak or absent DR5 signals during initial cell divisions in the pericycle have been reported in rice (Ni *et al.*, 2014), barley (Kirschner *et al.*, 2017), and maize (Jansen *et al.*, 2012). This contrasts with Arabidopsis, where a strong DR5 signal is typically detected during early LRP stages (Dubrovsky et al., 2000; Vanneste et al., 2005; Marhavý et al., 2013). The weak or absent DR5 signal in monocots suggests differences in auxin response mechanisms compared to Arabidopsis. This likely indicates a distinct set root developmental processes and alternative regulatory pathways in monocots. The synthetic DR5 promoter contains medium-affinity binding sites for ARF transcriptional regulators (Ulmasov *et al.*, 1997; Boer *et al.*, 2014). In

monocots, this likely captures only part of the transcriptional response to auxin. Thus, the DR5 promoter may not fully reflect auxin signaling nuances during early LRP development in Brachypodium. Nevertheless, we showed that auxin induces LRP formation in Brachypodium and expression of auxin transporters were detected in early LRP stages. Using promoters with higher affinity binding sites could improve understanding auxin transcriptional dynamics (Liao *et al.*, 2015; Hao *et al.*, 2021). More sensitive reporters could further enhance auxin signaling detection during early stages. Brighter and/or triple-fluorescent protein fusions targeted to the nucleus, or ratiometric reporters like R2D2, may provide a more accurate and detailed representation of auxin signaling dynamics (Hao *et al.*, 2021). These advanced reporters could capture subtle changes in auxin activity undetected by the standard DR5 reporter.

Hydropatterning directs LR development and modulates suberization in Brachypodium.

LR emergence is a complex process involving various cellular and tissue-specific interactions (Vermeer *et al.*, 2014; Vermeer and Geldner, 2015). In Brachypodium, key tissues such as the endodermis and exodermis are involved in this process. Water availability is a potent regulator of plant development, including the establishment of suberin lamellae, and induces root branching through a process called hydropatterning (Robbins and Dinneny, 2018). Hydropatterning enables roots to position LRs toward regions of high-water availability, such as wet soil or agar media, while preventing their emergence in areas with less water, such as air (Orman-Ligeza *et al.*, 2018; Orosa-Puente *et al.*, 2018). In this study, we demonstrate that Brachypodium roots initiate LRs in response to contact with nutrient medium. Furthermore, the lack of Fluorol Yellow signal (a probe for suberin) suggests that endodermal or exodermal suberization does not occur on the root side (close to meristematic zone) in contact with the nutrient medium. Hydropatterning has been shown to alter root architecture in response to water contact, eliciting SUMOylation of the auxin response factor ARF7 on air-exposed root sides of Arabidopsis (Orosa-Puente *et al.*, 2018). Additionally, nutritional changes can promote endodermal differentiation, influenced by the suberization status of this cell layer (Barberon *et al.*, 2016). Thus, it is likely that in Brachypodium, the suberization status of the endodermis is significantly influenced by hydropatterning and LR emergence. Furthermore, it is possible that the dynamics of suberin biosynthesis and degradation during LR formation in Brachypodium differ from those presented in some recent studies (Shukla and Barberon, 2021). Further studies could explore if the lack of suberization on the nutrient-contacting root side aids nutrient and water uptake, as well as LRP emergence. In addition, we still do not know if suberin degradation would be required locally at the LRP emergence site of Brachypodium roots when plants are

grown, such as in soil or hydroponics, where there is no direct contact with air as on medium plates.

Dividing endodermal cells do not establish a Casparian Strip Domain.

We demonstrate that the daughter cells of divided endodermal cells do not form a CSD in their cross walls. Although the endodermis in Arabidopsis does not divide during LRP development, the Casparian Strip (CS) seems to detach longitudinally with local breaks. There is a growing interest in understanding the function and formation of the CS in monocots such as rice and maize (Karahara *et al.*, 2004; Wang *et al.*, 2022). However, most of the recent studies focus on the function of the apoplastic barriers of the endodermis and exodermis as osmotic stress defenses (Chen *et al.*, 2022). In Arabidopsis, it has been described that CASPARIAN STRIP DOMAIN PROTEINs (CASP) proteins degrade to facilitate the "sliding" of the Casparian Strip during LR development (Vermeer *et al.*, 2014). In rice, a recent study revealed a new family of proteins containing a glycine/alanine/proline-rich domain, a lectin domain and a secretory signal peptide (GAPLESS) that mediates tethering of the plasma membrane to the CS (Song *et al.*, 2023). It was shown that GAPLESS proteins are specifically localized in the CS of root endodermal cells, and their loss of function results in a non-functional cell–cell junction (suberin is deposition is observed where the CSD normally is formed) and disrupted nutrient homoeostasis. GAPLESS1 forms a tight complex with OsCASP1 in the plasma membrane, thereby mediating the tethering of the CS to the CSD (Song *et al.*, 2023). Therefore, exploring whether Brachypodium orthologs of GAPLESS1 and/or CASPs are degraded during LR formation to facilitate the local breaking and sliding of the CS could provide important insights regarding LR growth through the endodermis.

A role for the exodermis in Brachypodium as mechanical barrier to restrict LR emergence.

The exodermis (hypodermis with Casparian bands) of plant roots is proposed to serve as a barrier with variable resistance to the radial flow of both water and solutes, contributing significantly to the overall structural resistance of the root (Hose *et al.*, 2001; Enstone, Peterson and Ma, 2003). Our results indicate that Brachypodium exhibits exodermal lignification comparable to Casparian bands. Some studies suggest that the exodermis might be induced by particular environmental stresses (Tylová *et al.*, 2017; Liu and Kreszies, 2023). The induction of an exodermis underscores its important role in helping plants cope with changing or extreme environments. For instance, exodermis development did not occur in the primary root of cotton seedlings grown in vermiculite with nutrient solution; however, exposure to 200 mM NaCl can induce the formation of the exodermis with

suberin lamellae and Casparian strips (Kotula *et al.*, 2017). This raises the question of whether the Brachypodium exodermis is a natural feature of the species or if, in our conditions, it was induced by exposing one side of the root to the air on the nutrient medium plates or a secondary effect of the RTE approach. Conversely, in cultivated barley (Hordeum vulgare spp. vulgare), especially in seminal roots, an exodermis is commonly absent (Kreszies, Schreiber and Ranathunge, 2018). However, in some barley cultivars, an exodermis has been observed in adventitious (nodal) roots (Gierth, Stelzer and Lehmann, 1998; Lehmann *et al.*, 2000). Furthermore, seaside barley (Hordeum marinum), a waterlogging-tolerant species, induces an exodermis to prevent radial oxygen loss under hypoxic conditions (Kotula *et al.*, 2017). The position and steps during exodermal lignification may also change depending on the plant species. In tomato, the exodermis undergoes two stages of differentiation: first, a polar lignin cap is deposited and localized on the epidermal face of exodermal cells (Manzano *et al.*, 2022). In the context of LR formation, the position of the initial lignin impregnation in the exodermis might confer different properties to the cell layer, such as altered rigidity (Enstone, Peterson, and Ma, 2003). Our observations based on the Basic Fuchsin staining (a lignin probe) suggest increased exodermal lignification in Bd21-3 delays LR emergence, unlike Bd21, which shows absent lignification before LRP emergence. It would be interesting to determine if the polarly localized lignin barrier in the tomato exodermis has different mechanical effects during the emergence of the LRP, especially under abiotic stresses. Although this demonstrates the highly variable nature of the exodermis, not just under stress but also within and across plant species, our findings rely only on anatomical observations and histological staining. More studies will be necessary to uncover the molecular insights of the exodermis and its function during LRP emergence.

6.2 CONCLUSION AND FUTURE PROSPECTS

GDSL-domain proteins as great tools for understanding CW modifications

Root branching is a major determinant for root system architecture (RSA) and plant adaptation across diverse environmental conditions (Bishopp and Bennett, 2019; Amtmann, Bennett and Henry, 2022). The primary focus of this thesis was to elucidate the mechanisms by which accommodation responses and cell wall modifications influence LR morphogenesis. Firstly, in Arabidopsis, we demonstrated that differentiated endodermal cells exhibit a specific auxin-mediated transcriptional response, primarily involving cell wall remodeling genes (Ursache *et al.*, 2021). The Arabidopsis family of GELP proteins contains more than one hundred members, for which little functional information is available (Shi et al., 2011; Yeats et al., 2012). We demonstrate that five members of this family are essential for suberin formation. This highlights the need for further studies on other members, as they

may be involved in crucial biological roles in CW modifications during plant development or in response to abiotic and biotic stresses. Despite the significant functional redundancy within this family, modern gene-editing technologies now allow us to overcome these challenges, as demonstrated with the GELP cluster required for suberin polymerization. By using endodermal-specific promoters, we could relatively quickly verify which additional GELPs can synthesize or degrade suberin. Additionally, we could test if cutin synthases, such as CD1, are specific for cutin or whether they are also involved in the other suberin-related pathways (Yeats *et al.*, 2012). We propose that it is now clear that not all GELPs act redundantly. The findings on the suberin-degrading subgroups show great potential to broaden our understanding of how these lipases can act during cell wall changes in plant development. It also remains the question of their activity in other plant species such as in Brachypodium.

Uncovering CW modifications during the LRP emergence in Brachypodium

We showed in Brachypodium that the endodermis divides and they do not seem to undergo a related volume loss to get flattened, as reported in Arabidopsis. This finding raises fundamental questions about the mechanisms by which the already differentiated endodermal cells re-enter the cell cycle and change their identity. Although we were able to detect *DR5pro::ER-mRFP* fluorescence in the overlying dividing endodermis cells and subsequently in the overlying cortical cell layers, the DR5 signal was not evident in the pericycle during the early cell divisions. Furthermore, it is still unclear how these endodermal cells disassemble or bypass the CS in order to divide again and without necessarily forming a Casparian strip Domain (CSD). This raises further inquiries into the cellular and molecular mechanisms governing identity changes in the endodermis and how these cells can undergo such transitions twice within a single developmental sequence.

To address some of these questions, ongoing work in comparative genomics and transcriptomics will analyze gene expression profiles and genomic sequences of Arabidopsis and Brachypodium. This project aims to identify conserved and divergent pathways involved in LR development. Furthermore, lineage tracing will be essential for tracking the fate of endodermal cells during LR formation. Using cell division markers like CYCB1::GUS could also help visualize and monitor the divisions of endodermal and cortical cells throughout the emergence of the new organ (Crombez *et al.*, 2016). State-of-the-art approaches, such as single-cell RNA sequencing of root sections at various time points after RTE, could also provide a spatiotemporal resolution view of the genetic program driving spatial accommodation. This would then be focused on the de-differentiation of endodermis cells, reactivation of their cell cycle, and their eventual transformation into root cap cells.

Another critical point for further studies involves the potential extensive cell wall remodeling during the Brachypodium LRP emergence, not only in the endodermis but also in the overlying cell layers. As demonstrated in Arabidopsis (Vermeer *et al.*, 2014), it is likely that there is direct cell-to-cell communication coordinating CW remodeling to facilitate LRP emergence in Brachypodium. This also includes the role of the exodermis in LRP emergence, as our findings suggest that auxin acts within this layer and increased lignification may limit or delay both the emergence and subsequent development of LRP. The use of expression data from scRNAseq experiments to identify exodermis-specific promoters (Cantó-Pastor *et al.*, 2024) would be crucial to scrutinize the role of this layer during LRP emergence. Also, it would help to clarify whether, for instance, blocking auxin signaling in the exodermis influences LR emergence in a similar way as the endodermis in Arabidopsis (Vermeer *et al.*, 2014). Or if the exodermis lignification indeed act a later modulator of LRP emergence as suggested for Bd21-3 in Chapter 5. To answer the other questions, the use of this single-cell atlas could help to select genes predicted to encode CW remodeling enzymes during the LRP emergence. A large collection of chemically-induced mutants (some candidates already in-house) will be useful for forward genetics with focus on CW modifications during LR development. Alternatively, the generation of knockouts using CRISPR/Cas9 in Brachypodium could be an option since transformation protocols are getting more efficient. Complementing these methods, advanced CW immunohistochemistry, biochemistry, and microscopy will be essential for acquiring a detailed cellular and molecular analysis of each stage in the LRP development. Most of this work is planned for the coming months in the lab, led by Dr. Kevin Bellande and Dr. Thomas Badet, who are following up the results described in Chapter 5.

6.3 Final remarks

The past few decades have seen extensive transcriptome analyses of root development in the plant model Arabidopsis. Recently, there has been a growing interest in extending these studies to crop species and/or closely related plant models, such as Brachypodium. In hand of the results of this thesis and forthcoming research, mutual comparisons between datasets from Arabidopsis and Brachypodium will likely help distinguish between false positives and true candidates, and cross-species comparisons will likely help to identify conserved developmental mechanisms related to LR development. As the number of datasets increases across different species, the resolution of the results will improve, leading to more refined conclusions.

A deeper examination of spatial accommodating responses also may uncover new research directions, such as root nodule formation during the symbiosis between

leguminous plants and Rhizobia bacteria. We believe that the tools we have developed, combined with expertise in transcriptome analysis and high-throughput phenotypic characterization of candidate regulators, will aid in identifying genes whose expression impacts LR development. Although our work focuses on the fundamental aspects of root development and may not immediately translate into new breeding strategies, understanding the molecular mechanisms by which these genes influence RSA formation could eventually help to generate or select better-performing plants for agricultural purposes.

REFERENCE LIST

Aki, S.S. *et al.* (2019) 'Cytokinin Signaling Is Essential for Organ Formation in Marchantia polymorpha', *Plant and Cell Physiology*, 60(8), pp. 1842–1854. Available at: https://doi.org/10.1093/pcp/pcz100.

Amtmann, A., Bennett, M.J. and Henry, A. (2022) 'Root Phenotypes for the Future', *Plant, Cell & Environment* [Preprint]. Available at: https://doi.org/10.1111/PCE.14269.

Andersen, T.G., Barberon, M. and Geldner, N. (2015) 'Suberization-the second life of an endodermal cell', *Current Opinion in Plant Biology*. Elsevier Ltd, pp. 9–15. Available at: https://doi.org/10.1016/j.pbi.2015.08.004.

Babé, A. *et al.* (2012) 'Repression of early lateral root initiation events by transient water deficit in barley and maize', *Philosophical Transactions of the Royal Society B: Biological Sciences*, 367(1595), pp. 1534–1541. Available at: https://doi.org/10.1098/rstb.2011.0240.

Barberon, M. *et al.* (2016) 'Adaptation of Root Function by Nutrient-Induced Plasticity of Endodermal Differentiation', *Cell*, 164(3), pp. 447–459. Available at: https://doi.org/10.1016/j.cell.2015.12.021.

Beeckman, T. and Eshel, A. (2024) *Plant Roots: The Hidden Half, Fifth Edition*. CRC Press. Available at: https://books.google.ch/books?id=FmVx0AEACAAJ.

De Bellis, D. *et al.* (2022) 'Extracellular vesiculo-tubular structures associated with suberin deposition in plant cell walls', *Nature Communications 2022 13:1*, 13(1), pp. 1–11. Available at: https://doi.org/10.1038/s41467-022-29110-0.

Belsson, F. *et al.* (2007) 'The acyltransferase GPAT5 is required for the synthesis of suberin in seed coat and root of Arabidopsis', *Plant Cell*, 19(1), pp. 351–368. Available at: https://doi.org/10.1105/tpc.106.048033.

Berhin, A. *et al.* (2019) 'The Root Cap Cuticle: A Cell Wall Structure for Seedling Establishment and Lateral Root Formation In Brief', *Cell*, 176. Available at: https://doi.org/10.1016/j.cell.2019.01.005.

Birnbaum, K.D. (2018) 'Power in Numbers: Single-Cell RNA-Seq Strategies to Dissect Complex Tissues', *Annual Review of Genetics*, 52(1), pp. 203–221. Available at: https://doi.org/10.1146/annurev-genet-120417-031247.

Bishopp, A. and Bennett, M.J. (2019) 'Turning lateral roots into nodules.', *Science (New York, N.Y.)*, 366(6468), pp. 953–954. Available at: https://doi.org/10.1126/science.aay8620.

Boer, D.R. *et al.* (2014) 'Structural Basis for DNA Binding Specificity by the Auxin-Dependent ARF Transcription Factors', *Cell*, 156(3), pp. 577–589. Available at: https://doi.org/10.1016/J.CELL.2013.12.027.

Calloni, R. *et al.* (2013) 'Reviewing and updating the major molecular markers for stem cells', *Stem Cells and Development*, 22(9), pp. 1455–1476. Available at: https://doi.org/10.1089/scd.2012.0637.

Cantó-Pastor, A. *et al.* (2024) 'A suberized exodermis is required for tomato drought tolerance', *Nature Plants*, 10(1), pp. 118–130. Available at: https://doi.org/10.1038/s41477-023-01567-x.

Casero, P.J. *et al.* (1993) 'Lateral root initiation by asymmetrical transverse divisions of pericycle cells in adventitious roots ofAllium cepa', *Protoplasma*, 176(3), pp. 138–144. Available at: https://doi.org/10.1007/BF01378950.

Casero, P.J., Casimiro, I. and Lloret, P.G. (1995) 'Lateral root initiation by asymmetrical transverse divisions of pericycle cells in four plant species:Raphanus sativus, Helianthus annuus, Zea mays, andDaucus carota', *Protoplasma*, 188(1), pp. 49–58. Available at: https://doi.org/10.1007/BF01276795.

Cavallari, N., Artner, C. and Benkova, E. (2021) 'Auxin-regulated lateral root organogenesis', *Cold Spring Harbor Perspectives in Biology*, 13(7). Available at: https://doi.org/10.1101/cshperspect.a039941.

Chen, A. *et al.* (2022) 'Plant root suberin: A layer of defence against biotic and abiotic stresses', *Frontiers in Plant Science*. Frontiers Media S.A. Available at: https://doi.org/10.3389/fpls.2022.1056008.

Chu, T.T.H. *et al.* (2018) 'Sub-cellular markers highlight intracellular dynamics of membrane proteins in response to abiotic treatments in rice', *Rice*, 11(1), p. 23. Available at: https://doi.org/10.1186/s12284-018-0209-2.

Cohen, H. *et al.* (2020) 'SUBERMAN regulates developmental suberization of the Arabidopsis root endodermis', *The Plant Journal*, p. tpj.14711. Available at: https://doi.org/10.1111/tpj.14711.

Crombez, H. *et al.* (2016) 'Lateral Root Inducible System in Arabidopsis and Maize', *J. Vis. Exp*, 107, p. 53481. Available at: https://doi.org/10.3791/53481.

Das, S., Weijers, D. and Borst, J.W. (2021) 'Auxin Response by the Numbers', *Trends in Plant Science*, pp. 1–10. Available at: https://doi.org/10.1016/j.tplants.2020.12.017.

Debeaujon, I. *et al.* (2003) 'Proanthocyanidin-Accumulating Cells in Arabidopsis Testa: Regulation of Differentiation and Role in Seed Development', *Plant Cell*, 15(11), pp. 2514–2531. Available at: https://doi.org/10.1105/tpc.014043.

Ditengou, F.A. *et al.* (2008) 'Mechanical induction of lateral root initiation in Arabidopsis thaliana', *Proceedings of the National Academy of Sciences of the United States of America*, 105(48), pp. 18818–18823. Available at: https://doi.org/10.1073/pnas.0807814105.

Dubrovsky, J.G. *et al.* (2008) *Auxin acts as a local morphogenetic trigger to specify lateral root founder cells*. Available at: www.pnas.orgcgidoi10.1073pnas.0712307105.

Du, Y. and Scheres, B. (2017) 'PLETHORA transcription factors orchestrate de novo organ patterning during Arabidopsis lateral root outgrowth', *Proceedings of the National Academy of Sciences of the United States of America*, 114(44), pp. 11709–11714. Available at: https://doi.org/10.1073/pnas.1714410114.

Eliyahu, A. *et al.* (2020) 'Vegetative propagation of elite Eucalyptus clones as food source for honeybees (Apis mellifera); adventitious roots versus callus formation', *Israel Journal of Plant Sciences*, 67(1–2), pp. 83–97. Available at: https://doi.org/10.1163/22238980-20191112.

Enstone, D.E., Peterson, C.A. and Ma, F. (2003) 'Root Endodermis and Exodermis: Structure, Function, and Responses to the Environment'. Available at: https://doi.org/10.1007/s00344-003-0002-2.

Figueiredo, M.R.A. de and Strader, L.C. (2022) 'Intrinsic and extrinsic regulators of Aux/IAA protein degradation dynamics', *Trends in Biochemical Sciences*, 47(10), pp. 865–874. Available at: https://doi.org/10.1016/j.tibs.2022.06.004.

Friero, I. *et al.* (2022) 'Abscisic acid is involved in several processes associated with root system architecture in maize', *Acta Physiologiae Plantarum*, 44(3), pp. 1–12. Available at: https://doi.org/10.1007/S11738-022-03360-3/TABLES/5.

Gierth, M., Stelzer, R. and Lehmann, H. (1998) 'An analytical microscopical study on the role of the exodermis in apoplastic Rb+(K+) transport in barley roots', *Plant and Soil*, 207(2), pp. 209–218. Available at: https://doi.org/10.1023/A:1004437516331.

Hao, Z. *et al.* (2021) 'Conserved, divergent and heterochronic gene expression during Brachypodium and Arabidopsis embryo development', *Plant Reproduction*, 34(3), pp. 207–224. Available at: https://doi.org/10.1007/S00497-021-00413-4/FIGURES/7.

Herrbach, V., Maillet, F. and Bensmihen, S. (2018) 'Adapting the lateral root-inducible system to medicago truncatula', in *Methods in Molecular Biology*. Humana Press Inc., pp. 77–83. Available at: https://doi.org/10.1007/978-1-4939-7747-5_5.

Hochholdinger, F. and Zimmermann, R. (2008) 'Conserved and diverse mechanisms in root development', *Current Opinion in Plant Biology*, pp. 70–74. Available at: https://doi.org/10.1016/j.pbi.2007.10.002.

Hose, E. *et al.* (2001) 'The exodermis: a variable apoplastic barrier', *Journal of Experimental Botany*, 52(365), pp. 2245–2264. Available at: https://doi.org/10.1093/jexbot/52.365.2245.

Ho, W.W.H. *et al.* (2020) 'Integrative Multi-omics Analyses of Barley Rootzones under Salinity Stress Reveal Two Distinctive Salt Tolerance Mechanisms', *Plant Communications*, 1(3). Available at: https://doi.org/10.1016/j.xplc.2020.100031.

Jansen, L. *et al.* (2012) 'Phloem-associated auxin response maxima determine radial positioning of lateral roots in maize'. Available at: https://doi.org/10.1098/rstb.2011.0239.

Karahara, I. *et al.* (2004) 'Development of the Casparian strip in primary roots of maize under salt stress', *Planta*, 219(1), pp. 41–47. Available at: https://doi.org/10.1007/s00425-004-1208-7.

Kawa, D. and Brady, S.M. (2022) 'Root cell types as an interface for biotic interactions', *Trends in Plant Science*. Elsevier Ltd, pp. 1173–1186. Available at: https://doi.org/10.1016/j.tplants.2022.06.003.

Kawai, T. (2022) 'Developmental and genetic analysis of compensatory growth of lateral roots in rice'.

Kawai, T., Chen, Y., *et al.* (2022) 'Rice Genotypes Express Compensatory Root Growth With Altered Root Distributions in Response to Root Cutting', *Frontiers in Plant Science*, 13. Available at: https://doi.org/10.3389/fpls.2022.830577.

Kawai, T., Shibata, K., *et al.* (2022) 'WUSCHEL-related homeobox family genes in rice control lateral root primordium size', *Proceedings of the National Academy of Sciences of the United States of America*, 119(1). Available at: https://doi.org/10.1073/PNAS.2101846119/-/DCSUPPLEMENTAL.

Kelliher, T. *et al.* (2017) 'MATRILINEAL, a sperm-specific phospholipase, triggers maize haploid induction', *Nature*, 542(7639), pp. 105–109. Available at: https://doi.org/10.1038/nature20827.

Kircher, S. and Schopfer, P. (2016) 'Priming and positioning of lateral roots in Arabidopsis. An approach for an integrating concept', *Journal of Experimental Botany*, 67(5), pp. 1411–1420. Available at: https://doi.org/10.1093/jxb/erv541.

Kirschner, G.K. *et al.* (2017) 'Unique and Conserved Features of the Barley Root Meristem', *Frontiers in Plant Science*, 8, p. 1240. Available at: https://doi.org/10.3389/fpls.2017.01240.

Kiryushkin, A.S. *et al.* (2019) 'Lateral root initiation in the parental root meristem of cucurbits: Old players in a new position', *Frontiers in Plant Science*, 10. Available at: https://doi.org/10.3389/fpls.2019.00365.

Kotula, L. *et al.* (2017) 'Anatomical and biochemical characterisation of a barrier to radial O2 loss in adventitious roots of two contrasting Hordeum marinum accessions', *Functional Plant Biology*, 44(9), p. 845. Available at: https://doi.org/10.1071/FP16327.

Kreszies, T., Schreiber, L. and Ranathunge, K. (2018) 'Suberized transport barriers in Arabidopsis, barley and rice roots: From the model plant to crop species', *Journal of Plant Physiology*, 227, pp. 75–83. Available at: https://doi.org/10.1016/j.jplph.2018.02.002.

Kurihara, D. *et al.* (2015) 'ClearSee: a rapid optical clearing reagent for whole-plant fluorescence imaging.', *Development (Cambridge, England)*, 142(23), pp. 4168–79. Available at: https://doi.org/10.1242/dev.127613.

Kurihara, D. *et al.* (2021) 'ClearSeeAlpha: Advanced Optical Clearing for Whole-Plant Imaging', *Plant and Cell Physiology* [Preprint]. Available at: https://doi.org/10.1093/pcp/pcab033.

Leftley, N. *et al.* (2021) 'Uncovering How Auxin Optimizes Root Systems Stresses', pp. 1–16. Available at: https://doi.org/10.1101/cshperspect.a040014.

Lehmann, H. *et al.* (2000) 'Analytical electron microscopical investigations on the apoplastic pathways of lanthanum transport in barley roots', *Planta*, 211(6), pp. 816–822. Available at: https://doi.org/10.1007/s004250000346.

Lewis, D.R. *et al.* (2013) 'A kinetic analysis of the auxin transcriptome reveals cell wall remodeling proteins that modulate lateral root development in Arabidopsis', *Plant Cell*, 25(9), pp. 3329–3346. Available at: https://doi.org/10.1105/tpc.113.114868.

Liao, C.Y. *et al.* (2015) 'Reporters for sensitive and quantitative measurement of auxin response', *Nature Methods*, 12(3), pp. 207–210. Available at: https://doi.org/10.1038/nmeth.3279.

Liu, T. and Kreszies, T. (2023) 'The exodermis: A forgotten but promising apoplastic barrier', *Journal of Plant Physiology*, 290, p. 154118. Available at: https://doi.org/https://doi.org/10.1016/j.jplph.2023.154118.

Lu, C. *et al.* (2019) 'Abscisic Acid Regulates Auxin Distribution to Mediate Maize Lateral Root Development Under Salt Stress', *Frontiers in Plant Science*, 10. Available at: https://doi.org/10.3389/fpls.2019.00716.

Lucob-Agustin, N. *et al.* (2021) 'Morpho-physiological and molecular mechanisms of phenotypic root plasticity for rice adaptation to water stress conditions', *Breeding Science*, 71(1), pp. 20–29. Available at: https://doi.org/10.1270/jsbbs.20106.

Malamy, J.E. and Benfey, P.N. (1997) 'Organization and cell differentiation in lateral roots of Arabidopsis thaliana', *Development*, 124(1), pp. 33 LP – 44. Available at: http://dev.biologists.org/content/124/1/33.abstract.

Manzano, C. *et al.* (2022) 'Regulation and Function of a Polarly Localized Lignin Barrier in the Exodermis', *bioRxiv*, p. 2022.10.20.513117. Available at: https://doi.org/10.1101/2022.10.20.513117.

Meng, F. *et al.* (2019) 'Molecular Mechanisms of Root Development in Rice', *Rice (New York, N.Y.)*, 12(1), p. 1. Available at: https://doi.org/10.1186/s12284-018-0262-x.

Mo, B. and Weijers, D. (2009) 'Auxin Control of Embryo Patterning', pp. 1–13.

Mustroph, A. and Bailey-Serres, J. (2010) 'The Arabidopsis translatome cell-specific mRNA atlas: Mining suberin and cutin lipid monomer biosynthesis genes as an example for data application', *Plant signaling & behavior*. 2010/03/07, 5(3), pp. 320–324. Available at: https://doi.org/10.4161/psb.5.3.11187.

Nagaki, K., Yamaji, N. and Murata, M. (2017) 'ePro-ClearSee: a simple immunohistochemical method that does not require sectioning of plant samples', *Scientific Reports*, 7(1), p. 42203. Available at: https://doi.org/10.1038/srep42203.

Nakayama, T. *et al.* (2017) 'A peptide hormone required for Casparian strip diffusion barrier formation in Arabidopsis roots', *Science*, 355(6322), pp. 284–286. Available at: https://doi.org/10.1126/science.aai9057.

Naseer, S. *et al.* (2012) 'Casparian strip diffusion barrier in Arabidopsis is made of a lignin polymer without suberin', *Proceedings of the National Academy of Sciences of the United States of America*. 2012/06/04, 109(25), pp. 10101–10106. Available at: https://doi.org/10.1073/pnas.1205726109.

Ni, J. *et al.* (2014) 'Histological characterization of the lateral root primordium development in rice', *Botanical Studies*, 55(1), pp. 1–6. Available at: https://doi.org/10.1186/s40529-014-0042-x.

Van Norman, J.M. *et al.* (2013) 'To branch or not to branch: the role of pre-patterning in lateral root formation', *Development*, 140(21), pp. 4301–4310. Available at: https://doi.org/10.1242/DEV.090548.

Ohashi-Ito, K. and Bergmann, D.C. (2007) 'Regulation of the *Arabidopsis* root vascular initial population by *LONESOME HIGHWAY*', *Development*, 134(16), pp. 2959–2968. Available at: https://doi.org/10.1242/dev.006296.

Okuda, A. *et al.* (2017) 'Identification and characterization of GmPDIL7, a soybean ER membrane-bound protein disulfide isomerase family protein', *FEBS Journal*, 284(3), pp. 414–428. Available at: https://doi.org/10.1111/febs.13984.

Orman-Ligeza, B. *et al.* (2018) 'The Xerobranching Response Represses Lateral Root Formation When Roots Are Not in Contact With Water', *SSRN Electronic Journal* [Preprint]. Available at: https://doi.org/10.2139/ssrn.3188447.

Orosa-Puente, B. *et al.* (2018) 'Root branching toward water involves posttranslational modification of transcription factor ARF7', *Science*, 362(6421), pp. 1407–1410. Available at: https://doi.org/10.1126/science.aau3956.

Parizot, B. *et al.* (2008) 'Diarch Symmetry of the Vascular Bundle in Arabidopsis Root Encompasses the Pericycle and Is Reflected in Distich Lateral Root Initiation', *Plant Physiology*, 146(1), pp. 140–148. Available at: https://doi.org/10.1104/pp.107.107870.

Pende, M. *et al.* (2018) 'High-resolution ultramicroscopy of the developing and adult nervous system in optically cleared Drosophila melanogaster', *Nature Communications*, 9(1), pp. 1–12. Available at: https://doi.org/10.1038/s41467-018-07192-z.

Pende, M. *et al.* (2020) 'A versatile depigmentation, clearing, and labeling method for exploring nervous system diversity', *Science Advances*, 6(22). Available at: https://doi.org/10.1126/sciadv.aba0365.

Péret, B., Larrieu, A. and Bennett, M.J. (2009) 'Lateral root emergence: A difficult birth', *Journal of Experimental Botany*, 60(13), pp. 3637–3643. Available at: https://doi.org/10.1093/jxb/erp232.

Powers, S.K. *et al.* (2019) 'Nucleo-cytoplasmic Partitioning of ARF Proteins Controls Auxin Responses in Arabidopsis thaliana', *Molecular Cell*, 76(1), pp. 177-190.e5. Available at: https://doi.org/10.1016/j.molcel.2019.06.044.

Robbins, N.E. and Dinneny, J.R. (2018) 'Growth is required for perception of water availability to pattern root branches in plants', *Proceedings of the National Academy of Sciences of the United States of America*, 115(4), pp. E822–E831. Available at: https://doi.org/10.1073/pnas.1710709115.

Robin, A.H.K. and Saha, P.S. (2015) 'Morphology of lateral roots of twelve rice cultivars of Bangladesh: Dimension increase and diameter reduction in progressive root branching at the vegetative stage', *Plant Root*, 9, pp. 34–42. Available at: https://doi.org/10.3117/plantroot.9.34.

De Rybel, B. *et al.* (2010) 'A novel Aux/IAA28 signaling cascade activates GATA23-dependent specification of lateral root founder cell identity', *Current Biology*, 20(19), pp. 1697–1706. Available at: https://doi.org/10.1016/j.cub.2010.09.007.

Schlereth, A. *et al.* (2010) 'MONOPTEROS controls embryonic root initiation by regulating a mobile transcription factor', *Nature*, 464(7290), pp. 913–916. Available at: https://doi.org/10.1038/nature08836.

Sexauer, M. *et al.* (2021) 'Visualizing polymeric components that define distinct root barriers across plant lineages', *Development (Cambridge)*, 148(23). Available at: https://doi.org/10.1242/DEV.199820/273645.

Shukla, V. and Barberon, M. (2021) 'Building and breaking of a barrier: Suberin plasticity and function in the endodermis', *Current Opinion in Plant Biology*, 64, p. 102153. Available at: https://doi.org/10.1016/J.PBI.2021.102153.

De Smet, I. and Beeckman, T. (2011) 'Asymmetric cell division in land plants and algae: the driving force for differentiation', *Nature Reviews Molecular Cell Biology*, 12(3), pp. 177–188. Available at: https://doi.org/10.1038/nrm3064.

Song, T. *et al.* (2023) 'A new family of proteins is required for tethering of Casparian strip membrane domain and nutrient homoeostasis in rice', *Nature Plants* [Preprint]. Available at: https://doi.org/10.1038/s41477-023-01503-z.

Van Staden, J. and Ntingane, M. (1996) *The effect of a combination of decapitation treatments, zeatin and benzyladenine on the initiation and emergence of lateral roots in Pisum sativum*, *S. Afr. J. Bot*.

Swarup, K. *et al.* (2008) 'The auxin influx carrier LAX3 promotes lateral root emergence', *Nature Cell Biology*, 10(8), pp. 946–954. Available at: https://doi.org/10.1038/ncb1754.

Torres-Martínez, H.H. *et al.* (2019) 'Lateral root primordium morphogenesis in angiosperms', *Frontiers in Plant Science*. Frontiers Media S.A. Available at: https://doi.org/10.3389/fpls.2019.00206.

Torres-Martínez, H.H. *et al.* (2020) 'From one cell to many: Morphogenetic field of lateral root founder cells in Arabidopsis thaliana is built by gradual recruitment', *Proceedings of the National Academy of Sciences*, 117(34), pp. 20943–20949. Available at: https://doi.org/10.1073/pnas.2006387117.

Torrey, J.G. (1950) 'The Induction of Lateral Roots by Indoleacetic Acid and Root Decapitation', *American Journal of Botany*, 37(4), p. 257. Available at: https://doi.org/10.2307/2437843.

Tylová, E. *et al.* (2017) 'Casparian bands and suberin lamellae in exodermis of lateral roots: An important trait of roots system response to abiotic stress factors', *Annals of Botany*, 120(1), pp. 71–85. Available at: https://doi.org/10.1093/aob/mcx047.

Ulmasov, T. *et al.* (1997) 'Aux/IAA proteins repress expression of reporter genes containing natural and highly active synthetic auxin response elements.', *The Plant Cell*, 9(11), pp. 1963–1971. Available at: https://doi.org/10.1105/tpc.9.11.1963.

Ursache, R. *et al.* (2018) 'A protocol for combining fluorescent proteins with histological stains for diverse cell wall components', *The Plant Journal*, 93(2), pp. 399–412. Available at: https://doi.org/10.1111/tpj.13784.

Ursache, R. *et al.* (2021) 'GDSL-domain proteins have key roles in suberin polymerization and degradation', *Nature Plants*, 7(3), pp. 353–364. Available at: https://doi.org/10.1038/s41477-021-00862-9.

Vermeer, J.E.M. *et al.* (2014) 'A spatial accommodation by neighboring cells is required for organ initiation in arabidopsis', *Science*, 343(6167), pp. 178–183. Available at: https://doi.org/10.1126/SCIENCE.1245871.

Vermeer, J.E.M. and Geldner, N. (2015) 'Lateral root initiation in Arabidopsis thaliana: a force awakens', *F1000Prime Reports*, 7. Available at: https://doi.org/10.12703/P7-32.

Voß, U. *et al.* (2015) 'The circadian clock rephases during lateral root organ initiation in Arabidopsis thaliana', *Nature Communications*, 6(1), p. 7641. Available at: https://doi.org/10.1038/ncomms8641.

Vysotskaya, L.B. *et al.* (2001) 'Growth rate, IAA and cytokinin content of wheat seedling after root pruning', *Plant Growth Regulation*, 33(1), pp. 51–57. Available at: https://doi.org/10.1023/A:1010700617829.

Wachsman, G. and Benfey, P.N. (2020) 'Lateral Root Initiation: The Emergence of New Primordia Following Cell Death', *Current Biology*, 30(3), pp. R121–R122. Available at: https://doi.org/10.1016/j.cub.2019.12.032.

Von Wangenheim, D. *et al.* (2016) 'Rules and self-organizing properties of post-embryonic plant organ cell division patterns', *Current Biology*, 26(4), pp. 439–449. Available at: https://doi.org/10.1016/j.cub.2015.12.047.

Wang, Y. *et al.* (2022) 'A dirigent family protein confers variation of Casparian strip thickness and salt tolerance in maize', *Nature Communications*, 13(1), p. 2222. Available at: https://doi.org/10.1038/s41467-022-29809-0.

Wu, Q., Pagès, L. and Wu, J. (2016) 'Relationships between root diameter, root length and root branching along lateral roots in adult, field-grown maize', *Annals of Botany*, 117(3), pp. 379–390. Available at: https://doi.org/10.1093/aob/mcv185.

Xiao, T.T. *et al.* (2019) 'Lateral root formation involving cell division in both pericycle, cortex and endodermis is a common and ancestral trait in seed plants', *Development (Cambridge)*, 146(20). Available at: https://doi.org/10.1242/dev.182592.

Xu, D. *et al.* (2017) 'YUCCA9-mediated auxin biosynthesis and polar auxin transport synergistically regulate regeneration of root systems following root cutting', *Plant and Cell Physiology*, 58(10), pp. 1710–1723. Available at: https://doi.org/10.1093/pcp/pcx107.

Yadav, V. *et al.* (2014) 'ABCG transporters are required for suberin and pollen wall extracellular barriers in Arabidopsis', *Plant Cell*, 26(9), pp. 3569–3588. Available at: https://doi.org/10.1105/tpc.114.129049.

Yeats, T.H. *et al.* (2012) 'The identification of cutin synthase: formation of the plant polyester cutin', *Nature Chemical Biology*, 8(7), pp. 609–611. Available at: https://doi.org/10.1038/nchembio.960.

Yu, P., Hochholdinger, F. and Li, C. (2019) 'Plasticity of Lateral Root Branching in Maize', *Frontiers in Plant Science*, 10. Available at: https://doi.org/10.3389/fpls.2019.00363.